University of Warsaw
Institute of Theoretical Physics
Faculty of Physics

Paulina Michalak

Spontaneous Scale Symmetry Breaking and Inflation in a Higgs-Dilaton-Weyl Framework

Doctoral dissertation

Thesis Advisor:
prof. dr hab. Zygmunt Lalak
Chair of Theory of Particles and Fundamental Interactions
Institute of Theoretical Physics

Warsaw, 2025r.

Acknowledgements

I would like to thank my supervisor, Professor Zygmunt Lalak, for supporting my work from the start of my master's studies and throughout my entire time in the doctoral school. His guidance was essential in completing this thesis.

I am also deeply grateful to my parents, who believed in me from the very beginning and made it possible for me to fulfill my high school dream of becoming a scientist.

A heartfull thank you to my fellow PhD students and colleagues from earlier years. Your scientific support was invaluable, but even more so were the friendships and the countless joyful moments that made this journey truly special.

A very special thanks to my life partner, Michał. Your unwavering support, patience, and kindness made this journey so much easier and more meaningful. Thank you for always being there, for believing in me even when I doubted myself, for answering my endless questions, and for filling this time with love and encouragement. I couldn't have done this without you.

Finally, I would like to extend my gratitude to my high school physics teacher, Jan Kowalczyk, who introduced me to the fascinating world of physics by lending me my first popular science books. Your passion and encouragement set me on this path, and for that, I am forever grateful.

Abstract

This dissertation explores scale-invariant extensions of the Standard Model (SM) Higgs scalar sector, addressing the unexplained origin of mass scales such as the electroweak scale and the Planck mass. We explore frameworks where scale symmetry is preserved at the classical and quantum levels and broken dynamically. We also focus on incorporating the Weyl gravity prescription, which naturally introduces a dilaton field coupled to the Higgs boson.

Theoretical foundations, including the quantum effective potential and scale-symmetric regularization, Weyl geometry, and quantum field theory at finite temperature, are reviewed. We then analyze a scale-invariant Higgs sector, incorporating quantum corrections, and examine the roles of gravity, dilaton effects, and the Weak Gravity Conjecture. One of the key contributions is the study of spontaneous scale symmetry breaking at high temperature, providing a natural mechanism for mass generation in the early Universe. We analyze temperature corrections to the one-loop effective potential and simulate the evolution of the Higgs and dilaton fields in a hot expanding Universe. We show that certain initial conditions for this evolution can lead to a physically viable vacuum state. Finally, we explore inflation in this framework, introducing a kinetic term for the dilaton and extending gravity to Weyl geometry, which affects the model's inflationary dynamics. These findings support the search for a more fundamental theory where mass scales arise from underlying symmetries rather than arbitrary parameters.

Streszczenie

Niniejsza rozprawa doktorska bada oparte na symetrii skalowania rozszerzenie skalarnego sektora Higgsa Modelu Standardowego, mające na celu wyjaśnienie nierozwiązanego problemu pochodzenia skal masowych, takich jak skala elektrosłaba i skala Plancka. Rozpatrujemy modele, w których symetria skalowania zachowana jest zarówno na poziomie klasycznym, jak i kwantowym, oraz łamana jest w sposób dynamiczny. Szczególną uwagę poświęcamy również zastosowaniu grawitacji Weyla, która w naturalny sposób wprowadza cząstkę dylaton, sprzężoną z bozonem Higgsa.
Przedstawiamy podstawy teoretyczne, takie jak kwantowy potencjał efektywny i regularyzację zachowującą symetrię skalowania, geometrię Weylowską oraz teorię pól kwantowych w skończonej temperaturze. Następnie analizujemy sektor Higgsa niezmienniczy ze względu na symetrię skalowania uwzględniając poprawki kwantowe, oraz badamy rolę grawitacji, efektów dylatonowych i hipotezy słabej grawitacji (Weak Gravity Conjecture).
Jednym z kluczowych wyników pracy jest analiza spontanicznego łamania symetrii skalowania w wysokiej temperaturze, oferująca naturalny mechanizm generowania mas we wczesnym Wszechświecie. Badamy poprawki temperaturowe do jednopętlowego efektywnego potencjału i symulujemy ewolucję pól Higgsa oraz dylatonu w gorącym, rozszerzającym się Wszechświecie, wykazując, że odpowiednie warunki początkowe mogą doprowadzić do fizycznie stabilnego stanu próżniowego. Na koniec omawiamy inflację w tym modelu, wprowadzając człon kinetyczny dla dylatonu oraz rozszerzając grawitację do geometrii Weyla, co wpływa na dynamikę inflacyjną modelu.
Otrzymane wyniki wspierają poszukiwania bardziej fundamentalnej teorii, w której skale masowe wynikają z podstawowych symetrii, a nie z arbitralnych parametrów.

Contents

Chapter 1

Introduction

While the Standard Model (SM) successfully describes particle interactions at currently accessible collider energies, it still faces unresolved problems, suggesting that it is a part of a more fundamental theory. Among those problems is the hierarchy problem, which arises due to the quantum corrections that tend to drive the Higgs mass, m_H, towards the Planck scale, M_P, at high energies. Maintaining m_H significantly below the Planck mass requires highly precise fine-tuning of the theory and exact cancellation of independent contributions. This suggests the need for a deeper underlying principle to resolve the problem. A natural way is to impose scale or conformal symmetry by setting $m_H = 0$ at the classical level. However, the Higgs mass is non-zero, and it must be generated through some symmetry-breaking mechanism. This mechanism can be explicit, like in radiative symmetry breaking with a fixed renormalization scale $\mu = const$ or cutoff $\Lambda = const$, or spontaneous, without introducing any direct mass scales. For such a model to explain the origin of the electroweak scale along with the Planck mass, it needs to be coupled to a version of gravity respecting the scale symmetry.

Various models have been proposed in which the Higgs scalar sector is extended by introducing a scalar singlet with $m_H = 0$, preserving the scale symmetry [1–8]. These models are often coupled to either Einstein's or Brans-Dicke gravity. However, an alternative and particularly compelling approach involves using the Weyl geometry [9–20], a natural extension of Riemannian geometry. One of the key advantages of this approach is that it offers a geometric origin for the additional scalar degree of freedom, the dilaton ϕ_0, as opposed to the Einstein's formulation, where it is introduced ad hoc. This new scalar field's vacuum expectation value (vev) generates all mass scales in the theory, including m_H and M_P. Moreover, it allows for the construction of a field-dependent subtraction scale $\mu(\phi_0)$ in dimensional regularization, preserving the scale symmetry at the quantum level, unlike a fixed renormalization scale $\mu = const$ or a dimensionful cutoff Λ. Previous studies [21–28] have demonstrated that the renormalization scale can be dynamically linked to the dilaton, such that after spontaneous scale symmetry breaking (SSSB), it is generated dynamically as $\mu(\langle\phi_0\rangle)$. This approach modifies quantum corrections, introducing new finite, non-polynomial contributions that are absent in the standard Coleman-Weinberg results [29, 30], as discussed in earlier works.

This study explores a scale-symmetric extension of the SM, where the Higgs scalar sector is coupled to Weyl gravity, leading to the emergence of an additional scalar singlet, the dilaton, which interacts with the Higgs neutral component. We analyze the fundamental classical and quantum properties of the model and highlight its most important applications as discussed in the literature. Then we proceed with our independent contributions, which include the study of gravity-dilaton effects, Weak Gravity Conjecture, SSSB in high temperature, and cosmological inflation within this framework.

The thesis is organized as follows. Chapter 2 briefly outlines the basic concept of Quantum Field Theory (QFT), quantum effective potential V_{eff}. We derive expressions for one-loop contributions to V_{eff} from scalar, fermion, and boson fields. Next, in Chapter 3 we extend the conventional approach to dimensional regularization by incorporating a scale-symmetric version with a dilaton-dependent subtraction scale $\mu(\phi_0)$. The analysis, based on existing works [22–25, 28], is included to keep the thesis self-consistent. Chapter 4 introduces the fundamental properties of Weyl conformal geometry, in which Einstein's gravity emerges as a low-energy limit. Similar descriptions can be found in literature [9–20].

Building on these theoretical foundations, Chapter 5 examines the scale-symmetric Higgs scalar sector extended with Weyl geometry and the dilaton. We demonstrate how the dilaton emerges naturally from Weyl conformal geometry and how it couples to the Higgs neutral component, and we continue with an extensive analysis of the classical and one-loop quantum potential of the resulting scalar sector. Although these results have been discussed in previous works [22–25, 28, 31], we include them to maintain the completeness of our study, as they serve as the basis for subsequent analysis. Next, in Chapter 6, we present an independent study of the gravity-dilaton effects, especially their decoupling limits, where the standard Higgs sector in flat spacetime is recovered. We finish the Chapter with an analysis of the realization of the Weak Gravity Conjecture in the model, which imposes constraints on the Weyl gauge coupling q.

Chapter 7 provides an extensive theoretical introduction to Quantum Field Theory in Finite Temperature, following standard textbook material. These concepts are then applied in Chapter 8, which presents an independent analysis of thermal effects in the scale-symmetric model under consideration. Understanding thermal corrections to the Higgs-dilaton potential is essential for describing the cosmological evolution of the system, as the Universe was hot during its early expansion. Since temperature introduces an explicit mass scale, it breaks the scale symmetry directly. Close analysis of the nature of electroweak symmetry breaking (EWSB) at finite temperature aligns with results obtained in the models involving only the Higgs boson, namely, that thermal effects restore electroweak symmetry at high temperatures, driving the Higgs vev to zero, after which EWSB occurs as smooth crossover [32–34]. The presence of an additional dilaton scalar and the inclusion of scale-invariant quantum corrections do not change these conclusions. Next, we follow with an analysis of the time evolution of the fields in a hot Universe within the FLRW gravitational background, reinforcing our results. This chapter, based on a paper co-authored by the author and her supervisor [35], provides a mechanism for dynamical mass generation as the dilaton settles into its final vev $\langle\phi_0\rangle$.

Chapter 9 explores the inflationary dynamics in the considered model, based on a paper co-authored by the author and her supervisor [36]. Three key aspects distinguish our approach from the previous studies on inflation in Higgs-dilaton models [2, 3, 6, 37–45]: the embedding of the theory in Weyl geometry, the explicit inclusion of a kinetic term for the dilaton, and incorporation of the so-called suppression factors, which all significantly impact inflationary dynamics. We first analyze the classical potential in inflationary regimes and then incorporate quantum corrections through the running of coupling constants in the inflationary potential. Our findings indicate that a viable parameter space exists that is consistent with experimental constraints, leading to successful slow-roll inflation. Additionally, we compute the gravitational wave spectrum resulting from inflationary dynamics of the considered framework. We conclude the chapter with a discussion of potential unitarity violation, a common challenge in inflationary models, particularly when energy scales during inflation approach or exceed the Planck scale.

Finally, Chapter 10 summarizes our results and outlines open questions that must be addressed to further refine the model. The thesis is also supplemented with appendices containing supplementary results and derivations essential to our analysis. Appendix A presents the beta functions for the couplings constants in the Higgs-dilaton potential, as well as those from the SM weak, strong, and top-Yukawa interactions, along with plots of their running with respect to the dilaton field and discussion on the choice of subtraction scale. Appendix B derives thermally averaged products of annihilation (a) and creation ($a^\dagger$) operators for scalars and fermions, which are used in QFT in finite temperature to compute Green's functions and propagators for the corresponding particles. Appendix C discusses the resummation procedure required for a consistent perturbative expansion in thermal QFT. Appendix D provides an approximate constraint for ensuring the dilaton field remains in thermal equilibrium. While these results are not exact, they serve as a useful approximation for the analysis presented in Chapter 8. Finally, Appendix E includes a brief derivation of statistical quantities in Thermal Field Theory, specifically the mean value and standard deviation of scalar field products at finite temperature.

Chapter 2

Quantum Effective Potential

This chapter reviews one of the fundamental concepts in Quantum Field Theory (QFT), the effective action and the effective potential. The effective potential, in particular, is crucial for studying spontaneous symmetry breaking, phase transitions, and vacuum structure in various quantum field theories. While the material covered here is standard QFT textbook content, we include it to keep the dissertation self-consistent and easy to understand. We focus on the effective potential derived from the generating functional in the path integral formulation so that, in the next chapters, we can explore these phenomena in a systematic and rigorous manner. This approach, along with the diagrammatic method, is covered in many educational resources, such as [29, 46–50].

2.1. Generating Functionals

Let's consider a real scalar field ϕ with Lagrangian density $\mathcal{L}_0(\phi)$ and an action:

$$S_0[\phi] = \int d^4x \mathcal{L}_0(\phi). \tag{2.1}$$

Denoting J as an external source and action $S[\phi]$ as:

$$S[\phi] = S_0[\phi] + J \cdot \phi, \tag{2.2}$$

where:

$$J \cdot \phi = \int d^4x J(x)\phi(x), \tag{2.3}$$

one can define generating functional $Z[J]$, which is a vacuum to vacuum amplitude in the presence of J source:

$$Z[J] = \langle 0_{\text{out}}|0_{\text{in}}\rangle_J = \int d\phi \exp\big\{iS_0[\phi] + iJ \cdot \phi\big\} = \int d\phi \exp\big\{iS[\phi]\big\}. \tag{2.4}$$

From definition (2.3) follows a functional derivative:

$$\frac{\delta}{\delta J(y)}\big(J\cdot\phi\big) = \int d^4x \delta^4(x-y)\phi(x) = \phi(y), \qquad \frac{\delta}{\delta \phi(y)}\big(J\cdot\phi\big) = \int d^4x J(x)\delta^4(x-y) = J(y). \tag{2.5}$$

Tylor expansion of $Z[J]$ in J provides Green's functions $G^{(n)}(x_1, \dots, x_n)$, containing all possible Feynman diagrams for considered process:

$$Z[J] = \sum_{n=0}^{\infty} \frac{i^n}{n!} \int d^4x_1 \dots d^4x_n J(x_1) \dots J(x_n) G^{(n)}(x_1, \dots, x_n), \tag{2.6}$$

so that:

$$G^{(n)}(x_1,\ldots,x_n) = (-i)^n \frac{\delta}{\delta J(x_1)} \cdots \frac{\delta}{\delta J(x_n)} Z[J]\Big|_{J=0}. \tag{2.7}$$

Using (2.4) one can define connected generating functional $W[J]$:

$$Z[J] = \exp\{iW[J]\}, \tag{2.8}$$

by which connected Green's functions $G^{(n)}_{conn}(x_1,\ldots,x_n)$ are generated:

$$iW[J] = \sum_{n=0}^{\infty} \frac{i^n}{n!} \int d^4x_1 \ldots d^4x_n J(x_1)\ldots J(x_n) G^{(n)}_{conn}(x_1,\ldots,x_n), \tag{2.9}$$

$$G^{(n)}_{conn}(x_1,\ldots,x_n) = \frac{\delta}{\delta J(x_1)} \cdots \frac{\delta}{\delta J(x_n)} W[J]\Big|_{J=0}. \tag{2.10}$$

One can now define the classical field ϕ_c as a vacuum expectation value (vev) of the field operator $\phi(x)$ in the presence of the given current J:

$$\phi_c(x) = \frac{\delta W[J]}{\delta J(x)} = \frac{\int d\phi \exp\{iS_0[\phi] + iJ\cdot\phi\}\cdot\phi(x)}{\int d\phi \exp\{iS_0[\phi] + iJ\cdot\phi\}} = \frac{\langle 0_{\mathrm{out}}|\phi(x)|0_{\mathrm{in}}\rangle}{\langle 0_{\mathrm{out}}|0_{\mathrm{in}}\rangle}\Bigg|_J. \tag{2.11}$$

The Above relation determines ϕ_c as a functional of J (as it is shown below in equation (2.14), ϕ_c and J are conjugated, so $\frac{\delta J(x)}{\delta\phi_c(y)} \neq 0$). In particular, in the absence of source, $J = 0$:

$$\phi_c(x)\Big|_{J=0} = \langle\phi\rangle = \frac{\int d\phi \exp\{iS_0[\phi]\}\cdot\phi(x)}{\int d\phi \exp\{iS_0[\phi]\}} = \frac{\langle 0_{\mathrm{out}}|\phi(x)|0_{\mathrm{in}}\rangle}{\langle 0_{\mathrm{out}}|0_{\mathrm{in}}\rangle}\Bigg|_{J=0} \tag{2.12}$$

and $\langle\phi\rangle$ is vev of field operator $\phi(x)$ in the true vacuum of the theory.

Functional Legendre transformation of $W[J]$ is the so-called effective action $\Gamma[\phi_c]$:

$$\Gamma[\phi_c] = W[J] - \int d^4x J(x)\phi_c(x). \tag{2.13}$$

The functional derivative of effective action with respect to ϕ_c gives:

$$\frac{\delta\Gamma[\phi_c(x)]}{\delta\phi_c(y)} = \int d^4x \frac{\delta W[J]}{\delta J(x)} \frac{\delta J(x)}{\delta\phi_c(y)} - \int d^4x \frac{\delta J(x)}{\delta\phi_c(y)}\phi_c(x) - J(y) = -J(y), \tag{2.14}$$

which, in the absence of external sources, will define the true vacuum of the theory:

$$\frac{\delta\Gamma[\phi_c(x)]}{\delta\phi_c(y)}\Bigg|_{J=0} = 0. \tag{2.15}$$

The effective action $\Gamma[\phi_c]$ can be expanded in two ways. First, Taylor expansion in ϕ_c provides 1PI (one-particle irreducible) Green's functions $\Gamma^{(n)}(x_1,\ldots,x_n)$:

$$\Gamma[\phi_c] = \sum_{n=0}^{\infty} \frac{1}{n!} \int d^4x_1 \ldots d^4x_n \phi_c(x_1)\ldots\phi_c(x_n)\Gamma^{(n)}(x_1,\ldots,x_n). \tag{2.16}$$

A 1PI Feynman diagram is a connected diagram that cannot be disconnected by cutting a single internal line. $\Gamma^{(n)}$ is the sum of all such diagrams with n external legs. Example 1PI diagrams in $\lambda\phi^4$ theory are shown in Figure 2.1. An alternative way is to expand the effective action in external momenta about the point for which all external momenta are zero. This gives:

$$\Gamma[\phi_c] = \int d^4x \Big[-V_{eff}(\phi_c) + \frac{1}{2}(\partial_\mu\phi_c)^2 Z(\phi_c) + \ldots \Big], \tag{2.17}$$

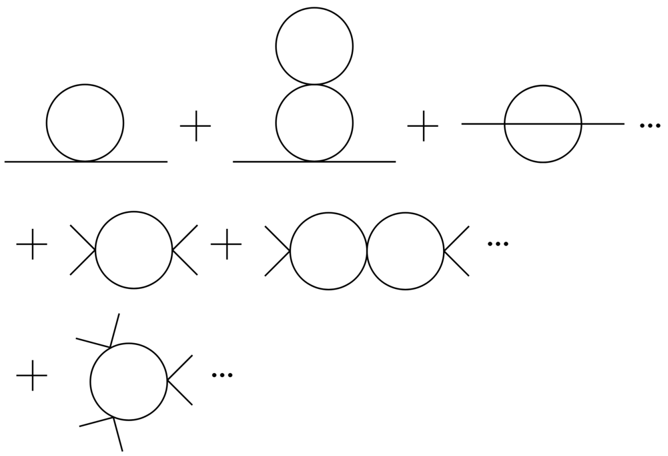

Figure 2.1: 1PI Feynman diagrams for $\lambda\phi^4$ theory.

where other terms contain higher derivatives of ϕ_c. The term with zero power of momentum, $V_{eff}(\phi_c)$, is the so-called effective potential. For homogeneous ϕ_c and J, independent of x, we find:

$$\Gamma[\phi_c] = -V_{eff}(\phi_c)\int d^4x \quad \Rightarrow \quad \frac{\delta\Gamma[\phi_c]}{\delta\phi_c} = -J = -V'_{eff}(\phi_c). \tag{2.18}$$

Using the above equation and (2.15), in the absence of external sources, we have:

$$\left.\frac{\delta\Gamma[\phi_c]}{\delta\phi_c}\right|_{J=0} = -V'_{eff}(\phi_c)\Big|_{J=0} = 0. \tag{2.19}$$

Consequently, the value $\phi_c\big|_{J=0} = \langle\phi\rangle$, for which the first derivative of the effective potential $V'_{eff}(\langle\phi\rangle)$ vanishes, is the vacuum expectation value of the ϕ field. Therefore, to study the vacuum structure of the model presented in this work, we will limit ourselves to the constant classical fields ϕ_c.

Let's write the 1PI Green's function $\Gamma^{(n)}(x_1,\ldots,x_n)$ as its Fourier transform:

$$\Gamma^{(n)}(x_1,\ldots,x_n) = \int\frac{d^4k_1}{(2\pi)^4}\cdots\frac{d^4k_n}{(2\pi)^4}(2\pi)^4\delta^{(4)}(k_1+\ldots+k_n)e^{i(k_1x_1+\ldots+k_nx_n)}\tilde{\Gamma}^{(n)}(k_1,\ldots,k_n), \tag{2.20}$$

which gives in (2.16):

$$\begin{aligned}\Gamma[\phi_c] =& \sum_{n=0}^{\infty}\frac{1}{n!}\int d^4x_1\ldots d^4x_n\int\frac{d^4k_1}{(2\pi)^4}\cdots\frac{d^4k_n}{(2\pi)^4}(2\pi)^4\delta^{(4)}(k_1+\ldots+k_n)e^{i(k_1x_1+\ldots+k_nx_n)}\times\\ &\times\tilde{\Gamma}^{(n)}(k_1,\ldots,k_n)\phi_c(x_1)\ldots\phi_c(x_n).\end{aligned} \tag{2.21}$$

Then, we express the delta function as:

$$(2\pi)^4\delta^{(4)}(k_1+\ldots k_n) = \int d^4x e^{-i(k_1+\ldots k_n)x}, \tag{2.22}$$

and in (2.21), after evaluation of the $\frac{d^4k_i}{(2\pi)^4}$ integrals we obtain:

$$\begin{aligned}\Gamma[\phi_c] =& \sum_{n=0}^{\infty}\frac{1}{n!}\int d^4x_1\ldots d^4x_n\int d^4x\ \delta^{(4)}(x-x_1)\ldots\delta^{(4)}(x-x_n)\tilde{\Gamma}^{(n)}(k_1,\ldots,k_n)\times\\ &\times\phi_c(x_1)\ldots\phi_c(x_n) = \int d^4x\sum_{n=0}^{\infty}\frac{1}{n!}\tilde{\Gamma}^{(n)}(k_1,\ldots,k_n)\phi_c^n(x).\end{aligned} \tag{2.23}$$

We expand the above expression around zero momenta:

$$\Gamma[\phi_c] = \int d^4x \sum_{n=0}^{\infty} \frac{1}{n!}\tilde{\Gamma}^{(n)}(0,\dots,0)\phi_c^n(x) + \dots \tag{2.24}$$

where terms in $+\dots$ are higher powers of momenta. One compares it to (2.18), in which the 0-th order term is the effective potential. The final result is:

$$V_{eff}(\phi_c) = -\sum_{n=0}^{\infty} \frac{1}{n!}\tilde{\Gamma}^{(n)}(0,\dots,0)\phi_c^n(x), \tag{2.25}$$

with $\tilde{\Gamma}^{(n)}(0,\dots,0)$ being 1PI diagrams with vanishing external momenta. The zero-loop order contribution to (2.25) is the tree-level potential $V_0(\phi_c)$ of a considered theory as a function of a classical field ϕ_c. Then, we have:

$$V_{eff}(\phi_c) = V_0(\phi_c) - \sum_{n=0}^{\infty} \frac{1}{n!}\tilde{\Gamma}^{(n)}_{\text{loops}}(0,\dots,0)\phi_c^n(x) = V_0(\phi_c) + V_1(\phi_c) + V_2(\phi_c) + \dots, \tag{2.26}$$

where $V_i(\phi_c)$ is the i-th loop order contribution to (2.25). As can be seen from equation (2.25), the specific form of the effective potential depends on the theory and, in particular, on its particle content, as different particles will contribute differently to the loop calculations. In chapter 7, we present the diagrammatic approach to finding $V_{eff}(\phi_c)$ in scalar field theory in finite temperature. In the following section, we present a derivation of the effective potential using a functional integration method, which provides a more efficient approach.

2.2. The One-Loop Effective Potential in Scalar Field Theory

To obtain effective potential V_{eff}, which comes from $\Gamma[\phi_c]$, one needs to calculate $W[J]$ first. From (2.4) and (2.8) we have:

$$\exp\big\{\frac{i}{\hbar}W[J]\big\} = \int d\phi \exp\big\{\frac{i}{\hbar}S[\phi]\big\} = \int d\phi \exp\big\{\frac{i}{\hbar}(S_0[\phi] + J\cdot\phi)\big\}, \tag{2.27}$$

where we inserted back $\hbar$. We want to evaluate $W[J]$ to the 1-loop order, hence, to the first order in $\hbar$. For $\hbar \to 0$, one can use the so-called steepest descend (or stationary phase) approximation. The main contribution to the integral (2.27) comes from the minimum of the exponent argument $S[\phi]$. Let's assume that it is minimized for some stationary "point" ϕ_s in field space:

$$\frac{\delta S[\phi]}{\delta\phi(x)}\bigg|_{\phi_s} = \frac{\delta\Big[S_0[\phi(y)] + J(y)\cdot\phi(y)\Big]}{\delta\phi(x)}\bigg|_{\phi_s} = 0. \tag{2.28}$$

For a real scalar field with potential $V(\phi)$, the action reads:

$$S_0[\phi] = \int d^4x\Big[\frac{1}{2}(\partial\phi)^2 - V(\phi)\Big] = -\int d^4x\Big[\frac{1}{2}\phi\partial^2\phi + V(\phi)\Big]. \tag{2.29}$$

This implicates in (2.28):

$$-\frac{\delta S_0[\phi(y)]}{\delta\phi(x)}\bigg|_{\phi_s} = \partial^2\phi_s(x) + V'(\phi_s(x)) = J(x), \tag{2.30}$$

hence ϕ_s can be regarded as a function of J and vice versa. Now we take $\phi = \phi_s + \tilde{\phi}$, where $\tilde{\phi}$ is a quantum field, and expand $S[\phi = \phi_s + \tilde{\phi}]$ around its stationary point ϕ_s:

$$
\begin{aligned}
&S_0[\phi_s + \tilde{\phi}] = -\int d^4x \frac{1}{2}\Big[\phi_s\partial^2\phi_s + 2\tilde{\phi}\partial^2\phi_s + \tilde{\phi}\partial^2\tilde{\phi}\Big] - \int d^4x\Big[V(\phi_s) + \tilde{\phi}V'(\phi_s) + \frac{1}{2}\tilde{\phi}^2V''(\phi_s) + \dots\Big],\\
&J\cdot(\phi_s + \tilde{\phi}) = J\cdot\phi_s + \int d^4x\Big[\tilde{\phi}\partial^2\phi_s + \tilde{\phi}V'(\phi_s)\Big],\\
&S[\phi_s + \tilde{\phi}] = S_0[\phi_s] + J\cdot\phi_s - \int d^4x\frac{1}{2}\Big[\tilde{\phi}(\partial^2 + V''(\phi_s))\tilde{\phi}\Big],
\end{aligned}
\tag{2.31}
$$

where (2.30) was used. A shift $\phi = \phi_s + \tilde{\phi}$ just changes the measure in (2.27) to $d\phi = d\tilde{\phi}$, and one has[1]:

$$
\begin{aligned}
\exp\big\{\frac{i}{\hbar}W[J]\big\} &= \exp\big\{\frac{i}{\hbar}(S[\phi_s] + J\cdot\phi_s)\big\}\int d\tilde{\phi}\exp\Big\{-\frac{i}{\hbar}\int d^4x\frac{1}{2}\tilde{\phi}\big[\partial^2 + V''(\phi_s)\big]\tilde{\phi}\Big\} =\\
&= \exp\big\{\frac{i}{\hbar}(S[\phi_s] + J\cdot\phi_s)\big\}\cdot\det\Big[\partial^2 + V''(\phi_s)\Big]^{-\frac{1}{2}}.
\end{aligned}
\tag{2.32}
$$

Finally, using:

$$
\det A = \exp\Big\{\mathrm{Tr}\big(\log A\big)\Big\} \quad\Rightarrow\quad \det\Big[\partial^2 + V''(\phi_s)\Big]^{-\frac{1}{2}} = \exp\Big\{-\frac{1}{2}\mathrm{Tr}\big(\log[\partial^2 + V''(\phi_s)]\big)\Big\},
\tag{2.33}
$$

generating functional $W[J]$ becomes:

$$
W[J] = S_0[\phi_s] + J\cdot\phi_s + \frac{i\hbar}{2}\mathrm{Tr}\Big(\log\big[\partial^2 + V''(\phi_s)\big]\Big).
\tag{2.34}
$$

Now with the above result, the next step in obtaining $\Gamma[\phi_c]$ is to find ϕ_c according to (2.11):

$$
\phi_c = \frac{\delta W[J]}{\delta J} = \phi_s.
\tag{2.35}
$$

Thus:

$$
\Gamma[\phi_c] = W[J] - J\cdot\phi_c = S_0[\phi_c] + \frac{i\hbar}{2}\mathrm{Tr}\Big(\log\big[\partial^2 + V''(\phi_c)\big]\Big).
\tag{2.36}
$$

The trace can be written as an integral over d^4x:

$$
\mathrm{Tr}\Big(\log\big[\partial^2 + V''(\phi_c)\big]\Big) = \int d^4x\langle x|\log\big[\partial^2 + V''(\phi_c)\big]|x\rangle.
\tag{2.37}
$$

This integral can be evaluated easily if ϕ_c is independent of x. Let's assume homogeneous $\phi_c = const$ and insert a complete set of momentum states $\int\frac{d^4k}{(2\pi)^4}|k\rangle\langle k| = \mathbb{1}$, which gives:

$$
\mathrm{Tr}\Big(\log\big[\partial^2 + V''(\phi_c)\big]\Big) = \int d^4x\int\frac{d^4k}{(2\pi)^4}\log\big[-k^2 + V''(\phi_c)\big].
\tag{2.38}
$$

For $\phi_c = const$, according to (2.18), we finally have:

$$
V_{eff}(\phi_c) = V(\phi_c) - \frac{i\hbar}{2}\int\frac{d^4k}{(2\pi)^4}\log\left[\frac{k^2 - V''(\phi_c)}{k^2}\right] + \mathcal{O}(\hbar^2),
\tag{2.39}
$$

where we have inserted $\log(-k^2)$, which is ϕ_c independent, to make the argument of logarithm dimensionless. We obtained the order $\hbar$ correction to the classical potential $V(\phi_c)$ known as

[1] Technically the integral $\int d\tilde{\phi}\exp\{-\frac{i}{\hbar}\int d^4x\frac{1}{2}\tilde{\phi}[\partial^2 + V''(\phi_s)]\tilde{\phi}\}$ results in infinite factor $\lim_{N\to\infty}(-2\pi i\hbar)^{N/2}$, but it is canceled by normalization factors included in the measure definition $\int d\tilde{\phi}$.

the Coleman-Weinberg effective potential. We set again $\hbar = 1$ and do Wick's rotation so equation (2.39) takes form:

$$V_{eff}(\phi_c) = V(\phi_c) + \frac{1}{2}\int \frac{d^4k_E}{(2\pi)^4}\log\left[\frac{k_E^2 + V''(\phi_c)}{k_E^2}\right] + \mathcal{O}(\hbar^2). \tag{2.40}$$

For example, if $V(\phi_c) = \frac{1}{2}m^2\phi_c^2 + \frac{\lambda}{4!}\phi_c^4$, then $V''(\phi_c) = m^2 + \frac{\lambda}{2}\phi_c^2$ can be interpreted as effective mass squared m_{eff}^2. The generalization to theory with many scalar fields ϕ_i is straightforward, one substitutes:

$$V''(\phi_c) \quad \rightarrow \quad (M^2)_{jk}\big|_{\phi_c} = \frac{\partial^2 V(\phi_i)}{\partial\phi_j\partial\phi_k}\Big|_{\phi_c}, \tag{2.41}$$

where ϕ_c here can be thought of as a vector of vacuum expectation values for ϕ_i fields and $M^2(\phi_c)$ is just the mass matrix from the potential $V(\phi_i)$ evaluated at ϕ_c. Finally, the one-loop contribution to the effective potential for scalar fields is given by:

$$V_1(\phi_c) = \frac{1}{2}\int \frac{d^4k_E}{(2\pi)^4}\log\Big[k_E^2 + M^2(\phi_c)\Big], \tag{2.42}$$

where we neglected the field independent term and $M^2(\phi_c)$ is defined as in (2.41).

2.3. Fermions

Let's consider adding fermionic fields so that the action reads:

$$S[\psi] = \int d^4x\left[\bar{\psi}\Big(i\gamma^\mu\partial_\mu - M_F(\phi)\Big)\psi\right], \tag{2.43}$$

where the mass matrix $M_F(\phi)$ is a linear function of the scalar field ϕ. In particular, it can be of the form $M_F(\phi) = m_F + y\cdot\phi$. Fermionic contribution to the functional $W[J]$ can be calculated from:

$$\exp\big\{\frac{i}{\hbar}W_F[J]\big\} = \int d\bar{\psi}d\psi\exp\big\{\frac{i}{\hbar}S[\psi]\big\}. \tag{2.44}$$

The action (2.43) is quadratic in spinor fields, therefore, we can perform the functional integral for the anti-commuting variables $d\bar{\psi}d\psi$:

$$\int d\bar{\psi}d\psi\exp\big\{\frac{i}{\hbar}\bar{\psi}\Big(i\gamma^\mu\partial_\mu - M_F(\phi)\Big)\psi\big\} = \det\Big[i\gamma^\mu\partial_\mu - M_F(\phi)\Big] = \exp\Big\{\mathrm{Tr}\log\Big(i\gamma^\mu\partial_\mu - M_F(\phi)\Big)\Big\}. \tag{2.45}$$

We write the trace as:

$$\begin{aligned}\mathrm{Tr}\log\Big(i\gamma^\mu\partial_\mu - M_F(\phi)\Big) &= \int d^4x\langle x|\mathrm{tr}\log\Big(i\gamma^\mu\partial_\mu - M_F(\phi)\Big)|x\rangle = \\ &= \int d^4x\int\frac{d^4k}{(2\pi)^4}\mathrm{tr}\log\Big(\not{k} - M_F(\phi)\Big),\end{aligned} \tag{2.46}$$

where tr is taken over the gamma matrices. Next, we use:

$$\det A = \exp\big\{\mathrm{tr}\log A\big\} \quad \Rightarrow \quad \mathrm{tr}\log A = \log\det A, \tag{2.47}$$

and the cyclic property of the determinant, inserting $\gamma^5\gamma^5 = \mathbb{1}$:

$$\begin{aligned}\mathrm{tr}\log\Big(\not{k} - M_F(\phi)\Big) &= \log\det\left[\gamma^5\Big(\not{k} - M_F(\phi)\Big)\gamma^5\right] = \log\det\Big(-\not{k} - M_F(\phi)\Big) = \\ &= \log\det(-1) + \log\det\Big(\not{k} + M_F(\phi)\Big) = \mathrm{tr}\log\Big(\not{k} + M_F(\phi)\Big) + \mathrm{tr}\log(-1),\end{aligned} \tag{2.48}$$

$$
\begin{aligned}
\operatorname{tr}\log\Big(\not{k}-M_F(\phi)\Big) =& \frac{1}{2}\Bigg[\operatorname{tr}\log\Big(\not{k}-M_F(\phi)\Big)+\operatorname{tr}\log\Big(\not{k}-M_F(\phi)\Big)\Bigg] = \\
=& \frac{1}{2}\Bigg[\operatorname{tr}\log\Big(\not{k}-M_F(\phi)\Big)+\operatorname{tr}\log\Big(\not{k}+M_F(\phi)\Big)+\operatorname{tr}\log(-1)\Bigg] = \\
=& \frac{1}{2}\operatorname{tr}\log\Big(-k^2+M_F(\phi)^2\Big) = 2\log\Big(-k^2+M_F(\phi)^2\Big).
\end{aligned}
\tag{2.49}
$$

We are left with:

$$
\exp\Big\{\frac{i}{\hbar}W_F[J]\Big\} = \exp\Big\{2\int d^4x\int\frac{d^4k}{(2\pi)^4}\log\Bigg[\frac{k^2-M_F(\phi)^2}{k^2}\Bigg]\Big\},
\tag{2.50}
$$

where we inserted field independent $\log(-k^2)$ to make the argument of logarithm dimensionless. Therefore, fermions contribute to the effective action as:

$$
\Gamma_F[\phi_c] = -2i\hbar\int d^4x\int\frac{d^4k}{(2\pi)^4}\log\Bigg[\frac{k^2-M_F(\phi_c)^2}{k^2}\Bigg],
\tag{2.51}
$$

giving in the effective potential:

$$
V_{eff}(\phi_c) = 2i\hbar\int\frac{d^4k}{(2\pi)^4}\log\Bigg[\frac{k^2-M_F(\phi_c)^2}{k^2}\Bigg]+\mathcal{O}(\hbar^2).
\tag{2.52}
$$

Finally, we do Wick's rotation, neglect the field independent term, and set $\hbar = 1$, so the one-loop contribution to the effective potential for fermions is:

$$
V_1(\phi_c) = (-4)\cdot\frac{1}{2}\int\frac{k_E^4}{(2\pi)^4}\log\Big[k_E^2+M_F^2(\phi_c)\Big].
\tag{2.53}
$$

The result differs from (2.42) by a factor -4, where 4 comes from the trace over gamma matrices and corresponds to the number of degrees of freedom of a fermion and -1 accounts for fermionic loop calculation.

2.4. Gauge Bosons

Now, we consider a theory described by the action of a gauge boson field with the R_ξ gauge-fixing term:

$$
S[A_\mu^a] = \int d^4x\Bigg(-\frac{1}{4}F_{\mu\nu}^aF^{a\mu\nu}+\frac{1}{2}g^{\mu\nu}M_{GB}^2(\phi_c)A_\mu^aA_\nu^a-\frac{1}{2\xi}\Big(\partial^\mu A_\mu^a\Big)\Big(\partial_\nu A_\nu^a\Big)+\mathcal{L}_{ghost}\Bigg),
\tag{2.54}
$$

where $F_{\mu\nu}^a = \partial_\mu A_\nu^a - \partial_\nu A_\mu^a - g\cdot f^{abc}A_\mu^bA_\nu^c$ and $M_{GB}^2(\phi_c)$ is the scalar interaction giving the gauge boson its mass term (e.g., $M_{GB}^2(\phi_c) = g^2\phi^2$) [2]. The form of the ghost's Lagrangian, which emerges due to the gauge fixing in Faddeev-Popov procedure, is of no interest in the pure gauge boson contribution to the effective potential (for more details see e.g., [51]: Appendix C.3). To find an inverse propagator, we need the part of the action that is quadratic in A_μ^a fields. One has:

$$
\Big(S[A_\mu^a]\Big)_{A^2\text{ terms}} = \int d^4x\frac{1}{2}A_\mu^a\Bigg[g^{\mu\nu}\partial^2+\Big(1-\frac{1}{\xi}\Big)\overleftarrow{\partial}^\mu\partial^\nu+g^{\mu\nu}M_{GB}^2(\phi_c)\Bigg]A_\nu^a,
\tag{2.55}
$$

[2] Of course, a scalar field coupled to a gauge field must be charged and therefore complex. Since we are interested only in gauge-bosons contribution to the effective potential, we consider the ϕ field as the real part of the full complex scalar field.

where the $\overleftarrow{\partial}^\mu$ operator acts to the left. The functional integral is:

$$\begin{aligned}
&\int dA \exp\left\{\frac{i}{\hbar}\int d^4x \frac{1}{2} A^a_\mu \left[g^{\mu\nu}\partial^2 + \Big(1-\frac{1}{\xi}\Big)\overleftarrow{\partial}^\mu\partial^\nu + g^{\mu\nu}M^2_{GB}(\phi_c)\right] A^a_\nu\right\} = \\
&= \det\left[g^{\mu\nu}\partial^2 + \Big(1-\frac{1}{\xi}\Big)\overleftarrow{\partial}^\mu\partial^\nu + g^{\mu\nu}M^2_{GB}(\phi_c)\right]^{-\frac{1}{2}} = \det\left[\mathcal{D}^{-1}\right]^{-\frac{1}{2}}.
\end{aligned} \tag{2.56}$$

Using the same methods as before, we get:

$$\det\left[\mathcal{D}^{-1}\right]^{-\frac{1}{2}} = \exp\Big\{-\frac{1}{2}\mathrm{Tr}\log\left[\mathcal{D}^{-1}\right]\Big\}. \tag{2.57}$$

$$\begin{aligned}
&\mathrm{Tr}\log\left[g^{\mu\nu}\partial^2 + \Big(1-\frac{1}{\xi}\Big)\overleftarrow{\partial}^\mu\partial^\nu + g^{\mu\nu}M^2_{GB}(\phi_c)\right] = \\
&= \int d^4x \int \frac{d^4k}{(2\pi)^4}\mathrm{tr}\log\left[g^{\mu\nu}\big(-k^2 + M^2_{GB}(\phi_c)\big) + \Big(1-\frac{1}{\xi}\Big)k_\mu k_\nu\right] = \\
&= \int d^4x \int \frac{d^4k}{(2\pi)^4}\log\det\left[g^{\mu\nu}\big(-k^2 + M^2_{GB}(\phi_c)\big) + \Big(1-\frac{1}{\xi}\Big)k_\mu k_\nu\right],
\end{aligned} \tag{2.58}$$

where (2.47) was used and the trace is over $\mu\nu$ indices. Evaluating the determinant yields:

$$\exp\big\{\frac{i}{\hbar}W_{GB}[J]\big\} = \exp\big\{-\frac{1}{2}\int d^4x \int \frac{d^4k}{(2\pi)^4}\Big(3\log\left[-k^2+M^2_{GB}(\phi_c)\right]+\log\left[k^2-\xi M^2_{GB}(\phi_c)\right]+\dots\Big)\big\}, \tag{2.59}$$

where $+\dots$ are constant terms, irrelevant for the effective potential. The $\log\left[k^2 - \xi M^2_{GB}(\phi_c)\right]$ cancels out due to the ghosts and would-be-Goldstone bosons contributions [51], and the effective action reads:

$$\Gamma_{GB}[\phi_c] = \frac{i\hbar}{2}\int d^4x \int \frac{d^4k}{(2\pi)^4}\Big(3\log\left[-k^2 + M^2_{GB}(\phi_c)\right]\Big). \tag{2.60}$$

Finally, after Wick's rotation, the effective potential reads:

$$V_1(\phi_c) = 3\cdot\frac{1}{2}\int \frac{d^4k_E}{(2\pi)^4}\log\left[k_E^2 + M^2_{GB}(\phi_c)\right]. \tag{2.61}$$

The result differs from (2.42) by a factor of 3, which accounts for the number of degrees of freedom of a vector gauge boson in $d = 4$ dimensions. In arbitrary d dimensions, this factor is equal to $n_{GB} = d - 1$ and will affect the form of the renormalized potential in dimensional regularization.

Chapter 3

Quantum Scale Symmetry

The integrals (2.42), (2.53) and (2.61) are divergent in $d = 4$ dimensions. To evaluate them, we need to specify which form of regularization we want to apply. In this work, we employ the dimensional regularization (DR). The conventional DR introduces the so-called subtraction parameter μ, which has the dimension of mass. The couplings, which enter the Lagrangian, are infinite bare parameters (λ_B), and the renormalized, physical couplings are finite (λ_R). The theory is continued analytically from $d = 4$ to $d = 4 - 2\epsilon$ dimensions. The subtraction parameter relates the bare couplings of the theory to the physically measurable quantities. For example, in ϕ^4 theory, the quartic coupling λ_B has a dimension 2ϵ and is related to dimensionless λ_R as:

$$\lambda_B = \mu^{2\epsilon}\Big[\lambda_R + \sum_{n=1}^{\infty}\frac{a_n}{\epsilon^n}\Big]. \tag{3.1}$$

The power n corresponds to the loop expansion so that for 1-loop effective potential, the sequence ends at $n = 1$. The a_n parameters are found using the renormalization conditions. The one-loop effective potential, to have a proper mass dimension, has a form:

$$V_1(\phi_c) = \mu^{4-d}V(\phi_c) + \frac{1}{2}\mu^{4-d}\sum_i n_i \int \frac{d^d k_E}{(2\pi)^d}\log\big[k_E^2 + M_i^2(\phi_c)\big], \tag{3.2}$$

where n_i are the factors appropriate for the contributions of particular particles. The one-loop effective potential $V_1(\phi_c)$ contains divergent terms as $\epsilon \to 0$. These divergences are canceled by the counterterms $\delta V_{c.t.}$, the form of which depends on the renormalization conditions and renormalization scheme.

In this chapter, we will analyze the behavior of the scalar, fermion, and gauge boson contributions to the one-loop effective potential, derived in the previous chapter, in two regimes: $\mu = const$ breaking the scale symmetry, and $\mu = \mu(\phi_i)$ preserving it. We will observe the differences in these two prescriptions, specifically, that the scale-invariant procedure introduces new finite corrections that are absent in the $\mu = const$ regime.

3.1. Breaking of the Scale Invariance at the Quantum Level

In this section, we consider the usual DR prescription with just a constant mass scale as a subtraction parameter. The divergent integrals (2.42), (2.53) and (2.61) are regularized in DR as follows:

$$\int \frac{d^4 k_E}{(2\pi)^4}\log\big[k_E^2 + M^2(\phi_c)\big] \xrightarrow{d=4-2\epsilon} \mu^{4-d}\int \frac{d^d k_E}{(2\pi)^d}\log\big[k_E^2 + M^2(\phi_c)\big]. \tag{3.3}$$

The above integral gives the standard result [52]:

$$\int \frac{d^d k_E}{(2\pi)^d}\log\big[k_E^2 + M^2(\phi_c)\big] = \frac{1}{(4\pi)^{\frac{d}{2}}}\frac{2}{d}\Gamma\Big(1 - \frac{d}{2}\Big)\mathrm{Tr}\big(M^2(\phi_c)\big)^{\frac{d}{2}}, \tag{3.4}$$

where $\Gamma(x) = (x-1)!$ is the Gamma function. Scalar and fermion contributions to the one-loop effective potential have the form:

$$V_1(\phi_c) = \mu^{4-d}\left[V(\phi_c) + \frac{1}{2}\sum_i n_i \int \frac{d^d k_E}{(2\pi)^d} \log\left[k_E^2 + M_i^2(\phi_c)\right]\right], \tag{3.5}$$

with constant n_i coefficients. Taking limit $\epsilon \to 0$ and keeping only divergent and finite non-zero terms, we get:

$$V_1(\phi_c) = V(\phi_c) + \frac{1}{64\pi^2}\sum_i n_i \cdot \mathrm{Tr}\big(M_i^2(\phi_c)\big)^2\left[\frac{1}{\epsilon} + \log\left[\frac{\mathrm{Tr}\big(M_i^2(\phi_c)\big)}{\kappa\cdot\mu^2}\right]\right], \qquad \kappa = 4\pi e^{\frac{3}{2}-\gamma}. \tag{3.6}$$

The gauge boson case is a bit different since the factor $n_{GB} = (d-1) = 3 - 2\epsilon$ in front of the integral will change the result slightly. The difference is in the κ factor, namely, for gauge bosons one gets $\kappa = 4\pi e^{\frac{5}{2}-\gamma}$. Finally, in the mass eigenbasis, we have:

$$V_1(\phi_c) = V(\phi_c) + \frac{1}{64\pi^2}\sum_i n_i \cdot M_i^4(\phi_c)\left[\frac{1}{\epsilon} + \log\left[\frac{M_i^2(\phi_c)}{\kappa\cdot\mu^2}\right]\right], \quad \kappa = \begin{cases} 4\pi e^{\frac{3}{2}-\gamma} & \text{scalars, fermions} \\ 4\pi e^{\frac{5}{2}-\gamma} & \text{gauge bosons}\end{cases} \tag{3.7}$$

where we sum over all particles present in the theory with field-dependent masses $M_i(\phi_c)$ and the number of degrees of freedom:

$$n_i = (-1)^{2s_i} Q_i C_i (2s_i + 1), \tag{3.8}$$

where s_i is the spin of the particle i, $Q_i = 1$ for neutral and $Q_i = 2$ for charged particles and C_i counts the number of colors of the particle i.

3.2. Scale Symmetric Effective Potential

We want to consider a scale symmetric theory at the quantum level. The concept of scale-invariant regularization was originally proposed in [53, 54]. To prevent $\mu = const$ from explicitly breaking the scale symmetry, one uses the subtraction function $\mu = \mu(\phi_0)$, which depends on the scalar field ϕ_0 present in the model. When this field acquires a vacuum expectation value $\langle\phi_0\rangle$, the subtraction scale is generated dynamically as $\mu(\langle\phi_0\rangle)$. This choice affects the outcome of the renormalized one-loop effective potential, as previously explored in [21–25, 31, 55]. Here, we briefly review those results and compare them to the usual $\mu = const$ method.

Consider a theory with a scalar dilaton field (denoted by ϕ_0) and real scalar fields ϕ_i, with a classical Lagrangian in $d = 4$ dimensions:

$$\mathcal{L} = \frac{1}{2}\sum_k \partial_\mu\phi_k\partial^\mu\phi_k - V(\phi_k), \qquad k = \{0, i\}. \tag{3.9}$$

The theory is scale-invariant in $d = 4$ dimensions if the potential satisfies the condition:

$$\left(4 - \Delta_\phi \phi_k \frac{\partial}{\partial\phi_k}\right) V(\phi_k) = 0, \tag{3.10}$$

where Δ_ϕ is the scaling dimension of the scalar field, determining how it transforms under the scale transformations given by:

$$\begin{aligned} x^\mu &\longmapsto x'^\mu = s x^\mu, \qquad s \in \mathbb{R}^+ \\ \phi(x) &\longmapsto \phi'(x) = s^{-\Delta_\phi}\phi(s^{-1}x). \end{aligned} \tag{3.11}$$

In $d = 4$ dimensions, $\Delta_\phi = \frac{d-2}{2} \xrightarrow{d=4} 1$. The condition (3.10) reflects the fact that the potential $V(\phi_k)$ has no dimensionful parameters and depends only on even power of fields, summing up to $d = 4$, for instance:

$$V(\phi_0, \phi_1) \propto \lambda_0 \phi_0^4 + \lambda_1 \phi_0^2 \phi_1^2 + \lambda_2 \phi_1^4 + \lambda_3 \phi_0^{-2} \phi_1^6 + \dots \tag{3.12}$$

The particular form of the potential in the model considered in this work will be specified later. Now, we emphasize that non-polynomial operators such as $\phi_0^{-2}\phi_1^6$ are scale-invariant and can be present in the potential, making it non-renormalizable. Further chapters will elaborate on this subject in more detail.

Now, we analytically continue the theory to $d = 4 - 2\epsilon$ dimensions. The mass dimensions read $[\mathcal{L}] = d$, $[\phi_k] = (d-2)/2 = 1 - \epsilon$, and the couplings are replaced by $\lambda \to \mu(\phi_0)^{2\epsilon}\lambda$, so that they remain dimensionless and the subtraction function is field dependent. This modifies the potential to $V(\phi_k) \to \tilde{V}(\phi_k) \equiv \mu(\phi_0)^{2\epsilon} V(\phi_k)$, with mass dimensions $[\tilde{V}] = d$, $[V] = 2d - 4$. Consequently, the scale-invariant tree level Lagrangian in d dimensions reads:

$$\tilde{\mathcal{L}} = \frac{1}{2} \sum_k \partial_\mu \phi_k \partial^\mu \phi_k - \tilde{V}(\phi_k), \qquad k = \{0, i\}, \qquad \tilde{V}(\phi_k) \equiv \mu(\phi_0)^{2\epsilon} V(\phi_k). \tag{3.13}$$

In this work, the subtraction function μ is chosen to be a function of the ϕ_0 dilaton field only. Specifically:

$$\mu(\phi_0)^{4-d} = \mu(\phi_0)^{2\epsilon} = \left[z \cdot \phi_0^{\frac{1}{1-\epsilon}} \right]^{2\epsilon}, \tag{3.14}$$

where z is an arbitrary dimensionless scaling parameter, defining the subtraction scale after the spontaneous breaking of scale symmetry as $\mu(\langle \phi_0 \rangle) = z \langle \phi_0 \rangle$. This will be relevant in the renormalization group equations and Callan-Symanzik equation, as quantities will be differentiated with respect to z [55]. While alternative choices for μ are possible, they are considered non-physical [23]. Consequently, the subtraction scale is generated by the dilaton alone and has a mass dimension $[\mu(\phi_0)] = [z \cdot \phi_0^{\frac{1}{1-\epsilon}}] = [\phi_0] \cdot \frac{1}{1-\epsilon} = (1-\epsilon) \cdot \frac{1}{1-\epsilon} = 1$ (this holds in any spacetime dimensions d).

To dynamically generate the subtraction scale, the dilaton must be a dynamical field with a non-zero vev. Therefore, the kinetic term for ϕ_0 is necessary, which is important in the analysis in Chapter 5. Usually, considering the origin of the dilaton from Weyl geometry, the kinetic term for ϕ_0 is absent (see, e.g., [9–11]). The possible mechanism for $\langle \phi_0 \rangle$ generation is explored in Chapter 8, where temperature corrections and gravity are added to the model.

First, we focus only on the scalar one-loop contribution, then we generalize to other fields. The prescription for the one-loop effective potential described in Chapter 2 must be applied with some caution. Firstly, the mass matrix under the logarithm must be changed to:

$$\tilde{M}^2_{ab} = \partial^2 \tilde{V} / \partial \phi_a \partial \phi_b, \tag{3.15}$$

as it is the $\tilde{V}(\phi_k)$ that enters the Lagrangian and is used in the expansion of the action $S[\phi_k]$. Secondly, it is unnecessary to include a μ^{4-d} factor in front of the integral since the dimension of potential $[\tilde{V}] = d$ matches $[d^d k_E] = d$. Therefore, the quantum effective potential for real scalar fields ϕ_i and the dilaton ϕ_0 reads:

$$V_1(\phi_k) = \left[z \cdot \phi_0^{\frac{1}{1-\epsilon}} \right]^{2\epsilon} V(\phi_k) + \frac{1}{2} \int \frac{d^d k_E}{(2\pi)^d} \log \left[k_E^2 + \tilde{M}^2(\phi_k) \right], \tag{3.16}$$

which results in:

$$V_1(\phi_k) = \left[z \cdot \phi_0^{\frac{1}{1-\epsilon}} \right]^{2\epsilon} V(\phi_k) + \frac{1}{2} \sum_i \frac{\Gamma\Big(\epsilon - 1\Big)}{(4\pi)^{\epsilon-1} (2-\epsilon)} \mathrm{Tr} \Bigg(\tilde{M}^2(\phi_k) \Bigg)^{2-\epsilon}. \tag{3.17}$$

Keeping only divergent and finite non-zero terms in the limit $\epsilon \to 0$, one obtains:

$$V_1(\phi_k) = V(\phi_k) + \frac{1}{64\pi^2}\mathrm{Tr}\big(\tilde{M}^2(\phi_k)\big)^2\left[\frac{1}{\epsilon} + \log\left[\frac{\mathrm{Tr}\big(\tilde{M}^2(\phi_k)\big)}{\kappa\cdot\mu^2}\right]\right], \qquad \kappa = 4\pi e^{\frac{3}{2}-\gamma}. \tag{3.18}$$

Since the μ is a field-dependent function, the mass matrix in the scale symmetric regime is non-trivial:

$$\tilde{M}^2_{ab} = \frac{\partial^2\tilde{V}(\phi_k)}{\partial\phi_a\partial\phi_b} = \mu^{2\epsilon}\left[M^2_{ab} + \frac{2\epsilon}{\mu^2}\Big(\big(\mu\mu_{ab} - \mu_a\mu_b\big)V + \mu\big(\mu_a V_b + \mu_b V_a\big)\Big)\right] + \mathcal{O}(\epsilon^2), \tag{3.19}$$

where the subscripts on μ and V denote derivatives, $\hat{O}_a = \partial\hat{O}/\partial\phi_a$. For the dilaton dependent function (3.14), the above expression simplifies to:

$$\tilde{M}^2_{ab} = \mu^{2\epsilon}\left[M^2_{ab} + \delta^0_a\delta^0_b\frac{2\epsilon}{\mu^2}\Big(\big(\mu\mu_{00} - \mu_0^2\big)V + 2\mu\mu_0 V_0\Big)\right] + \mathcal{O}(\epsilon^2). \tag{3.20}$$

The trace under the logarithm in $\epsilon \to 0$ limit yields just:

$$\log\left[\frac{\mathrm{Tr}\big(\tilde{M}^2(\phi_k)\big)}{\kappa\cdot\mu^2}\right] \xrightarrow{\epsilon\to 0} \log\left[\frac{\mathrm{Tr}\big(M^2(\phi_k)\big)}{\kappa\cdot\mu^2}\right]. \tag{3.21}$$

The $\mathrm{Tr}\big(\tilde{M}^2(\phi_k)\big)^2$ term, however, is multiplied by a factor $1/\epsilon$. Consequently, one gets a new finite correction, due to the presence of the ϵ proportional term in $\tilde{M}^2$, which is absent in the dimensional regularization with $\mu = const$:

$$\begin{aligned}\mathrm{Tr}\big(\tilde{M}^2(\phi_k)\big)^2\cdot\frac{1}{\epsilon} \quad \xrightarrow{\epsilon\to 0} \quad & \mathrm{Tr}\big(M^2(\phi_k)\big)^2\cdot\frac{1}{\epsilon} + \\ & + \frac{4\mathrm{Tr}\big(M^2(\phi_k)\big)}{\mu^2}\cdot\Big(\big(\mu\mu_{00} - \mu_0^2\big)V + 2\mu\mu_0 V_0\Big).\end{aligned} \tag{3.22}$$

Finally, the scale-invariant one-loop effective potential with scalar contributions in the mass eigenbasis reads:

$$V_1(\phi_k) = V(\phi_k) + \frac{1}{64\pi^2}\sum_i M_i^4(\phi_k)\left[\frac{1}{\epsilon} + \log\left[\frac{M_i^2(\phi_k)}{\kappa\cdot\mu^2}\right]\right] + \frac{1}{64\pi^2}\delta V_1, \qquad \kappa = 4\pi e^{\frac{3}{2}-\gamma}, \tag{3.23}$$

$$\delta V_1 = \frac{4}{\mu^2}\sum_i M_i^2(\phi_k)\cdot\Big(\big(\mu\mu_{00} - \mu_0^2\big)V + 2\mu\mu_0 V_0\Big), \tag{3.24}$$

where $M_i^2(\phi_k)$ are the eigenvalues of the tree-level mass matrix.

To generalize the above result to a theory with fermions and gauge bosons, let us first study the example scale-invariant mass terms in d dimensions[1]:

$$\tilde{\mathcal{L}}_{mass} \propto \tilde{m}^2_{GB}(\phi_k)A_\mu A^\mu - \tilde{m}_f(\phi_k)\bar{f}_L f_R, \tag{3.25}$$

where the field-dependent masses are:

$$\tilde{m}^2_{GB}(\phi_k) = \mu(\phi_0)^{2\epsilon}\cdot m^2_{GB}(\phi_k), \qquad \tilde{m}_f(\phi_k) = \mu(\phi_0)^{\epsilon}\cdot m_f(\phi_k). \tag{3.26}$$

[1] Actually, the scale-invariant dimensional regularization procedure for gauge bosons requires more caution to ensure that the gauge symmetry is not spoiled. However, this subject is beyond the scope of this work and does not affect the result for gauge boson one-loop contributions to the effective potential. For more details, we refer the reader to [26, 27].

Due to the change in coupling constants $\lambda \to \mu^{2\epsilon}\lambda$, the masses change to $m^2(\phi_k) \to \tilde{m}^2(\phi_k) = \mu^{2\epsilon}m^2(\phi_k)$. Notice that the inclusion of the μ factor to the proper power preserves the dimension of the mass parameter: in $d = 4$ dimensions $[m(\phi_k)] = 1$, and in $d = 4 - 2\epsilon$ dimensions $[\tilde{m}(\phi_k)] = 1$. In contrast to the scalar fields case, as in (3.19) and (3.20), the fermions and gauge bosons do not acquire ϵ-proportional corrections to their masses. Consequently, their contributions to the one-loop effective potential are the same as in the $\mu = const$ case, except we change the subtraction scale to its scale-symmetric counterpart $\mu(\phi_0)$ under the logarithms in the Coleman-Weinberg potential. Finally, one obtains the one-loop effective potential in the mass eigenbasis:

$$V_1(\phi_k) = V(\phi_k) + \frac{1}{64\pi^2}\sum_i n_i M_i^4(\phi_k)\left[\frac{1}{\epsilon} + \log\left[\frac{M_i^2(\phi_k)}{\kappa \cdot \mu(\phi_0)^2}\right]\right] + \frac{1}{64\pi^2}\delta V_1,$$
$$\text{where } \kappa = \begin{cases} 4\pi e^{\frac{3}{2}-\gamma} & \text{scalars, fermions} \\ 4\pi e^{\frac{5}{2}-\gamma} & \text{gauge bosons} \end{cases}. \tag{3.27}$$

We sum over all particles present in the theory with field-dependent masses $M_i(\phi_k)$ and the number of degrees of freedom n_i given in equation (3.8). The new contribution δV_1 comes from the scalar sector only and is given in equation (3.24).

3.3. Conclusions

The one-loop effective potential (3.27) is scale symmetric. While it is not yet renormalized, the renormalization procedure will not change the conclusion that scale-invariance is preserved at the quantum level due to the field-dependent subtraction function $\mu(\phi_0)$. This will be demonstrated in the analysis of a scale-invariant Standard Model in Chapter 5. The new finite contribution δV_1 comes solely from the scalar sector and appears as a result of a scale-symmetric, dynamical variant of μ. This contribution leads to non-polynomial operators suppressed by higher powers of the dilaton, such as $\frac{\phi_1^6}{\phi_0^2}, \frac{\phi_1^8}{\phi_0^4}, \ldots$. Although these operators maintain scale symmetry, they imply the non-renormalizability of the theory. The above conclusions are valid at the one-loop level. For a detailed discussion on higher-loop effects, see [24, 26, 28].

Chapter 4

Weyl Conformal Geometry

Proposed in 1918, Weyl conformal geometry [56, 57] was an attempt to describe electromagnetism as a geometrical property of spacetime, similar to gravity in Einstein's theory. Weyl's conformal geometry consists of Riemannian geometry equipped with an additional massless vector gauge field ω_μ. Weyl proposed that after parallel transport of a vector, not only its direction is changed but also its length, and in Weyl geometry $\tilde{\nabla}_\mu g_{\alpha\beta} = -q\omega_\mu g_{\alpha\beta}$. As a consequence, there's no absolute way to compare lengths in space-time, and a standard ruler needs to be defined. Because of this issue and the fact that electromagnetism is considered an internal property rather than a spacetime one, Weyl's conformal theory was criticized by Einstein and other physicists and forgotten for a time. Later, Dirac in 1973 [58] proposed a new approach to Weyl's theory, and it started to be reconsidered as Weyl's conformal gravity. In this revised theory, the gauge vector field ω_μ becomes massive (m_{ω_μ} close to Planck mass M_P) and it decouples for energies below that scale, thus Einstein general relativity can be considered as the low energy limit of Weyl conformal gravity. The decoupling occurs after the spontaneous breaking of Weyl conformal symmetry via the Stueckelberg mechanism. Since physicists lack detailed knowledge of the Universe's conditions at energies $E > M_P$, Weyl conformal gravity may play an important role in early cosmology and theories of inflation [1–4, 6, 12, 21].

We will explore the foundational properties of Weyl's conformal geometry to construct an action invariant under conformal Weyl transformations. Through this discussion, we will arrive at a very important conclusion: Einstein's gravity emerges as a low energy limit of Weyl gravity. Furthermore, the Weyl Ricci scalar squared term $\tilde{R}^2$ is the source of an additional scalar, the dilaton. This new sector, originating from Weyl conformal gravity, can be coupled to the Higgs doublet, and its vacuum expectation value will generate mass scales, particularly the Higgs mass and Planck mass. The material presented in this chapter is not novel and has been previously analyzed in [9–20, 59, 60]. Here, we briefly review the essential information for our subsequent analysis.

4.1. Weyl Conformal Geometry

The main difference between Riemannian gravity and Weyl gravity is the presence of the Weyl gauge vector field ω_μ. Weyl quantities will be denoted with a tilde. The Weyl connection represented by $\tilde{\Gamma}^\rho_{\mu\nu}$ is expressed as follows[1]:

$$\tilde{\Gamma}^\rho_{\mu\nu} = \Gamma^\rho_{\mu\nu} + \frac{q}{2}\Big[\delta^\rho_\mu \omega_\nu + \delta^\rho_\nu \omega_\mu - g_{\mu\nu}\omega^\rho\Big], \tag{4.1}$$

where $\Gamma^\rho_{\mu\nu}$ denotes the Riemannian connection given by:

$$\Gamma^\rho_{\mu\nu} = \frac{1}{2} g^{\rho\alpha}\big[\partial_\nu g_{\alpha\mu} + \partial_\mu g_{\alpha\nu} - \partial_\alpha g_{\mu\nu}\big], \tag{4.2}$$

[1] We adopt the metric convention $(+,-,-,-)$ with $g = |\det g_{\mu\nu}| > 0$.

and q is the gauge coupling between ω_μ and a scalar field, emerging from a covariant derivative to be shown later. The system is torsion free, i.e. $\tilde{\Gamma}^\rho_{\mu\nu} = \tilde{\Gamma}^\rho_{\nu\mu}$. Notably, if we take the limit $\omega_\mu \to 0$, Riemannian geometry is restored, resulting in $\tilde{\Gamma}^\rho_{\mu\nu} \to \Gamma^\rho_{\mu\nu}$. In contrast to Riemannian geometry, where $\nabla_\mu g_{\alpha\beta} = 0$, the Weyl covariant derivative of the metric is non-zero:

$$\begin{aligned}\tilde{\nabla}_\mu g_{\alpha\beta} =& \partial_\mu g_{\alpha\beta} - \tilde{\Gamma}^\sigma_{\mu\alpha} g_{\sigma\beta} - \tilde{\Gamma}^\sigma_{\mu\beta} g_{\alpha\sigma} = \nabla_\mu g_{\alpha\beta} - \frac{q}{2}\Big[g_{\mu\beta}\omega_\alpha + g_{\alpha\beta}\omega_\mu - g_{\mu\alpha}\omega_\beta\Big] - \\ &- \frac{q}{2}\Big[g_{\mu\alpha}\omega_\beta + g_{\alpha\beta}\omega_\mu - g_{\mu\beta}\omega_\alpha\Big] = -q\omega_\mu g_{\alpha\beta} \neq 0.\end{aligned} \tag{4.3}$$

Therefore, in Weyl geometry, parallel transport along a closed curve of a vector changes its direction (as in Einstein's gravity framework) and its length.

With (4.1), the Riemann tensor in Weyl geometry takes the form:

$$\tilde{R}^\rho_{\mu\nu\sigma} = \partial_\nu \tilde{\Gamma}^\rho_{\mu\sigma} - \partial_\sigma \tilde{\Gamma}^\rho_{\mu\nu} + \tilde{\Gamma}^\rho_{\nu\lambda}\tilde{\Gamma}^\lambda_{\mu\sigma} - \tilde{\Gamma}^\rho_{\sigma\lambda}\tilde{\Gamma}^\lambda_{\mu\nu}. \tag{4.4}$$

Then Ricci tensor is $\tilde{R}_{\mu\sigma} = \tilde{R}^\rho_{\mu\rho\sigma}$, and Ricci scalar $\tilde{R} = g^{\mu\nu}\tilde{R}_{\mu\nu}$ reads:

$$\tilde{R} = R - 3q\nabla_\mu\omega^\mu - \frac{3}{2}q^2\omega_\mu\omega^\mu, \tag{4.5}$$

where R is Ricci scalar in Riemannian geometry, and similarly, $\nabla_\mu\omega_\alpha = \partial_\mu\omega_\alpha - \Gamma^\sigma_{\mu\alpha}\omega_\sigma$. Weyl gauge vector field ω_μ is abelian. Consequently, the field strength tensor $\tilde{F}_{\mu\nu}$ corresponding to ω_μ is equal to the Riemannian counterpart:

$$\tilde{F}_{\mu\nu} = \tilde{\nabla}_\mu\omega_\nu - \tilde{\nabla}_\nu\omega_\mu = \partial_\mu\omega_\nu - \partial_\nu\omega_\mu = F_{\mu\nu}, \tag{4.6}$$

where $\tilde{\nabla}_\mu$ is the covariant derivative with connection $\tilde{\Gamma}^\sigma_{\mu\nu}$:

$$\tilde{\nabla}_\mu\omega_\nu = \partial_\mu\omega_\nu - \tilde{\Gamma}^\sigma_{\mu\nu}\omega_\sigma = \partial_\mu\omega_\nu - \Gamma^\sigma_{\mu\nu}\omega_\sigma - \frac{q}{2}\Big[\delta^\sigma_\mu\omega_\nu + \delta^\sigma_\nu\omega_\mu - g_{\mu\nu}\omega^\sigma\Big]\omega_\sigma. \tag{4.7}$$

We aim to construct a Lagrangian invariant under local Weyl gauge conformal transformations. For the metric $g_{\mu\nu}$, scalar field ϕ, fermion field ψ and Weyl vector field ω_μ, these are:

$$\begin{aligned} g_{\mu\nu} \quad &\longrightarrow \quad g'_{\mu\nu} = \Omega^2 g_{\mu\nu}, \\ \phi \quad &\longrightarrow \quad \phi' = \frac{\phi}{\Omega}, \\ \psi \quad &\longrightarrow \quad \psi' = \frac{\psi}{\Omega^{3/2}}, \\ \omega_\mu \quad &\longrightarrow \quad \omega'_\mu = \omega_\mu - \frac{1}{q}\partial_\mu \ln\Omega^2, \end{aligned} \tag{4.8}$$

where Ω is a dimensionless real parameter that, in general can be field-dependent. Consequently, we obtain $g'^{\mu\nu} = \Omega^{-2}g^{\mu\nu}$ and $\sqrt{g'} = \Omega^4\sqrt{g}$. Unlike the Riemannian connection $\Gamma^\sigma_{\mu\nu}$, the Weyl geometry connection $\tilde{\Gamma}^\sigma_{\mu\nu}$ is invariant under (4.8). The Weyl curvature transforms as $\tilde{R}' = \Omega^{-2}\tilde{R}$, while the Weyl field strength remains unchanged $\tilde{F}'_{\mu\nu} = \tilde{F}_{\mu\nu}$.

4.2. Stueckelberg Breaking of Weyl Conformal Geometry

4.2.1. Weyl Quadratic Gravity

First, we will consider the theory of Weyl quadratic gravity with gauge vector field ω_μ in the absence of matter. The Lagrangian for Weyl quadratic gravity invariant under (4.8) is given by[2]:

$$\frac{\mathcal{L}_\omega}{\sqrt{g}} = \frac{\xi_0}{4!}\tilde{R}^2 - \frac{1}{4}\tilde{F}_{\mu\nu}\tilde{F}^{\mu\nu}, \tag{4.10}$$

where $\xi_0 > 0$. The inclusion of the $\tilde{R}^2$ term introduces an additional scalar state, so we can express this term equivalently as:

$$\tilde{R}^2 \quad \rightarrow \quad -2\phi_0^2\tilde{R} - \phi_0^4. \tag{4.11}$$

Solving the equation of motion for ϕ_0 yields $\phi_0^2 = -\tilde{R}$, and recovers the Weyl quadratic gravity term. Consequently, we can consider an equivalent Lagrangian, invariant under (4.8), of the form:

$$\frac{\mathcal{L}_\omega}{\sqrt{g}} = -\frac{\xi_0}{12}\phi_0^2\tilde{R} - \frac{1}{4}\tilde{F}_{\mu\nu}\tilde{F}^{\mu\nu} - \frac{\xi_0}{4!}\phi_0^4. \tag{4.12}$$

The above Lagrangian includes a massless scalar field ϕ_0, referred to as the dilaton[3], with quartic interaction, and a massless vector field ω_μ present in $\tilde{R}$ and $\tilde{F}_{\mu\nu}$ terms. We choose $\Omega^2 = \xi_0\phi_0^2/6M^2$ in the conformal transformation (4.8), effectively gauge fixing ϕ_0 field to a constant:

$$\phi_0'^2 = \frac{\phi_0^2}{\Omega^2} = \frac{6M^2}{\xi_0}. \tag{4.13}$$

Finally, the Lagrangian (4.12) becomes (up to a total derivative term):

$$\frac{\mathcal{L}'_\omega}{\sqrt{g'}} = -\frac{1}{2}M^2\tilde{R}' - \frac{1}{4}\tilde{F}_{\mu\nu}\tilde{F}^{\mu\nu} - \frac{3}{2}\frac{M^4}{\xi_0} = -\frac{1}{2}M^2R' + \frac{3q^2}{4}M^2\omega_\mu\omega^\mu - \frac{1}{4}\tilde{F}_{\mu\nu}\tilde{F}^{\mu\nu} - \frac{3}{2}\frac{M^4}{\xi_0}, \tag{4.14}$$

where (4.5) was used. R' is the Riemannian curvature scalar after the transformation (4.8). The Weyl vector field became massive via the Stueckelberg mechanism with $m_\omega^2 = \frac{3}{2}q^2M^2$. Since the term $-\frac{1}{2}M^2R'$ represents the Einstein-Hilbert term in (4.14), M aligns with the Planck mass scale M_P. Consequently, the Planck mass scale is naturally generated after the breaking of the Weyl conformal symmetry. These phenomena, unachievable within Riemannian gravity, offer a solution to the hierarchy problem and the origin of mass scales in physics.

The Lagrangian (4.14) represents the Einstein-Proca action for the Weyl gauge field with a positive cosmological constant term. It is worth highlighting the conservation of the number of degrees of freedom in the presented mechanism. Initially, we had a massless vector and a scalar field, resulting in $n_{d.o.f.} = 3$. Following the gauge symmetry transformation, we are left with only one massive vector field, maintaining $n_{d.o.f.} = 3$. This arises from the absorption of the dilaton mode ϕ_0 by the vector field ω_μ. Without ω_μ, the conservation of degrees of freedom wouldn't be possible. For a coupling q not too small (see: Section 6.3), the mass of the Weyl vector field is close to the Planck mass. Below this scale, ω_μ decouples, and the entire theory transitions to a Riemannian framework. Consequently, Einstein's gravity emerges as the low-energy limit of Weyl gravity.

4.2.2. Matter Fields

Matter fields couple to the Weyl gauge vector field via a covariant derivative, the form of which depends on the specific type of field under consideration. Each type of field F has an associated

[2]The original Weyl Lagrangian contains also the Weyl-tensor term:

$$\mathcal{L}_{Weyl} \sim -\frac{1}{\eta^2}\tilde{C}^2_{\mu\nu\rho\sigma}, \qquad \tilde{C}^2_{\mu\nu\rho\sigma} = C^2_{\mu\nu\rho\sigma} + \frac{3}{2}q^2\tilde{F}^2_{\mu\nu} \tag{4.9}$$

and is invariant under (4.8). However, this term is not relevant to the analysis of this work and was not included in (4.10).

[3]Specifically, the real dilaton being $\ln\phi_0^2$ with shift symmetry: $\ln\phi_0^2 \rightarrow \ln\phi_0^2 - \ln\Omega$. However, for simplicity, we refer to ϕ_0 field as the dilaton in this work, as it will remain approximately massless.

conformal weight w, which determines its behavior under conformal transformation (4.8), i.e., we have:

$$F \to F' = \Omega^w F, \qquad w_{scalar} = -1, \quad w_{fermion} = -\frac{3}{2}, \quad w_{gauge} = 0. \tag{4.15}$$

Then, the gauge covariant derivative for conformal transformations involving the Weyl vector field ω_μ has the form:

$$\tilde{D}_\mu F = \big(\partial_\mu + w \cdot \frac{q}{2}\omega_\mu\big)F. \tag{4.16}$$

Since $\omega'_\mu = \omega_\mu - \frac{1}{q}\partial_\mu \ln \Omega^2$, the $\tilde{D}_\mu F$ transforms as:

$$\tilde{D}'_\mu F' = \big(\partial_\mu + w \cdot \frac{q}{2}\omega'_\mu\big)F' = \Omega^w \tilde{D}_\mu F. \tag{4.17}$$

Gauge Bosons

Let's consider a general case of a non-Abelian gauge vector field A^a_μ, where a is an internal index from the Lie algebra of the gauge group. In the Riemannian geometry, the field strength for A^a_μ is expressed as:

$$F^a_{\mu\nu} = \nabla_\mu A^a_\nu - \nabla_\nu A^a_\mu + g f^{abc} A^b_\mu A^c_\nu, \tag{4.18}$$

where g is the gauge coupling constant, f^{abc} are the structure constants and ∇_μ is evaluated with the Riemannian Levi-Civita torsion-free connection $\Gamma^\rho_{\mu\nu} = \Gamma^\rho_{\nu\mu}$. For any torsion-free connection, the above expression reduces to:

$$F^a_{\mu\nu} = \partial_\mu A^a_\nu - \partial_\nu A^a_\mu + g f^{abc} A^b_\mu A^c_\nu. \tag{4.19}$$

Extending to the Weyl conformal geometry, one just changes the $\nabla_\mu \to \tilde{\nabla}_\mu$ with Weyl connection $\tilde{\Gamma}^\rho_{\mu\nu}$:

$$\tilde{F}^a_{\mu\nu} = \tilde{\nabla}_\mu A^a_\nu - \tilde{\nabla}_\nu A^a_\mu + g f^{abc} A^b_\mu A^c_\nu. \tag{4.20}$$

Since $\tilde{\Gamma}^\rho_{\mu\nu}$ is torsion-free, this reduces to $F^a_{\mu\nu}$ from equation (4.19). Hence, there is no direct coupling of the gauge bosons and the Weyl vector field.

Gauge bosons remain invariant under (4.8). To understand this, let's consider a field F with a conformal weight w, charged under a gauge symmetry represented by the group G with the gauge boson A_μ[4]. The covariant derivative respecting conformal symmetry (4.8) for the F field is:

$$\tilde{D}_\mu F = \Big(\partial_\mu - igA_\mu + w \cdot \frac{q}{2}\omega_\mu\Big)F. \tag{4.21}$$

The gauge field A_μ transforms according to its G group, while ω_μ accounts for the conformal transformation. The coordinates and ∂_μ remain unaffected by G and (4.8). Therefore, the kinetic terms for gauge bosons and their inclusion in covariant derivatives are not affected by the (4.8) symmetry.

Fermions

Fermionic sector coupled to gravity requires introduction of a tetrad e^a_μ and a spin connection w^{ab}_μ:

$$e^a_\mu e^b_\nu \eta_{ab} = g_{\mu\nu}, \qquad w^{ab}_\mu = w^{ab}_\mu = e^{\rho b}(-\partial_\mu e^a_\rho + e^a_\nu \Gamma^\nu_{\mu\rho}), \tag{4.22}$$

where η_{ab} is the Minkowski metric $diag(+,-,-,-)$. The covariant derivative for fermions in the Riemannian case is:

$$D_\mu \psi = \Big(\partial_\mu + \frac{1}{2}w^{ab}_\mu \sigma_{ab}\Big)\psi, \qquad \sigma_{ab} = \frac{1}{4}[\gamma_a, \gamma_b], \tag{4.23}$$

[4]Whether the group G is Abelian or non-Abelian doesn't matter in this context.

with antisymmetric gamma matrices fulfilling $\{\gamma^a, \gamma^b\} = 2\eta^{ab}$. The Lagrangian for a massless Dirac fermion reads:

$$\frac{\mathcal{L}_f}{\sqrt{g}} = \bar{\psi} i \gamma^a e_a^\mu D_\mu \psi. \tag{4.24}$$

Generalization to Weyl geometry is straightforward:

$$w_\mu^{ab} \to \tilde{w}_\mu^{ab} = e^{\rho b}(-\partial_\mu e_\rho^a + e_\nu^a \tilde{\Gamma}^\nu_{\mu\rho}) = w_\mu^{ab} + \frac{q}{2}\big(e_\mu^a e^{\nu b} - e_\mu^b e^{\nu a}\big)\omega_\nu, \tag{4.25}$$

and with (4.16), one obtains a Weyl covariant derivative for the fermionic field:

$$\tilde{D}_\mu \psi = \Big(\partial_\mu + \frac{1}{2}\tilde{\omega}_\mu^{ab}\sigma_{ab} - \frac{3}{4} q \omega_\mu\Big)\psi. \tag{4.26}$$

The Lagrangian invariant under (4.8) has the following form:

$$\frac{\tilde{\mathcal{L}}_f}{\sqrt{g}} = \bar{\psi} i \gamma^a e_a^\mu \tilde{D}_\mu \psi, \tag{4.27}$$

where tetrad transforms as $e_\mu^{\prime a} \to \Omega e_\mu^a$ and $\tilde{w}_\mu^{ab}$ is invariant under (4.8). We will show that Lagrangians (4.24) and (4.27) are equal and, as a consequence, the fermions do not couple to ω_μ vector field.

All terms involving ω_μ field in the Lagrangian (4.27) are:

$$\left(\frac{\tilde{\mathcal{L}}_f}{\sqrt{g}}\right)_\omega \sim \bar{\psi} i \gamma^c e_c^\mu \left[\frac{1}{2}\cdot\frac{q}{2}\big(e_\mu^a e^{\nu b} - e_\mu^b e^{\nu a}\big)\omega_\nu \sigma_{ab} - \frac{3}{4} q \omega_\mu\right]\psi. \tag{4.28}$$

We have:

$$\begin{aligned}
&\gamma^c e_c^\mu \frac{q}{4}\big(e_\mu^a e^{\nu b} - e_\mu^b e^{\nu a}\big)\omega_\nu \sigma_{ab} = \frac{q}{4}\gamma^c\big(\eta_c^a e^{\nu b} - \eta_c^b e^{\nu a}\big)\omega_\nu \cdot \frac{1}{4}[\gamma_a, \gamma_b] = \\
&= \frac{q}{16}\big(\gamma^a e^{\nu b} - \gamma^b e^{\nu a}\big)\omega_\nu [\gamma_a, \gamma_b] = \frac{q}{8}\big(\gamma^a e^{\nu b} - \gamma^b e^{\nu a}\big)\omega_\nu \cdot 2\gamma_a\gamma_b\Big|_{a\neq b} = \frac{3}{4} q \gamma_b e^{\nu b}\omega_\nu,
\end{aligned} \tag{4.29}$$

where $e_a^\mu e_\mu^b = \eta_a^b$ was used and $\gamma^b\gamma_b\gamma_a\Big|_{b\neq a} = 3\gamma_a$. The above result cancels out the $-\frac{3}{4}q\omega_\mu$ factor from the covariant derivative in (4.28). Consequently, Lagrangians (4.24) and (4.27) are equivalent, and the Weyl gauge vector field ω_μ doesn't couple to fermions.

Scalar Fields

Terms permitted by the symmetry (4.8) for a scalar coupled to a Weyl vector ω_μ are the covariant derivative $\tilde{D}_\mu \phi_i$ and a non-minimal coupling term $\xi_i \phi_i^2 \tilde{R}$. The Lagrangian for a scalar field ϕ_i that remains invariant under conformal transformations is given by:

$$\frac{\mathcal{L}_s}{\sqrt{g}} = -\frac{\xi_i}{12}\phi_i^2 \tilde{R} + \frac{1}{2}\tilde{D}_\mu \phi_i \tilde{D}^\mu \phi_i - V(\phi_i), \tag{4.30}$$

where $\tilde{R}$ is defined in (4.5), and the covariant derivative, according to (4.16), is:

$$\tilde{D}_\mu \phi_i = \big(\partial_\mu - \frac{q}{2}\omega_\mu\big)\phi_i. \tag{4.31}$$

To ensure invariance under conformal transformations, the potential $V(\phi_i)$ must be a homogeneous function of degree four in the scalar fields ϕ_i:

$$V(\phi_i) = \phi_k^4 V\left(\frac{\phi_i}{\phi_k}\right). \tag{4.32}$$

One can expand $\tilde{R}$ and $\tilde{D}_\mu\phi_i$ terms to explicitly see the ω_μ interactions:

$$\begin{aligned}
\frac{\mathcal{L}_s}{\sqrt{g}} \sim &-\frac{\xi_i}{12}\phi_i^2 R + \frac{q}{4}\big[\xi_i\phi_i^2\big]\nabla_\mu\omega^\mu + \frac{q^2}{8}\big[(\xi_i+1)\phi_i^2\big]\omega_\mu\omega^\mu - \frac{q}{4}(\partial_\mu\phi_i^2)\omega^\mu + \frac{1}{2}(\partial_\mu\phi_i)(\partial^\mu\phi_i) = \\
= &-\frac{\xi_i}{12}\phi_i^2 R + \frac{q^2}{8}\big[(\xi_i+1)\phi_i^2\big]\omega_\mu\omega^\mu - \frac{q}{4}\partial_\mu\big[(\xi_i+1)\phi_i^2\big]\omega^\mu + \frac{1}{2}(\partial_\mu\phi_i)(\partial^\mu\phi_i) = \\
= &-\frac{\xi_i}{12}\phi_i^2 R + \frac{q^2}{8}K\omega_\mu\omega^\mu - \frac{q}{4}K_\mu\omega^\mu + \frac{1}{2}(\partial_\mu\phi_i)(\partial^\mu\phi_i),
\end{aligned} \tag{4.33}$$

where we defined:

$$K = (\xi_i+1)\phi_i^2, \qquad K_\mu = \partial_\mu K. \tag{4.34}$$

To obtain the second line of (4.33), one needs to integrate by parts:

$$\partial_\mu\big(\sqrt{g}\phi_i^2\omega^\mu\big) = \sqrt{g}\phi_i^2\left[\frac{1}{2}g^{\alpha\beta}\partial_\mu g_{\alpha\beta}\omega^\mu + \partial_\mu\omega^\mu + \frac{\partial_\mu\phi_i^2}{\phi_i^2}\omega^\mu\right] = \sqrt{g}\phi_i^2\left[\nabla_\mu\omega^\mu + \frac{\partial_\mu\phi_i^2}{\phi_i^2}\omega^\mu\right], \tag{4.35}$$

where the $\partial_\mu g = g g^{\alpha\beta}\partial_\mu g_{\alpha\beta}$ relation was used, and:

$$\nabla_\mu\omega^\mu = \frac{1}{\sqrt{g}}\partial_\mu\big(\sqrt{g}\omega^\mu\big) = \partial_\mu\omega^\mu + \frac{1}{2}g^{\alpha\beta}\partial_\mu g_{\alpha\beta}\omega^\mu. \tag{4.36}$$

The complete Lagrangian describing a scalar field ϕ_i and the Weyl vector ω_μ, invariant under conformal transformations (4.8), is given by:

$$\frac{\mathcal{L}_s}{\sqrt{g}} = -\frac{\xi_i}{12}\phi_i^2 R + \frac{q^2}{8}K\omega_\mu\omega^\mu - \frac{q}{4}K_\mu\omega^\mu + \frac{1}{2}(\partial_\mu\phi_i)(\partial^\mu\phi_i) - V(\phi_i). \tag{4.37}$$

Here, $-\frac{\xi_i}{12}\phi_i^2 R$ represents the non-minimal coupling term for ϕ^2, where R denotes the Riemannian Ricci scalar. In a subsequent section, we will demonstrate that by including the Lagrangian for the Weyl vector field (4.10), this term contributes to the generation of the Planck mass, resulting in the Einstein-Hilbert term $-\frac{1}{2}M_P^2 R$. The Lagrangian (4.37) includes both a mass term for the ω_μ field and a derivative coupling to the scalar field. Additionally, we will show that upon gauge fixing with an appropriate choice of Ω^2, the generalization of the mixing K_μ term is "eaten" by the ω_μ field, leaving only the mass term.

4.3. Higgs Scalar Sector and Weyl Quadratic Gravity

This section explores an extension of the Standard Model coupled to Weyl geometry. We focus on the Higgs sector, specifically the neutral Higgs component ϕ_1, interacting with the Weyl vector field ω_μ. The Lagrangian invariant under conformal transformations (4.8) is:

$$\frac{\mathcal{L}}{\sqrt{g}} = -\frac{1}{4}\tilde{F}_{\mu\nu}\tilde{F}^{\mu\nu} + \frac{\xi_0}{4!}\tilde{R}^2 - \frac{\xi_1}{12}\phi_1^2\tilde{R} + \frac{1}{2}\tilde{D}_\mu\phi_1\tilde{D}^\mu\phi_1 - \frac{\lambda}{4!}\phi_1^4. \tag{4.38}$$

We proceed by applying a substitution: $\tilde{R}^2 \to -2\phi_0^2\tilde{R} - \phi_0^4$ (where ϕ_0 satisfies its equation of motion, $\phi_0^2 = -\tilde{R}$, restoring the original Lagrangian). This leads to:

$$\frac{\mathcal{L}}{\sqrt{g}} = -\frac{1}{4}\tilde{F}_{\mu\nu}\tilde{F}^{\mu\nu} - \frac{\xi_0}{12}\phi_0^2\tilde{R} - \frac{\xi_1}{12}\phi_1^2\tilde{R} + \frac{1}{2}\tilde{D}_\mu\phi_1\tilde{D}^\mu\phi_1 - \frac{\lambda}{4!}\phi_1^4 - \frac{\xi_0}{4!}\phi_0^4. \tag{4.39}$$

To explicitly see the ω_μ and scalars interaction, one expands the $\tilde{R}$ and $\tilde{D}_\mu\phi_1$ terms, performing the same calculations as in equations (4.33), (4.35), (4.36):

$$\begin{aligned}
\frac{\mathcal{L}}{\sqrt{g}} \sim &-\frac{1}{12}\rho^2 R + \frac{q}{4}\rho^2\nabla_\mu\omega^\mu + \frac{q^2}{8}K\omega_\mu\omega^\mu - \frac{q}{4}\big(\partial_\mu\phi_1^2\big)\omega^\mu + \frac{1}{2}\big(\partial_\mu\phi_1\big)\big(\partial^\mu\phi_1\big) = \\
&-\frac{1}{12}\rho^2 R + \frac{q^2}{8}K\omega_\mu\omega^\mu - \frac{q}{4}K_\mu\omega^\mu + \frac{1}{2}\big(\partial_\mu\phi_1\big)\big(\partial^\mu\phi_1\big),
\end{aligned} \tag{4.40}$$

where we defined:

$$\rho^2 = \xi_0\phi_0^2 + \xi_1\phi_1^2, \qquad K = \xi_0\phi_0^2 + (\xi_1 + 1)\phi_1^2 = \rho^2 + \phi_1^2, \qquad K_\mu = \partial_\mu K. \tag{4.41}$$

We fix the gauge with the choice of Ω as:

$$\Omega^2 = \frac{\xi_0\phi_0^2 + \xi_1\phi_1^2}{6M^2} = \frac{\rho^2}{6M^2} \quad \Rightarrow \quad \rho'^2 = \frac{\rho^2}{\Omega^2} = 6M^2, \qquad K' = \frac{K}{\Omega^2} = \frac{\rho^2 + \phi_1^2}{\rho^2}6M^2 = \phi_1'^2 + 6M^2. \tag{4.42}$$

Following the conformal transformation (4.8) and expanding $\tilde{R}'$ using (4.5) with integration by parts, we transform the Lagrangian (4.39) to:

$$\frac{\mathcal{L}'}{\sqrt{g'}} = -\frac{1}{4}\tilde{F}'_{\mu\nu}\tilde{F}'^{\mu\nu} - \frac{1}{2}M^2 R + \frac{3}{4}q^2 M^2 \omega'_\mu \omega'^\mu + \frac{1}{2}\tilde{D}'_\mu\phi'_1\tilde{D}'^\mu\phi'_1 - V'(\phi'_1). \tag{4.43}$$

The potential transforms according to:

$$\begin{aligned} V(\phi_1, \rho) &= \frac{\lambda}{4!}\phi_1^4 + \frac{1}{24\xi_0}\left(\rho^2 - \xi_1\phi_1^2\right)^2 \to V'(\phi'_1) \\ V'(\phi'_1) &= \frac{\lambda}{4!}\phi_1'^4 + \frac{1}{24\xi_0}\left(6M^2 - \xi_1\phi_1'^2\right)^2 = \frac{1}{4!}\Big(\lambda + \frac{\xi_1^2}{\xi_0}\Big)\phi_1'^4 - \frac{1}{2}M^2\frac{\xi_1}{\xi_0}\phi_1'^2 + \frac{3}{2}\frac{M^4}{\xi_0}. \end{aligned} \tag{4.44}$$

The Weyl vector field acquires a mass term by absorbing the radial mode ρ^2. We identify the mass scale M with the Planck mass M_P, as the non-minimal term, $-\frac{1}{12}\rho^2 R$, became the Einstein-Hilbert term, $-\frac{1}{2}M^2 R$. However, the derivative coupling $\omega_\mu\partial^\mu\phi'_1$ remains within the kinetic term $\frac{1}{2}\tilde{D}'_\mu\phi'_1\tilde{D}'^\mu\phi'_1$. To achieve the canonical kinetic term for the scalar field, a further field redefinition is introduced:

$$\hat{\omega}_\mu = \omega'_\mu - \frac{1}{q}\partial_\mu \ln\left(\phi_1'^2 + 6M_P^2\right) = \omega'_\mu - \frac{1}{q}\partial_\mu \ln K', \qquad \phi'_1 = \sqrt{6}M_P \sinh\Big(\frac{\sigma}{\sqrt{6}M_P}\Big). \tag{4.45}$$

With this redefinition, the Lagrangian becomes:

$$\frac{\mathcal{L}'}{\sqrt{g'}} = -\frac{1}{4}\hat{F}_{\mu\nu}\hat{F}^{\mu\nu} - \frac{1}{2}M_P^2 R + \frac{3}{4}q^2 M_P^2 \cosh^2\Big(\frac{\sigma}{\sqrt{6}M_P}\Big)\hat{\omega}_\mu\hat{\omega}^\mu + \frac{1}{2}\partial_\mu\sigma\partial^\mu\sigma - V'(\sigma). \tag{4.46}$$

Here, $\hat{\omega}_\mu$ represents the redefined Weyl vector field with the field strength $\hat{F}_{\mu\nu} = \partial_\mu\hat{\omega}_\nu - \partial_\nu\hat{\omega}_\mu$. The transformed potential for the scalar σ is:

$$V'(\sigma) = \frac{1}{4!}\Big(\lambda + \frac{\xi_1^2}{\xi_0}\Big)\sinh^4\Big(\frac{\sigma}{\sqrt{6}M_P}\Big) - \frac{1}{2}M_P^2\frac{\xi_1}{\xi_0}\sinh^2\Big(\frac{\sigma}{\sqrt{6}M_P}\Big) + \frac{3}{2}\frac{M_P^4}{\xi_0}. \tag{4.47}$$

The mass term for the redefined Weyl vector field $\hat{\omega}_\mu$ in the transformed Lagrangian depends on the scalar field σ. In the limit where $\sigma \ll M_P$, we can expand this term:

$$\frac{3}{4}q^2 M_P^2 \cosh^2\Big(\frac{\sigma}{\sqrt{6}M_P}\Big)\hat{\omega}_\mu\hat{\omega}^\mu = \frac{3}{4}q^2 M_P^2\hat{\omega}_\mu\hat{\omega}^\mu + \frac{q^2}{8}\sigma^2\hat{\omega}_\mu\hat{\omega}^\mu + \mathcal{O}(M_P^{-2}), \tag{4.48}$$

where $\mathcal{O}(M_P^{-2})$ terms are negligible. The expansion of the mass term reveals two key aspects of the Weyl vector boson's behavior. Firstly, the leading coupling $\frac{q^2}{8}\sigma^2\hat{\omega}_\mu\hat{\omega}^\mu$, describes the only interaction between the ω_μ and the scalar σ (which is related to the Higgs field) and therefore the only relevant coupling to the Standard Model. Secondly, the Weyl vector boson acquires a mass proportional to the Planck mass:

$$m_\omega^2 = \frac{3}{2}q^2 M_P^2\Big(1 + \frac{\langle\sigma^2\rangle}{6M_P^2}\Big), \tag{4.49}$$

where the Higgs vev correction arising after the electroweak spontaneous symmetry breaking is negligible. Effectively, for energies below the M_P scale, the Weyl vector decouples from the theory, and the description of spacetime becomes well-approximated by Riemannian geometry, which is the standard framework used in General Relativity. It's important to note that the transformation preserves the total number of degrees of freedom. Initially, we had a massless vector boson ω_μ and two massless real scalars ϕ_0, ϕ_1 (total: $n_{d.o.f.} = 2 + 1 + 1 = 4$). After the transformation, we have a massive vector boson $\hat{\omega}_\mu$ and a massless real scalar σ (total: $n_{d.o.f.} = 3 + 1 = 4$).

The next chapter explores the possibility of the dilaton field being dynamical, which is necessary to generate the subtraction scale $\mu(\langle\phi_0\rangle)$, as described in Chapter 3. We will investigate the potential coupling between the dilaton field and the Higgs scalar field and its implications for the theory. In particular, we will demonstrate that in this scenario, the mass of the Weyl vector remains proportional to the Planck mass, M_P. Consequently, for energies significantly lower than M_P, the theory can effectively be described by Riemannian geometry.

Chapter 5

Scale Symmetric Standard Model

In this chapter, we examine the theory of the Higgs scalar sector coupled with Weyl conformal gravity and the dilaton field. We investigate the Stueckelberg mechanism, in which the Weyl vector field ω_μ becomes massive, to understand the theory's behavior in the low-energy limit (after the decoupling of ω_μ). Then, we describe the properties arising from the scale-symmetric tree-level potential and determine the mass scales of the theory, outlining the possible parameter space. We finish with a comprehensive analysis of the quantum scale-invariant renormalization procedure of the model, including the beta functions and the renormalization group (RG) improvement of the potential. A similar analysis focused on Standard Model renormalization can be found in [22, 27, 31].

First, we provide the basic structure of the classical Lagrangian in the considered theory. The Lagrangian for the Standard Model in Weyl conformal geometry, invariant under (4.8) and $SU(2)_L \times U(1)_Y$ gauge group, is given by:

$$\mathcal{L} = \mathcal{L}_{g.b.} + \mathcal{L}_{\Phi-\phi_0} + \mathcal{L}_\psi. \tag{5.1}$$

The $\mathcal{L}_{g.b.}$ term includes the kinetic terms (field strengths) for the gauge bosons of the Standard Model:

$$\frac{\mathcal{L}_{g.b.}}{\sqrt{g}} = -\frac{1}{4}\Big(\partial_\mu A^a_\nu - \partial_\nu A^a_\mu + g_2 \varepsilon^{abc} A^b_\mu A^c_\nu\Big)^2 - \frac{1}{4}\Big(\partial_\mu B_\nu - \partial_\nu B_\mu\Big)^2, \tag{5.2}$$

where A^a_μ and B_μ are gauge bosons of strong and weak interactions, whose mixtures will become the massive W^+, W^- and Z^0 bosons. The $SU(2)_L$ Higgs doublet is given by:

$$\Phi = \frac{1}{\sqrt{2}} \begin{pmatrix} G_1 + iG_2 \\ \phi_1 + v + iG_3 \end{pmatrix}, \tag{5.3}$$

where ϕ_1 is the Higgs field, v is its vacuum expectation value, and G_1, G_2, and G_3 are Goldstone bosons associated with the three spontaneously broken generators of the $SU(2)_L \times U(1)_Y$ gauge group. After the Electroweak symmetry breaking, these Goldstone bosons are "eaten" by the W^+, W^-, and Z^0 bosons, which as a consequence, acquire mass generated by the Higgs vacuum expectation value.

The Lagrangian for Φ and dilaton ϕ_0 is:

$$\frac{\mathcal{L}_{\Phi-\phi_0}}{\sqrt{g}} = -\frac{1}{12}\xi_0 \phi_0^2 \tilde{R} - \frac{1}{12}\xi_1 \phi_1^2 \tilde{R} + \big(\tilde{D}_{\Phi\mu}\Phi\big)^\dagger \big(\tilde{D}^\mu_\Phi \Phi\big) + \frac{1}{2}\tilde{D}_\mu \phi_0 \tilde{D}^\mu \phi_0 - V(\Phi, \phi_0), \tag{5.4}$$

with the covariant derivatives defined as:

$$\tilde{D}_{\Phi\mu}\Phi = \Big[\partial_\mu + i g_2 \tau^a A^a_\mu + i g_1 Y_\Phi B_\mu - \frac{q}{2}\omega_\mu\Big]\Phi, \tag{5.5}$$

$$\tilde{D}_\mu \phi_0 = \Big[\partial_\mu - \frac{q}{2}\omega_\mu\Big]\phi_0. \tag{5.6}$$

Here, $\tau^a = \frac{\sigma^a}{2}$ are the $SU(2)_L$ Pauli matrices, and g_1 and g_2 are the couplings of the weak $U(1)_Y$ and strong $SU(2)_L$ gauge interactions respectively[1]. The charges for the Higgs doublet are $Y = \frac{1}{2}$ and $Q = \frac{\tau^3}{2} + Y$. The scale-invariant tree-level potential for the Higgs and dilaton is:

$$V(\Phi, \phi_0) = \lambda_0 \phi_0^2 + 2\lambda_1 \big(\Phi^\dagger \Phi\big) \phi_0^2 + 4\lambda_2 \big(\Phi^\dagger \Phi\big)^4, \tag{5.8}$$

which for the Higgs neutral component ϕ_1 gives:

$$V(\phi_1, \phi_0) = \lambda_0 \phi_0^4 + \lambda_1 \phi_0^2 \phi_1^2 + \lambda_2 \phi_1^4. \tag{5.9}$$

In the fermionic Lagrangian, we include only the top quark, which gives the leading fermionic contribution at the quantum level:

$$\frac{\mathcal{L}_\psi}{\sqrt{g}} = \overline{Q}_L i\gamma^a e_a^\mu D_\mu Q_L + \bar{t}_R i\gamma^a e_a^\mu D_\mu t_R + \Big(- y_t \overline{Q}_L \tilde{\Phi} t_R + h.c.\Big), \tag{5.10}$$

where:

$$Q_L = \begin{pmatrix} t_L \\ b_L \end{pmatrix}, \qquad \tilde{\Phi} = i\tau^2 \Phi = \frac{1}{\sqrt{2}} \begin{pmatrix} \phi_1 + iG_3 \\ -G1 - iG2 \end{pmatrix}, \tag{5.11}$$

and the top quark mass is $m_t^2(\phi_1) = \frac{y_t^2}{2}\phi_1^2$. The mass terms for gauge bosons arising from (5.4) are:

$$\frac{\mathcal{L}_{g.b.mass}}{\sqrt{g}} = \frac{g_2^2}{4} W_\mu^+ W^{-\mu} \phi_1^2 + \frac{1}{8}(g_1^2 + g_2^2) Z_\mu^0 Z^{0\mu} \phi_1^2 = m_W^2(\phi_1) W_\mu^+ W^{-\mu} + \frac{1}{2} m_Z^2(\phi_1) Z_\mu^0 Z^{0\mu}. \tag{5.12}$$

5.1. Scale Symmetric Higgs Scalar Sector

In this section, we will demonstrate that the theory with the kinetic term for the dilaton field ϕ_0, emerging from the $\tilde{R}^2$ term in Weyl quadratic gravity, coupled to the Higgs neutral component, can be considered as embedded in regular Riemannian geometry for mass scales lower than the Planck mass. As discussed earlier in Chapter 3, the presence of the kinetic term for the dilaton is essential, as this field is responsible for the generation of mass scales in the presented model (the subtraction scale $\mu(\langle \phi_0 \rangle)$ in particular) and, therefore, must be dynamical. Using the tools introduced in Chapter 4, we begin with the following Lagrangian:

$$\frac{\mathcal{L}}{\sqrt{g}} = -\frac{1}{12}\Big(\xi_0 \phi_0^2 + \xi_1 \phi_1^2\Big)\tilde{R} - \frac{1}{4}\tilde{F}_{\mu\nu}\tilde{F}^{\mu\nu} + \frac{1}{2}\tilde{D}_\mu \phi_0 \tilde{D}^\mu \phi_0 + \frac{1}{2}\tilde{D}_\mu \phi_1 \tilde{D}^\mu \phi_1 - V(\phi_0, \phi_1), \tag{5.13}$$

invariant under Weyl conformal transformations (4.8). One can expand the covariant derivatives $\tilde{D}_i \phi_i$ and the Weyl scalar $\tilde{R}$, and obtain, up to a total derivative:

$$\frac{\mathcal{L}}{\sqrt{g}} = -\frac{1}{12}\rho^2 R - \frac{q}{4} K_\mu \omega^\mu + \frac{q^2}{8} K \omega_\mu \omega^\mu + \frac{1}{2}\partial_\mu \phi_0 \partial^\mu \phi_0 + \frac{1}{2}\partial_\mu \phi_1 \partial^\mu \phi_1 - \frac{1}{4}\tilde{F}_{\mu\nu}\tilde{F}^{\mu\nu} - V(\phi_0, \phi_1), \tag{5.14}$$

where:

$$\rho^2 = \xi_0 \phi_0^2 + \xi_1 \phi_1^2, \tag{5.15}$$

$$K = \rho^2 + \phi_0^2 + \phi_1^2 = (\xi_0 + 1)\phi_0^2 + (\xi_1 + 1)\phi_1^2, \qquad K_\mu = \partial_\mu K. \tag{5.16}$$

[1] The gauge transformations for the Higgs doublet are:

$$\begin{aligned} SU(2)_L: &\qquad \Phi \to e^{-i\theta^a(x)\tau^a}\Phi \\ U(1)_Y: &\qquad \Phi \to e^{-i\omega(x)Y_\Phi}\Phi. \end{aligned} \tag{5.7}$$

We fix the scale symmetry gauge of (5.13), with:

$$\Omega^2 = \frac{\rho^2}{6M^2} = \frac{\xi_0\phi_0^2 + \xi_1\phi_1^2}{6M^2}, \qquad \rho'^2 = \frac{\rho^2}{\Omega^2} = 6M^2. \tag{5.17}$$

The (5.13) Lagrangian becomes:

$$\frac{\mathcal{L}'}{\sqrt{g'}} = -\frac{1}{2}M^2R' - \frac{1}{4}\tilde{F}'_{\mu\nu}\tilde{F}'^{\mu\nu} + \frac{3}{4}q^2M^2\omega'_\mu\omega'^\mu + \frac{1}{2}\tilde{D}'_\mu\phi'_0\tilde{D}'^\mu\phi'_0 + \frac{1}{2}\tilde{D}'_\mu\phi'_1\tilde{D}'^\mu\phi'_1 - V'(\phi'_0, \phi'_1), \tag{5.18}$$

where the $\tilde{R}'$ has been expanded, and the integration by parts was performed. Let's take a careful look at the $\tilde{D}'_\mu\phi_i$ and $\omega'_\mu\omega'^\mu$ terms:

$$\frac{\mathcal{L}'}{\sqrt{g'}} \supset \frac{q^2}{8}\Big[6M^2 + \phi_0'^2 + \phi_1'^2\Big]\omega'_\mu\omega'^\mu + \frac{1}{2}\Big[\partial_\mu\phi'_0\partial^\mu\phi'_0 + \partial_\mu\phi'_1\partial^\mu\phi'_1\Big] - \frac{q}{4}\omega'_\mu\partial^\mu\Big[\phi_0'^2 + \phi_1'^2\Big]. \tag{5.19}$$

The derivative coupling $\omega'_\mu\partial^\mu(\phi_0'^2 + \phi_1'^2)$ needs to be removed. Therefore, we introduce new variables:

$$\hat{\omega}_\mu = \omega'_\mu - \frac{1}{q}\partial_\mu \ln\Big[6M^2 + \phi_0'^2 + \phi_1'^2\Big] = \omega'_\mu - \frac{1}{q}\partial_\mu \ln K', \tag{5.20}$$

$$\tan\theta = \frac{\phi'_0}{\phi'_1}, \qquad \phi_0'^2 + \phi_1'^2 = 6M^2\sinh^2\frac{\sigma}{\sqrt{6}M}, \tag{5.21}$$

where $K' = K/\Omega^2 =$, with K defined in (5.16). The (5.18) Lagrangian becomes:

$$\frac{\hat{\mathcal{L}}}{\sqrt{g'}} = -\frac{1}{2}M^2R - \frac{1}{4}\hat{\tilde{F}}_{\mu\nu}\hat{\tilde{F}}^{\mu\nu} + \frac{1}{2}m^2_{\hat{\omega}}(\sigma)\hat{\omega}_\mu\hat{\omega}^\mu + 3M^2\sinh^2\frac{\sigma}{\sqrt{6}M}\partial_\mu\theta\partial^\mu\theta + \frac{1}{2}\partial_\mu\sigma\partial^\mu\sigma - V(\sigma,\theta), \tag{5.22}$$

with the $\hat{\omega}_\mu$ mass:

$$m^2_{\hat{\omega}}(\sigma) = \frac{3}{2}q^2M^2\cosh^2\frac{\sigma}{\sqrt{6}M}, \tag{5.23}$$

and the potential:

$$V(\sigma,\theta) = 36M^4\cos^4\theta\sinh^4\frac{\sigma}{\sqrt{6}M}\Big[\lambda_2 + \lambda_1\tan^2\theta + \lambda_0\tan^4\theta\Big]. \tag{5.24}$$

Both fields ω'_μ and $\hat{\omega}_\mu$ have masses proportional to qM:

$$m^2_{\omega'} = \frac{3}{2}q^2M^2, \qquad m^2_{\hat{\omega}}(\sigma) = \frac{3}{2}q^2M^2\cosh^2\frac{\sigma}{\sqrt{6}M}. \tag{5.25}$$

For q not too small (see Section 6.3), both masses are greater than the M scale, which is associated with the Planck mass scale M_P. Consequently, the ω_μ vector boson decouples for energies below M_P. Therefore, in further analysis, we can consider a theory within Riemannian geometry only.

The M appearing in the definition of Ω^2 in equation (5.17) is an arbitrary mass parameter. We choose it as $M^2 = \xi_0\langle\phi_0^2\rangle + \xi_1\langle\phi_1^2\rangle$. Consequently, the mechanism of fixing a gauge and breaking the scale symmetry happens when fields acquire their vacuum expectation values. The ρ^2 mass scale transforms to:

$$\rho^2 = \xi_0\phi_0^2 + \xi_1\phi_1^2 \quad \xrightarrow{\text{gauge fixing}} \quad \rho'^2 = \frac{\rho^2}{\Omega^2} = 6M^2 = \xi_0\langle\phi_0^2\rangle + \xi_1\langle\phi_1^2\rangle, \tag{5.26}$$

and the Planck mass is generated as:

$$M_P^2 = \frac{1}{6}\Big[\xi_0\langle\phi_0^2\rangle + \xi_1\langle\phi_1^2\rangle\Big]. \tag{5.27}$$

5.2. Scale Symmetric Higgs Potential

As we showed in the previous section, for energies below the Planck mass scale, the Weyl vector boson decouples, and the geometry becomes Riemannian. Since this is the case for energies that are considered in the evolution of the hot Universe (as $E \gtrsim M_{Pl}$, one enters the quantum gravity era), in this section, we consider the Lagrangian (5.13), without the ω_μ field. The theory is described by:

$$\frac{\mathcal{L}}{\sqrt{g}} = -\frac{1}{12}\Big(\xi_0\phi_0^2 + \xi_1\phi_1^2\Big)R + \frac{1}{2}\partial_\mu\phi_0\partial^\mu\phi_0 + \frac{1}{2}\partial_\mu\phi_1\partial^\mu\phi_1 - V(\phi_0, \phi_1), \tag{5.28}$$

where R is the Ricci scalar in Riemannian geometry, ϕ_0 is the dilaton field originating from the Weyl quadratic term $\tilde{R}^2$ and ϕ_1 is the Higgs neutral component from the Higgs doublet. The above Lagrangian is scale symmetric, with the potential:

$$V(\phi_0, \phi_1) = \lambda_0\phi_0^4 + \lambda_1\phi_0^2\phi_1^2 + \lambda_2\phi_1^2. \tag{5.29}$$

The coupling constants fulfill the hierarchy relation:

$$\lambda_2 \gg |\lambda_1| \gg \lambda_0, \qquad \lambda_2, \lambda_0 > 0, \lambda_1 < 0, \tag{5.30}$$

so that the new sector is weakly coupled to the Higgs neutral component. This relation, maintained at the quantum level, will be significant in the context of mass scales generation.

Equations of motion from (5.28) read[2]:

$$\begin{aligned}
\phi_0 : \qquad & \ddot{\phi_0} + 3H\dot{\phi_0} + \frac{\xi_0}{6}\phi_0 R + 4\lambda_0\phi_0^3 + 2\lambda_1\phi_0\phi_1^2 = 0 \\
\phi_1 : \qquad & \ddot{\phi_1} + 3H\dot{\phi_1} + \frac{\xi_1}{6}\phi_1 R + 4\lambda_2\phi_1^3 + 2\lambda_1\phi_0^2\phi_1 = 0 \\
g_{\mu\nu} : \qquad & \frac{1}{12}\Big(\xi_0\phi_0^2 + \xi_1\phi_1^2\Big)R - \frac{1}{2}\dot{\phi_0}^2 - \frac{1}{2}\dot{\phi_1}^2 + 2\big(\lambda_0\phi_0^4 + \lambda_1\phi_0^2\phi_1^2 + \lambda_2\phi_1^4\big) = 0
\end{aligned} \tag{5.31}$$

We enforce the additional condition of zero cosmological constant:

$$V(\langle\phi_0\rangle, \langle\phi_1\rangle) = 0, \tag{5.32}$$

and find the stationary solutions of (5.31). The ground state is a flat direction in the ϕ_i field space with zero curvature scalar:

$$\langle\phi_1^2\rangle = -\frac{\lambda_1}{2\lambda_2}\langle\phi_0^2\rangle, \qquad \lambda_0 = \frac{\lambda_1^2}{4\lambda_2}, \qquad \langle R\rangle = 0. \tag{5.33}$$

With λ_0 from (5.33), the potential becomes:

$$V(\phi_0, \phi_1) = \lambda_2\phi_0^4\left(\frac{\phi_1^2}{\phi_0^2} + \frac{\lambda_1}{2\lambda_2}\right)^2. \tag{5.34}$$

The mass matrix of (5.29) is:

$$M^2 = \begin{pmatrix} 2\lambda_1\phi_1^2 + 12\lambda_0\phi_0^2 & 4\lambda_1\phi_1\phi_0 \\ 4\lambda_1\phi_1\phi_0 & 12\lambda_2\phi_1^2 + 2\lambda_1\phi_0^2 \end{pmatrix}, \tag{5.35}$$

and has two eigenvalues at the ground state:

$$m_G^2 = 0, \qquad m_H^2 = -4\lambda_1\left(1 - \frac{\lambda_1}{2\lambda_2}\right)\langle\phi_0^2\rangle. \tag{5.36}$$

[2]We use the Friedmann–Lemaître–Robertson–Walker metric $(1, -a^2(t), -a^2(t), -a^2(t))$ with the Hubble parameter $H = \dot{a}(t)/a(t)$ and $\sqrt{g} = \sqrt{|\det g|} = a^3(t)$.

The Goldstone mode related to the scale symmetry is massless and generates the mass for the other state. Mass eigenstates are obtained from:

$$\begin{pmatrix} G \\ H \end{pmatrix} = \begin{pmatrix} \cos\theta & \sin\theta \\ -\sin\theta & \cos\theta \end{pmatrix} \begin{pmatrix} \phi_0 \\ \phi_1 \end{pmatrix}, \tag{5.37}$$

$$\cos\theta = \frac{1}{\sqrt{1+\delta}} \approx 1 - \frac{\delta}{2}, \qquad \sin\theta = \sqrt{\frac{\delta}{1+\delta}} \approx \sqrt{\delta}, \qquad \delta = -\frac{\lambda_1}{2\lambda_2}, \tag{5.38}$$

$$G = \cos\theta\phi_0 + \sin\theta\phi_1 \approx \phi_0, \tag{5.39}$$

$$H = -\sin\theta\phi_0 + \cos\theta\phi_1 \approx \phi_1. \tag{5.40}$$

The hierarchy described by equation (5.30) dictates that the interaction basis fields coincide with the mass basis fields. Hence, ϕ_1 corresponds to the massive Higgs scalar. Throughout our discussion, we will interchangeably refer to ϕ_0 as G and ϕ_1 as H.

After fields acquire their vevs (which mechanism will be discussed in Chapter 8), the Ricci scalar term plays a role of the Einstein-Hilbert term:

$$\frac{\mathcal{L}_{E-H}}{\sqrt{g}} = -\frac{1}{12}\Big(\xi_0\langle\phi_0^2\rangle + \xi_1\langle\phi_1^2\rangle\Big)R = -\frac{1}{12}\Big(\xi_0 - \xi_1\frac{\lambda_1}{2\lambda_2}\Big)\langle\phi_0^2\rangle R = -\frac{1}{2}M_P^2 R. \tag{5.41}$$

Consequently, the Planck mass scale, (5.27), is determined as:

$$M_P^2 = \frac{1}{6}\Big(\xi_0 - \xi_1\frac{\lambda_1}{2\lambda_2}\Big)\langle\phi_0^2\rangle. \tag{5.42}$$

The vacuum expectation value of the dilaton field plays a central role in determining mass scales. Specifically, it governs the emergence of fundamental mass parameters such as the Higgs vev $\langle\phi_1\rangle$, the Higgs mass m_H, and the Planck mass M_P. In scale-symmetric theories, the value of $\langle\phi_0\rangle$ remains arbitrary, as only the relative ratios of mass scales can be established. The hierarchy of couplings (5.30) ensures that $\langle\phi_0\rangle \gg \langle\phi_1\rangle$, allowing the dilaton vev to be of the order of Planck mass. In further discussions, it will be demonstrated that this hierarchy persists at the quantum level, and no additional tuning is needed beyond (5.30) at the classical level.

5.2.1. Parameter Space

Mass scales relations (5.33), (5.36), and (5.42) provide a way to determine the allowed values of λ_1, λ_2, ξ_0, and ξ_1 within our theoretical framework. The forthcoming calculations will use the approximate experimental values, which are [61, 62]:

$$m_H = 125 \text{ GeV}, \qquad \langle\phi_1\rangle = 250 \text{ GeV}, \qquad M_P = 2.44\cdot 10^{18} \text{ GeV}. \tag{5.43}$$

First, the relation of λ_1 and λ_2 satisfying the hierarchy (5.30) is:

$$\frac{m_H^2}{\langle\phi_1^2\rangle} = 4(2\lambda_2 - \lambda_1) \quad\Rightarrow\quad \lambda_2 = \frac{1}{32}\big(1+16\lambda_1\big), \qquad 0 > \lambda_1 \gg -\frac{1}{48} \approx -0.021. \tag{5.44}$$

For the non-minimal couplings, we get:

$$M_P^2 = \frac{1}{6}\Big(\xi_1 - \xi_0\frac{2\lambda_2}{\lambda_1}\Big)\langle\phi_1^2\rangle \quad\Rightarrow\quad \frac{1}{\lambda_1} = -16\left(\frac{6M_P^2}{\xi_0\langle\phi_1^2\rangle} - \frac{\xi_1}{\xi_0} + 1\right), \qquad 2\xi_0 + \xi_1 \ll \frac{6M_P^2}{\langle\phi_1^2\rangle} \approx 5.72\cdot 10^{32} \tag{5.45}$$

We provide the possible parameter space plots in Figure 5.1. The next sections of this chapter analyze the scalar sector without gravity couplings. For simplicity, we will set $\lambda_1 = -10^{-6}$ and $\lambda_2 = 0.03125$.

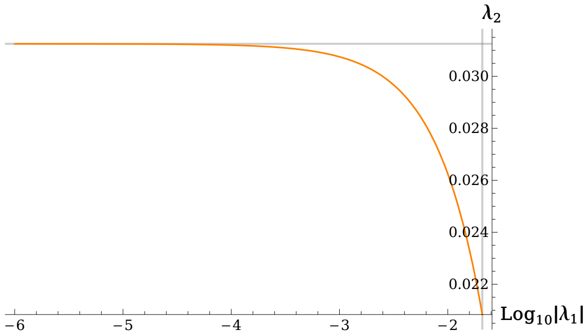

(a) Relation $\lambda_2 = \frac{1}{32}(1 + 16\lambda_1)$ for possible λ_1 values. For $|\lambda_1| \ll 1$, λ_2 tends to a constant value of 0.03125 (gray grid line on y axis). The gray grid line on x axis correspond to the boundary value $\lambda_1 = -\frac{1}{48}$.

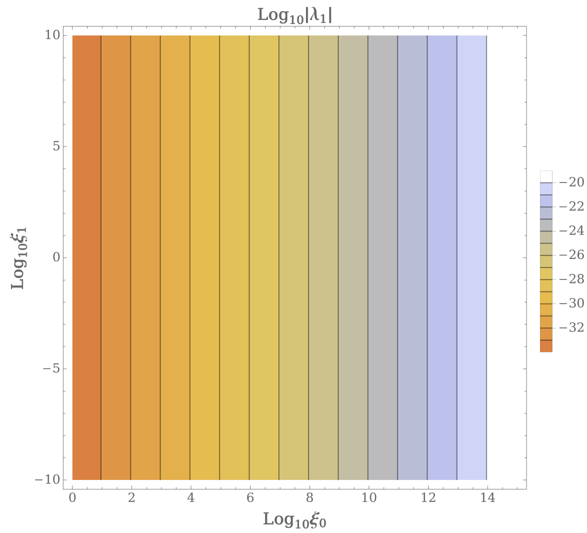

(b) Possible values of λ_1 as a function of non-minimal couplings ξ_i, according to relation (5.45).

Figure 5.1: Plots illustrating the allowed parameter space.

5.3. Non-Polynomial Operators

In the context of scale symmetry, the potential $V(\phi_0, \phi_1)$ can generally take the form:

$$V(\phi_0, \phi_1) = \sum_{n=0}^{\infty} \lambda_n \phi_0^{4-2n} \phi_1^{2n}, \tag{5.46}$$

where terms for $n > 2$ are of importance since even if one sets them initially to zero, they are generated at the quantum level using scale symmetric regularization prescription, as will be shown in the forthcoming analysis. They can be expanded into polynomial effective operators, for instance:

$$\lambda_3 \frac{\phi_1^6}{\phi_0^2} = \lambda_3 \frac{\phi_1^6}{\langle \phi_0^2 \rangle} \left(1 - 2\frac{\phi_0'}{\langle \phi_0 \rangle} + 3\frac{\phi_0'^2}{\langle \phi_0^2 \rangle} + \dots \right), \qquad \phi_0 = \langle \phi_0 \rangle + \phi_0', \tag{5.47}$$

where ϕ_0' is a fluctuation. However, the scale symmetry is better manifested in their non-polynomial form, which we will adopt in our study. The expansion (5.47) reveals that each following term λ_n becomes increasingly suppressed by the large dilaton vev $\langle \phi_0 \rangle \sim M_P$. Therefore, one can freely impose the hierarchy:

$$\lambda_2 \gg |\lambda_1| \gg \lambda_0 \gg |\lambda_3| \gg \dots \tag{5.48}$$

We will briefly examine the potential with $\lambda_n = 0$ for $n > 3$ and demonstrate that this only introduces negligible corrections to our previous analysis.

Let's consider:

$$V = \lambda_0 \phi_0^4 + \lambda_1 \phi_0^2 \phi_1^2 + \lambda_2 \phi_1^4 + \lambda_3 \frac{\phi_1^6}{\phi_0^2}, \tag{5.49}$$

with:

$$\lambda_0, \lambda_2, \lambda_3 > 0, \quad \lambda_1 < 0, \tag{5.50}$$

where only for positive values of λ_3 the potential is well-defined at the large ϕ_1. Finding the ground state with zero cosmological constant, one gets:

$$V = \lambda_3 \phi_0^4 \left(\frac{\phi_1^2}{\phi_0^2} - x_0 \right)^2 \left(\frac{\phi_1^2}{\phi_0^2} - y_0 \right) \tag{5.51}$$

where:

$$x_0 = \frac{-\lambda_2 + \sqrt{\lambda_2^2 - 3\lambda_1\lambda_3}}{3\lambda_3}, \qquad y_0 = -\frac{\lambda_2 + 2\sqrt{\lambda_2^2 - 3\lambda_1\lambda_3}}{3\lambda_3}. \tag{5.52}$$

$$\lambda_0 = -\frac{1}{27\lambda_3^2}\Big(- \lambda_2 + \sqrt{\lambda_2^2 - 3\lambda_1\lambda_3}\Big)\Big(- \lambda_2^2 + 6\lambda_1\lambda_3 + \lambda_2\sqrt{\lambda_2^2 - 3\lambda_1\lambda_3}\Big) \tag{5.53}$$

Expanding above results for small λ_3:

$$x_0 = -\frac{\lambda_1}{2\lambda_2} - \frac{3\lambda_1^2\lambda_3}{8\lambda_2^3} + \mathcal{O}(\lambda_3^2), \qquad y_0 = \frac{\lambda_1}{\lambda_2} - \frac{\lambda_2}{\lambda_3} + \frac{3\lambda_1^2\lambda_3}{4\lambda_2^3} + \mathcal{O}(\lambda_3^2) \tag{5.54}$$

$$\lambda_0 = \frac{\lambda_1^2}{4\lambda_2} + \frac{\lambda_1^3\lambda_3}{8\lambda_2^3} \; + \mathcal{O}(\lambda_3^2) \tag{5.55}$$

and taking the limit $\lambda_3 \to 0$, one recovers the previous results:

$$V = \phi_0^4\left(\frac{\phi_1^2}{\phi_0^2} - x_0^2\right)^2\left(\lambda_3\frac{\phi_1^2}{\phi_0^2} - \lambda_3 y_0\right) \xrightarrow{\lambda_3\to 0} \lambda_2\phi_0^4\left(\frac{\phi_1^2}{\phi_0^2} + \frac{\lambda_1}{2\lambda_2}\right)^2. \tag{5.56}$$

The mass matrix is given by:

$$M^2 = \begin{pmatrix} 12\lambda_0\phi_0^2 + 2\lambda_1\phi_1^2 + 6\lambda_3\frac{\phi_1^6}{\phi_0^4} & 4\lambda_1\phi_0\phi_1 - 12\lambda_3\frac{\phi_1^5}{\phi_0^3} \\ 4\lambda_1\phi_0\phi_1 - 12\lambda_3\frac{\phi_1^5}{\phi_0^3} & 2\lambda_1\phi_0^2 + 12\lambda_2\phi_1^2 + 30\lambda_3\frac{\phi_1^4}{\phi_0^2} \end{pmatrix}, \tag{5.57}$$

with eigenvalues at the ground state:

$$m_G^2 = 0, \qquad m_H^2 = \left[- 4\lambda_1\left(1 - \frac{\lambda_1}{2\lambda_2}\right) + \frac{3\lambda_1^2\lambda_3}{\lambda_2^2} + \mathcal{O}(\lambda_3^2)\right]\langle\phi_0^2\rangle. \tag{5.58}$$

Mass eigenstates obtain small corrections:

$$\cos\theta \approx 1 - \frac{\delta}{2} - \frac{\delta_3}{2}, \qquad \sin\theta \approx \sqrt{\delta} - \frac{\delta_3}{2\sqrt{\delta}}, \qquad \delta = -\frac{\lambda_1}{2\lambda_2}, \quad \delta_3 = -\frac{3\lambda_1^2}{8\lambda_2^3}\lambda_3, \tag{5.59}$$

$$G = \cos\theta\phi_0 + \sin\theta\phi_1 \approx \phi_0, \tag{5.60}$$

$$H = \sin\theta\phi_0 - \cos\theta\phi_1 \approx \phi_1. \tag{5.61}$$

Again, the interaction basis fields coincide with the mass basis fields, if the hierarchy (5.48) is fulfilled.

Including non-polynomial terms in tree-level potential leads to corrections of order λ_3 or higher. According to equation (5.48), these corrections are negligible compared to the results presented in Section 5.2. However, we will address them in our examination of the quantum effective potential to show that their respective one-loop beta functions are insignificant, allowing them to be safely omitted at the classical level[3].

[3]This can be done at the one-loop level. However, at two loops, the beta functions for λ_3 and higher receive corrections that do not vanish when $\lambda_3, \lambda_4, \ldots$ are set to zero [24,28]. Nevertheless, they remain small and safely negligible.

5.4. Scale-Symmetric One-Loop Corrections in the Absence of Gravity

In this section, we employ dimensional regularization maintaining quantum scale symmetry from Chapter 3. The choice of the subtraction function is given by:

$$\mu^{2\epsilon} = \mu(\phi_0)^{2\epsilon} = \left(z \cdot \phi_0^{\frac{1}{1-\epsilon}}\right)^{2\epsilon}. \tag{5.62}$$

To sustain dimensionless λ_i couplings, we replace $\lambda_i \to \mu(\phi_0)^{2\epsilon}\lambda_i$. Consequently, this transformation changes the potential to $V(\phi_0, \phi_1) \to \tilde{V}(\phi_0, \phi_1) = \mu(\phi_0)^{2\epsilon} V(\phi_0, \phi_1)$, making it scale invariant in $d = 4 - 2\epsilon$ dimensions. Due to the field dependence of $\mu(\phi_0)$, new finite corrections emerge at the quantum level, beyond the usual Coleman-Weinberg terms in the $\mu = const$ prescription.

Consider the Lagrangian for the Higgs scalar ϕ_1 coupled to the dilaton ϕ_0 of the form:

$$\mathcal{L} = \frac{1}{2}\left(\partial_\mu \phi_0\right)^2 + \frac{1}{2}\left(\partial_\mu \phi_1\right)^2 - \tilde{V}(\phi_0, \phi_1) + \mathcal{L}_{SM} + \delta\mathcal{L}_{c.t.}, \tag{5.63}$$

where:

$$\tilde{V}(\phi_0, \phi_1) = \mu(\phi_0)^{2\epsilon} V(\phi_0, \phi_1), \qquad V(\phi_0, \phi_1) = \lambda_0 \phi_0^4 + \lambda_1 \phi_0^2 \phi_1^2 + \lambda_2 \phi_1^4 + \lambda_3 \frac{\phi_1^6}{\phi_0^2}. \tag{5.64}$$

The counter-term Lagrangian will cancel the poles of the one-loop corrections:

$$\begin{aligned}\delta\mathcal{L}_{c.t.} =& \frac{1}{2}\left(Z_G - 1\right)\left(\partial_\mu \phi_0\right)^2 + \frac{1}{2}\left(Z_H - 1\right)\left(\partial_\mu \phi_1\right)^2 \\ &- \mu(\phi_0)^{2\epsilon}\Bigg[\left(Z_0 Z_G^2 - 1\right)\lambda_0 \phi_0^4 + \left(Z_1 Z_G Z_H - 1\right)\lambda_1 \phi_0^2 \phi_1^2 + \left(Z_2 Z_H^2 - 1\right)\lambda_2 \phi_1^4 + \\ &+ \sum_{n=3,4,5,6} \left(Z_n Z_G^{-n+2} Z_H^n - 1\right)\lambda_n \frac{\phi_1^{2n}}{\phi_0^{2n-4}}\Bigg],\end{aligned} \tag{5.65}$$

where the sum over n is essential, as these terms will arise at the quantum level. The Lagrangian $\mathcal{L}_{SM}$ contains the interactions of the Higgs boson with other SM particles, specifically the top quark, $W^{\pm}$, and Z gauge bosons. The field-dependent square masses for these particles can be read from (5.10) and (5.12):

$$m_t^2(\phi_1) = \frac{1}{2} y_t^2 \phi_1^2, \qquad m_W^2(\phi_1) = \frac{1}{4} g_2^2 \phi_1^2, \qquad m_Z^2(\phi_1) = \frac{1}{4}(g_1^2 + g_2^2)\phi_1^2. \tag{5.66}$$

The mass for the Higgs doublet Goldstones is:

$$m_\chi^2(\phi_0, \phi_1) = 2\lambda_1 \phi_0^2 + 4\lambda_2 \phi_1^2 + 6\lambda_3 \frac{\phi_1^4}{\phi_0^2} \xrightarrow{\text{ground state}} m_\chi^2 = 0. \tag{5.67}$$

The field dependent masses for Higgs $m_H^2(\phi_0, \phi_1)$ and Goldstone $m_G^2(\phi_0, \phi_1)$ are the eigenvalues of the mass matrix (5.57). With the above particle content, the one-loop effective potential, using the equation (3.27), is given by:

$$V_1(\phi_0, \phi_1) = V(\phi_0, \phi_1) + \frac{1}{64\pi^2} \sum_{i=G,H,\chi,W,Z,t} n_i \cdot m_i^4 \left(-\frac{1}{\epsilon} + \ln \frac{m_i^2}{\kappa_i \mu^2(\phi_0)}\right) + \frac{1}{64\pi^2} \delta V_1(\phi_0, \phi_1), \tag{5.68}$$

where the numbers of degrees of freedom are $n_i = \{1, 1, 3, 6, 3, -12\}$ for $i = \{G, H, \chi, W, Z, t\}$ and $\kappa_i = 4\pi e^{3/2-\gamma_E}$ for $i = G, H, \chi, t$ and $\kappa_i = 4\pi e^{5/2-\gamma_E}$ if $i = W, Z$. The contribution $\delta V_1(\phi_0, \phi_1)$

is novel, and is absent in the $\mu = const$ regime. It is derived according to the equation (3.24), with the result:

$$\begin{aligned}\delta V_1(\phi_0,\phi_1) = & -336\lambda_0^2\phi_0^4 - 8\lambda_1(25\lambda_0+8\lambda_1)\phi_0^2\phi_1^4 + 8(6\lambda_0\lambda_2 - 3\lambda_1^2 - 16\lambda_1\lambda_2)\phi_1^4 + \\ & + 8(\lambda_1\lambda_2+9\lambda_0\lambda_3)\frac{\phi_1^6}{\phi_0^2} - 32\lambda_3(\lambda_1-12\lambda_2)\frac{\phi_1^8}{\phi_0^4} + 24\lambda_3(\lambda_2+24\lambda_3)\frac{\phi_1^{10}}{\phi_0^6} + 120\lambda_3^2\frac{\phi_1^{12}}{\phi_0^8}.\end{aligned} \tag{5.69}$$

New interactions have emerged due to the inclusion of higher non-polynomial operators, which were originally absent at the tree-level in potential (5.64). Therefore, the general form of the classical potential should be in fact as in (5.46), where each non-polynomial term with the power of ϕ_1^n $(n > 4)$ generates higher-order terms. Note that, even for $\lambda_3 = 0$ at the classical level, $\lambda_1\lambda_2\frac{\phi_1^6}{\phi_0^2}$ is still present in δV_1, making the higher terms inevitable. Nevertheless, considering the hierarchy (5.48), these contributions are negligible. Additionally, the beta functions of their corresponding couplings can be safely set to zero by assigning $\lambda_n \to 0$ for $n > 2$ (see the equation (A.1) in Appendix A).

To renormalize the divergences of (5.68), we adopt the $\overline{\text{MS}}$ scheme. Consequently, in counter-terms, Z_i factors absorbing the divergences are defined as:

$$Z_i = 1 + \frac{1}{\epsilon}\frac{\delta_i}{(4\pi)^2}, \tag{5.70}$$

and the subtraction function is rescaled to $\mu^2 \to \mu^2\frac{e^{\gamma_E}}{4\pi}$. One identifies:

$$\begin{gathered}\delta_0 = 36\lambda_0 + \frac{4\lambda_1^2}{\lambda_0}, \qquad \delta_1 = 4\big(3\lambda_0 + 2\lambda_1 + 6\lambda_2\big), \\ \delta_2 = \frac{\lambda_1^2}{\lambda_2} + 48\lambda_2 + 30\frac{\lambda_1\lambda_3}{\lambda_2} + \frac{3}{64\lambda_2}\Big(\big(g_1^2+g_2^2\big)^2 + 2g_2^4 - 16y_t^4\Big), \\ \delta_3 = 12\big(3\lambda_0 - 4\lambda_1 + 15\lambda_2\big), \qquad \delta_4 = \frac{3\lambda_3}{\lambda_4}\big(2\lambda_1 + 75\lambda_3\big), \\ \delta_5 = 72\frac{\lambda_3^2}{\lambda_5}, \qquad \delta_6 = 9\frac{\lambda_3^2}{\lambda_6}.\end{gathered} \tag{5.71}$$

Factors renormalizing the kinetic terms for the Higgs and dilaton field, Z_G and Z_H, are given by [22, 63, 64][4]:

$$\begin{aligned} & Z_G = 1, \qquad \delta_G = 0, \qquad \gamma_G = -\frac{1}{2}\frac{\partial \ln Z_G}{\partial \ln z} = 0 \\ & Z_H = 1 + \frac{1}{\epsilon}\frac{\delta_H}{(4\pi)^2}, \qquad \delta_H = \left[\frac{9}{4}g_1^2 + \frac{3}{4}g_2^2 - 3y_t^2\right], \qquad \gamma_H = -\frac{1}{2}\frac{\partial \ln Z_H}{\partial \ln z} = \frac{\partial \ln \phi_1}{\partial \ln z} = \frac{2}{(4\pi)^2}\delta_H,\end{aligned} \tag{5.72}$$

where γ_G and γ_H are the so-called anomalous dimensions. The Renormalization Group Equation (RGE) for each coupling can be derived by differentiation [55]:

$$0 = \frac{d}{d\ln z}\lambda_n^{(BARE)} = \frac{d}{d\ln z}\Big(\mu(\phi_0)^{2\epsilon}Z_n Z_H^{-n}\lambda_n\Big), \tag{5.73}$$

where index $(BARE)$ denotes a bare coupling constant, which is independent of the renormalization group (RG) factor z, and $Z_G = 1$ does not have to be included. From the above differentiation, we obtain the equations for the beta functions $\beta_n = \frac{d}{d\ln z}\lambda_n$:

$$2\epsilon + \frac{\beta_n}{\lambda_n} + \sum_{\alpha_i}\beta_{\alpha_i}\frac{d}{d\alpha_i}\ln Z_n Z_H^{-n} = 0, \tag{5.74}$$

[4]At the one-loop level, $\gamma_G = \gamma_H = 0$ if one considers only the potential (5.64) [24, 28]. However, the Higgs neutral component receives the corrections from the Standard Model particles and γ_H is the same as for $\mu = const$.

where $\alpha_i = \{\lambda_0, \lambda_1, \ldots, \lambda_6, g_1, g_2, y_t\}$. To the order $\mathcal{O}(\lambda_n)$ they are:

$$\beta_n = -2\epsilon\lambda_n + \mathcal{O}(\lambda_n^2). \tag{5.75}$$

Using this result for β_{α_i} in (5.74), one gets:

$$\beta_n = -2\epsilon\lambda_n + 2\epsilon\lambda_n \sum_{\alpha_i} \alpha_i \frac{d}{d\alpha_i} \ln Z_n Z_H^{-n} = -2\epsilon\lambda_n + \frac{2\lambda_n}{(4\pi)^2} \sum_{\alpha_i} \alpha_i \frac{d}{d\alpha_i}\Big(\delta_n - n\cdot\delta_H\Big). \tag{5.76}$$

Since one has:

$$\alpha_i \frac{d}{d\alpha_i}\delta_n = \delta_n, \qquad \alpha_i \frac{d}{d\alpha_i}\delta_H = 2\delta_H, \tag{5.77}$$

the final result reads:

$$\beta_n = -2\epsilon\lambda_n + \frac{2\lambda_n}{(4\pi)^2}\Big(\delta_n - 2n\delta_H\Big). \tag{5.78}$$

The explicit formulas for beta functions of λ_n couplings are presented in Appendix A[5], along with the Standard Model results for g_1, g_2 and y_t, taken from [63,64]. Additionally, the appendix includes plots illustrating the running of λ_n.

The renormalized one-loop potential is:

$$V_1(\phi_0,\phi_1) = V(\phi_0,\phi_1) + \frac{1}{64\pi^2}\sum_{i=G,H,\chi,W,Z,t} n_i \cdot m_i^4 \ln\frac{m_i^2}{c_i(z\phi_0)^2} + \frac{1}{64\pi^2}\delta V_1(\phi_0,\phi_1), \tag{5.79}$$

where $c_i = \{e^{3/2}, e^{5/2}\}$ for $i = \{\{G,H,\chi,t\},\{W,Z\}\}$. The $V_1(\phi_0,\phi_1)$ is manifestly scale invariant. The Coleman-Weinberg potential is modified due to the scale-symmetric choice of subtraction scale $\mu = z\phi_0$. Figure 5.2 illustrates the RG-improved potential V_1[6], with the RG parameter $z = z_0 = \langle\phi_1\rangle/\langle\phi_0\rangle$, chosen as described in the following discussion. All parameters run with the dilaton field ϕ_0, as discussed in Appendix A. We also include the running of the ϕ_1 field, the details of which are described in Section A.1.

The Callan-Symanzik equation for the scalar potential ensures that the potential remains independent of the subtraction scale. At the one-loop level, this leads to the following expression [55]:

$$\frac{d}{d\ln z}V_1(\phi_0,\phi_1,\alpha_i) = \left[z\frac{\partial}{\partial z} + \beta_{\alpha_i}\frac{\partial}{\partial\alpha_i} + \gamma_H\phi_1\frac{\partial}{\partial\phi_1}\right]V_1(\phi_0,\phi_1,\alpha_i) = \mathcal{O}(\alpha_i^3), \tag{5.80}$$

where $V_1(\phi_0,\phi_1,\alpha_i)$ is the RG-improved one-loop potential found in (5.79) with all couplings running with the $\mu = z\cdot\phi_0$ scale. In particular, since λ_n for $n>3$ have non-zero β functions, the tree-level potential $V(\phi_0,\phi_1)$ is completed with higher order polynomial terms:

$$V(\phi_0,\phi_1) \quad\to\quad V(\phi_0,\phi_1) + \lambda_4\frac{\phi_1^8}{\phi_0^4} + \lambda_5\frac{\phi_1^{10}}{\phi_0^6} + \lambda_6\frac{\phi_1^{12}}{\phi_0^8}. \tag{5.81}$$

The explicit dependence on z appears only in the Coleman-Weinberg part of V_1, under the logarithms. At the one-loop level, the operators $\beta_{\alpha_i}\frac{\partial}{\partial\alpha_i} + \gamma_H\phi_1\frac{\partial}{\partial\phi_1}$ act solely on the classical potential. Therefore, the Callan-Symanzik one-loop equation is validated, allowing the RG factor

[5]At the one-loop level, beta functions for λ_n couplings are the same as when $\mu = const$. However, at the two-loop level, they start to differ due to the ϵ corrections in the scalar field dependent masses emerging from $\mu(\phi_0)^{2\epsilon}$, [24,28].

[6]It is well known that the Standard Model Higgs effective potential generally suffers from infrared (IR) divergences due to the inclusion of the field-dependent tree-level masses of the Goldstone bosons, which vanish at the ground state. Following the analysis given in [65] and [66], the resummation of IR-problematic terms can resolve these divergences, and one can neglect the Goldstone bosons' contribution. Consequently, we do not include $m_\chi^2(\phi_0,\phi_1)$ in the numerical analysis of the potential of one loop (5.79).

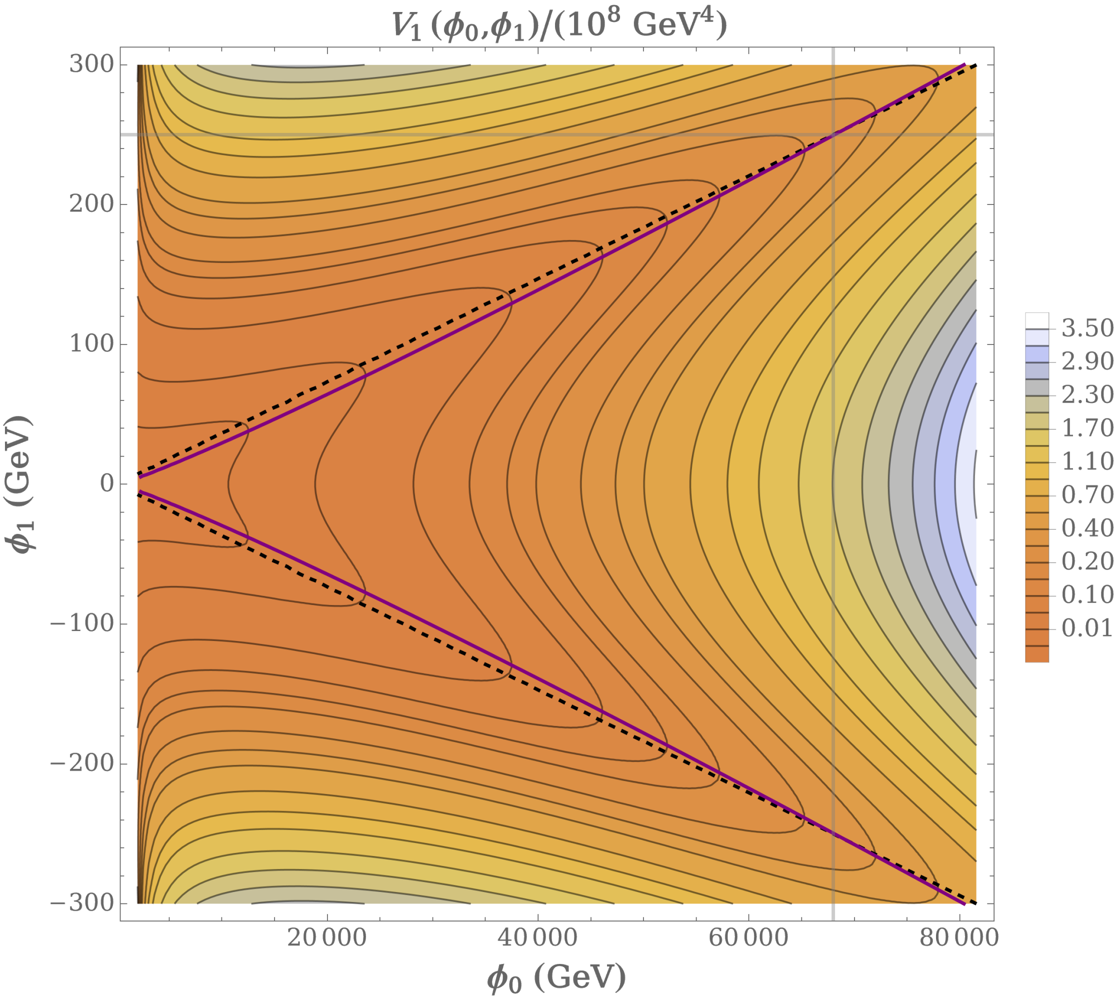

Figure 5.2: Plot of the renormalized RG-improved potential $V_1(\phi_0, \phi_1)$ from equation (5.79). The RG parameter is equal to $z = \langle\phi_1\rangle/\langle\phi_0\rangle$ and $\lambda_1 = -10^{-6}$. The black dashed lines depict the quantum flat direction according to (5.83), and the gray grid lines correspond to the vacuum expectation values of fields for given λ_1. The true quantum flat direction in the RG improved potential $V_1(\phi_0, \phi_1)$, for which its first derivatives vanish, is not a straight line and has been marked with the thick purple line.

z and the subtraction scale $z\langle\phi_0\rangle$ to be fixed since the one-loop potential remains independent of it. To minimize the logarithmic terms in the potential, we set $z = z_0 = \langle\phi_1\rangle/\langle\phi_0\rangle$. This choice ensures that, after the spontaneous scale symmetry breaking, the subtraction scale is $\mu(\langle\phi_0\rangle) = z_0\langle\phi_0\rangle = \langle\phi_1\rangle$. However, fixing the RG parameter z does not mean that the coupling constants do not run. To apply the RG improvement of the potential, we set the subtraction scale to $\mu(\phi_0) = z_0 \cdot \phi_0 = \langle\phi_1\rangle/\langle\phi_0\rangle \cdot \phi_0$. Consequently, all parameters run with the dilaton field ϕ_0, as discussed in the Appendix A.

Given the hierarchy (5.48), we can express the couplings as:

$$\lambda_2 = \tilde{\lambda}_2, \quad \lambda_1 = \varepsilon \cdot \tilde{\lambda}_1, \quad \lambda_0 = \varepsilon^2 \cdot \tilde{\lambda}_0, \quad \lambda_3 = \varepsilon^3 \cdot \tilde{\lambda}_3, \quad \dots, \tag{5.82}$$

where $\varepsilon \ll 1$, the $\tilde{\lambda}_n$ terms are of the same order, and we can expand the quantities to the desired order in ε. The new flat direction, for which $V_1(\langle\phi_0\rangle, \langle\phi_1\rangle) = 0 + \mathcal{O}(\varepsilon^2)$, is modified to:

$$\frac{\langle\phi_1^2\rangle}{\langle\phi_0^2\rangle} = -\frac{\lambda_1}{2\lambda_2} \cdot \frac{8\lambda_2}{X}\left[Y + \sqrt{Y^2 - 2X}\right] + \mathcal{O}(\varepsilon^2) = -\frac{\lambda_1}{2\lambda_2} \cdot \delta, \qquad \delta \approx 0.845 \text{ for } \lambda_2 = 0.03125, \tag{5.83}$$

$$X = 3g^4\left[\log\frac{g^2}{4}-2\right]+6g_2^4\left[\log\frac{g_2^2}{4}-2\right]-48y_t^4\left[\log\frac{y_t^2}{2}-1\right]+256\lambda_2\left[9\lambda_2\Big(\log 12\lambda_2-1\Big)+4\pi^2\right], \tag{5.84}$$

$$Y = 16\big(4\pi^2+3\lambda_2\log 12\lambda_2\big). \tag{5.85}$$

The one-loop Higgs mass is given by:

$$m_H^2 = \left[\frac{\partial^2 V_1}{\partial\phi_0^2}+\frac{\partial^2 V_1}{\partial\phi_1^2}\right]\Bigg|_{\phi_i=\langle\phi_1\rangle}, \tag{5.86}$$

which yields the correction to the classical value:

$$\begin{aligned}\delta m_H^2 = -\frac{\lambda_1}{2\lambda_2}\frac{3\langle\phi_0^2\rangle}{16\cdot(4\pi)^2}\Bigg[&-16y_t^4\left(3\ln\frac{y_t^2}{2}-1\right)+(g_1^2+g_2^2)^2\left(3\ln\frac{g_1^2+g_2^2}{4}-4\right)+\\ &+g_2^4\left(6\ln\frac{g_2^2}{4}-8\right)+512\lambda_2^2\Big(4\ln 8\lambda_2-1\Big)\Bigg]+\mathcal{O}(\varepsilon^2).\end{aligned} \tag{5.87}$$

Given that $\langle\phi_0^2\rangle = -\frac{2\lambda_2}{\lambda_1}\cdot\frac{1}{\delta}\langle\phi_1^2\rangle$, the Higgs mass quantum correction is proportional to $\frac{1}{\delta}\langle\phi_1^2\rangle$, maintaining the hierarchy $m_H^2\sim\langle\phi_1^2\rangle\ll\langle\phi_0^2\rangle$. The numerical values for different λ_1 (note that the λ_2 coupling and the dilaton vev $\langle\phi_0\rangle$ are both λ_1 functions), give a correction of about 7.5% to the tree-level value $m_H = 125$ GeV. This indicates that the original classical hierarchy is preserved at the quantum level, and there is no need for additional fine-tuning of the couplings λ_n.

5.5. Conclusions

We demonstrated that with the kinetic term for the dilaton field, arising from the Weyl quadratic gravity term, the conclusions of the previous chapter are maintained. The theory behaves within a regular Riemannian geometric framework for energy scales below the Planck mass. This chapter provides an insight into the realization of the scale symmetry at both the classical and quantum levels in the Standard Model Higgs scalar sector coupled to the dilaton. The classical hierarchy of the coupling constants, maintained at the quantum level, ensures a weak interaction between the new sector and the Higgs field, supporting the naturalness of the electroweak scale, as the quantum Higgs mass correction is small. Consequently, the realization of scale symmetry through Weyl conformal gravity offers a consistent way of adding a new sector to the model, responsible for generating mass scales and realizing a scale-symmetric quantum regularization method. This approach provides a promising solution to the hierarchy problem.

Chapter 6

Gravity and Dilaton Effects

In the previous chapter, we presented a scale-symmetric theory of a Higgs-like field ϕ_1 non-minimally coupled to Weyl conformal gravity. Due to the presence of the $\tilde{R}^2$ term, a dilaton mode ϕ_0 emerges and interacts with ϕ_1 and Weyl gravity. This chapter focuses on the dilaton and gravity sector, specifically exploring conditions under which one can decouple both and recover a pure Higgs sector. Such a scenario would correspond to the physics observed in the present Universe. We focus solely on the classical Lagrangian and neglect the quantum effects. In the last section, we explore the implications of the Weak Gravity Conjecture (WGC) in our model. This analysis imposes constraints on the Weyl gauge coupling q and provides insight into the interplay between gravity, gauge interactions, and scale symmetry. This entire chapter presents a novel analysis that is not found in any papers known to the authors.

6.1. Dilaton Decoupling

The analysis of the classical potentials (5.29) and (5.49), with and without non-polynomial operators, respectively, showed that the massless component can be approximated as:

$$G = \cos\theta\phi_0 - \sin\theta\phi_1 \approx \phi_0, \tag{6.1}$$

provided the coupling hierarchy $\lambda_3 \ll \lambda_0 \ll |\lambda_1| \ll \lambda_2$ is maintained. Consequently, the dilaton mode ϕ_0 can be regarded as a pure, massless Goldstone particle. Its vacuum expectation value contributes to the mass of the neutral Higgs component:

$$m_H^2 = \left[-4\lambda_1\left(1 - \frac{\lambda_1}{2\lambda_2}\right) + (\text{corrections})\right]\langle\phi_0^2\rangle, \tag{6.2}$$

where the corrections come from non-polynomial operators and are significantly smaller than the rest of the terms.

The classical dilaton decoupling limit is realized by setting all dilaton couplings to zero $(\lambda_1, \lambda_3, \lambda_4, \ldots \to 0)$ and allowing the vev of the dilaton to approach infinity $(\langle\phi_0\rangle \to \infty)$ while keeping a fixed value for m_H^2. In the following analysis, we examine the model's behavior in this context, disregarding the contributions from non-polynomial operators, as their impact is negligible.

Let's denote the vacuum expectation values of the fields as $\langle\phi_i\rangle = v_i$ with:

$$v_1^2 = -\frac{\lambda_1}{2\lambda_2}v_0^2 = \delta\cdot v_0^2, \qquad \delta = -\frac{\lambda_1}{2\lambda_2}. \tag{6.3}$$

We expand the classical potential around the ground state:

$$V(\phi_0,\phi_1) = \lambda_2\phi_0^4\left(\frac{\phi_1^2}{\phi_0^2} + \frac{\lambda_1}{2\lambda_2}\right)^2 \quad \xrightarrow{\phi_i = v_i + \tilde{\phi}_i} \quad V(\tilde{\phi}_0,\tilde{\phi}_1) = \lambda_2\Big(\tilde{\phi}_1^2 + 2\sqrt{\delta}v_0\tilde{\phi}_1 - 2\delta v_0\tilde{\phi}_0 - \delta\tilde{\phi}_0^2\Big)^2, \tag{6.4}$$

where $\tilde{\phi}_i$ are quantum fluctuations with zero vevs. The mass matrix at the ground state is:

$$M_{gr}^2 = 8\lambda_2\delta v_0^2 \cdot \begin{pmatrix} \delta & -\sqrt{\delta} \\ -\sqrt{\delta} & 1 \end{pmatrix} \tag{6.5}$$

The normalized eigenvectors of (6.5), give the transition matrix so that the M_{gr}^2 can be transformed to its diagonal form:

$$\mathcal{R}^T M_{gr}^2 \mathcal{R} = M_{diag}^2, \qquad \mathcal{R} = \frac{1}{\sqrt{1+\delta}} \cdot \begin{pmatrix} 1 & -\sqrt{\delta} \\ \sqrt{\delta} & 1 \end{pmatrix}, \qquad M_{diag}^2 = \begin{pmatrix} 0 & 0 \\ 0 & 8\lambda_2\delta(\delta+1)v_0^2 \end{pmatrix}. \tag{6.6}$$

Therefore, the mass eigenstates are:

$$\begin{pmatrix} \tilde{\phi}_0 \\ \tilde{\phi}_1 \end{pmatrix} = \frac{1}{\sqrt{1+\delta}} \begin{pmatrix} G - \sqrt{\delta}H \\ \sqrt{\delta}G + H \end{pmatrix}, \qquad \begin{pmatrix} G \\ H \end{pmatrix} = \frac{1}{\sqrt{1+\delta}} \begin{pmatrix} \tilde{\phi}_0 + \sqrt{\delta}\tilde{\phi}_1 \\ -\sqrt{\delta}\tilde{\phi}_0 + \tilde{\phi}_1 \end{pmatrix} \tag{6.7}$$

We write the potential (6.4) in terms of the new fields:

$$V(G,H) = \lambda_2 \cdot H^2\Big((1-\delta)H + 2\sqrt{\delta}G + 2\sqrt{\delta(1+\delta)}v_0\Big)^2, \tag{6.8}$$

which after the spontaneous symmetry breaking (the Goldstone mode acquires its vev: $\langle G\rangle = 0$), one has:

$$\begin{aligned} V(H) =& 4\lambda_2\delta(1+\delta)v_0^2 \cdot H^2 + 4\lambda_2\sqrt{\delta(1+\delta)}(1-\delta)v_0 \cdot H^3 + \lambda_2(1-\delta)^2 \cdot H^4 = \\ =& \frac{1}{2}m_H^2 \cdot H^2 + \sqrt{2\lambda_2}(1-\delta)m_H \cdot H^3 + \lambda_2(1-\delta)^2 \cdot H^4. \end{aligned} \tag{6.9}$$

To decouple the dilaton, one applies the limits $\lambda_1 \to 0 \Rightarrow \delta \to 0$ and $v_0 \to \infty$ with the m_H^2 fixed. This results in the Higgs potential:

$$V(H) = \frac{1}{2}m_H^2 \cdot H^2 + \sqrt{2\lambda_2}m_H \cdot H^3 + \lambda_2 \cdot H^4. \tag{6.10}$$

To compare the result (6.10) to the Standard Model Higgs potential, we expand the latter around the ground state:

$$V_{SM}(h) = \lambda_{SM}\left(\frac{1}{2}(v_h+h)^2 + \frac{\mu^2}{2\lambda_{SM}}\right)^2, \qquad v_h^2 = -\frac{\mu^2}{\lambda_{SM}}, \quad \mu^2 = -\frac{1}{2}m_H^2. \tag{6.11}$$

This gives:

$$V_{SM}(h) = \frac{1}{2}m_H^2 \cdot h^2 + \sqrt{\frac{\lambda_{SM}}{2}}m_H \cdot h^3 + \frac{\lambda_{SM}}{4} \cdot h^4. \tag{6.12}$$

The potentials (6.10) and (6.12) are equivalent if $\lambda_2 = \frac{1}{4}\lambda_{SM}$. At the electroweak scale, where $\lambda_2 = 0.03125$ and $\lambda_{SM} = 0.125$, this condition is satisfied as a result of the conditions established in the analysis from Section 5.2.1.

To summarize, the mass scales in the theory are dynamically generated after the spontaneous breaking of scale symmetry, when the Goldstone mode acquires its vev. Specifically, both the Higgs mass and vev are proportional to $\langle\phi_0\rangle$. Upon the decoupling of the dilaton, the Standard Model Higgs scalar sector is recovered. Incorporating the gravity sector, discussed in the next section, shows that the dilaton vev also gives rise to the Planck mass, M_P. Therefore, those two sectors are related, and as will be shown, gravity decoupling (in the flat limit) aligns with the decoupling of the dilaton. The exact mechanism by which the ϕ_0 field acquires its vev is studied in Chapter 8, where the time evolution of the fields is further improved with temperature corrections.

6.2. Gravity Decoupling

Weyl conformal gravity introduces Weyl vector field ω_μ which is coupled to ϕ_i fields via Weyl curvature scalar $\tilde{R}$ and covariant derivative $\tilde{D}_\mu$, which are:

$$\tilde{R} = R - 3qD_\mu\omega^\mu - \frac{3}{2}q^2\omega_\mu\omega^\mu, \tag{6.13}$$

$$\tilde{D}_\mu\phi_i = \Big(\partial_\mu - \frac{q}{2}\omega_\mu\Big)\phi_i. \tag{6.14}$$

We have shown that after the breaking of Weyl conformal symmetry via the Stueckelberg mechanism, ω_μ acquires a mass $m^2_{\omega_\mu} = \frac{3}{4}q^2M^2$, where M is arbitrary. The presence of the Einstein-Hilbert term in the broken Lagrangian allows us to identify M with the Planck mass scale, so that $m^2_{\omega_\mu} \sim M_P^2$ (see Section 6.3 for the details of the possible q coupling values). For energies below the Planck mass scale, the Weyl vector field decouples, and the theory becomes Riemannian. The Weyl geometric approach is important in at least two aspects:

- It provides a natural mass generation, even in the absence of matter, through the geometric origin of the new scalar sector, ϕ_0, which is not added to the theory ad hoc. This occurs due to the spontaneous breaking of the scale symmetry and the ω_μ field "eating" the dilaton.
- The presence of the Weyl vector field ensures the conservation of degrees of freedom in the Stueckelberg mechanism. This wouldn't be possible without ω_μ, as there would be nothing to absorb the dilaton mode. Similar theories embedded in Riemannian geometry result in the presence of unphysical ghosts (see, e.g., [7,67]).

One can now consider the gravity decoupling limit, $M_P \to \infty$ or more precisely, the flat limit $g_{\mu\nu} \to \eta_{\mu\nu}$. In Section 5.1, we showed that after the spontaneous breaking of the Weyl conformal symmetry in a theory with two scalar fields ϕ_0 and ϕ_1, we obtain the Lagrangian of the form:

$$\frac{\mathcal{L}'}{\sqrt{g'}} = -\frac{1}{2}M_P^2R' - \frac{1}{4}\tilde{F}'_{\mu\nu}\tilde{F}'^{\mu\nu} + \frac{3}{4}q^2M_P^2\omega'_\mu\omega'^\mu + \frac{1}{2}\tilde{D}'_\mu\phi'_0\tilde{D}'^\mu\phi'_0 + \frac{1}{2}\tilde{D}'_\mu\phi'_1\tilde{D}'^\mu\phi'_1 - V'(\phi'_0,\phi'_1), \tag{6.15}$$

where quantities with prime are rescaled after the conformal transformation (4.8), and in particular, R' is the Riemannian curvature scalar. From now on, the primes will be omitted. In order to remove the derivative coupling $\omega_\mu\partial^\mu\big(\phi_0^2+\phi_1^2\big)$, we introduce a new variable (5.20):

$$\omega_\mu \quad\longrightarrow\quad \hat{\omega}_\mu + \frac{1}{q}\partial_\mu \ln\Big[6M_P^2 + \phi_0^2 + \phi_1^2\Big]. \tag{6.16}$$

The Lagrangian becomes:

$$\begin{aligned}\frac{\mathcal{L}}{\sqrt{g}} =& -\frac{1}{2}M_P^2R - \frac{1}{4}\tilde{F}_{\mu\nu}\tilde{F}^{\mu\nu} + \frac{1}{8}q^2\Big(6M_P^2+\phi_0^2+\phi_1^2\Big)\hat{\omega}_\mu\hat{\omega}^\mu + \\ &+\frac{1}{2}\frac{\big(6M_P^2+\phi_1^2\big)\big(\partial_\mu\phi_0\big)^2 - 2\phi_0\phi_1\partial_\mu\phi_0\partial^\mu\phi_1 + \big(6M_P^2+\phi_0^2\big)\big(\partial_\mu\phi_1\big)^2}{6M_P^2+\phi_0^2+\phi_1^2} - V(\phi_0,\phi_1).\end{aligned} \tag{6.17}$$

The Planck mass is associated with the dilaton vev, as seen from equation (5.27):

$$M_P^2 = \frac{1}{6}\Big[\xi_0\langle\phi_0^2\rangle + \xi_1\langle\phi_1^2\rangle\Big] = \frac{1}{6}\Big[\xi_0 - \frac{\lambda_1}{2\lambda_2}\xi_1\Big]\langle\phi_0^2\rangle \quad\Rightarrow\quad M_P\to\infty \equiv \langle\phi_0\rangle\to\infty. \tag{6.18}$$

Consequently, the gravity decoupling is related to the dilaton decoupling in our model. This is unsurprising, as the ϕ_0 field originates from the $\tilde{R}^2$ term. We expand the Lagrangian (6.17) around the ground state $\phi_i = v_i + \tilde{\phi}_i$, rewrite it in terms of the mass eigenstates G, H (6.7) and provide its form after the spontaneous symmetry breaking when $\langle G \rangle = 0$:

$$\begin{aligned}\frac{\mathcal{L}}{\sqrt{g}} =& -\frac{1}{2}M_P^2 R - \frac{1}{4}\tilde{F}_{\mu\nu}\tilde{F}^{\mu\nu} + \frac{1}{8}q^2\Big[M_P^2\big(6+\alpha^2(1+\delta)\big) + H^2\Big]\hat{\omega}_\mu\hat{\omega}^\mu + \\ &+ \frac{1}{2}\frac{6+\alpha^2(1+\delta)}{6+\alpha^2(1+\delta)+\frac{H^2}{M_P^2}}\partial_\mu H\partial^\mu H - V(H),\end{aligned} \tag{6.19}$$

where $V(H)$ has the form (6.9), $\delta = -\frac{\lambda_1}{2\lambda_2}$ and $M_P^2 = \alpha^2\langle\phi_0^2\rangle$ from equation (6.18). In the above Lagrangian, we have the Einstein-Hilbert action for Riemannian gravity and the matter Lagrangian $\mathcal{L}_M$:

$$S = \int \sqrt{g}\Big[-\frac{1}{2}M_P^2 R + \mathcal{L}_M\Big]d^4x = \int \sqrt{g}\Big[-\frac{1}{2\kappa}R + \mathcal{L}_M\Big]d^4x = S_G + S_M, \tag{6.20}$$

where $\kappa = 8\pi G = 1/(2M_P^2)$. From the action S, one obtains Einstein's field equations:

$$R_{\mu\nu} - \frac{1}{2}g_{\mu\nu}R = 8\pi G T_{\mu\nu}, \tag{6.21}$$

where $T_{\mu\nu}$ is an energy-stress tensor for matter fields:

$$T_{\mu\nu} = \frac{-2}{\sqrt{g}}\frac{\delta S_M}{\delta g^{\mu\nu}} = \frac{-2}{\sqrt{g}}\frac{\partial\big(\sqrt{g}\mathcal{L}_M\big)}{\partial g^{\mu\nu}} = -2\frac{\partial\mathcal{L}_M}{\partial g^{\mu\nu}} + g_{\mu\nu}\mathcal{L}_M. \tag{6.22}$$

Expanding the metric around the Minkowski background, $g_{\mu\nu} = \eta_{\mu\nu} + h_{\mu\nu}$, up to linear order in $h_{\mu\nu}$, (6.21) becomes [68,69]:

$$\Box\hat{h}_{\mu\nu} = -16\pi G T_{\mu\nu} = -\frac{1}{M_P^2}T_{\mu\nu}, \tag{6.23}$$

where $\hat{h}_{\mu\nu} = h_{\mu\nu} - \frac{1}{2}\eta_{\mu\nu}h$ is the so called trace-reversed perturbation variable with $h = h^\alpha_\alpha$. The gravity decoupling $M_P \to \infty$ provides a flat limit only if the energy-momentum tensor $T_{\mu\nu}$ does not contain powers of M_P higher than 2.

If one takes into account the analysis from the previous Section 6.1, then $\phi_0 \to \infty$ limit provides the Higgs potential (6.10), with zero Planck mass power. The only significant contribution to the $T_{\mu\nu}$ with non-zero Planck mass powers is the $\hat{\omega}_\mu$ mass term:

$$\frac{\mathcal{L}_M}{\sqrt{g}} \xrightarrow{M_P} \frac{q^2}{8}M_P^2\big(6+\alpha^2(1+\delta)\big)\hat{\omega}_\mu\hat{\omega}_\nu g^{\mu\nu}. \tag{6.24}$$

$$-2\frac{\partial\mathcal{L}_M}{\partial g^{\mu\nu}} + g_{\mu\nu}\mathcal{L}_M \xrightarrow{M_P} \frac{q^2}{8}M_P^2\big(6+\alpha^2(1+\delta)\big)\Big[g_{\mu\nu}\hat{\omega}_\alpha\hat{\omega}^\alpha - 2\hat{\omega}_\mu\hat{\omega}_\nu\Big] \tag{6.25}$$

Substituting the result to the equation (6.23) gives:

$$\Box\hat{h}_{\mu\nu} = \frac{q^2}{8}\big(6+\alpha^2(1+\delta)\big)\Big[-g_{\mu\nu}\hat{\omega}_\alpha\hat{\omega}^\alpha + 2\hat{\omega}_\mu\hat{\omega}_\nu\Big] + \mathcal{O}(M_P^{-1}). \tag{6.26}$$

The graviton couples to the Weyl vector boson but does not interact with the remaining matter sector. The contribution of the $\hat{\omega}_\mu$ field to the Einstein equation modifies the dynamics of metric perturbations. However, analyzing the individual terms in the Lagrangian (6.19), we find that taking the $M_P \to \infty$ limit has two significant implications:

- $-\frac{1}{2}M_P^2 R$: To keep the action finite as $M_P \to \infty$, the curvature R must approach zero. Since the strength of the gravitational interaction is given by $G \sim M_P^{-2}$, it effectively decreases to zero.

- $\frac{1}{8}q^2\Big[M_P^2+H^2\Big]\hat{\omega}_\mu\hat{\omega}^\mu$: The Higgs field is finite and independent of M_P, so in the $M_P\to\infty$ limit, the Planck mass term dominates the Weyl vector field mass term. Consequently, the $\hat{\omega}_\mu$ field acquires a very large mass, causing its dynamics to decouple from the low-energy effective theory.

Therefore, in the gravity decoupling limit, the Lagrangian (6.19) effectively reduces to:

$$\mathcal{L}_{eff}=\frac{1}{2}\partial_\mu H\partial^\mu H-V(H), \tag{6.27}$$

where the potential $V(H)$ is given by (6.10).

6.3. Weak Gravity Conjecture

The notion of the Weak Gravity Conjecture (WGC) originates from the Swampland program, which aims to determine the constraints required for quantum field theories to be consistently embedded in quantum gravity. Although Swampland conjectures are usually motivated by or validated within the string theory and black hole physics, they offer a way to validate theories of particle physics and cosmology beyond the Standard Model. While we do not consider the quantum gravity regime in this work, the WGC will serve as a qualitative check on the possible values of the conformal symmetry gauge coupling q. Here, we briefly review the application of WGC to a model with massless scalar fields. For a more detailed introduction to the Swampland program and the WGC, we refer the reader to Refs. [70–72]. The information presented below is derived from these references, while the final analysis applying the WGC to the specific Higgs−dilaton model is original.

The Weak Gravity Conjecture states that in a theory that is coupled to gravity with a gauge field, there must exist at least one charged state on which gravity acts as the weakest force. The charge in question can be of any type, specifically associated with the relevant gauge group. For instance, the electromagnetic charge is the charge of a particle under the electromagnetic gauge group $U(1)_{em}$. Considering the $U(1)$ gauge group as an example, provides a straightforward way to derive the inequality that expresses the WGC. The $U(1)$ force, mediated by a massless gauge boson, acting on a particle with mass m, charge q, and gauge coupling g, is given by:

$$F_g=\frac{1}{4\pi r^2}\Big(g\cdot q\Big)^2, \tag{6.28}$$

while the gravitational force is equal to:

$$F_G=\frac{1}{4\pi r^2}\left(\frac{m}{\sqrt{2}M_P}\right)^2, \tag{6.29}$$

with the gravitational charge being the mass m and the gravitational gauge coupling defined as $\big(\sqrt{2}M_P\big)^{-1}$. The WGC then leads to the condition:

$$F_g\geq F_G \quad \Rightarrow \quad \frac{m}{g\cdot q}\leq\sqrt{2}M_P. \tag{6.30}$$

This is known as the Electric WGC. The Magnetic WGC states that the cut-off Λ of a theory is bounded from above. The Magnetic WGC can be derived from equation (6.30) by considering a magnetic monopole with mass m_M instead of an electrically charged particle and changing the gauge coupling to its magnetic dual g^{-1}:

$$m_M\leq\frac{\sqrt{2}}{g}M_P. \tag{6.31}$$

The mass of a monopole is related to the cut-off of the theory as $m_M \sim \frac{\Lambda}{g^2}$ leading to:

$$\Lambda \lesssim g \cdot M_P. \tag{6.32}$$

This implies that if the gauge coupling g is set to zero, restoring a global symmetry, the cut-off also goes to zero, invalidating such theory. This statement is connected to the broader Swampland conjecture, which claims that there are no global symmetries in a consistent Quantum Gravity theory. Every symmetry must be either broken or gauged.

The equations (6.30) and (6.32) apply only to theories with a single $U(1)$ symmetry and a massless gauge boson. Application to more complex theories requires some modifications to the WGC. Here, we list three relevant to our work:

- **Massive gauge field:** If the gauge field is massive, with mass M_g, the gauge potential V_g changes, resulting in a modified force:

$$V_g = e^{-M_g \cdot r} \cdot \frac{g^2 \cdot q^2}{4\pi r} \quad \Rightarrow \quad F_g = -\frac{d}{dr} V_g = \frac{e^{-M_g \cdot r}}{4\pi r^2}\Big(1 + M_g \cdot r\Big)\big(g \cdot q\big)^2. \tag{6.33}$$

The above formula for the gauge force applies to any gauge theory where the gauge boson has a mass M_g and a momentum-space propagator of the form $\frac{1}{k^2+M_g^2}$. It is relevant for any $U(1)$, $SU(2)$, etc. group as well as for continuous non-compact groups like the dilatation group isomorphic to $\mathbb{R}_+$.

- **Multiple gauge symmetries:** For theories with multiple gauge symmetries with gauge couplings g_a, for each particle with mass m_i, one can define a vector:

$$\vec{Q}_i = \frac{\vec{q}_i \cdot M_P}{m_i}, \qquad \vec{q}_i = \big(g_{i,1} \cdot q_{i,1}, g_{i,2} \cdot q_{i,2}, \dots\big), \tag{6.34}$$

where $\vec{q}_i$ is the charge vector in the gauge space for the i-th particle. The WGC states that the convex hull of the $\vec{Q}_i$ vectors must contain the unit ball. This is a rather rigorous requirement, so a weaker version can be considered: for each particle, the condition is:

$$|\vec{Q}_i| \geq 1. \tag{6.35}$$

This ensures that each particle's $\vec{Q}_i$ vector satisfies the WGC condition individually, which is more easily verifiable than the convex hull condition.

- **Massless scalar fields:** To incorporate massless scalar fields into a theory, let's consider a different interpretation of the Electric WGC inequality. For two particles of the same kind, the gauge force between them is self-repulsive, while gravity is self-attractive. The Electric WGC (6.30) implies that those particles should be self-repelling. This observation leads to a modification of (6.30) in the presence of massless scalar fields, which introduce an additional self-attractive force. If the massless scalar fields s_i have a field metric k_{ij}, with kinetic term $k_{ij}\partial_\mu s^i \partial^\mu s^j$, and the massive particle considered in the WGC inequality have field dependent mass $m(s_i)$ with ground state value $m(\langle s_i \rangle) = m$, then the force mediated by massless scalars is:

$$F_S = \frac{1}{4\pi r^2}\mu^2, \tag{6.36}$$

where μ is the scalar interaction strength, defined as:

$$\mu^2 = k_{ij}\mu^i\mu^j\Big|_{\langle s_i \rangle}, \qquad \mu^i = \frac{\partial}{\partial s_i} m(s_i). \tag{6.37}$$

Consequently, for the two identical particles to be self-repulsive, the WGC is modified to:

$$\sum_i F_{g_i} \geq F_G + F_S, \tag{6.38}$$

where F_{g_i} are the forces associated with gauge groups. This is the so-called Repulsive Force Condition, which ensures that the gauge repulsion is stronger than the attractive forces between two identical charged states.

In this work, we want to apply the refined WGC for our theory with a massless dilaton scalar state and massive Higgs scalar, both coupled to a gauge boson ω_μ, to find constraints on the values of Weyl gauge coupling q. First, one has to transform the Lagrangian (6.17) to a form in which the mass eigenstates are manifested. Using (6.7) and neglecting the gravity part, one obtains:

$$\begin{aligned}\mathcal{L}_{GH\omega} =& -\frac{1}{4}\tilde{F}_{\mu\nu}\tilde{F}^{\mu\nu} + \frac{q^2}{8}\Big(6M_P^2 + G^2 + H^2\Big)\hat{\omega}_\mu\hat{\omega}^\mu + \\ &+ \frac{1}{2}\frac{\big(6M_P^2 + H^2\big)\big(\partial_\mu G\big)^2 - 2GH\partial_\mu G\partial^\mu H + \big(6M_P^2 + G^2\big)\big(\partial_\mu H\big)^2}{6M_P^2 + G^2 + H^2} - V(G,H).\end{aligned} \tag{6.39}$$

Note that we didn't expand the Lagrangian around the ground state $\phi_i = v_i + \tilde{\phi}_i$, so the mass eigenstates G, H have non-zero vevs. The potential $V(G,H)$ is given by:

$$V(G,H) = 4\lambda_2\delta H^4\left(\frac{G}{H} + \frac{1-\delta}{2\sqrt{\delta}}\right)^2, \qquad \langle H\rangle = 0, \tag{6.40}$$

where $\langle H\rangle = 0$ correspond to proper values of ϕ_i fields vevs, i.e., $\langle\phi_1^2\rangle = \delta\langle\phi_0^2\rangle$. The Planck mass in terms of $\langle G\rangle$, using (6.18), reads:

$$M_P^2 = \frac{1}{6}\frac{1}{\big(1+\delta\big)}\big(\xi_0 + \delta\xi_1\big)\langle G^2\rangle. \tag{6.41}$$

The field metric for scalars k_{ij} is given by:

$$k_{ij} = \frac{1}{2}\frac{1}{6M_P^2 + G^2 + H^2}\begin{pmatrix} 6M_P^2 + H^2 & -GH \\ -GH & 6M_P^2 + G^2\end{pmatrix}. \tag{6.42}$$

Since μ^2 from (6.37) is evaluated at the ground state, using (6.40), (6.41), and expanding in δ, we obtain:

$$k_{ij} = \frac{1}{2}\begin{pmatrix} \frac{\xi_0}{\xi_0+1} & 0 \\ 0 & 1\end{pmatrix} + \mathcal{O}\Big(\frac{\delta}{\xi_0}\Big). \tag{6.43}$$

Consequently, the massless G scalar has a separate kinetic term, equal to:

$$\frac{1}{2}\frac{\xi_0}{\xi_0+1}\cdot\partial_\mu G\partial^\mu G = k_{GG}\cdot\partial_\mu G\partial^\mu G. \tag{6.44}$$

The scalar dependent mass of a massive H state is the eigenvalue of the second derivative matrix derived from $V(G,H)$ potential:

$$\begin{aligned}&m_H^2(G,H) = 12\lambda_2 H^2 + 24\lambda_2\sqrt{\delta}\cdot GH + 4\lambda_2\delta\big(2G^2 - 3H^2\big) + \mathcal{O}\big(\delta^{3/2}\big),\\ &m_H^2(\langle G\rangle,\langle H\rangle) = m_H^2 = 8\lambda_2\delta\langle G^2\rangle.\end{aligned} \tag{6.45}$$

Then, the scalar interaction strength reads:

$$\mu^2 = k_{GG}\cdot\left(\frac{\partial m_H(G,H)}{\partial G}\right)^2\Bigg|_{\langle G\rangle} = \frac{4\lambda_2\delta\xi_0}{1+\xi_0}. \tag{6.46}$$

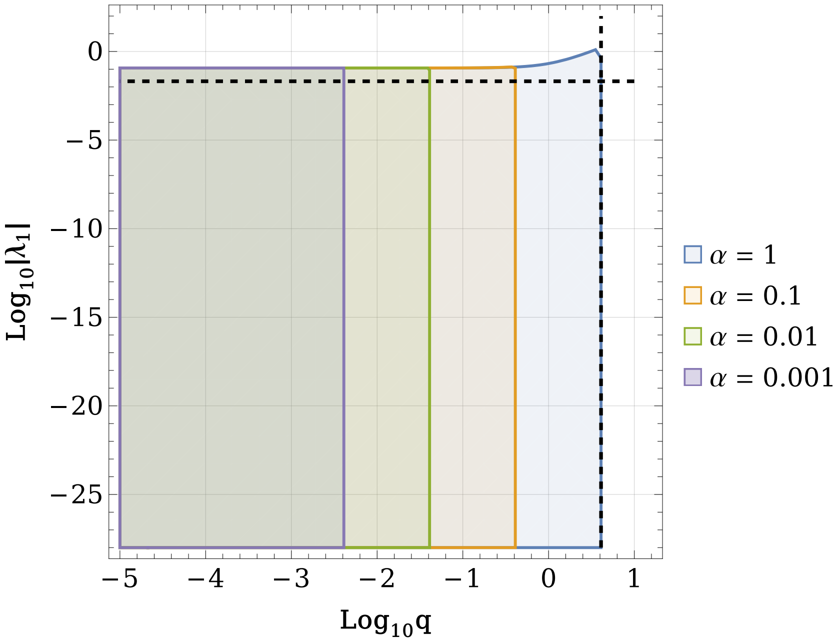

Figure 6.1: The constraints on λ_1 and q values, resulting from the WGC inequality for the H state (6.50). Different values of α reflect different energy scales, as $E \sim \frac{1}{r} = \frac{1}{\alpha \cdot r_\omega} = \sqrt{\frac{3}{2}}\frac{q}{\alpha}M_P$ (see discussion after equation (6.51)). Black dashed lines mark $q = 4\sqrt{\frac{\pi}{3}}$, the value for which $m_\omega = \sqrt{8\pi}M_P$, and $\lambda_1 = -\frac{1}{48}$, the boundary value obtained in Section 5.2.1 from equation (5.44)

The charges of the H state for each gauge group are the same as for the ϕ_1 Higgs neutral component, which couples directly to the SM particles, and read:

$$\begin{aligned} SU(2)_L: &\qquad g_{SU(2)} = g_2, &\qquad q_{SU(2)} = -\frac{1}{2}, \\ U(1)_Y: &\qquad g_{U(1)} = g_1, &\qquad q_{U(1)} = 1, \\ \omega_\mu: &\qquad g_\omega = q, &\qquad q_\omega = \frac{1}{2}. \end{aligned} \tag{6.47}$$

First, we check the simplified version of the convex hull condition. The charge vector for the H field equals:

$$\vec{Q}_H = \frac{M_P}{m_H}\left(-\frac{1}{2}g_2, g_1, \frac{q}{2}\right), \tag{6.48}$$

$$|\vec{Q}_H| = \frac{1}{8\sqrt{3}}\sqrt{\frac{(4g_1^2 + g_2^2 + q^2)(\xi_0 + \delta\xi_1)}{\delta\lambda_2(1+\delta)}}. \tag{6.49}$$

The condition $|Q_H| \geq 1$ is fulfilled for any q and λ_1, ξ_0, ξ_1 values. Note that this result does not include the effects of the massless scalar force contribution nor the fact that the Weyl gauge force is mediated by a massive particle.

The proper WGC, with the F_S force, has the form:

$$F_\omega + F_{g_1} + F_{g_2} \geq F_G + F_S, \tag{6.50}$$

where F_{g_i} are forces associated with SM gauge groups, F_G is the gravity force and F_S is the force mediated by massless scalar G. The Weyl vector field has a mass $m_\omega^2 = \frac{3}{2}q^2M_P^2$ (see, Lagrangian (6.15)), and the Weyl force equals:

$$F_\omega = \frac{q^2/4}{4\pi r^2}\left(1 + m_\omega \cdot r\right) \cdot e^{-m_\omega \cdot r}. \tag{6.51}$$

The interaction range for F_ω force is given by $r_\omega = m_\omega^{-1}$. We check the WGC condition (6.50) for $r = \alpha \cdot r_\omega$, for $0 < \alpha \leq 1$ and $r_{M_P} \leq r \leq r_{EW}$, where $r_{M_P} = \left(\sqrt{8\pi} M_P\right)^{-1}$ and $r_{EW} = (125 \text{ GeV})^{-1}$ are lengths associated with the Planck mass scale[1] M_P and electroweak scale respectively. Therefore, we consider energies above the EW scale and below the quantum gravity effects. Consequently, F_{g_i} are mediated by massless gauge bosons and have the following form:

$$F_{g_i} = \frac{g_i^2 q_H^2}{4\pi r^2}. \tag{6.52}$$

Figure 6.1 illustrates the q and λ_1 constraints obtained from (6.50), where the parameter space relations from Section 5.2.1 were used. For $r = \alpha \cdot r_\omega$, the Weyl gauge force has a form:

$$4\pi r^2 \cdot F_\omega\big(r = \alpha \cdot r_\omega\big) = \frac{q^2}{4}\big(1+\alpha\big)e^{-\alpha}, \tag{6.53}$$

and is a decreasing function of α. Consequently, larger values of α allow larger values of q that still satisfy the bound (6.50). We conclude that there exist values of q for which the Weyl vector field mass reaches the Planck mass scale, $m_\omega \approx M_P$. This supports the assumption made in Chapter 5 that the ω_μ field decouples from the low-energy theory for scales below M_P.

[1] Thorough the work, we use the reduced Planck mass $M_P = 2.44 \cdot 10^{18}$ GeV, whereas the approximate quantum gravity cutoff is equal to $\sqrt{8\pi} M_P = 1.22 \cdot 10^{19}$ GeV.

Chapter 7

Quantum Field Theory in Finite Temperature

7.1. Motivation

Quantum field theory at finite temperature is an essential framework for understanding the behavior of matter and energy in the hot, evolving universe. While conventional quantum field theory offers valuable insights into the fundamental nature of particles and their interactions, it overlooks a significant aspect—the thermal nature of the universe throughout its evolution. Ignoring the influence of temperature can result in incomplete descriptions of phenomena crucial in high-energy physics and cosmology. Quantum field theory at finite temperature allows us to account for the effects of thermal equilibrium, thermal fluctuations, and the creation and annihilation of particles in a hot environment. By incorporating temperature into the theoretical framework, we can gain a deeper understanding of phase transitions, thermalization processes, and the behavior of matter under extreme conditions. Therefore, quantum field theory at finite temperature must not be neglected to fully comprehend the complexity of the universe's thermal evolution. The material presented in this chapter is not original and is derived from existing articles and books [32,73–78], which serve as excellent resources in the field of finite-temperature quantum field theory.

7.2. Review of Quantum Statistical Mechanics

In this section, we will shortly review the concepts from Quantum Statistical Mechanics essential to describe a dynamical system in thermal equilibrium characterized by a time-independent Hamiltonian $\hat{H}$ and a set of conserved charges $\hat{Q}_i$. One of these concepts is the notion of an ensemble:

- **the microcanonical ensemble** describes an isolated system which has fixed energy E, particle number N and volume V;
- **the canonical ensemble** is used to describe a system in contact with a heat reservoir at temperature T, can exchange the energy with it and T, N, and V are fixed;
- **the great canonical ensemble** specifies a system that can exchange energy and particles with the heat reservoir, and T, V, and chemical potentials μ_i are fixed.

To describe the evolution of a system in the hot Universe, where chemical potentials are negligible, the right variant is the canonical ensemble. With this choice, the fundamental object in equilibrium statistical mechanics, the so-called density matrix $\hat{\rho}$, is of the form:

$$\hat{\rho} = \exp\big\{ -\beta\hat{H}\big\}, \tag{7.1}$$

where $\beta = T^{-1}$. It is used to calculate an ensemble average of any specified observable, represented by the operator $\hat{A}$, giving its expectation value:

$$\langle \hat{A} \rangle = A = \frac{\mathrm{Tr}\big[\hat{\rho}\hat{A}\big]}{\mathrm{Tr}\big[\hat{\rho}\big]}, \tag{7.2}$$

where Tr is a trace operation:

$$\mathrm{Tr}\big[\dots\big] = \sum_{\alpha} \langle \alpha | \dots | \alpha \rangle \tag{7.3}$$

and the sum is performed over a complete set of states of the system under consideration. The partition function, which carries complete information on the thermodynamic properties of the system in equilibrium, is defined as:

$$Z(T) = \mathrm{Tr}\big[\hat{\rho}\big]. \tag{7.4}$$

It is connected to fundamental quantities such as the system's average energy U, pressure p, particle number N_i, and entropy S:

$$U = \langle \hat{H} \rangle = \frac{\mathrm{Tr}\big[\hat{\rho}\hat{H}\big]}{\mathrm{Tr}\big[\hat{\rho}\big]} = \frac{1}{Z(T)}\mathrm{Tr}\big[e^{-\beta\hat{H}}\hat{H}\big] = -\frac{d}{d\beta}\ln Z(T), \tag{7.5}$$

$$p = T\frac{\partial\big(\ln Z(T)\big)}{\partial V}, \tag{7.6}$$

$$N_i = \frac{\partial\big(T\ln Z(T)\big)}{\partial \mu_i}, \tag{7.7}$$

$$S = \frac{\partial\big(T\ln Z(T)\big)}{\partial T}. \tag{7.8}$$

7.3. Imaginary Time Formalism and Green's functions

There are two equivalent formulations of statistical QFT: the imaginary-time or Matsubara formalism and the real-time or Keldysh-Schwinger formalism. In this work, we employ the Matsubara method, which was introduced by Matsubara in 1955 [79]. We will also work in the Heisenberg picture.

The basic idea of the Matsubara imaginary time formalism is that the density matrix $\hat{\rho}$ can be treated as a quantum evolution operator for an imaginary time from $t = 0$ to $t = -i\beta$ so that we have:

$$\hat{\rho} = e^{-\beta\hat{H}} \quad \longrightarrow \quad e^{-i\hat{H}t} \qquad \text{for } -i\beta < t < 0. \tag{7.9}$$

The justification of the above statement will become apparent in the later analysis in this section and comes from the periodicity of the two-point Green's function. We introduce the following notation: t stands for the imaginary time variable, so $-i\beta < t < 0$ and $\tau = it$ stands for the real time variable and $0 < \tau < \beta$. From now on, we will omit the hats when denoting operators.

7.3.1. Scalar Fields

Consider a real scalar field operator $\phi(x)$ with a time-independent Hamiltonian H. Its time evolution satisfies:

$$\phi(x) = \phi(\vec{x}, t) = e^{iHt}\phi(\vec{x}, 0)e^{-iHt} = e^{H\tau}\phi(\vec{x}, 0)e^{-H\tau}. \tag{7.10}$$

We define the temperature Green's function for n scalar field operators as:

$$G^{(n)}(x_1, \dots, x_n) \equiv \langle \mathcal{T}\phi(x_1), \dots, \phi(x_n) \rangle, \tag{7.11}$$

where $\langle \ldots \rangle$ denotes the ensemble average:

$$\langle \ldots \rangle = \frac{1}{Z} \mathrm{Tr}\Big[e^{-\beta H} \ldots\Big], \tag{7.12}$$

and $\mathcal{T}$ represents time ordering in the complex plane:

$$\begin{aligned} \mathcal{T}\phi(x_1)\phi(x_2) = \mathcal{T}\phi(\vec{x_1}, -i\tau_1)\phi(\vec{x_2}, -i\tau_2) \quad &= \quad \Theta(\tau_1 - \tau_2)\phi(\vec{x_1}, -i\tau_1)\phi(\vec{x_2}, -i\tau_2) \\ &+ \quad \Theta(\tau_2 - \tau_1)\phi(\vec{x_2}, -i\tau_2)\phi(\vec{x_1}, -i\tau_1). \end{aligned} \tag{7.13}$$

For a translationally invariant system, the two-point Green's function $G^{(2)}(x_1, x_2)$ can be denoted as:

$$G^{(2)}(x_1, x_2) \quad \longrightarrow \quad \Delta(\vec{x}, \tau) = \langle \mathcal{T}\phi(\vec{x}, -i\tau)\phi(\vec{0}, 0)\rangle. \tag{7.14}$$

The relation $0 < \tau < \beta$ (and from it $-i\beta < t < 0$), comes from the fact that $\Delta(\vec{x}, \tau)$ is periodic in τ with period β:

$$\begin{aligned} \Delta(\vec{x}, \tau) =& \frac{1}{Z}\mathrm{Tr}\Big[e^{-\beta H}\mathcal{T}\phi(\vec{x}, -i\tau)\phi(\vec{0}, 0)\Big] = \frac{1}{Z}\mathrm{Tr}\Big[e^{-\beta H}\phi(\vec{x}, -i\tau)\phi(\vec{0}, 0)\Big] = \\ =& \frac{1}{Z}\mathrm{Tr}\Big[\phi(\vec{0}, 0)e^{-\beta H}\phi(\vec{x}, -i\tau)\Big] = \frac{1}{Z}\mathrm{Tr}\Big[e^{-\beta H}e^{\beta H}\phi(\vec{0}, 0)e^{-\beta H}\phi(\vec{x}, -i\tau)\Big] = \\ =& \frac{1}{Z}\mathrm{Tr}\Big[e^{-\beta H}\phi(\vec{0}, -i\beta)\phi(\vec{x}, -i\tau)\Big] = \frac{1}{Z}\mathrm{Tr}\Big[e^{-\beta H}\mathcal{T}\phi(\vec{x}, -i\tau)\phi(\vec{0}, -i\beta)\Big] = \\ =& \Delta(\vec{x}, \tau - \beta). \end{aligned} \tag{7.15}$$

The equality $\Delta(\vec{x}, \tau) = \Delta(\vec{x}, \tau - \beta)$ is known as the Kubo-Martin-Schwinger relation. Let's introduce two additional Green's functions:

$$\Delta^{+}(\vec{x}, \tau) \equiv \langle \phi(\vec{x}, -i\tau)\phi(\vec{0}, 0)\rangle, \tag{7.16}$$

$$\Delta^{-}(\vec{x}, \tau) \equiv \langle \phi(\vec{0}, 0)\phi(\vec{x}, -i\tau)\rangle, \tag{7.17}$$

so that:

$$\Delta(\vec{x}, \tau) = \Theta(\tau)\Delta^{+}(\vec{x}, \tau) + \Theta(-\tau)\Delta^{-}(\vec{x}, \tau). \tag{7.18}$$

In the next part, we will find formulas for $\Delta^{\pm}(\vec{x}, \tau)$ in order to obtain $\Delta(\vec{x}, \tau)$ for scalar fields from (7.18).

Free scalar field plane wave decomposition reads:

$$\phi(x) = \int \frac{d^3k}{(2\pi)^3}\frac{1}{\sqrt{2\omega_k}}\Big[a(\vec{k})e^{-ikx} + a^{\dagger}(\vec{k})e^{ikx}\Big], \tag{7.19}$$

where $k^{\mu} = (\omega_k, \vec{k})$ and $\omega_k^2 = \vec{k}^2 + m^2$. The normally ordered Hamiltonian for the scalar field is:

$$H = \int \frac{d^3k}{(2\pi)^3}\omega_k a^{\dagger}(\vec{k})a(\vec{k}). \tag{7.20}$$

Equal time commutation relations for field operators are:

$$\big[\phi(\vec{x}, t), \dot{\phi}(\vec{y}, t)\big] = i\delta^{(3)}(\vec{x} - \vec{y}), \qquad \big[\phi(\vec{x}, t), \phi(\vec{y}, t)\big] = \big[\dot{\phi}(\vec{x}, t), \dot{\phi}(\vec{y}, t)\big] = 0, \tag{7.21}$$

which gives commutation relations for creation and annihilation operators:

$$\big[a(\vec{p}), a^{\dagger}(\vec{k})\big] = (2\pi)^3\delta^{(3)}(\vec{p} - \vec{k}), \qquad \big[a(\vec{p}), a(\vec{k})\big] = \big[a^{\dagger}(\vec{p}), a^{\dagger}(\vec{k})\big] = 0. \tag{7.22}$$

In Appendix B, we derive the ensemble averages for the products of $a(\vec{p})$ and $a^{\dagger}(\vec{p})$. The results obtained are as follows:

$$\begin{aligned} &\langle a(\vec{p})a(\vec{k})\rangle = \langle a^{\dagger}(\vec{p})a^{\dagger}(\vec{k})\rangle = 0, \\ &\langle a(\vec{p})a^{\dagger}(\vec{k})\rangle = [1 + n_B(\omega_k)](2\pi)^3\delta^{(3)}(\vec{p} - \vec{k}), \\ &\langle a^{\dagger}(\vec{p})a(\vec{k})\rangle = n_B(\omega_k)(2\pi)^3\delta^{(3)}(\vec{p} - \vec{k}), \end{aligned} \tag{7.23}$$

where $n_B(\omega_k)$ is the Bose-Einstein distribution function:

$$n_B(\omega_k) = \frac{1}{e^{\beta\omega_k} - 1}. \tag{7.24}$$

From (7.23), we see, that the n_B is the eigenvalue of the number operator $N = a^\dagger a$.

Explicit evaluation of $\Delta^+(\vec{x}, \tau)$ gives:

$$\begin{aligned}
\Delta^+(\vec{x}, \tau) = & \int \frac{d^3p}{(2\pi)^3} \frac{d^3k}{(2\pi)^3} \frac{1}{2\sqrt{\omega_p\omega_k}} \langle \left[a(\vec{p})e^{-ipx} + a^\dagger(\vec{p})e^{ipx}\right] \cdot \left[a(\vec{k}) + a^\dagger(\vec{k})\right]\rangle = \\
= & \int \frac{d^3p}{(2\pi)^3} \frac{d^3k}{(2\pi)^3} \frac{1}{2\sqrt{\omega_p\omega_k}} \left[e^{-ipx}\langle a(\vec{p})a^\dagger(\vec{k})\rangle + e^{ipx}\langle a^\dagger(\vec{p})a(\vec{k})\rangle\right] = \\
= & \int \frac{d^3p}{(2\pi)^3} \frac{d^3k}{(2\pi)^3} \frac{1}{2\sqrt{\omega_p\omega_k}} \left[e^{-ipx}[1 + n_B(\omega_k)] + e^{ipx} n_B(\omega_k)\right](2\pi)^3\delta^{(3)}(\vec{p} - \vec{k}) = \\
= & \int \frac{d^3k}{(2\pi)^3} \frac{1}{2\omega_k} \left[e^{-\omega_k\tau} e^{i\vec{k}\cdot\vec{x}}[1 + n_B(\omega_k)] + e^{\omega_k\tau} e^{-i\vec{k}\cdot\vec{x}} n_B(\omega_k)\right].
\end{aligned} \tag{7.25}$$

Same calculation for $\Delta^-(\vec{x}, \tau)$ gives:

$$\Delta^-(\vec{x}, \tau) = \int \frac{d^3k}{(2\pi)^3} \frac{1}{2\omega_k} \left[e^{-\omega_k\tau} e^{i\vec{k}\cdot\vec{x}} n_B(\omega_k) + e^{\omega_k\tau} e^{-i\vec{k}\cdot\vec{x}}[1 + n_B(\omega_k)]\right]. \tag{7.26}$$

From equation (7.18) we obtain:

$$\begin{aligned}
\Delta(\vec{x}, \tau) = \int \frac{d^3k}{(2\pi)^3} \frac{1}{2\omega_k} \Bigg[& n_B(\omega_k) \cdot \left(e^{-\omega_k\tau} e^{i\vec{k}\cdot\vec{x}} + e^{\omega_k\tau} e^{-i\vec{k}\cdot\vec{x}}\right) + \\
& + \left(\Theta(\tau) e^{-\omega_k\tau} e^{i\vec{k}\cdot\vec{x}} + \Theta(-\tau) e^{\omega_k\tau} e^{-i\vec{k}\cdot\vec{x}}\right)\Bigg].
\end{aligned} \tag{7.27}$$

The Fourier transformation of $\Delta(\vec{x}, \tau)$ is:

$$\Delta(\vec{p}, \omega_n) \equiv \int_0^\beta d\tau \int d^3x e^{i(\omega_n\tau - \vec{p}\cdot\vec{x})} \Delta(\vec{x}, \tau), \tag{7.28}$$

and its inverse:

$$\Delta(\vec{x}, \tau) = \frac{1}{\beta} \sum_{n=-\infty}^{n=+\infty} \int \frac{d^3p}{(2\pi)^3} e^{-i(\omega_n\tau - \vec{p}\cdot\vec{x})} \Delta(\vec{p}, \omega_n), \tag{7.29}$$

where the periodicity constraint $\Delta(\vec{x}, \tau) = \Delta(\vec{x}, \tau + \beta)$ causes the Fourier expansion to be no longer a continuous integral but a discrete Fourier series instead:

$$\int \frac{d^4k}{(2\pi)^4} \quad \longrightarrow \quad \frac{1}{\beta} \sum_{n=-\infty}^{n=+\infty} \int \frac{d^3k}{(2\pi)^3} \tag{7.30}$$

with:

$$e^{-i\omega_n\tau} = e^{-i\omega_n(\tau+\beta)} \qquad \Rightarrow \qquad \omega_n \equiv \frac{2\pi n}{\beta} = 2\pi T n, \tag{7.31}$$

and ω_n being the so-called Matsubara frequencies. Using the formula for $\Delta(\vec{x}, \tau)$ in equation (7.27), we can perform the Fourier transformation in (7.28). For the τ variable, we have the integral:

$$\int_0^\beta d\tau \; e^{\tau(i\omega_n \pm \omega_k)} = \frac{e^{\beta(i\omega_n \pm \omega_k)} - 1}{i\omega_n \pm \omega_k} = \frac{e^{\pm\beta\omega_k} - 1}{i\omega_n \pm \omega_k}, \tag{7.32}$$

where we used the fact that $e^{i\beta\omega_n} = e^{2\pi i n} = 1$. Note, that the τ integral is performed from 0 to β and $\tau > 0$, so $\Theta(\tau) = 1$ and $\Theta(-\tau) = 0$. To avoid confusion, we remind that $\omega_n = 2\pi T n$ and $\omega_k = \sqrt{\vec{k}^2 + m^2}$. For the $\vec{x}$ variable, we get:

$$\int d^3x\; e^{-i(\vec{p}\pm\vec{k})\cdot\vec{x}} = (2\pi)^2\delta^{(3)}(\vec{p}\pm\vec{k}). \tag{7.33}$$

Then:

$$\begin{aligned}
&\Delta(\vec{p},\omega_n) = \\
&= \int \frac{d^3k}{(2\pi)^3}\frac{1}{2\omega_k}\left[\big(n_B(\omega_k)+1\big)\frac{e^{-\beta\omega_k}-1}{i\omega_n-\omega_k}(2\pi)^3\delta^{(3)}(\vec{p}-\vec{k}) + n_B(\omega_k)\frac{e^{\beta\omega_k}-1}{i\omega_n+\omega_k}(2\pi)^3\delta^{(3)}(\vec{p}+\vec{k})\right] \\
&= \frac{1}{2\omega_p}\left[\big(n_B(\omega_p)+1\big)\frac{e^{-\beta\omega_p}-1}{i\omega_n-\omega_p} + n_B(\omega_p)\frac{e^{\beta\omega_p}-1}{i\omega_n+\omega_p}\right] = \frac{1}{2\omega_p}\left[\frac{-1}{i\omega_n-\omega_p}+\frac{1}{i\omega_n+\omega_p}\right] \\
&= \frac{1}{\omega_n^2+\omega_p^2} = \frac{1}{\vec{p}^2+m^2+\omega_n^2},
\end{aligned} \tag{7.34}$$

where in the second line we used the fact that $\omega_p = \sqrt{\vec{p}^2+m^2} = \sqrt{(\vec{-p})^2+m^2} = \omega_{-p}$ and substituted $n_B(\omega) = (e^{\beta\omega}-1)^{-1}$. Using (7.29) and (7.34), we get:

$$\begin{aligned}
&\Delta(\vec{x},\tau) = \\
&= \frac{1}{\beta}\sum_{n=-\infty}^{n=+\infty}\int\frac{d^3p}{(2\pi)^3}e^{-i(\omega_n\tau-\vec{p}\cdot\vec{x})}\frac{1}{\vec{p}^2+m^2+\omega_n^2} = \frac{i}{\beta}\sum_{n=-\infty}^{n=+\infty}\int\frac{d^3p}{(2\pi)^3}e^{-i(\omega_n\tau-\vec{p}\cdot\vec{x})}\frac{-i}{\vec{p}^2+m^2+\omega_n^2} \\
&= \frac{i}{\beta}\sum_{n=-\infty}^{n=+\infty}\int\frac{d^3p}{(2\pi)^3}e^{-i(\omega_n\tau-\vec{p}\cdot\vec{x})}\frac{i}{(i\omega_n)^2-\vec{p}^2-m^2} = \frac{i}{\beta}\sum_{n=-\infty}^{n=+\infty}\int\frac{d^3p}{(2\pi)^3}e^{-i(\omega_n\tau-\vec{p}\cdot\vec{x})}\frac{i}{p^2-m^2},
\end{aligned} \tag{7.35}$$

where, to get the proper i factor in the propagator, we multiplied by $-i^2 = 1$. Notice, that the thermal four-momentum has a discrete 0−th component, given by $p^\mu = (i\omega_n, \vec{p})$. All the propagators and the complete Feynman rules, including those for fermions, are provided in Table 7.1.

7.3.2. Fermion Fields

Consider a complex fermion field operator $\psi(x)$ with time-independent Hamiltonian H. Its time evolution, similarly to bosons, satisfies:

$$\psi(x) = \psi(\vec{x},t) = e^{iHt}\psi(\vec{x},0)e^{-iHt} = e^{H\tau}\psi(\vec{x},0)e^{-H\tau}. \tag{7.36}$$

In contrast to bosons, fermionic fields fulfill anti-commutation relations. Therefore, to obtain the Lorentz invariant Feynman propagator, we have to change the time ordering formula (7.13) to:

$$\begin{aligned}
\mathcal{T}_F\psi(x_1)\bar{\psi}(x_2) = \mathcal{T}_F\psi(\vec{x_1},-i\tau_1)\bar{\psi}(\vec{x_2},-i\tau_2) \;&=\; \Theta(\tau_1-\tau_2)\psi(\vec{x_1},-i\tau_1)\bar{\psi}(\vec{x_2},i\tau_2) \\
&-\; \Theta(\tau_1-\tau_2)\bar{\psi}(\vec{x_2},i\tau_2)\psi(\vec{x_1},-i\tau_1).
\end{aligned} \tag{7.37}$$

Analogously, we define the two-point Green's function as:

$$\Delta_F(\vec{x},\tau) = \langle\mathcal{T}_F\psi(\vec{x},-i\tau)\bar{\psi}(\vec{0},0)\rangle. \tag{7.38}$$

Anti-commuting relations imply anti-periodicity of $\Delta_F(\vec{x},\tau)$ in τ with period β:

$$\begin{aligned}\Delta_F(\vec{x},\tau) =&\frac{1}{Z}\mathrm{Tr}\Big[e^{-\beta H}\mathcal{T}_F\psi(\vec{x},-i\tau)\bar{\psi}(\vec{0},0)\Big] = \frac{1}{Z}\mathrm{Tr}\Big[e^{-\beta H}\psi(\vec{x},-i\tau)\bar{\psi}(\vec{0},0)\Big] = \\ =&\frac{1}{Z}\mathrm{Tr}\Big[\bar{\psi}(\vec{0},0)e^{-\beta H}\psi(\vec{x},-i\tau)\Big] = \frac{1}{Z}\mathrm{Tr}\Big[e^{-\beta H}e^{\beta H}\bar{\psi}(\vec{0},0)e^{-\beta H}\psi(\vec{x},-i\tau)\Big] = \\ =&\frac{1}{Z}\mathrm{Tr}\Big[e^{-\beta H}\bar{\psi}(\vec{0},-i\beta)\psi(\vec{x},-i\tau)\Big] = \frac{1}{Z}\mathrm{Tr}\Big[e^{-\beta H}(-1)\cdot\mathcal{T}_F\psi(\vec{x},-i\tau)\bar{\psi}(\vec{0},-i\beta)\Big] = \\ =&-\Delta_F(\vec{x},\tau-\beta),\end{aligned} \tag{7.39}$$

so that the Kubo-Martin-Schwinger relation for fermions reads $\Delta_F(\vec{x},\tau) = -\Delta_F(\vec{x},\tau-\beta)$. We introduce two additional Green's functions:

$$\Delta_F^+(\vec{x},\tau) \equiv \langle\psi(\vec{x},-i\tau)\bar{\psi}(\vec{0},0)\rangle, \tag{7.40}$$

$$\Delta_F^-(\vec{x},\tau) \equiv \langle\bar{\psi}(\vec{0},0)\psi(\vec{x},-i\tau)\rangle, \tag{7.41}$$

for which:

$$\Delta_F(\vec{x},\tau) = \Theta(\tau)\Delta_F^+(\vec{x},\tau) - \Theta(-\tau)\Delta_F^-(\vec{x},\tau). \tag{7.42}$$

Free fermion field plane wave decomposition reads:

$$\psi(x) = \sum_s\int\frac{d^3k}{(2\pi)^3}\frac{1}{\sqrt{2\omega_k}}\Big[a_s(\vec{k})u_s(\vec{k})e^{-ikx} + b_s^\dagger(\vec{k})v_s(\vec{k})e^{ikx}\Big], \tag{7.43}$$

$$\bar{\psi}(x) = \sum_s\int\frac{d^3k}{(2\pi)^3}\frac{1}{\sqrt{2\omega_k}}\Big[a_s^\dagger(\vec{k})\bar{u}_s(\vec{k})e^{ikx} + b_s(\vec{k})\bar{v}_s(\vec{k})e^{-ikx}\Big], \tag{7.44}$$

where $u_s(\vec{k})$ and $v_s(\vec{k})$ are free solutions of the Dirac equation, $(i\partial\!\!\!/ - m)\psi(x) = 0$, fulfilling:

$$\sum_s u_s(\vec{k})\bar{u}_s(\vec{k}) = k\!\!\!/ + m, \qquad\qquad \sum_s v_s(\vec{k})\bar{v}_s(\vec{k}) = k\!\!\!/ - m, \tag{7.45}$$

and s denotes two different spin states. Dispersion relation with four-momentum $k^\mu = (\omega_k,\vec{k})$ is $\omega_k^2 = \vec{k} + m^2$. The normally ordered Hamiltonian for the fermion field is:

$$H = \int\frac{d^3k}{(2\pi)^3}\omega_k\left(\sum_s a_s^\dagger(\vec{k})a_s(\vec{k}) + \sum_s b_s^\dagger(\vec{k})b_s(\vec{k})\right), \tag{7.46}$$

where $a_s^\dagger(\vec{k})a_s(\vec{k})$ represents the contribution from particles (fermions) and $b_s^\dagger(\vec{k})b_s(\vec{k})$ represents the contribution from antiparticles (antifermions). Equal time anti-commutation relations for fermion field operators are:

$$\{\psi_\alpha(\vec{x},t),\psi_\beta^\dagger(\vec{y},t)\} = \delta^{(3)}(\vec{x}-\vec{y})\delta_{\alpha\beta}, \qquad \{\psi_\alpha(\vec{x},t),\psi_\beta(\vec{y},t)\} = \{\psi_\alpha^\dagger(\vec{x},t),\psi_\beta^\dagger(\vec{y},t)\} = 0, \tag{7.47}$$

where α,β are spinor indices. This translates into annihilation and creation operators' relations:

$$\begin{gathered}\{a_r(\vec{k}),a_s^\dagger(\vec{p})\} = \{b_r(\vec{k}),b_s^\dagger(\vec{p})\} = (2\pi)^3\delta^{(3)}(\vec{k}-\vec{p})\delta_{rs}, \\ \{a_r(\vec{k}),a_s(\vec{p})\} = \{a_r^\dagger(\vec{k}),a_s^\dagger(\vec{p})\} = \{b_r(\vec{k}),b_s(\vec{p})\} = \{b_r^\dagger(\vec{k}),b_s^\dagger(\vec{p})\} = 0.\end{gathered} \tag{7.48}$$

From the Appendix B, we have the ensemble averages:

$$\begin{aligned}\langle a_s(\vec{p})a_r(\vec{k})\rangle &= \langle a_s^\dagger(\vec{p})a_r^\dagger(\vec{k})\rangle = 0, \\ \langle a_s(\vec{p})a_r^\dagger(\vec{k})\rangle &= [1-n_F(\omega_k)](2\pi)^3\delta^{(3)}(\vec{p}-\vec{k})\delta_{sr}, \\ \langle a_s^\dagger(\vec{p})a_r(\vec{k})\rangle &= n_F(\omega_k)(2\pi)^3\delta^{(3)}(\vec{p}-\vec{k})\delta_{sr},\end{aligned} \tag{7.49}$$

and same for $b_s(\vec{k})$, $b_s^\dagger(\vec{k})$ operators. Using this result, we evaluate $\Delta_F^+(\vec{x},\tau)$:

$$\begin{aligned}
&\Delta_F^+(\vec{x},\tau) = \\
&= \sum_{s,r}\int \frac{d^3p}{(2\pi)^3}\frac{d^3k}{(2\pi)^3}\frac{1}{2\sqrt{\omega_p\omega_k}}\langle\Big[a_s(\vec{p})u_s(\vec{p})e^{-ipx} + b_s^\dagger(\vec{p})v_s(\vec{p})e^{ipx}\Big]\cdot\Big[a_r^\dagger(\vec{k})\bar{u}_r(\vec{k}) + b_r(\vec{k})\bar{v}_r(\vec{k})\Big]\rangle \\
&= \sum_{s,r}\int \frac{d^3p}{(2\pi)^3}\frac{d^3k}{(2\pi)^3}\frac{1}{2\sqrt{\omega_p\omega_k}}\Big[e^{-ipx}u_s(\vec{p})\bar{u}_r(\vec{k})\langle a_s(\vec{p})a_r^\dagger(\vec{k})\rangle + e^{ipx}v_s(\vec{p})\bar{v}_r(\vec{k})\langle b_s^\dagger(\vec{p})b_r(\vec{k})\rangle\Big] \\
&= \sum_{s,r}\int \frac{d^3p}{(2\pi)^3}\frac{d^3k}{(2\pi)^3}\frac{1}{2\sqrt{\omega_p\omega_k}}\Big[e^{-ipx}u_s(\vec{p})\bar{u}_r(\vec{k})[1-n_F(\omega_k)] + e^{ipx}v_s(\vec{p})\bar{v}_r(\vec{k})n_F(\omega_k)\Big](2\pi)^3\delta^{(3)}(\vec{p}-\vec{k})\delta_{sr} \\
&= \int\frac{d^3k}{(2\pi)^3}\frac{1}{2\omega_k}\Big[e^{-\omega_k\tau}e^{i\vec{k}\cdot\vec{x}}[1-n_F(\omega_k)][\not{k}+m] + e^{\omega_k\tau}e^{-i\vec{k}\cdot\vec{x}}n_F(\omega_k)[\not{k}-m]\Big].
\end{aligned} \tag{7.50}$$

Same calculation for $\Delta_F^-(\vec{x},\tau)$ gives:

$$\Delta_F^-(\vec{x},\tau) = \int\frac{d^3k}{(2\pi)^3}\frac{1}{2\omega_k}\Big[e^{-\omega_k\tau}e^{i\vec{k}\cdot\vec{x}}n_F(\omega_k)\cdot(2m) + e^{\omega_k\tau}e^{-i\vec{k}\cdot\vec{x}}[1-n_F(\omega_k)]\cdot(-2m)\Big]. \tag{7.51}$$

From equation (7.42) we get:

$$\begin{aligned}
\Delta_F(\vec{x},\tau) = \int\frac{d^3k}{(2\pi)^3}\frac{1}{2\omega_k}\Bigg[&2m\Big(e^{\omega_k\tau}e^{-i\vec{k}\cdot\vec{x}}[1-n_F(\omega_k)] - e^{-\omega_k\tau}e^{i\vec{k}\cdot\vec{x}}n_F(\omega_k)\Big) + \\
&+\Theta(\tau)\Big(e^{-\omega_k\tau}e^{i\vec{k}\cdot\vec{x}}\big[\not{k}(1-n_F(\omega_k)) + m(1+n_F(\omega_k))\big] + \\
&+ e^{\omega_k\tau}e^{-i\vec{k}\cdot\vec{x}}\big[\not{k}n_F(\omega_k) + m(n_F(\omega_k)-2)\big]\Big)\Bigg],
\end{aligned} \tag{7.52}$$

where we used $\Theta(-\tau) = 1-\Theta(\tau)$. The Fourier transformation of $\Delta_F(\vec{x},\tau)$ is:

$$\Delta_F(\vec{p},\omega_n) \equiv \int_0^\beta d\tau\int d^3x e^{i(\omega_n\tau-\vec{p}\cdot\vec{x})}\Delta_F(\vec{x},\tau), \tag{7.53}$$

and its inverse:

$$\Delta_F(\vec{x},\tau) = \frac{1}{\beta}\sum_{n=-\infty}^{n=+\infty}\int\frac{d^3p}{(2\pi)^3}e^{-i(\omega_n\tau-\vec{p}\cdot\vec{x})}\Delta_F(\vec{p},\omega_n). \tag{7.54}$$

Fermion propagator is anti-periodic in τ, so $\Delta_F(\vec{x},\tau) = -\Delta_F(\vec{x},\tau+\beta)$ imposes constraint on ω_n frequencies:

$$e^{-i\omega_n\tau} = -e^{-i\omega_n(\tau+\beta)} \qquad \Rightarrow \qquad \omega_n \equiv \frac{(2n+1)\pi}{\beta} = (2n+1)\pi T. \tag{7.55}$$

To perform the Fourier transformation in equation (7.53), one can observe that the τ integral is performed from 0 to β and $\tau > 0$, so $\Theta(\tau) = 1$ and $\Theta(-\tau) = 0$:

$$\Delta_F(\vec{x},\tau) = \int\frac{d^3k}{(2\pi)^3}\frac{1}{2\omega_k}\Big[e^{\omega_k\tau}e^{-i\vec{k}\cdot\vec{x}}[\not{k}-m]n_F(\omega_k) + e^{-\omega_k\tau}e^{i\vec{k}\cdot\vec{x}}[\not{k}+m][1-n_F(\omega_k)]\Big]. \tag{7.56}$$

Therefore, for the τ variable, we have the same integral as before, with $e^{i\beta\omega_n} = e^{(2n+1)i\pi} = -1$:

$$\int_0^\beta d\tau\; e^{\tau(i\omega_n\pm\omega_k)} = \frac{e^{\beta(i\omega_n\pm\omega_k)}-1}{i\omega_n\pm\omega_k} = -\frac{e^{\pm\beta\omega_k}+1}{i\omega_n\pm\omega_k}, \tag{7.57}$$

and for the $\vec{x}$ variable integral:

$$\int d^3x \; e^{-i(\vec{p}\pm\vec{k})\cdot\vec{x}} = (2\pi)^2\delta^{(3)}(\vec{p}\pm\vec{k}). \tag{7.58}$$

Therefore, we obtain:

$$\begin{aligned}
&\Delta_F(\vec{p},\omega_n) = \\
&= \frac{1}{2\omega_p}\left[(-1)\frac{e^{\beta\omega_p}+1}{i\omega_n+\omega_p}[-\not{p}-m]n_F(\omega_p) + (-1)\frac{e^{-\beta\omega_p}+1}{i\omega_n-\omega_p}[\not{p}+m](1-n_F(\omega_p))\right] \\
&= \frac{\not{p}+m}{2\omega_p}\left[\frac{e^{\beta\omega_p}+1}{i\omega_n+\omega_p}n_F(\omega_p) - \frac{e^{-\beta\omega_p}+1}{i\omega_n-\omega_p}(1-n_F(\omega_p))\right] = \frac{\not{p}+m}{2\omega_p}\left[\frac{1}{i\omega_n+\omega_p} - \frac{1}{i\omega_n-\omega_p}\right] \\
&= \frac{\not{p}+m}{\omega_n^2+\omega_p^2} = \frac{\not{p}+m}{\vec{p}^2+m^2+\omega_n^2}.
\end{aligned} \tag{7.59}$$

Finally, the inverse transform reads:

$$\Delta_F(\vec{x},\tau) = \frac{i}{\beta}\sum_{n=-\infty}^{n=+\infty}\int\frac{d^3p}{(2\pi)^3}e^{-i(\omega_n\tau-\vec{p}\cdot\vec{x})}\frac{i[\not{p}+m]}{p^2-m^2}, \tag{7.60}$$

where $p^\mu = (i\omega_n,\vec{p})$, with fermionic Matsubara frequencies $\omega_n = (2n+1)\pi T$. Feynman rules for bosons and fermions are provided in Table 7.1.

Table 7.1: Comparison of momentum-space Feynman rules for zero and finite temperature quantum field theories.

	ZERO TEMPERATURE	FINITE TEMPERATURE
boson propagator:	$\frac{i}{p^2-m^2}, \quad p^\mu = \big(p_0,\vec{p}\big)$	$\frac{i}{p^2-m^2}, \quad p^\mu = \big(2\pi i n\beta^{-1},\vec{p}\big)$
fermion propagator:	$\frac{i[\not{p}+m]}{p^2-m^2}, \quad p^\mu = \big(p_0,\vec{p}\big)$	$\frac{i[\not{p}+m]}{p^2-m^2}, \quad p^\mu = \big((2n+1)\pi i\beta^{-1},\vec{p}\big)$
loop integral:	$\int\frac{d^4p}{(2\pi)^4}$	$\frac{i}{\beta}\sum_{n=-\infty}^{n=+\infty}\int\frac{d^3p}{(2\pi)^3}$
vertex δ functions:	$(2\pi)^4\delta^{(4)}\Big(\sum p_i\Big)$	$i\beta(2\pi)^3\delta\Big(\sum\omega_i\Big)\delta^{(3)}\Big(\sum\vec{p}_i\Big)$

7.4. Effective Potential at Finite Temperature

Using all the tools developed in the previous sections, we will derive the one-loop effective potential at finite temperature, incorporating contributions from scalars, fermions, and gauge bosons. As we will show, the effective potential at finite temperature naturally includes the effective potential at zero temperature, calculated in Chapter 2. To obtain these results, we will employ the diagrammatic approach and the Feynman rules outlined in Table 7.1.

7.4.1. Scalars:

Let's consider the self-interacting scalar field ϕ with the Lagrangian:

$$\mathcal{L} = \frac{1}{2}(\partial_\mu\phi)(\partial^\mu\phi) - \frac{1}{2}m^2\phi^2 - \frac{\lambda}{4!}\phi^4, \tag{7.61}$$

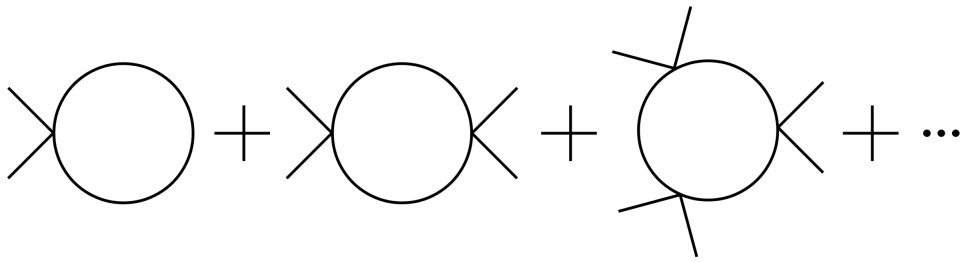

Figure 7.1: The 1PI diagrams for the scalar theory described by Lagrangian (7.61).

so the tree-level potential reads:

$$V_0(\phi) = \frac{1}{2}m^2\phi^2 + \frac{\lambda}{4!}\phi^4. \tag{7.62}$$

According to equation (2.26), to obtain the one-loop effective potential, one must sum all 1PI diagrams with 1-loop. For the scalar theory, these diagrams are illustrated in Figure 7.1. For ℓ-th diagram with 2ℓ external legs, ℓ propagators and ℓ vertices, we have the following contribution:

- ℓ propagators give $(i)^\ell(-\vec{p}^2 - \omega_n^2 - m^2)^{-\ell} = (i)^\ell(p^2 - m^2)^{-\ell}$;
- for 2ℓ external lines, we get $\phi_c^{2\ell}$ factor;
- each vertex gives $(-i\frac{\lambda}{2})$, where the factor $\frac{1}{2}$ comes from the symmetry of interchanging the 2 external lines entering the vertex;
- the overall symmetry factor for each diagram is $\frac{\ell!}{2\ell}$, which comes from the following argumentation: we have $\ell!$ combinations for choosing vertices, mirror symmetry of the graph gives factor $\frac{1}{2}$ and one also has symmetry under the discrete group of rotations $\mathbf{Z}_\ell$, producing $\frac{1}{\ell}$ factor;
- there's an extra global factor of i coming from the definition of the generating functional $W[J]$ and effective action $\Gamma[\phi_c]$[1].

The sum of one-loop diagrams gives the following potential:

$$V_1(\phi_c) = i \times \frac{i}{\beta}\sum_{l=1}^{\infty}\frac{1}{2l}\sum_{n=-\infty}^{n=+\infty}\int\frac{d^3p}{(2\pi)^3}\left(\frac{\frac{\lambda}{2}\phi_c^2}{(i\omega_n)^2 - \vec{p}^2 - m^2}\right)^l. \tag{7.64}$$

Using the relation:

$$\log(1-x) = -\sum_{l=1}^{\infty}\frac{x^l}{l}, \tag{7.65}$$

[1]The evaluation of the effective potential requires careful consideration of the formalism used, especially the distinction between Euclidean and Minkowski spaces. The functional $W[J]$ generates Feynman diagrams in Euclidean space, while $iW[J]$ generates them in the Minkowski space. Similarly, the effective action $\Gamma[\phi_c]$ represents the sum of 1PI diagrams in Euclidean space, while $i\Gamma[\phi_c]$ corresponds to the same sum in the Minkowski space. Consequently, when employing Minkowski-space propagators, as in the above derivation, the effective action and potential satisfy:

$$i\Gamma = \sum(\text{graphs}) \quad \Rightarrow \quad \Gamma = -i\sum(\text{graphs}) \quad \Rightarrow \quad V_{eff} = -\sum\Gamma = i\sum(\text{graphs}), \tag{7.63}$$

resulting in an additional factor of i.

we get:

$$
\begin{aligned}
&V_1(\phi_c) = \\
&= \frac{1}{2\beta}\sum_{n=-\infty}^{n=+\infty}\int \frac{d^3p}{(2\pi)^3}\log\left(1-\frac{\frac{\lambda}{2}\phi_c^2}{(i\omega_n)^2-\vec{p}^2-m^2}\right) = \frac{1}{2\beta}\sum_{n=-\infty}^{n=+\infty}\int \frac{d^3p}{(2\pi)^3}\log\left(1+\frac{\frac{\lambda}{2}\phi_c^2}{\omega_n^2+\vec{p}^2+m^2}\right) \\
&= \frac{1}{2\beta}\sum_{n=-\infty}^{n=+\infty}\int \frac{d^3p}{(2\pi)^3}\left[\log\left(\omega_n^2+\vec{p}^2+m^2+\frac{\lambda}{2}\phi_c^2\right)-\log\left(\omega_n^2+\vec{p}^2+m^2\right)\right] \\
&= \frac{1}{2\beta}\sum_{n=-\infty}^{n=+\infty}\int \frac{d^3p}{(2\pi)^3}\log\left(\omega_n^2+\omega^2\right)+(\phi_c \text{ independent terms}),
\end{aligned}
\tag{7.66}
$$

where in the last line we defined:

$$
\omega^2=\vec{p}^2+m^2(\phi_c), \qquad m^2(\phi_c)=m^2+\frac{\lambda}{2}\phi_c^2=\frac{\partial^2 V_0(\phi_c)}{\partial\phi_c^2}. \tag{7.67}
$$

The sum over n can be easily computed using the formulas:

$$
\sum_{n=0}^{n=+\infty}\frac{1}{n^2+a^2}=\frac{\pi}{2a}\coth(\pi a)+\frac{1}{2a^2} \quad \Rightarrow \quad \sum_{n=-\infty}^{n=+\infty}\frac{1}{n^2+a^2}=\frac{\pi}{a}\coth(\pi a). \tag{7.68}
$$

Denoting the sum from (7.66) as:

$$
f(\omega)=\sum_{n=-\infty}^{n=+\infty}\log\left(\omega_n^2+\omega^2\right), \tag{7.69}
$$

we have:

$$
\begin{aligned}
\frac{\partial f(\omega)}{\partial\omega} &= \sum_{n=-\infty}^{n=+\infty}\frac{2\omega}{\omega_n^2+\omega^2}=2\omega\sum_{n=-\infty}^{n=+\infty}\frac{1}{\frac{4\pi^2}{\beta^2}n^2+\omega^2}=\frac{\beta^2\omega}{2\pi^2}\sum_{n=-\infty}^{n=+\infty}\frac{1}{n^2+\frac{\beta^2\omega^2}{4\pi^2}}= \\
&= \frac{\beta^2\omega}{2\pi^2}\cdot\frac{2\pi^2}{\beta\omega}\coth\left(\frac{\beta\omega}{2}\right)=\beta\cdot\frac{e^{\beta\omega}+1}{e^{\beta\omega}-1},
\end{aligned}
\tag{7.70}
$$

which gives:

$$
f(\omega)=\beta\omega+2\log\left(1-e^{-\beta\omega}\right)+(\omega \text{ independent constant}). \tag{7.71}
$$

Substituting (7.71) into (7.66), we obtain:

$$
V_1(\phi_c)=\int\frac{d^3p}{(2\pi)^3}\left[\frac{\omega}{2}+\frac{1}{\beta}\log\left(1-e^{-\beta\omega}\right)\right]. \tag{7.72}
$$

The first term in the above result is temperature-independent. We will prove that this first integral is the 1-loop effective potential at zero temperature, given in the equation (2.40). Consider the integral:

$$
\omega\int_{-\infty}^{+\infty}\frac{dx}{2\pi i}\frac{1}{-x^2+\omega^2-i\epsilon}=\omega\int_{-\infty}^{+\infty}\frac{dx}{2\pi i}\frac{1}{\left[(\omega-i\tilde{\epsilon})-x\right]\cdot\left[(\omega-i\tilde{\epsilon})+x\right]}, \tag{7.73}
$$

where:

$$
\sqrt{\omega^2-i\epsilon}=\omega-\frac{i\epsilon}{2\omega}+\mathcal{O}(\epsilon^2)\approx\omega-i\tilde{\epsilon}. \tag{7.74}
$$

We have two residues $x = \pm(\omega - i\tilde{\epsilon})$. We choose to close the contour anticlockwise in the complex plane, picking the pole $x = -\omega + i\tilde{\epsilon}$ with residue $1/2\omega$. Therefore:

$$\omega \int_{-\infty}^{+\infty} \frac{dx}{2\pi i} \frac{1}{-x^2 + \omega^2 - i\epsilon} = \frac{1}{2}. \tag{7.75}$$

One can also write:

$$\frac{1}{2} = \omega \int_{-\infty}^{+\infty} \frac{dx}{2\pi i} \frac{1}{-x^2 + \omega^2 - i\epsilon} = \frac{\partial}{\partial \omega}\left[\frac{1}{2}\int_{-\infty}^{+\infty} \frac{dx}{2\pi i} \log\Big(- x^2 + \omega^2 - i\epsilon\Big)\right], \tag{7.76}$$

which gives:

$$-\frac{i}{2}\int_{-\infty}^{+\infty} \frac{dx}{2\pi} \log\Big(- x^2 + \omega^2 - i\epsilon\Big) = \frac{\omega}{2} + \text{const.} \tag{7.77}$$

Finally:

$$\int \frac{d^3p}{(2\pi)^3}\frac{\omega}{2} = -\frac{i}{2}\int \frac{d^4p}{(2\pi)^4} \log\Big(- p_0^2 + \omega^2 - i\epsilon\Big) = \frac{1}{2}\int \frac{d^4p}{(2\pi)^4} \log\Big(p^2 + m^2(\phi_c)\Big), \tag{7.78}$$

where in the last equality we performed the Wick rotation $p_0 \to ip_0$ and used $\omega^2 = \vec{p}^2 + m^2(\phi_c)$, giving $p^2 = p_0^2 + \vec{p}^2$. This result is identical to the one obtained in the equation (2.40) for the zero-temperature theory.

The temperature-dependent part of (7.72) can be written as:

$$\begin{aligned} V_1(\phi_c)|_T =& \ \frac{1}{\beta}\int \frac{d^3p}{(2\pi)^3} \log\Big(1 - e^{-\beta\omega}\Big) = \frac{T}{2\pi^2}\int_0^\infty dp\ p^2 \log\Big(1 - e^{-\beta\sqrt{\vec{p}^2 + m^2(\phi_c)}}\Big) = \\ =& \ \frac{T^4}{2\pi^2} J_B\big[m^2(\phi_c)/T^2\big], \end{aligned} \tag{7.79}$$

where $J_B[m^2(\phi_c)/T^2]$ is the thermal bosonic function defined as:

$$J_B[m^2(\phi_c)/T^2] = \int_0^\infty dx\ x^2 \log\Big(1 - e^{-\sqrt{x^2 + m^2(\phi_c)/T^2}}\Big). \tag{7.80}$$

The high-temperature expansion of J_B is very useful and reads:

$$\begin{aligned} J_B[m^2(\phi_c)/T^2]\Big|_{m \ll T} =& \ -\frac{\pi^4}{45} + \frac{\pi^2}{12}\frac{m^2(\phi_c)}{T^2} - \frac{\pi}{6}\Big(\frac{m^2(\phi_c)}{T^2}\Big)^{3/2} - \frac{1}{32}\frac{m^4(\phi_c)}{T^4}\log\frac{m^2(\phi_c)}{a_b T^2} \\ & - 2\pi^{7/2}\sum_{\ell=1}^{\infty}(-1)^\ell \frac{\zeta(2\ell+1)}{(\ell+1)!}\Gamma\Big(\ell + \frac{1}{2}\Big)\Big(\frac{m^2(\phi_c)}{4\pi^2 T^2}\Big)^{\ell+2}, \end{aligned} \tag{7.81}$$

where $a_b = 16\pi^2 \exp(3/2 - 2\gamma_E)$ ($\log a_b = 5.4076$), and ζ is the Riemann $\zeta-$function.

7.4.2. Fermions:

Let's consider the fermion field ψ interacting with the scalar ϕ described by the Lagrangian:

$$\mathcal{L} = \bar{\psi}(i\partial\!\!\!/ - m_F(\phi_c))\psi, \tag{7.82}$$

where $m_F(\phi_c) = y\phi_c$. To simplify further calculations, this will be treated as an interaction vertex with Feynman rule $-i(y\phi_c)$. Therefore, the mass parameter m in the fermion propagator is set to zero, and we will sum over fermion loops without external legs, as illustrated in Figure 7.2. The generalization to a massive theory is straightforward, requiring only the modification of m_F to $m_F(\phi_c) = m + y\phi_c$. Since ℓ fermion propagators introduce a factor of $\mathrm{Tr}\big[p\!\!\!/^\ell\big]$ and the trace of the odd number of γ matrices is zero, we sum only the diagrams with an even number of fermion propagators.

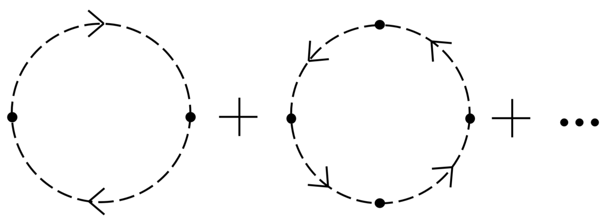

Figure 7.2: 1PI diagrams contributing to the 1-loop effective potential of (7.82). The fermionic propagators are massless, with momentum flow marked by arrows. Black dots denote the field-dependent fermion-scalar interaction with vertex contribution $-iy\phi_c$.

For ℓ-th diagram with 2ℓ fermionic propagators and 2ℓ vertices, we have the following contribution:

- the 2ℓ propagators give $\frac{(i)^{2\ell}}{(-\vec{p}^2-\omega_n^2)^{2\ell}}\mathrm{Tr}\left[\not{p}^{2\ell}\right] = \frac{(i)^{2\ell}}{(p^2)^{2\ell}} \cdot 4p^{2\ell} = \frac{4(i)^{2\ell}}{p^{2\ell}} = 4\left(\frac{-1}{p^2}\right)^{\ell}$, where we used $\mathrm{Tr}\left[p^{2\ell}\right] = 4p^{2\ell}$;
- 2ℓ vertices give $(-im_F(\phi_c))^{2\ell} = (-m_F^2(\phi_c))^{\ell}$;
- the overall symmetry factor, including $\frac{1}{(2\ell)!}$ from the effective potential definition (2.25), is $\frac{1}{2\ell}$, which comes from the following argumentation: we have $(2\ell)!$ combinations for choosing vertices, symmetry under the discrete group of rotations $\mathbf{Z}_{2\ell}$, produces $\frac{1}{2\ell}$ factor;
- there's an extra global factor of i coming from the definition of the generating functional $W[J]$ and effective action $\Gamma[\phi_c]$ and global factor (-1) coming from the fermion loop.

Consequently, the one-loop effective potential contribution from fermions reads:

$$V_1(\phi_c) = -i \times \frac{i}{\beta}\sum_{\ell=1}^{\infty}\frac{1}{2\ell}\sum_{n=-\infty}^{n=+\infty}\int\frac{d^3p}{(2\pi)^3}4\left(\frac{m_F^2(\phi_c)}{p^2}\right)^{\ell}. \tag{7.83}$$

Using the relation (7.65), we obtain:

$$\begin{aligned} &V_1(\phi_c) = \\ &= -\frac{2}{\beta}\sum_{n=-\infty}^{n=+\infty}\int\frac{d^3p}{(2\pi)^3}\log\left(1-\frac{m_F^2(\phi_c)}{(i\omega_n)^2-\vec{p}^2}\right) = -\frac{2}{\beta}\sum_{n=-\infty}^{n=+\infty}\int\frac{d^3p}{(2\pi)^3}\log\left(1+\frac{m_F^2(\phi_c)}{\omega_n^2+\vec{p}^2}\right) \\ &= -\frac{2}{\beta}\sum_{n=-\infty}^{n=+\infty}\int\frac{d^3p}{(2\pi)^3}\left[\log\left(\omega_n^2+\vec{p}^2+m_F^2(\phi_c)\right)-\log\left(\omega_n^2+\vec{p}^2\right)\right] \\ &= -\frac{2}{\beta}\sum_{n=-\infty}^{n=+\infty}\int\frac{d^3p}{(2\pi)^3}\log\left(\omega_n^2+\omega^2\right) + (\phi_c \text{ independent terms}), \end{aligned} \tag{7.84}$$

where in the last line we have:

$$\omega^2 = \vec{p}^2 + m_F^2(\phi_c), \qquad\qquad \omega_n = (2n+1)\pi T. \tag{7.85}$$

The sum over n will be calculated with the same method as for bosons. However, it is important to note that the Matsubara frequencies for fermions have an odd factor $(2n+1)$. Let us again define:

$$f(\omega) = \sum_{n=-\infty}^{n=+\infty}\log\left(\omega_n^2+\omega^2\right), \tag{7.86}$$

with its derivative:

$$\frac{\partial f(\omega)}{\partial \omega} = \sum_{n=-\infty}^{n=+\infty} \frac{2\omega}{\omega_n^2+\omega^2} = 2\omega \sum_{n=-\infty}^{n=+\infty} \frac{1}{\frac{\pi^2}{\beta^2}(2n+1)^2+\omega^2} = \frac{2\beta^2\omega}{\pi^2} \sum_{n=-\infty}^{n=+\infty} \frac{1}{(2n+1)^2+\frac{\beta^2\omega^2}{\pi^2}}. \tag{7.87}$$

Using the equation (7.68), let's define:

$$S(a) = \sum_{n=-\infty}^{n=+\infty} \frac{1}{n^2+a^2} = \frac{\pi}{a}\coth(\pi a), \tag{7.88}$$

and observe:

$$\sum_{n=(\text{even numbers})} \frac{1}{n^2+a^2} = \sum_{m=-\infty}^{m=+\infty} \frac{1}{(2m)^2+a^2} = \frac{1}{4}\sum_{m=-\infty}^{m=+\infty} \frac{1}{m^2+(a/2)^2} = \frac{1}{4}S(a/2), \tag{7.89}$$

$$\sum_{n=(\text{odd numbers})} \frac{1}{n^2+a^2} = S(a) - \frac{1}{4}S(a/2) = \frac{\pi}{a}\Big(\coth(\pi a) - \frac{1}{2}\coth(\pi a/2)\Big) = \frac{\pi}{2a}\tanh\Big(\frac{\pi a}{2}\Big). \tag{7.90}$$

With the above result, we obtain:

$$\frac{\partial f(\omega)}{\partial \omega} = \beta\cdot\tanh\Big(\frac{\beta\omega}{2}\Big) = \beta\cdot\frac{e^{\beta\omega}-1}{e^{\beta\omega}+1}, \tag{7.91}$$

and integration gives:

$$f(\omega) = \beta\omega + 2\log\Big(1+e^{-\beta\omega}\Big) + (\omega \text{ independent constant}). \tag{7.92}$$

Finally, (7.84) becomes:

$$V_1(\phi_c) = -4\int \frac{d^3p}{(2\pi)^3}\Bigg[\frac{\omega}{2} + \frac{1}{\beta}\log\Big(1+e^{-\beta\omega}\Big)\Bigg]. \tag{7.93}$$

The above result differs from the bosonic case by a factor (-4), which consists of the overall (-1) sign accounting for fermionic loop calculation, and number 4 comes from the trace over Dirac indices in $\mathrm{Tr}\big[\not{p}^{2\ell}\big] = 4p^{2\ell}$. The temperature-independent part, as proven previously in the bosonic case, is the 1-loop effective potential at zero temperature:

$$(-4)\cdot\frac{1}{2}\int\frac{d^4p}{(2\pi)^4}\Big[\log\big(p^2+m_F^2(\phi_c)\big)\Big]. \tag{7.94}$$

The second, temperature-dependent part, is:

$$\begin{aligned} V_1(\phi_c)|_T =& (-4)\cdot\frac{1}{\beta}\int\frac{d^3p}{(2\pi)^3}\log\Big(1+e^{-\beta\omega}\Big) = (-4)\cdot\frac{T}{2\pi^2}\int_0^\infty dp\, p^2\log\Big(1+e^{-\beta\sqrt{\vec{p}^2+m_F^2(\phi_c)}}\Big) = \\ =& (-4)\cdot\frac{T^4}{2\pi^2}J_F\big[m_F^2(\phi_c)/T^2\big], \end{aligned} \tag{7.95}$$

where $J_F[m_F^2(\phi_c)/T^2]$ is the thermal fermionic function defined as:

$$J_F[m_F^2(\phi_c)/T^2] = \int_0^\infty dx\, x^2\log\Big(1+e^{-\sqrt{x^2+m_F^2(\phi_c)/T^2}}\Big). \tag{7.96}$$

The high-temperature expansion of J_F is very useful and reads:

$$\begin{aligned} J_F[m_F^2(\phi_c)/T^2]\Big|_{m\ll T} =& \frac{7\pi^4}{360} - \frac{\pi^2}{24}\frac{m_F^2(\phi_c)}{T^2} - \frac{1}{32}\frac{m_F^4(\phi_c)}{T^4}\log\frac{m^2(\phi_c)}{a_f T^2} \\ & - \frac{\pi^{7/2}}{4}\sum_{\ell=1}^{\infty}(-1)^\ell\frac{\zeta(2\ell+1)}{(\ell+1)!}\Big(1-2^{-2\ell-1}\Big)\Gamma\Big(\ell+\frac{1}{2}\Big)\Big(\frac{m_F^2(\phi_c)}{\pi^2T^2}\Big)^{\ell+2}, \end{aligned} \tag{7.97}$$

where $a_f = \pi^2\exp(3/2-2\gamma_E)$ $(\log a_f = 2.6351)$, and ζ is the Riemann $\zeta-$function.

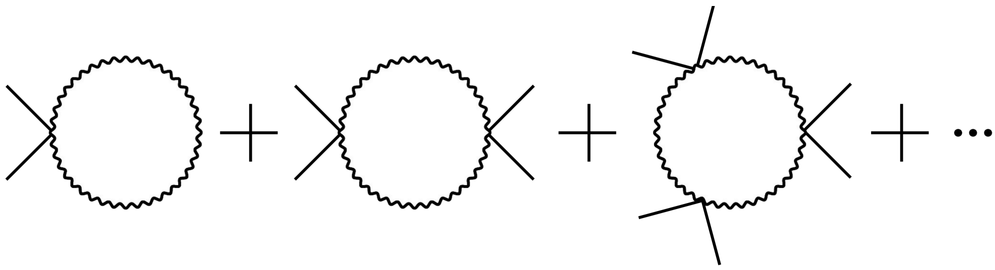

Figure 7.3: 1PI diagrams contributing to the 1-loop effective potential of (7.98). Solid lines are scalar external legs, and wavy lines in loops are gauge boson propagators.

7.4.3. Gauge Bosons:

When deriving the Feynman rules in momentum space, we did not explicitly calculate those for gauge bosons. However, as the reader can easily deduce, the propagators for bosons and fermions remain the same in both zero and finite temperature theories, with the only modification of the 0-th momentum component to $p^0 = i\omega_n$, where ω_n are the Matsubara frequencies relevant to the particle species under consideration. Since gauge bosons obey the Bose-Einstein statistics, their four-momentum is identical to that of scalars: $p^\mu = \big(i\omega_n, \vec{p}\big)$, with the bosonic Matsubara frequencies given by $\omega_n = 2n\pi\beta^{-1}$. With this in mind, we will use Feynman rules provided in Table 7.1 for a theory in which a gauge boson is coupled to the scalar field. One final remark is necessary: when coupling a scalar field to a gauge field, the scalar must be charged and, therefore, complex. Nonetheless, if we are only interested in how gauge bosons contribute to the thermal effective potential, we consider the ϕ field as the real part of a complex scalar field. Indeed, when studying mass generation for the Standard Model gauge bosons, it is the real part of the Higgs field h that is responsible for the Higgs mechanism. Hence, we consider the following scalar-gauge boson interaction:

$$\mathcal{L} \supseteq g^2 g_{\mu\nu} A^\mu A^\nu \phi_c^2, \tag{7.98}$$

giving the vertex rule $i2g_{\mu\nu}g^2$. The gauge boson propagator for a massless field in Lorenz gauge reads:

$$\frac{-i}{p^2}\Big[g^{\mu\nu} - \frac{p^\mu p^\nu}{p^2}\Big]. \tag{7.99}$$

We will sum the 1PI diagrams shown in Figure 7.3. For ℓ-th diagram with 2ℓ external scalar legs, ℓ gauge boson propagators and ℓ vertices, we have the following contribution:

- ℓ propagators give $\left(\frac{-i}{p^2}\right)^\ell\Big[g^{\mu\nu} - \frac{p^\mu p^\nu}{p^2}\Big]^\ell$ with $p^\mu = \big(i\omega_n, \vec{p}\big)$;
- for 2ℓ external lines, we get $\phi_c^{2\ell}$ factor;
- each vertex gives $\big(ig_{\mu\nu}g^2\big)$, where the factor 2 is canceled by $\frac{1}{2}$ coming from the symmetry of interchanging the 2 external lines entering the vertex;
- the overall symmetry factor is the same as for scalars: $\frac{\ell!}{2\ell}$;
- there's an extra global factor of i coming from the definition of the generating functional $W[J]$ and effective action $\Gamma[\phi_c]$.

The derivation of the contractions of vertices with propagators requires some caution. Let's calculate it for the first 2 diagrams visible in Figure 7.3. We have:

$$\begin{aligned}
\ell = 1: \quad & (ig_{\mu\nu}g^2)\cdot\left(\frac{-i}{p^2}\right)\Big[g^{\mu\nu} - \frac{p^\mu p^\nu}{p^2}\Big] = \frac{g^2}{p^2}\big[g^\mu_\mu - p^2/p^2\big] = \frac{g^2}{p^2}[4-1] = 3\cdot\frac{g^2}{p^2},\\
\ell = 2: \quad & (ig_{\mu\nu}g^2)\cdot\left(\frac{-i}{p^2}\right)\Big[g^{\mu\sigma} - \frac{p^\mu p^\sigma}{p^2}\Big](ig_{\rho\sigma}g^2)\cdot\left(\frac{-i}{p^2}\right)\Big[g^{\rho\nu} - \frac{p^\rho p^\nu}{p^2}\Big] =\\
& = \frac{g^4}{p^4}\Big[g^\mu{}_\rho g^\rho{}_\mu - 2\frac{p^\mu p_\mu}{p^2} + \frac{p^\mu p_\mu p^\rho p_\rho}{p^4}\Big] = \frac{g^4}{p^4}[4-2+1] = 3\cdot\frac{g^4}{p^4}.
\end{aligned} \tag{7.100}$$

It is easy to see that the proper contraction of vertices and propagators results in a global factor 3 (for arbitrary D dimensions, it would be $(D-1)$). Finally, performing the same steps as for scalar fields, we obtain:

$$\begin{aligned} V_1(\phi_c) = &\; i \times \frac{i}{\beta}\sum_{\ell=1}^{\infty}\frac{1}{2\ell}\sum_{n=-\infty}^{n=+\infty} 3\cdot\left(\frac{g^2\phi_c^2}{p^2}\right)^{\ell} = 3\cdot\frac{1}{2\beta}\sum_{n=-\infty}^{n=+\infty}\log\left(1-\frac{g^2\phi_c^2}{(i\omega_n)^2-\vec{p}^2}\right) = \\ = &\; 3\cdot\frac{1}{2\beta}\sum_{n=-\infty}^{n=+\infty}\log\left(1+\frac{g^2\phi_c^2}{\omega_n^2+\vec{p}^2}\right) = 3\cdot\frac{1}{2\beta}\sum_{n=-\infty}^{n=+\infty}\log\left(\omega_n^2+\omega^2\right)+(\phi_c \text{ independent terms}), \end{aligned} \tag{7.101}$$

where in the last line we defined:

$$\omega^2 = \vec{p}^2 + m_{GB}^2(\phi_c) = \vec{p}^2 + g^2\phi_c^2, \qquad\qquad \omega_n = 2n\pi T. \tag{7.102}$$

The sum over n is identical to that for the scalar field case, yielding:

$$V_1(\phi_c) = 3\cdot\int\frac{d^3p}{(2\pi)^3}\left[\frac{\omega}{2}+\frac{1}{\beta}\log\left(1-e^{-\beta\omega}\right)\right], \tag{7.103}$$

which differs from (7.72) by a factor of 3. This factor accounts for the number of degrees of freedom of the gauge boson, which in arbitrary D dimensions is equal to $D-1$. Once again, the temperature-independent part provides the one-loop zero-temperature contribution to the effective potential:

$$3\cdot\frac{1}{2}\int\frac{d^4p}{(2\pi)^4}\log\left(p^2+m_{GB}^2(\phi_c)\right), \tag{7.104}$$

and the temperature-dependent part is:

$$V_1(\phi_c)|_T = 3\cdot\frac{T^4}{2\pi^2}J_B\left[m_{GB}^2(\phi_c)/T^2\right], \tag{7.105}$$

with J_B being the thermal bosonic function defined in (7.80).

7.4.4. Thermal Potential

Summing up the results obtained in the previous section, we can write the thermal part of the effective potential for a model that includes scalars, fermions, and gauge bosons as follows:

$$\delta V_T = \frac{T^4}{2\pi^2}\left[\sum_{i=\text{bosons}} n_i\cdot J_B\left(\frac{m_i^2(\phi_c)}{T^2}\right)+\sum_{j=\text{fermions}} n_j\cdot J_F\left(\frac{m_j^2(\phi_c)}{T^2}\right)\right], \tag{7.106}$$

where $n_{i/j}$ are the numbers of degrees of freedom of the considered particle with field-dependent mass $m_{i/j}(\phi_c)$ and $J_{B/F}$ are thermal bosonic (B) and fermionic (F) functions defined in (7.80), (7.96) respectively. The number of degrees of freedom n_a for any particle can be written in a general form:

$$n_a = (-1)^{2s_a}Q_aC_a(2s_a+1), \tag{7.107}$$

where s_a is the spin of the particle a, $Q_a = 1$ for neutral and $Q_a = 2$ for charged particles and C_a counts the number of colors of the particle a.

7.4.5. Renormalization of Quantum Field Theory in Finite Temperature and Resummation

The potential in equation (7.106) represents the one-loop contribution of order λ. As we demonstrate in the Appendix C, the perturbation expansion in thermal QFT fails at high temperatures, where higher-order diagrams can contribute in the same order as the lower-order ones. Additionally, when the boson field-dependent mass $m(\phi_c)$ is negative, the effective potential acquires an imaginary part due to the term $m^3(\phi_c)T$ from the J_B function expansion at high temperature (7.81).

To improve the results, one must account for higher-order contributions, specifically those from the so-called daisy diagrams. This procedure, known as resummation, contributes terms of order $\lambda^{3/2}$, which is the same as the $m(\phi_c)^3T$ term. The detailed discussion of the resummation method and the accompanying renormalization procedure is presented in Appendix C.

Accordingly, the thermal part of the effective potential, instead of (7.106), must take the form:

$$\delta V_{T+daisy} = \frac{T^4}{2\pi^2}\left[\sum_{i=\text{bosons}} n_i \cdot J_B\left(\frac{\left(m_i^2\right)_{eff}(\phi_c,T)}{T^2}\right) + \sum_{j=\text{fermions}} n_j \cdot J_F\left(\frac{m_j^2(\phi_c)}{T^2}\right)\right], \tag{7.108}$$

where $\left(m_i^2\right)_{eff}(\phi_c,T)$ denote the thermally corrected bosonic masses, often referred to as thermal masses. These effective masses arise from the self-energy corrections in the bosonic propagators evaluated in the thermal background. Each bosonic degree of freedom acquires an additional temperature-dependent contribution, such that:

$$\left(m_i^2\right)_{eff}(\phi_c,T) = m_i^2(\phi_c) + \Pi_i(T), \tag{7.109}$$

where $\Pi_i(T) \sim \lambda T^2$ represents the leading thermal correction. These corrections ensure the validity of perturbative expansion of the thermal potential at high temperature. Fermionic masses remain unchanged, as fermions do not contribute to the daisy diagrams resummation in the same way due to the absence of zero Matsubara modes. The explicit form of $\Pi_i(T)$ and the corresponding effective masses used in this work will be specified in the next Chapter.

Chapter 8

Spontaneous Scale Symmetry Breaking at High Temperature

In this chapter, we incorporate the tools developed in Chapter 7, particularly the thermal effective potential, to explore the effects of temperature on scale symmetry breaking in a model with dilaton ϕ_0 coupled to the Higgs neutral component ϕ_1. We will demonstrate that the symmetry in the Higgs sector is restored at high temperatures, as indicated by $\langle\phi_1\rangle = 0$. After the temperature decreases, two degenerate minima emerge for the ϕ_1 field, allowing for electroweak symmetry breaking (EWSB) as a phase transition. We further investigate the nature of this transition and the time evolution of the fields when coupled to gravity in the Riemannian geometry, with their potential modified by temperature corrections. This approach is particularly relevant, considering the hot conditions of the early Universe during its evolution. Understanding the time evolution of the fields allows us to examine the characteristics of EWSB in our model and simulate the dynamic mass generation, in which dilaton plays a key role in establishing the mass scales: the Higgs mass m_H and vev $\langle\phi_1\rangle$, and the Planck mass M_P. The analysis presented in this chapter is novel and was briefly introduced in our paper [35][1]. Similar models incorporating quantum and thermal corrections have been explored in works such as [80–84].

8.1. Temperature Corrections and Electroweak Symmetry Breaking

We focus on the temperature corrections to the classical scale-symmetric potential (5.9):

$$V(\phi_0, \phi_1) = \lambda_0\phi_0^4 + \lambda_1\phi_0^2\phi_1^2 + \lambda_2\phi_1^4. \tag{8.1}$$

The complete one-loop thermal potential is given by:

$$V_{full}(\phi_0, \phi_1, T) = V_1(\phi_0, \phi_1) + \delta V_{T+daisy}(\phi_0, \phi_1, T), \tag{8.2}$$

where $V_1(\phi_0, \phi_1)$ is the one-loop potential at zero temperature, derived in Section 5.4, given in equation (5.79). We apply the RG improvement to the effective potential $V_{full}(\phi_0, \phi_1, T)$ from equation (8.2). The coupling constants run according to their one-loop β functions, provided

[1]The values of the non-minimal coupling ξ_0 used in Section 8.2 require a brief clarification. In this analysis, we adopt $\xi_0 = 10^{10}$, following our initial assumption that a large coupling is necessary to generate the correct Planck mass, as in equation (5.42). However, this choice predates the subsequent study of the author and her supervisor for a later paper on inflation in the same model, [36], which results are presented in Chapter 9. It is showed that ξ_0 should be significantly smaller, of the order of 10^{-2}. Nevertheless, this revision does not affect the main results or conclusions presented in this Chapter, and for consistency with the reference paper [35], we keep the large ξ_0 value here.

in Appendix A. The temperature corrections improved by daisy diagrams are represented by potential (7.108) supplemented with thermal-effective masses for boson particles:

$$\delta V_{T+daisy}(\phi_0,\phi_1,T)=\frac{T^4}{2\pi^2}\left[\sum_{i=\text{bosons}} n_i\cdot J_B\left(\frac{(m_i^2)_{eff}(\phi_k,T)}{T^2}\right)+\sum_{j=\text{fermions}} n_j\cdot J_F\left(\frac{m_j^2(\phi_k)}{T^2}\right)\right], \tag{8.3}$$

with J_B and J_F defined in (7.80) and (7.96), respectively. Their high temperature expansions are given in equation (7.81) for J_B and equation (7.97) for J_F[2]. Since fermions do not encounter infrared divergences, only bosons require ressumation. In principle, only the field-dependent masses of the Higgs and dilaton can have negative values, while the masses of the gauge bosons $W^\pm$ and Z^0 remain positive. Nevertheless, we include the daisy-resummed contributions for gauge particles for completeness in our calculations. As discussed earlier in Section 5.4, we do not include χ Goldstone bosons contributions in the numerical analysis.

The thermal effective masses for the scalar sector are calculated from the high-temperature expansion of the first-order thermal potential $\delta V_T(\phi_0,\phi_1,T)$, given in equation (7.106), to the T^2 order. The thermal mass matrix, including the tree-level potential $V(\phi_0,\phi_1)$, reads:

$$\begin{aligned} M^2_{eff}(\phi_0,\phi_1,T) &= \begin{pmatrix} \frac{\partial^2 V}{\partial\phi_0^2} & \frac{\partial^2 V}{\partial\phi_1\partial\phi_0} \\ \frac{\partial^2 V}{\partial\phi_0\partial\phi_1} & \frac{\partial^2 V}{\partial\phi_1^2}\end{pmatrix} + \left.\begin{pmatrix} \frac{\partial^2 \delta V_T}{\partial\phi_0^2} & \frac{\partial^2 \delta V_T}{\partial\phi_1\partial\phi_0} \\ \frac{\partial^2 \delta V_T}{\partial\phi_0\partial\phi_1} & \frac{\partial^2 \delta V_T}{\partial\phi_1^2}\end{pmatrix}\right|_{\frac{m}{T}\ll 1} = \\ &= \begin{pmatrix} 12\lambda_0\phi_0^2+2\lambda_1\phi_1^2 & 4\lambda_1\phi_0\phi_1^2 \\ 4\lambda_1\phi_0\phi_1^2 & 2\lambda_1\phi_0^2+12\lambda_2\phi_1^2\end{pmatrix} + \\ &\quad + T^2\begin{pmatrix} \lambda_0+\frac{1}{6}\lambda_1 & 0 \\ 0 & \lambda_2+\frac{1}{6}\lambda_1+\frac{1}{16}g_1^2+\frac{3}{16}g_2^2+\frac{1}{4}y_t^2\end{pmatrix}. \end{aligned} \tag{8.5}$$

The thermal effective masses for scalars are eigenvalues of the $M^2_{eff}(\phi_0,\phi_1,T)$ matrix:

$$\begin{aligned} (m_G^2)_{eff}(\phi_0,\phi_1,T) &= 2\lambda_1\phi_1^2+\frac{1}{6}\lambda_1 T^2+\mathcal{O}(\lambda_1^2), \\ (m_H^2)_{eff}(\phi_0,\phi_1,T) &= 12\lambda_2\phi_1^2+2\lambda_1\phi_0^2+\left(\lambda_2+\frac{1}{6}\lambda_1+\frac{1}{16}g_1^2+\frac{3}{16}g_2^2+\frac{1}{4}y_t^2\right)T^2+\mathcal{O}(\lambda_1^2). \end{aligned} \tag{8.6}$$

For the gauge bosons, one has to consider thermal corrections to the mass matrix in the gauge field basis, which is non-diagonal. One gets [85, 86]:

$$(M^2_{GB})_{eff}(\phi_1,T)=\frac{\phi_1^2}{4}\begin{pmatrix} g_2^2 & 0 & 0 & 0 \\ 0 & g_2^2 & 0 & 0 \\ 0 & 0 & g_2^2 & -g_1g_2 \\ 0 & 0 & -g_1g_2 & g_1^2\end{pmatrix}+\frac{11}{6}T^2\begin{pmatrix} g_2^2 & 0 & 0 & 0 \\ 0 & g_2^2 & 0 & 0 \\ 0 & 0 & g_2^2 & 0 \\ 0 & 0 & 0 & g_1^2\end{pmatrix}. \tag{8.7}$$

The eigenvalues, with the tree-level masses given in equation (5.66), are [87]:

$$(m_W^2)_{eff}(\phi_1,T)=m_W^2(\phi_1)+\frac{11}{6}g_2^2T^2, \tag{8.8}$$

$$(m_Z^2)_{eff}(\phi_1,T)=\frac{1}{2}m_Z(\phi_1)^2+\frac{11}{12}(g_1^2+g_2^2)T^2+\sqrt{\delta}, \tag{8.9}$$

[2] The high temperature expansion (HTE) of $J_B[x]$ works for $0<x<13$, while HTE of $J_F[x]$ is valid for $0<x<5.5$ (both within an 0.5% accuracy). One can establish the approximate minimal temperature sufficient for the HTE of J_B and J_F functions. Given that the top quark mass is always greater than any of the field-dependent masses $m_i(\phi_0,\phi_1)$, and the J_F HTE constraint is stronger, the top quark mass sets the minimal temperature for using HTE:

$$T_{min}\approx 0.32 y_t\phi_1 \xrightarrow{\phi_1=300\text{ GeV}} 90\text{ GeV}. \tag{8.4}$$

This value is valid for $\phi_1<300$ GeV and $\phi_0<\sqrt{-2\lambda_2/\lambda_1}\cdot 300$ GeV, which we use later in the numerical analysis in this work.

$$\left(m_\gamma^2\right)_{eff}(\phi_1,T) = \frac{1}{2}m_Z(\phi_1)^2 + \frac{11}{12}\left(g_1^2+g_2^2\right)T^2 - \sqrt{\delta}, \tag{8.10}$$

$$\delta = \frac{1}{4}m_Z(\phi_1)^4 + \frac{11}{144}\frac{\left(g_1^2-g_2^2\right)^2}{\left(g_1^2+g_2^2\right)}\left[12m_Z^2(\phi_1) + 11\left(g_1^2+g_2^2\right)T^2\right]T^2. \tag{8.11}$$

Note that there is a non-zero thermal mass for the photon, which is massless when $T = 0$.

Symmetry Breaking at High Temperature

The scale symmetry breaking can be effectively discussed at the leading level of HTE of the potential (8.2):

$$V_{HTE}(\phi_0,\phi_1,T) = V(\phi_0,\phi_1) + \frac{1}{2}\phi_1^2\left(\lambda_2 + \frac{\lambda_1}{6} + \frac{g_1^2}{16} + \frac{3g_2^2}{16} + \frac{h_t^2}{4}\right)T^2 + \frac{1}{2}\phi_0^2\left(\lambda_0 + \frac{\lambda_1}{6}\right)T^2, \tag{8.12}$$

where the one-loop corrections were omitted for simplicity and only the classical potential $V(\phi_0,\phi_1)$ is present. Both ϕ_i fields obtain fully independent thermal corrections. The ϕ_1 Higgs field contribution is dominated by gauge bosons and top quark couplings. The dilaton ϕ_0 acquires corrections proportional to the λ_1, coupling of the mixing term in the scalar sector, only when it is in thermal equilibrium (for $|\lambda_1| \gtrsim 10^{-5}$, see Appendix D). Temperature influences the vacuum expectation values of the fields so that they are no longer proportional to each other, as indicated by the equations of motion derived from (8.12).

When the dilaton is in equilibrium, the equations of motion are modified to:

$$\begin{aligned} \phi_0: &\quad 6\lambda_0\left(4\phi_0^2+T^2\right) + \lambda_1\left(12\phi_1^2+T^2\right) = 0, \\ \phi_1: &\quad 8\lambda_1\left(12\phi_0^2+T^2\right) + 48\lambda_2\left(4\phi_1^2+T^2\right) + 3\left(g_1^2+3g_2^2+4y_t^2\right)T^2 = 0. \end{aligned} \tag{8.13}$$

Keeping in mind the classical relation $\lambda_0 = \frac{\lambda_1^2}{4\lambda_2}$ and parameter space constraint $\lambda_2 = \frac{1}{32}\left(1+16\lambda_1\right)$, the only valid physical solution becomes:

$$\langle\phi_1^2\rangle_T = 0, \qquad \langle\phi_0^2\rangle_T = -\frac{1+64\lambda_1}{192\lambda_1}T^2 = \alpha^2(\lambda_1)\cdot T^2. \tag{8.14}$$

Figure 8.1 depicts the $\alpha(\lambda_1)$ function for different λ_1 values for which dilaton can reach the thermal equilibrium. The values, obtained numerically for the full potential (8.2), with the inclusion of the quantum corrections and RG improvement, marked by the black dot points, agree with high accuracy.

The equations of motion, when the dilaton is not in equilibrium, are:

$$\begin{aligned} \phi_0: &\quad 4\lambda_0\phi_0 + 2\lambda_1\phi_1 = 0, \\ \phi_1: &\quad 8\lambda_1\left(12\phi_0^2+T^2\right) + 48\lambda_2\left(4\phi_1^2+T^2\right) + 3\left(g_1^2+3g_2^2+4y_t^2\right)T^2 = 0. \end{aligned} \tag{8.15}$$

The only possible solution for this set of equations is:

$$\langle\phi_1^2\rangle_T = \langle\phi_0^2\rangle_T = 0. \tag{8.16}$$

Figure 8.2 illustrates the exact behavior of $V_{full}(\phi_0,\phi_1,T)$ (8.2) for different temperature scales. For practical purposes, the value used in numerical calculations was set to $\lambda_1 = -10^{-4}$ so that the dilaton is in equilibrium and its thermal minimum is visible. The corresponding plot with $\lambda_1 = -10^{-10}$, where the dilaton is not in thermal equilibrium, is shown in Figure 8.3. Figures 8.4 and 8.6 show plots of the dilaton direction for $\langle\phi_1\rangle_T = 0$ GeV with different λ_1 values. The Higgs direction for $\lambda_1 = -10^{-4}$ at various dilaton values and temperatures is illustrated in Figure 8.5. However, due to the singularity in the one-loop potential at the dilaton temperature minimum $\phi_0 = \langle\phi_0\rangle_T = 0$ GeV when $\lambda_1 = -10^{-10}$, we do not provide a plot of the Higgs direction in this case. Figure 8.7 illustrates the Higgs field direction for different temperatures, with the dilaton value set to its zero-temperature vev, $\phi_0 = \langle\phi_0\rangle$. Due to quantum corrections that preserve scale symmetry, the potential remains flat at the origin, indicating that the electroweak symmetry-breaking (EWSB) phase transition is likely second order.

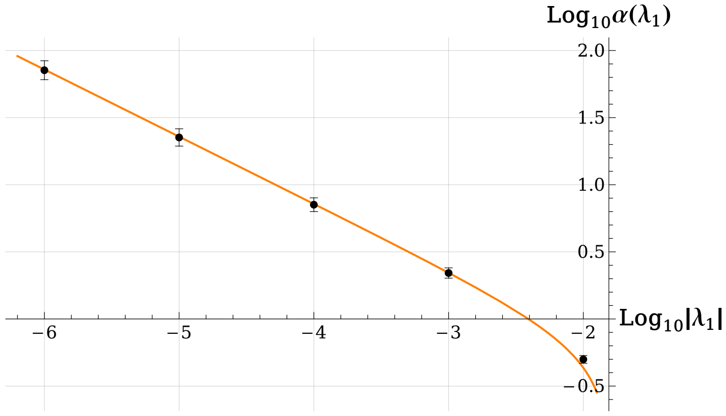

Figure 8.1: Plot of the parameter $\alpha(\lambda_1)$ from equation (8.14) for λ_1 ranges for which the dilaton can reach thermal equilibrium. The black dot points represent the numerical results obtained from the full potential (8.2). The error bars account for the variation in the actual $\langle\phi_0\rangle_T$ value across different temperatures spanning from 10 GeV to 10^8 GeV. These bars indicate the minimum and maximum values of $\langle\phi_0\rangle_T/T$ within this temperature range.

Both scenarios involving the dilaton thermal equilibrium lead to the restoration of electroweak symmetry, as $\langle\phi_1^2\rangle = 0$. As we will demonstrate later, after the temperature decreases, the Higgs field potential transitions to its characteristic shape with two degenerate minima, but this occurs only if the dilaton remains non-zero. However, equations (8.14) and (8.16) suggest that, either from the beginning of the hot phase or after the cooling process, the dilaton value tends towards zero. This would imply that the Universe remains in an electroweak and scale-symmetric phase, which is unrealistic. The actual situation is more subtle. Unlike the dilaton, the Higgs field interacts strongly with the rest of the SM particles and can easily reach thermal equilibrium. As discussed in Appendix E, even if the equation of motion for ϕ_1 drives its vev to zero, it still experiences significant thermal fluctuations, given by:

$$\sigma_{\phi_1}^2 = \frac{T^2}{12} - \langle\phi_1\rangle_T^2 = \frac{T^2}{12}. \tag{8.17}$$

Due to the mixing term $\lambda_1\phi_0^2\phi_1^2$ in the potential, the dilaton's equation of motion acquires a contribution, which acts as a force repulsing it from the origin:

$$-\frac{\partial V_{HTE}(\phi_0,\phi_1,T)}{\partial\phi_0} \sim -2\lambda_1\phi_1^2\phi_0 \sim -\lambda_1 T^2\phi_0. \tag{8.18}$$

Moreover, as highlighted in the analysis of the parameter space, the value of λ_1 in a realistic scenario is small, so the dilaton can't reach the thermal equilibrium. Its potential, dominated by the λ_1 interaction term, is nearly flat, allowing even a small force to drive the dilaton to higher field values. Consequently, a more plausible scenario involves non-zero, large values of ϕ_0, allowing the Universe during cooling to evolve into a vacuum state where both scale and electroweak symmetries are broken. Section 8.2 further examines the possible time dynamics of the fields in this scenario.

8.2. Time Evolution in the Hot Universe

In this section, we investigate the time evolution of fields in the scale symmetric scalar sector in the hot expanding universe. We demonstrate that there are reasonable initial conditions leading to the physically relevant vacuum configuration at the very late stages of the evolution. The analysis is performed in two scenarios: a realistic model (small $|\lambda_1|$, for which dilaton is

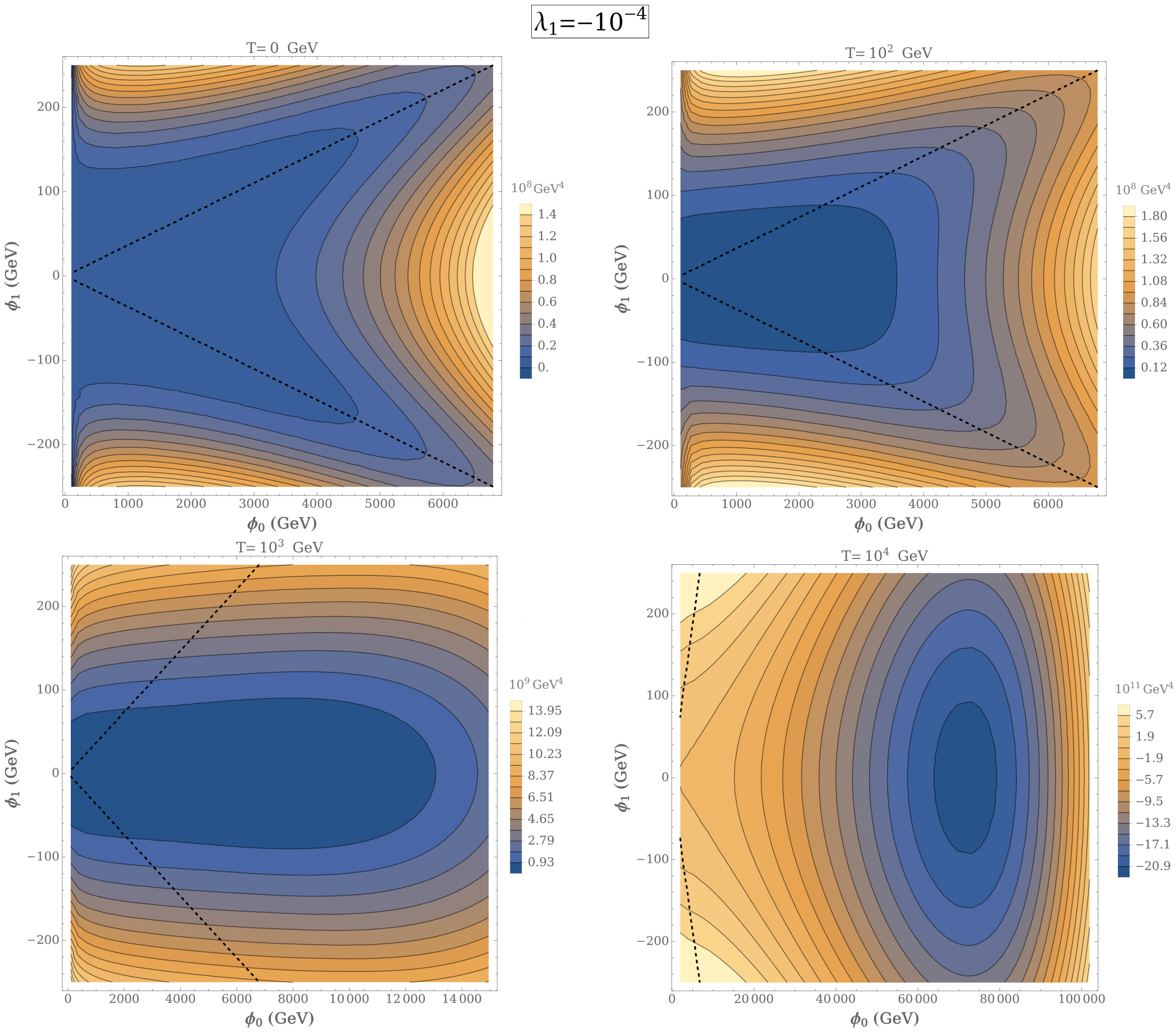

Figure 8.2: Plots of $V_{full}(\phi_0, \phi_1, T)$ for different temperatures and $\lambda_1 = -10^{-4}$, for which dilaton acquires thermal mass corrections. Black dashed lines mark the quantum flat direction (5.83). As the temperature increases, the flat direction no longer exists, and the scale symmetry is broken. The Higgs value is driven to $\langle \phi_1 \rangle_T = 0$ GeV. The dilaton ϕ_0 acquires a minimum value, proportional to the temperature (8.14). For this particular choice of λ_1, one has $\langle \phi_0 \rangle_T \approx 7.1 \cdot T$.

not in thermal equilibrium) and an unrealistic model (larger $|\lambda_1|$, for which dilaton is in thermal equilibrium), which reflect the parameter space used in simulations. Quantum corrections and running of the coupling constants in this section were neglected. We use the HTE expansion so that the potential reads:

$$V_{HTE}(\phi_0, \phi_1, T) = \lambda_0 \phi_0^4 + \lambda_1 \phi_0^2 \phi_1^2 + \lambda_2 \phi_1^4 + \frac{1}{2}\phi_1^2 \left(\lambda_2 + \frac{\lambda_1}{6} + \frac{g_1^2}{16} + \frac{3g_2^2}{16} + \frac{h_t^2}{4} \right) T^2 + \frac{1}{2}\phi_0^2 \left(\lambda_0 + \frac{\lambda_1}{6} \right) T^2, \tag{8.19}$$

where the dilaton thermal correction $\frac{1}{2}\phi_0^2 \left(\lambda_0 + \frac{\lambda_1}{6} \right) T^2$ is present only in the unrealistic model with larger $|\lambda_1|$.

The equations of motion (5.31) are supplemented with the thermal mass corrections so that,

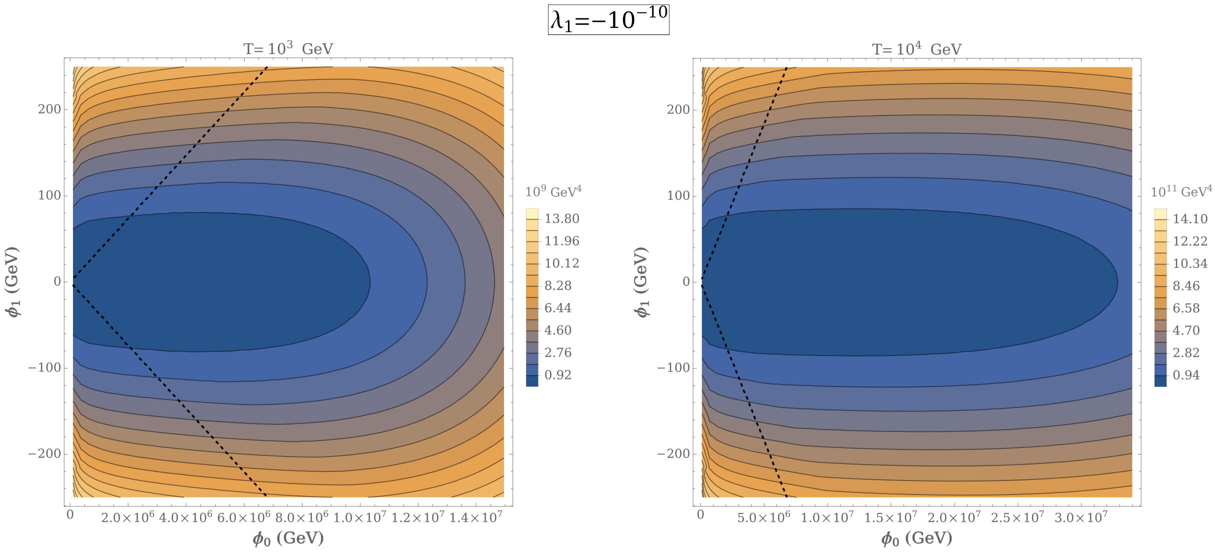

Figure 8.3: Plots of $V_{full}(\phi_0, \phi_1, T)$ for high temperatures and $\lambda_1 = -10^{-10}$, for which dilaton is not in thermal equilibrium. Black dashed lines mark the quantum flat direction (5.83). As the temperature increases, the flat direction no longer exists, and the scale symmetry is broken. Both the Higgs and dilaton values are driven to the origin. Precise dilaton direction for $\phi_1 = 0$ is illustrated in Figure 8.6.

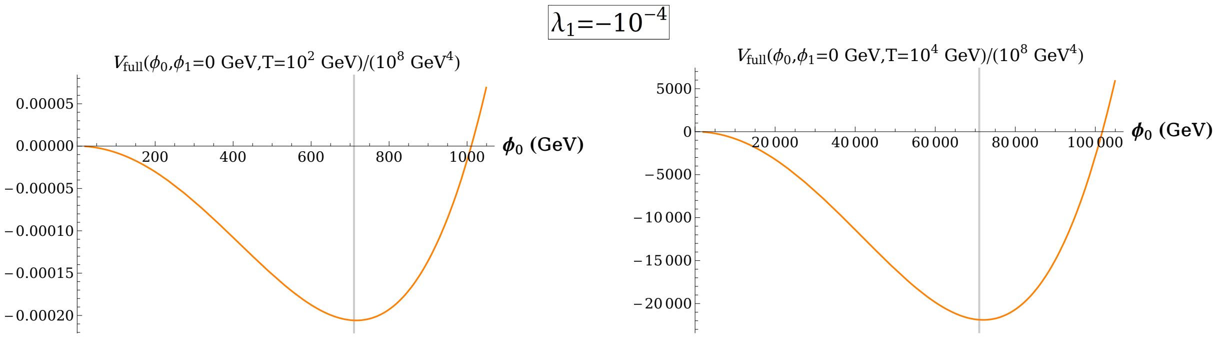

Figure 8.4: Plots of $V_{full}(\phi_0, \phi_1 = 0\text{ GeV}, T)$ for different temperatures and $\lambda_1 = -10^{-4}$, so that the dilaton is in thermal equilibrium. The gray grid lines mark the minimum (8.14).

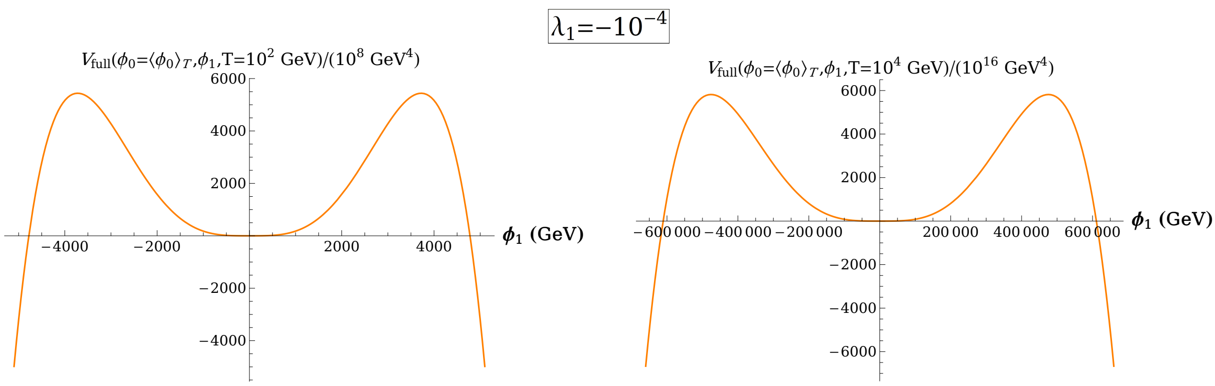

Figure 8.5: Plots of $V_{full}(\phi_0 = \langle\phi_0\rangle_T, \phi_1, T)$ for different temperatures and $\lambda_1 = -10^{-4}$, with $\langle\phi_0\rangle_T$ as in eq. (8.14). For the large Higgs field values, the potential goes to minus infinity: $\lim_{|\phi_1|\to\infty} V_{full}(\phi_0 = \langle\phi_0\rangle_T, \phi_1, T) = -\infty$.

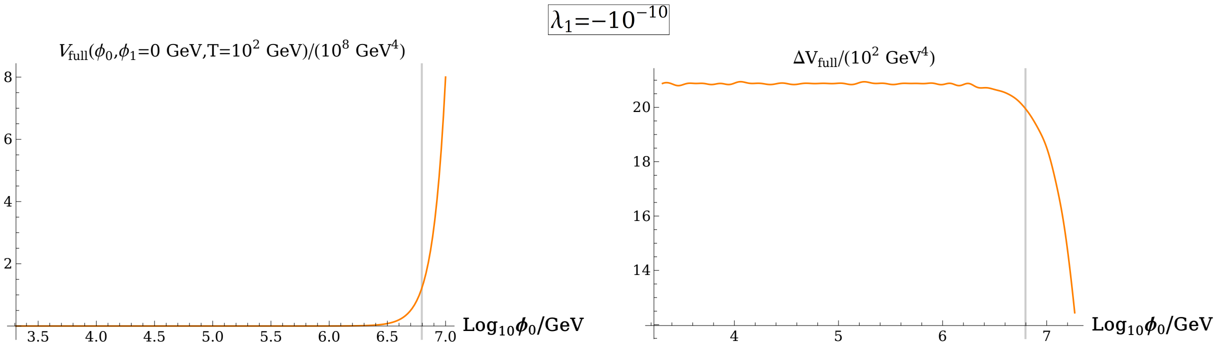

Figure 8.6: The plot of $V_{full}(\phi_0, \phi_1 = 0 \text{ GeV}, T)$ is shown with $\lambda_1 = -10^{-10}$, so that the dilaton is not in thermal equilibrium. The gray grid lines mark the zero-temperature vev of the dilaton $\langle \phi_0^2 \rangle = -\frac{2\lambda_2}{\lambda_1} \langle \phi_1^2 \rangle$. Since the dilaton does not acquire thermal mass corrections, the temperature affects the ϕ_0 direction only through the effective Higgs mass term, $\left(m_H^2\right)_{eff}(\phi_0, \phi_1, T)$, where the coupling of ϕ_0 is small parameter λ_1. This is evident in the second plot, where we defined $\Delta V_{full} = \left| V_{full}(T = 10^2 \text{ GeV}) - V_{full}(T = 10^4 \text{ GeV}) \right|$, where a temperature change of two orders of magnitude results in only a small shift in the values along the ϕ_0 direction values.

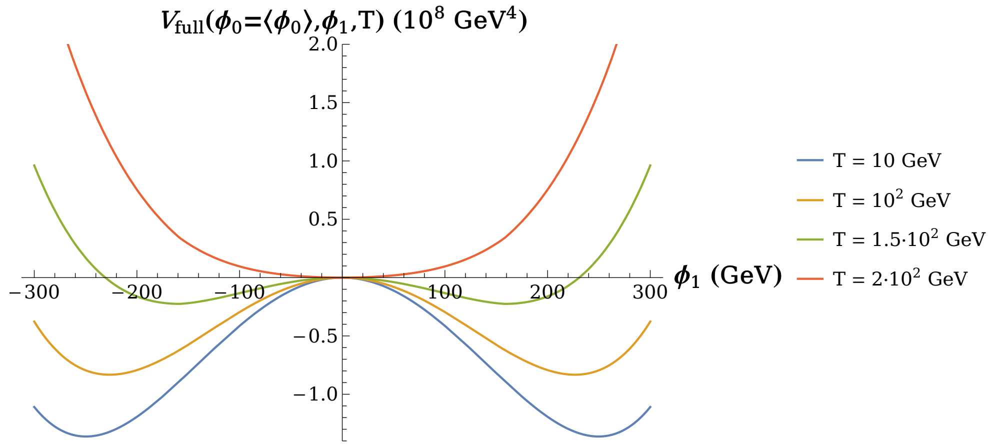

Figure 8.7: The plot of $V_{full}(\phi_0 = \langle \phi_0 \rangle, \phi_1, T)$ is shown for different temperatures, where $\langle \phi_0 \rangle = \sqrt{-\frac{2\lambda_2}{\lambda_1}} \cdot 250$ GeV. The differences between $\lambda_1 = -10^{-4}$ and $\lambda_1 = -10^{-10}$ are subtle, so the provided plot serves as a qualitative illustration of the Higgs potential behavior for both values. As the temperature decreases, the global minimum at $\langle \phi_1 \rangle_T = 0$ GeV becomes a maximum, and two degenerate minima begin to form.

with relation $R = 12H^2 + 6\dot{H}$, one has:

$$
\begin{aligned}
&\ddot{\phi}_0 + 3H\dot{\phi}_0 + 2\xi_0\phi_0 H^2 + \xi_0\phi_0\dot{H} + 4\lambda_0\phi_0^3 + 2\lambda_1\phi_0\phi_1^2 + \left(\lambda_0 + \frac{\lambda_1}{6}\right)\phi_0 T^2 = 0, \\
&\ddot{\phi}_1 + 3H\dot{\phi}_1 + 2\xi_1\phi_1 H^2 + \xi_1\phi_1\dot{H} + 4\lambda_2\phi_1^3 + 2\lambda_1\phi_0^2\phi_1 + \left(\lambda_2 + \frac{\lambda_1}{6} + \frac{g_1^2}{16} + \frac{3g_2^2}{16} + \frac{h_t^2}{4}\right)\phi_1 T^2 = 0, \\
&\frac{1}{2}\left(\xi_0\phi_0^2 + \xi_1\phi_1^2\right)\left(2H + \dot{H}\right) - \frac{1}{2}\dot{\phi_0}^2 - \frac{1}{2}\dot{\phi_1}^2 + 2\left(\lambda_0\phi_0^4 + \lambda_1\phi_0^2\phi_1^2 + \lambda_2\phi_1^4\right) + \\
&\quad + \phi_1^2\left(\lambda_2 + \frac{\lambda_1}{6} + \frac{g_1^2}{16} + \frac{3g_2^2}{16} + \frac{h_t^2}{4}\right)T^2 + \phi_0^2\left(\lambda_0 + \frac{\lambda_1}{6}\right)T^2 = 0.
\end{aligned}
\tag{8.20}
$$

The system evolves with temperature, which time dependence is changing as in the radiation-dominated era:

$$T\Big(H(t)\Big) = \sqrt{\frac{3\sqrt{10}M_P}{\pi\sqrt{g_*}}H(t)}, \tag{8.21}$$

where the Hubble parameter is treated as an independent variable, with its dynamics governed by (8.20). The number of effective degrees of freedom of relativistic particles during the radiation domination is approximately [88] $g_* \approx 100$, and the Planck mass is $M_P = 2.44 \cdot 10^{18}$ GeV.

Before discussing the exact results, let us examine the temperature contribution to the equation of motion for the ϕ_1 Higgs field. The factor $\left(\lambda_2 + \frac{\lambda_1}{6} + \frac{g_1^2}{16} + \frac{3g_2^2}{16} + \frac{h_t^2}{4}\right) = \gamma$ is positive for both λ_1 scenarios. The initial temperatures for both H_0 values (see further discussion about the initial conditions) are of the order of 10^8 GeV. As long as T remains high, the term $\gamma\phi_1 T^2$ dominates the equation of motion for ϕ_1, causing the field to oscillate around the minimum value $\phi_1 = 0$ with a very high frequency $\omega_1^2 = \gamma T^2$. These oscillations persist until the $3H\dot{\phi}_1$ term becomes significant. Since the Hubble parameter decreases during the evolution, the only aspect that effectively changes is the frequency ω_1, which decreases over time. Consequently, first, we consider the separate evolution of the dilaton sector with $\phi_1 = \dot{\phi}_1 = 0$. Then, we include the analysis of the Higgs evolution at lower temperatures, when the dilaton has settled at its final value. We provide plots illustrating the early system evolution with ϕ_1 oscillations in Figures 8.8 and 8.11.

Another important aspect to consider is the shape of the potential for dilaton in the realistic scenario (dilaton not in thermal equilibrium). For $\phi_1 = 0$, the potential is given by $V_{HTE} = \lambda_0\phi_0^4$. For small $|\lambda_1|$, the $\lambda_0 = \frac{\lambda_1^2}{4\lambda_2}$ is even smaller, making this potential nearly flat with a global minimum at $\langle\phi_0\rangle = 0$, which should be the natural starting point for the field. However, to obtain the proper Higgs vev in the later stages of evolution, the dilaton's value at late time t_k should be $\phi_0(t_k) = \sqrt{-\frac{2\lambda_2}{\lambda_1}} \cdot 250$ GeV, which is of the 10^{13} GeV order. To achieve this result, the starting point for ϕ_0 evolution should be close to $\phi_0(t_k)$, or it should begin with a large field space velocity $\dot{\phi}_0(t=0)$. This is possible after inflationary slow-roll (a detailed analysis of inflation in the Higgs-dilaton model is described in Chapter 9), where the inflaton field speeds up, enabling ϕ_0 to obtain large values of $\dot{\phi}_0$. Since the potential is nearly flat, a large field space velocity allows the dilaton to reach any value, including $\phi_0 \approx \phi_0(t_k)$ as the starting point. Therefore, we choose the initial conditions in a way that allows efficient comparison of the results in both λ_1 scenarios and to enable the dilaton to evolve to the desired $\phi_0(t_k)$ value.

The initial conditions were determined as follows:

- Two initial Hubble parameter values were chosen: $H_0 = \{0.1, 0.5\}$ GeV; this choice was arbitrary.
- The initial temperature was chosen as $T_0 = T(H_0)$ from equation (8.21), giving $T_0 = \{2.7 \cdot 10^8, 6.1 \cdot 10^8\}$ GeV.
- The initial Higgs field value $\phi_1(t=0)$ could be sampled from a normal distribution with a mean value equal to its temperature minimum value $\mu = \langle\phi_1\rangle_{T_0} = 0$ GeV and variance $\sigma^2 = \frac{T_0^2}{12}$, as ϕ_1 is in thermal equilibrium (see: Appendix E). This choice only affects the amplitude of the ϕ_1 oscillations. Consequently, for greater clarity in the plots, we set $\phi_1(t=0) = 10$ GeV.
- The initial Higgs field time derivative value $\dot{\phi}_1(t=0)$ could be sampled from a normal distribution with a mean value $\mu = 0$ and variance $\sigma^2 = \frac{\pi^2}{30}T^4$ for fields in thermal equilibrium (see: Appendix E). This choice only affects the amplitude of the ϕ_1 oscillations. Consequently, for greater clarity in the plots, we set $\dot{\phi}_1(t=0) = 300$ GeV^2.
- Following the previous discussion about the dilaton initial conditions, we set $\phi_0(t=0) = \sqrt{-\frac{2\lambda_2}{\lambda_1}} \cdot \phi_1(t=0)$ and $\dot{\phi}_0(t=0) = \sqrt{-\frac{2\lambda_2}{\lambda_1}} \cdot \dot{\phi}_1(t=0)$, which allows the dilaton to reach its desired final value $\phi_0(t_k) = \sqrt{-\frac{2\lambda_2}{\lambda_1}} \cdot 250$ GeV. This choice was implemented in both λ_1

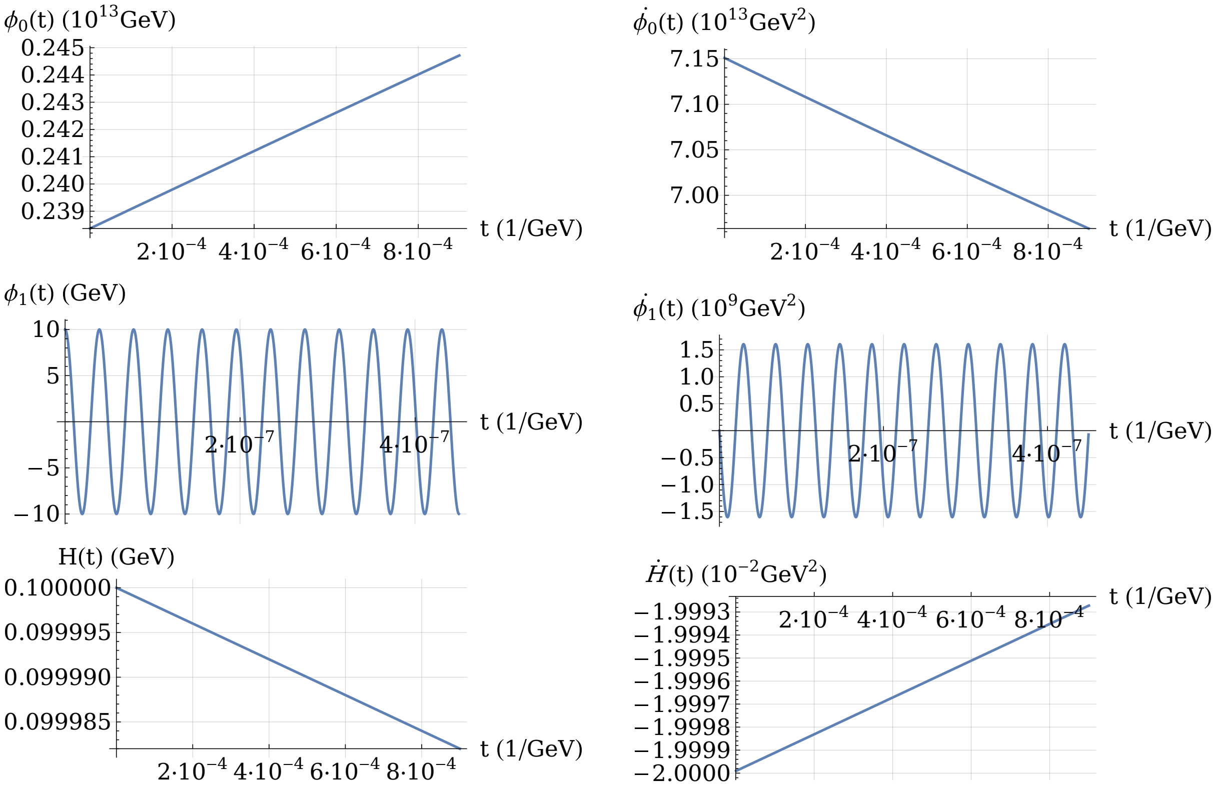

Figure 8.8: The evolution of the ϕ_i fields and Hubble parameter H for early times in the realistic model with $\lambda_1 = -1.1 \cdot 10^{-24}$. For greater clarity, only the $H_0 = 0.1$ GeV plots are included. Note the different time ranges at the Higgs field ϕ_1 plots, which were changed due to the high frequency of its oscillations.

scenarios to emphasize the effect of larger $|\lambda_1|$, resulting in the dilaton being in thermal equilibrium. However, the natural starting point for the dilaton in the case of larger $|\lambda_1|$ is its temperature minimum value $\langle\phi_0^2\rangle_T = -\frac{1+64\lambda_1}{192\lambda_1}T^2$ (see: equation (8.14)). Therefore, we provide an additional analysis of a case with $\phi_0(t=0) = \langle\phi_0\rangle_T + \delta_x$ and $\dot{\phi}_0(t=0) = \delta_v$, where δ_i are some relatively small quantities chosen arbitrarily so that the dilaton starts its evolution around its temperature minimum.

8.2.1. Realistic Model: dilaton out of the thermal equilibrium

The parameter space chosen in this section, fulfilling requirements from the Subsection 5.2.1, and motivated by the later analysis of inflation in Chapter 9, is given by:

$$\lambda_1 = -1.1 \cdot 10^{-24}, \qquad \lambda_2 = 0.03125, \qquad \lambda_0 = \frac{\lambda_1^2}{4\lambda_2}, \qquad \xi_0 = 10^{10}, \qquad \xi_1 = 10^5. \tag{8.22}$$

The initial phase of the field's evolution, including the Higgs field ϕ_1 oscillations, is shown in Figure 8.8. Figure 8.9 illustrates the separate evolution of the dilaton sector alone.

Interesting behavior can be observed in the evolution of the Hubble parameter H. As shown in Figure 8.10, for the same initial conditions, except for the initial H_0 value, all trajectories merge and evolve similarly after a sufficiently long time. This can be understood by examining the last equation from (8.20) in the limit ($v_h = 250$ GeV):

$$\phi_0 \to \sqrt{-\frac{2\lambda_2}{\lambda_1}}v_h, \quad \dot{\phi}_0 \to 0, \quad \phi_1 \to 0, \quad \dot{\phi}_1 \to 0, \tag{8.23}$$

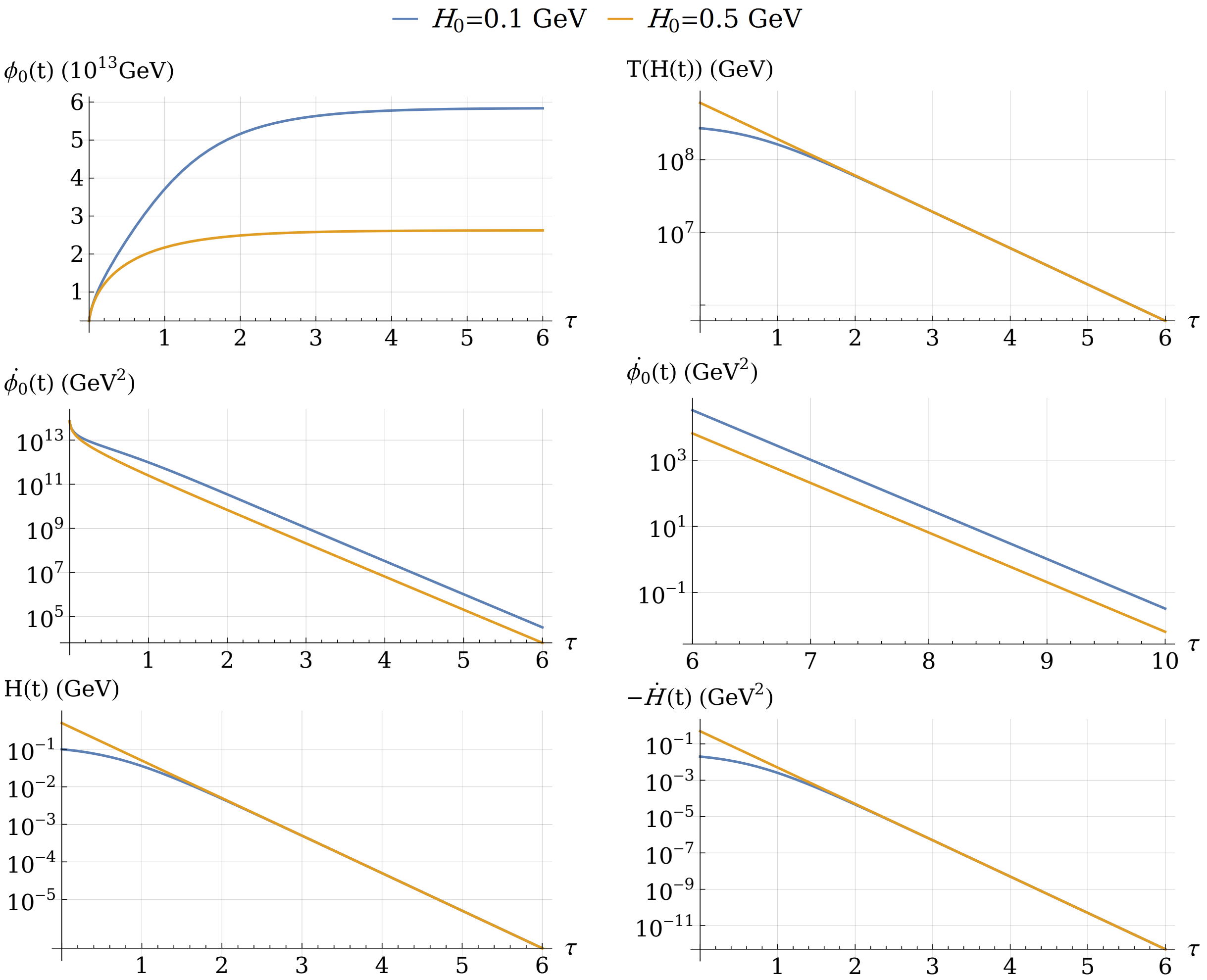

Figure 8.9: The evolution of the dilaton field ϕ_0 and Hubble parameter H over time in the realistic model with $\lambda_1 = -1.1 \cdot 10^{-24}$. An additional plot for $\dot{\phi}_0(t)$ is included for later times to demonstrate that ϕ_0 indeed stabilizes. The dimensionless time variable is given by $\tau = \log_{10}\left[t \cdot \text{GeV}\right]$. The $H_0 = 0.1$ GeV trajectories correspond to the physical evolution with $\phi_0(t_k) = \sqrt{-\frac{2\lambda_2}{\lambda_1}} \cdot 250$ GeV.

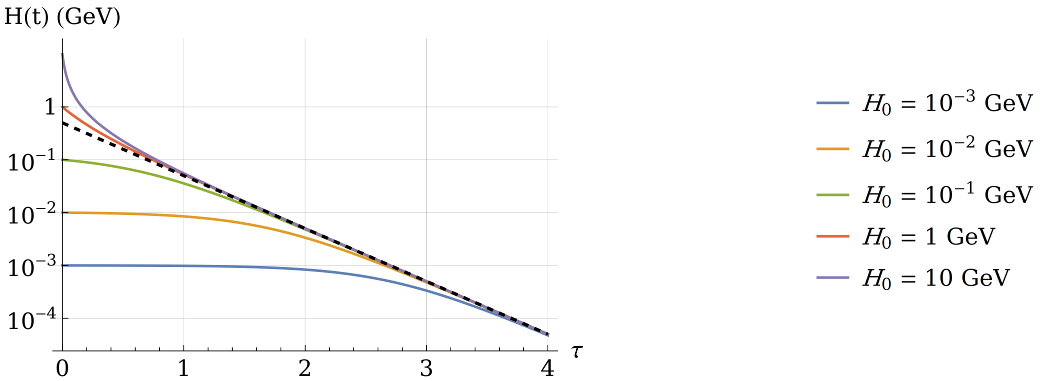

Figure 8.10: The evolution of the Hubble parameter H over time, for different initial H_0 values. The rest of the initial conditions were chosen the same as for plots in Figures (8.8) and (8.12). All solutions merge at the black dashed line, which represents the radiation-dominated Hubble parameter time dependence $H_{rad}(t) = \frac{1}{2t}$. The dimensionless time variable is given by $\tau = \log_{10}\left[t \cdot \text{GeV}\right]$.

where the fields settled at their final values, as depicted in Figure (8.9). This leaves us with:

$$\lambda_2 v_h \left(2\lambda_1 v_h^2 - \xi_0 \left(\dot{H} + 2H^2\right)\right) = 0, \tag{8.24}$$

yielding the solution:

$$H(t) = \sqrt{\delta} v_h \tan \left[\arctan \left(\frac{H_0}{\sqrt{\delta} v_h} \right) - 2\sqrt{\delta} v_h \cdot t \right], \tag{8.25}$$

where we have defined $\delta = -\frac{\lambda_1}{\xi_0} \lll 1$ (in a realistic model, $|\lambda_1| \ll 1$ and $\xi_0 \gg 1$). For $H_0 > 10^{-12}$ GeV, the argument of arctan is large enough, so $\arctan\left(\frac{H_0}{\sqrt{\delta} v_h}\right) \approx \frac{\pi}{2}$. Expanding further in δ:

$$H(t) = \frac{1}{2t} - \frac{2}{3}\delta v_h^2 \cdot t + \mathcal{O}(\delta^2). \tag{8.26}$$

This solution is independent of the initial conditions and, to the 0-th order, represents the radiation-dominated Hubble parameter time dependence $H_{rad}(t) = \frac{1}{2t}$.

8.2.2. Unrealistic Model: dilaton in the thermal equilibrium

The parameter space chosen in this section is:

$$\lambda_1 = -10^{-4}, \qquad \lambda_2 = 0.03125, \qquad \lambda_0 = \frac{\lambda_1^2}{4\lambda_2}, \qquad \xi_0 = 10^{10}, \qquad \xi_1 = 10^5, \tag{8.27}$$

where we changed only the λ_1 value to isolate its effects on the system evolution. With this choice, the dilaton is in thermal equilibrium and its thermal correction $\frac{1}{2}\phi_0^2\Big(\lambda_0 + \frac{\lambda_1}{6}\Big)T^2 = \frac{1}{2}\phi_0\gamma_0 T^2$ is present in $V_{HTE}(\phi_0, \phi_1, T)$.

In Figure 8.11, we present the early evolution of the system with the same initial conditions as in the realistic scenario (note that the $\phi_0(t=0)$ and $\dot{\phi}_0(t=0)$ are λ_1 dependent, so they are the same in a sense of the scale associated with λ_1 value). The whole system exhibits non-trivial oscillatory behavior and appears unstable due to the vastly increasing $\dot{H}$. The solutions with $\phi_1 = \dot{\phi}_1 = 0$ are depicted in Figure 8.12 and fully reveal the instability.

We present the effective potential $V_{eff}(\phi_0, t)$ for the dilaton in this case in Figure 8.13a:

$$V_{eff}^{(0)}(\phi_0, t) = \lambda_0 \phi_0^4 + \frac{1}{2}\phi_0^2\Big(\frac{\lambda_1}{6} + \lambda_0\Big)T^2\big(H(t)\big) + \frac{\xi_0}{12}\phi_0^2\big(12H(t) + 6\dot{H}(t)\big), \tag{8.28}$$

where the gravitational part is included as it affects the ϕ_0 evolution. The effective potential has a global minimum at $\phi_0 = 0$ for all t and becomes steeper over time. Consequently, the dilaton rolls towards the minimum faster and faster.

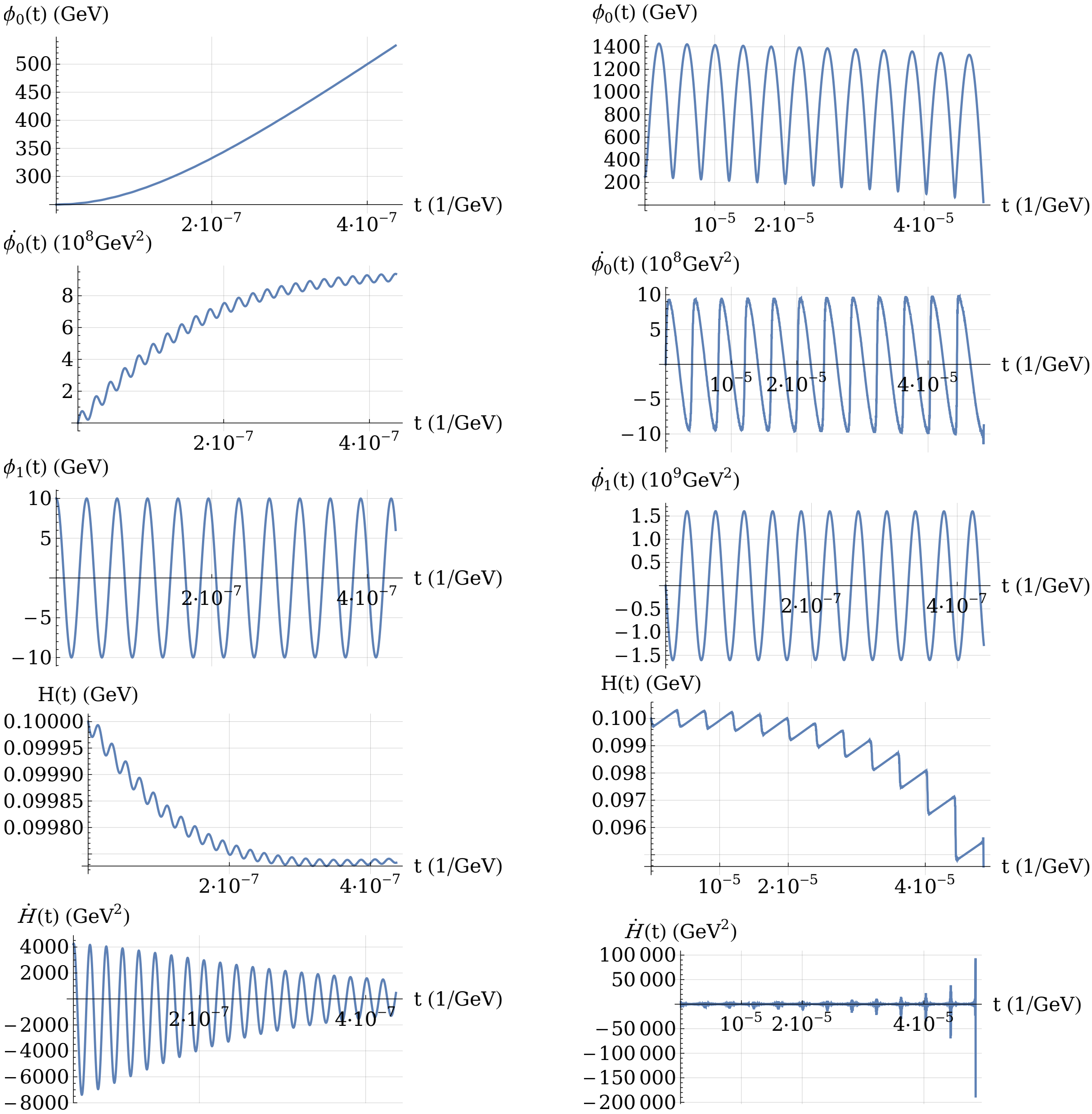

Figure 8.11: The evolution of the ϕ_i fields and Hubble parameter H for early times in the unrealistic model with $\lambda_1 = -10^{-4}$. For greater clarity, only the $H_0 = 0.1$ GeV plots are included.

One can also analyze the effective potential for the Hubble parameter H, treating it as a field:

$$V_{eff}^{(H)}(H, t) = \xi_0 \phi_0^2(t) \cdot H^2 + \frac{1}{2}\phi_0^2(t)\left(\frac{\lambda_1}{6} + \lambda_0\right)T^2(H). \tag{8.29}$$

As shown in Figure 8.13b, the potential has a global minimum at the value $H = 305$ GeV for all t and gets flatter over time. The Hubble parameter starts to roll rapidly in the early stages, which destabilizes the system even more.

Thermal minimum as a starting point for dilaton

Here, we briefly analyze the system's behavior when the dilaton field begins its evolution at $\phi_0(t=0) = \langle\phi_0\rangle_T + \delta_x$ and $\dot{\phi}_0(t=0) = \delta_v$, where $\langle\phi_0^2\rangle = -\frac{1+64\lambda_1}{192\lambda_1}T^2$ is its temperature minimum value and δ_i are some relatively small quantities chosen arbitrarily. The initial conditions are

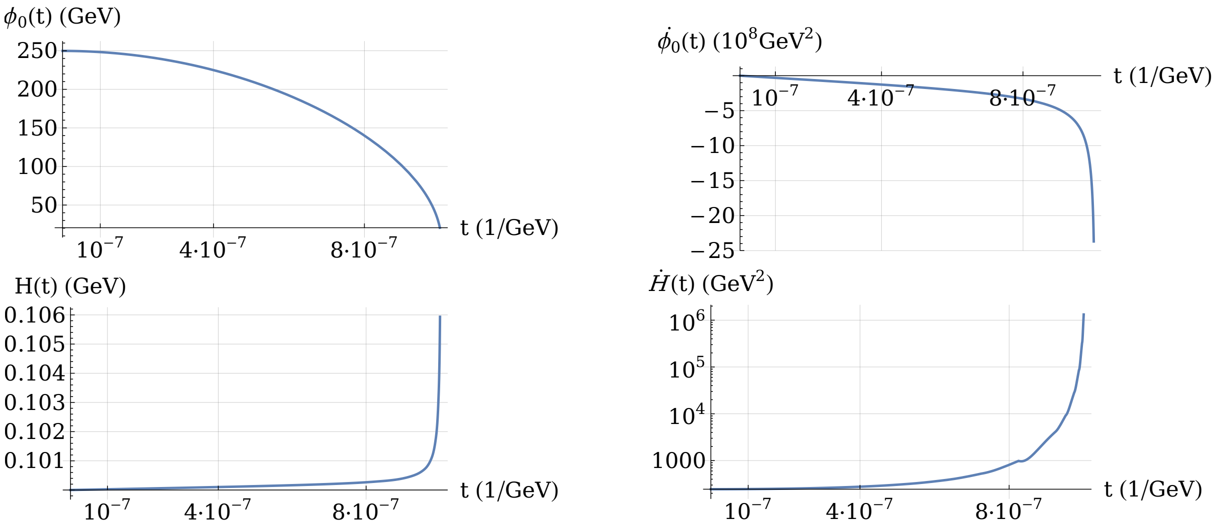

Figure 8.12: The evolution of the dilaton field ϕ_0 and Hubble parameter H in the unrealistic model with $\lambda_1 = -10^{-4}$. For greater clarity, only the $H_0 = 0.1$ GeV plots are included.

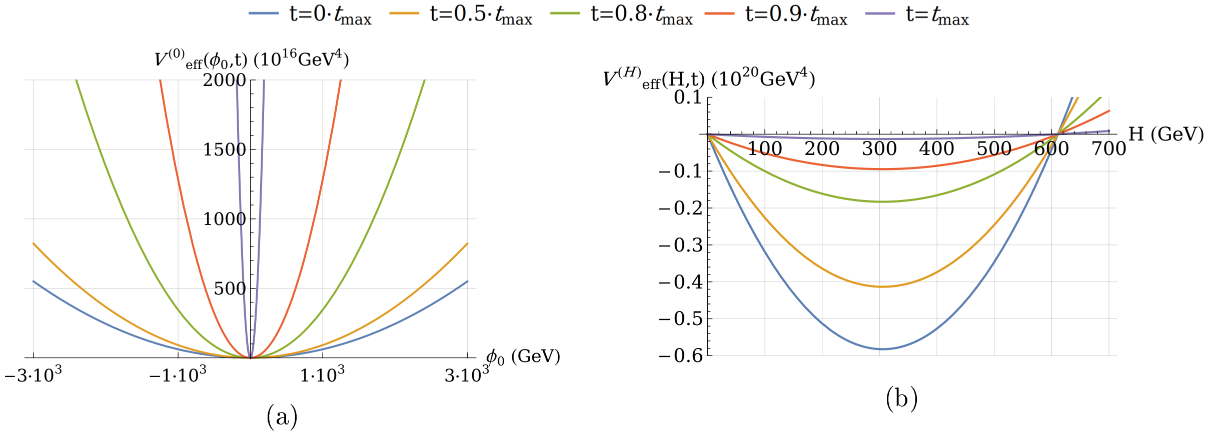

Figure 8.13: Plots showing the shape of the dilaton field potential (8.28) and of the Hubble parameter H potential (8.29) during the evolution depicted in Figure 8.12. The t_{max} is the maximum value of the time axis shown in Figure 8.12.

then as follows:

$$\phi_0(0) = \langle\phi_0\rangle_T + \delta_x, \quad \dot{\phi}_0(0) = \delta_v, \quad \phi_1(0) = 10 \text{ GeV}, \quad \dot{\phi}_1(0) = 300 \text{ GeV}^2, \quad H(0) = 0.1 \text{ GeV}. \tag{8.30}$$

Figure 8.14 illustrates the time evolution of both fields and the Hubble parameter in this scenario. Since the shape of the dilaton potential (8.28), depicted in Figure 8.13a, remains unchanged, the system is unstable. The dilaton rapidly approaches zero, while the Hubble parameter evolves to larger values. The potential for H (8.29) remains the same as in Figure 8.13b, but with a different minimum value, $H = 153$ GeV, due to the altered ϕ_0 values.

8.2.3. Electroweak Symmetry Breaking

We analyze the realistic model late-time evolution of the Higgs scalar field separately, at sufficiently low temperatures, after the dilaton has settled at its final value. At high temperatures, the Higgs mean value is zero $\langle\phi_1\rangle_T = 0$ GeV. However, since the Higgs field easily reaches the thermal equilibrium, its equilibrium value includes a variance $\sigma^2 = \frac{T^2}{12}$. Consequently, it can fluctuate away from the origin at any moment and evolve toward its physical ground state with $\langle\phi_1\rangle = 250$ GeV as the temperature approaches zero. The initial conditions were chosen as

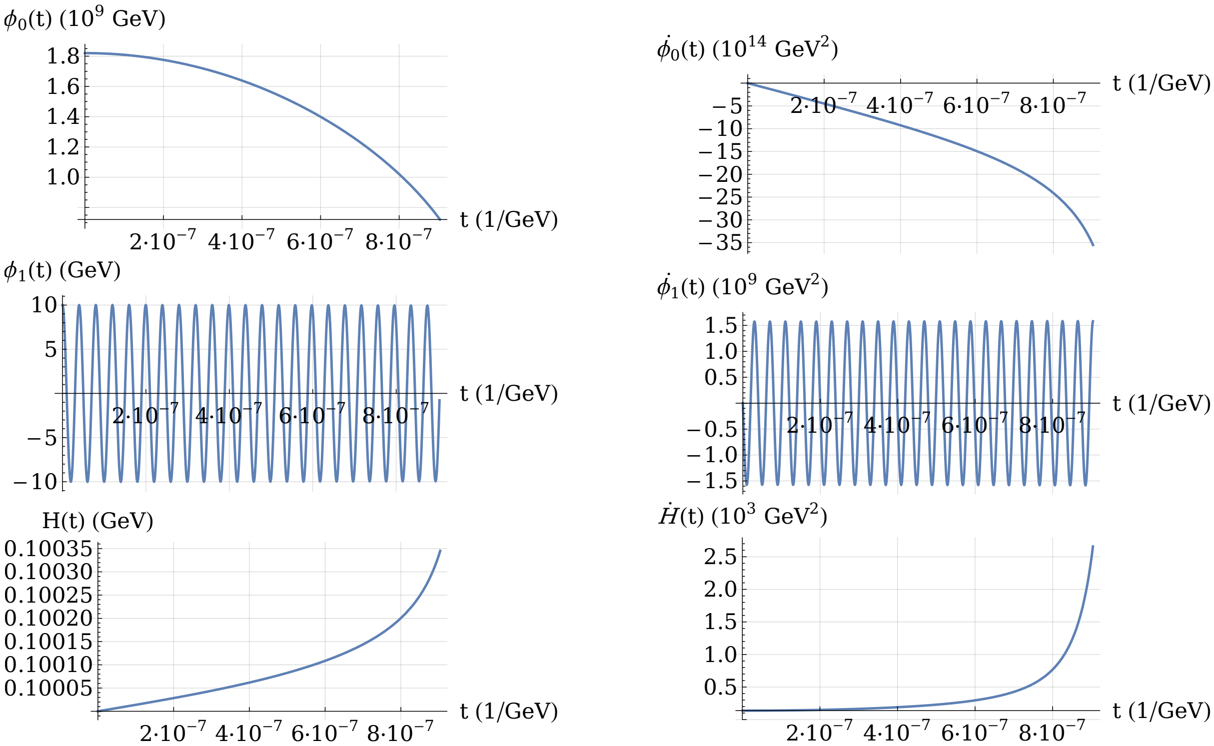

Figure 8.14: The evolution of the ϕ_i fields and Hubble parameter H for early times in the unrealistic model with $\lambda_1 = -10^{-4}$ and dilaton starting point as its thermal minimum $\langle\phi_0\rangle_T$. For greater clarity, only the $H_0 = 0.1$ GeV plots are included.

follows:

- As the dilaton stabilizes in the later stages of evolution, we fix its value at $\phi_0 = \sqrt{-\frac{2\lambda_2}{\lambda_1}} \cdot 250$ GeV and set its filed space velocity to zero, $\dot{\phi}_0 = 0$ GeV^2;
- The initial Hubble parameter and temperature are chosen so that the potential exhibits minima distinct from the origin, with $T_0 \approx 30$ GeV and $H_0 = 10^{-15}$ GeV.

Even at the lower temperatures, the Higgs oscillation frequency remains high. Through these oscillations, particle production can occur, causing the Higgs particle to lose energy and eventually stop. This process is implemented in the equations of motion by modifying the friction term for ϕ_1 to include an effective decay term:

$$3H\dot{\phi}_1 \quad \longrightarrow \quad (3H + \Gamma_H)\dot{\phi}_1, \tag{8.31}$$

where Γ_H is the total Higgs decay width [62]: $\Gamma_H \approx 4.1$ MeV. Figure 8.15 illustrates the Higgs field evolution incorporating the particle decay. The high oscillations are visible as the blue lines almost entirely cover both plots. The average behavior of the ϕ_1 field, marked by orange lines, shows that the Higgs settles at its physical vev $\langle\phi_1\rangle = 250$ GeV.

The evolution of the full Higgs potential over time, across different temperatures, was previously illustrated in Figure 8.7. Figure 8.16 represents a close-up view of the potential near the origin, allowing us to better examine the nature of the EWSB phase transition. Since the potential $V_{full}(\phi_0 = v_0, \phi_1, T)$ includes quantum corrections that preserve scale symmetry, it remains flat at the origin at all temperatures. The critical temperature is the only significant scale, marking the point at which the origin shifts from a minimum to a maximum and two degenerate minima emerge. The absence of a barrier for the ϕ_1 field signals a smooth, second-order phase transition. Consequently, in this model, there is no gravitational waves production from a first-order phase transition or bubble production.

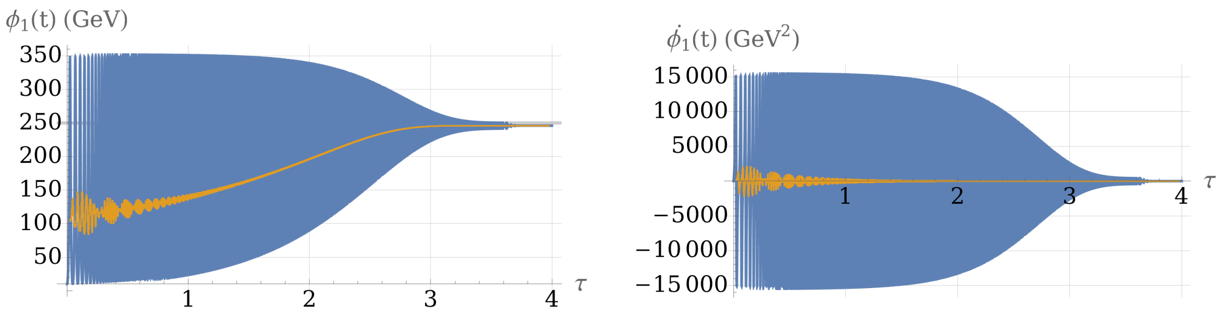

Figure 8.15: Plots of the further evolution of the Higgs field ϕ_1 and its field space velocity $\dot{\phi}_1$ are shown, with initial conditions set to $\phi_1(0) = 10$ GeV, $\dot{\phi}1(0) = 0$ GeV^2, $T_0 = 30$ GeV, and $H_0 = 10^{-15}$ GeV. At this stage, the Hubble parameter and temperature remain constant over time, therefore we do not present their plots. The blue lines represent the actual evolution, which is highly oscillatory and thus appears as a filled shape rather than a line. The orange lines indicate the time-averaged values of the blue lines. The dimensionless time variable used is $\tau = \log 10(t/\text{GeV})$.

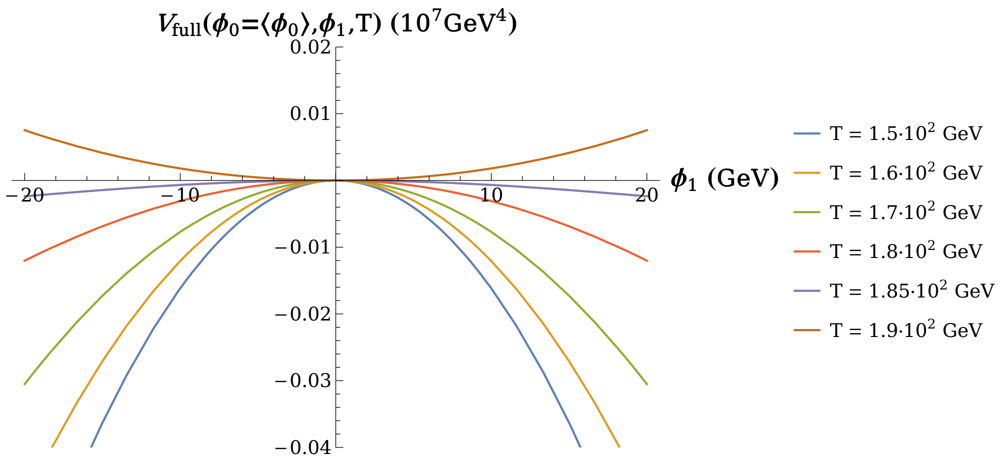

Figure 8.16: The close up of the plot of $V_{full}(\phi_0 = \langle\phi_0\rangle, \phi_1, T)$ for different temperatures around the critical temperature, where $\langle\phi_0\rangle = \sqrt{-\frac{2\lambda_2}{\lambda_1}} \cdot 250$ GeV. As the temperature decreases, the global minimum at $\langle\phi_1\rangle_T = 0$ GeV becomes a maximum, and two degenerate minima begin to form.

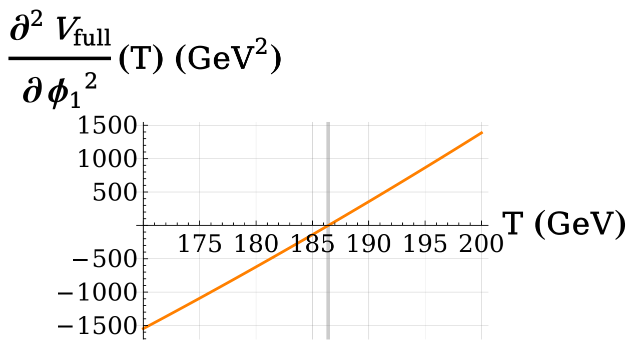

Figure 8.17: Plot of the second derivative of the potential, $V_{full}(\langle\phi_0\rangle, \phi_1, T)$, at the origin with marked critical temperature, $T_C \approx 186$ GeV, at which the second derivative changes sign. The absence of discontinuous jumps in the second derivative indicates that the EWSB phase transition is of second order.

8.3. Conclusions

Temperature explicitly breaks the scale symmetry, as it introduces a mass scale. As shown in Figure 8.7, the potential for the Higgs scalar, ϕ_1, takes on a characteristic shape with two degenerate minima after the temperature decreases, with the dilaton settling at its vev, $\langle\phi_0^2\rangle = -\frac{2\lambda_2}{\lambda_1}\langle\phi_1^2\rangle$. We demonstrated that there are possible initial conditions for the evolution of fields in the hot Universe to reach the physical vacuum state, where both scale and electroweak symmetry are broken.

The process proceeds as follows: First, the electroweak symmetry is restored by temperature corrections, keeping the Higgs field at the origin for high T. Meanwhile, the dilaton can evolve to its desired value, setting the proper EW scale, $\langle\phi_0^2\rangle = -\frac{2\lambda_2}{\lambda_1}\langle\phi_1^2\rangle$. Even after the dilaton settles at its vev, the temperature may still be too high for the electroweak symmetry breaking (EWSB) to occur. As T decreases, the Higgs scalar, which can easily reach the thermal equilibrium, can start its further evolution towards the 250 GeV minimum due to the thermal fluctuations. As the Higgs approaches its vev, it oscillates with a high frequency given by $\omega_1^2 = \left(\lambda_2 + \frac{\lambda_1}{6}\frac{\lambda_1}{6} + \frac{g_1^2}{16} + \frac{3g_2^2}{16} + \frac{h_t^2}{4}\right)T^2$. These oscillations can signal various physical phenomena. As the Universe cools, interactions with other SM particles in the hot plasma can dissipate the Higgs energy, leading to the damping of these oscillations. The Higgs may also decay into lighter SM particles, effectively converting its oscillatory energy into radiation and matter, eventually stabilizing at its minimum. We reject the possibility that the Higgs stops oscillating due to the Hubble friction, as the ω_1 frequency is dominated by the contributions from the top quark and gauge bosons, staying high compared to the Hubble parameter H, throughout most of the cooling process and time evolution.

As indicated in Figure 8.16, which includes full thermal corrections, one-loop effects, and RG improvement, the EW symmetry-breaking phase transition is second-order. Therefore, the transition is smooth and does not produce abrupt changes, bubble formation, or gravitational waves in this model.

Chapter 9

Inflation in the Scale Symmetric Standard Model

This Chapter explores the potential for inflation within the framework of the scale-symmetric Standard Model, focusing on the scalar sector of the Higgs field coupled with the dilaton immersed in Weyl conformal geometry, based on the paper by author and her supervisor [36]. The tree-level inflationary scenarios of the similar Higgs-dilaton models have been extensively studied in previous works in [2,6,37–39,43–45], including the implications of Weyl geometry [11,12,17], and the impact of quantum corrections [3,40–42]. The novelty of this work lies in three key aspects:

1. The analysis of the Higgs-dilaton model coupled to Weyl geometry incorporating the kinetic term for the dilaton. This addition is essential for dynamic mass generation, particularly the μ subtraction scale, as discussed in Chapter 3.
2. The inclusion of quantum corrections through one-loop beta function within the framework of Weyl conformal geometry, as this affects the form of the Einstein-Hilbert Lagrangian, which plays a key role in the inflationary dynamics of the model.
3. The incorporation of propagator suppression factors [41,42,89,90], present in models with scalar fields non-minimally coupled to the curvature. They impact the beta functions of couplings, changing their RG evolution.

This approach extends the existing literature by addressing the effects of the dilaton's dynamics and quantum corrections in the Weyl geometry model.

The chapter begins with a compact introduction to the notions necessary for understanding the inflationary theory discussed in subsequent sections. While these concepts are exhaustively covered in many standard textbooks and cosmology lectures [91–93], a brief overview is provided here for clarity and completeness of the work.

The large-scale homogeneity and isotropy of the Universe give rise to the Friedmann-Lemaître-Robertson-Walker FLRW metric:

$$\mathrm{d}s^2 = -\mathrm{d}t^2 + a^2(t)\left(\frac{\mathrm{d}r^2}{1-kr^2} + r^2\big(\mathrm{d}\theta^2 + \sin^2\theta\,\mathrm{d}\phi^2\big)\right), \tag{9.1}$$

where t is the cosmic time and $a(t)$ is the scale factor, characterizing the relative size of the Universe. The parameter k determines the curvature of spacetime, with $k = +1$ for positive curvature, $k = 0$ for flat geometry, and $k = -1$ for negative curvature. The evolution of the $a(t)$ reflects the dynamics of the Universe and depends on its matter content, energy density ρ, and isotropic pressure p. This evolution is governed by the Einstein field equations. Assuming a zero cosmological constant ($\Lambda = 0$), the equations reduce to the Friedmann equations:

$$\left(\frac{\dot{a}}{a}\right)^2 = H^2 = \frac{\rho}{3} - \frac{k}{a^2}, \tag{9.2}$$

$$\frac{\ddot{a}}{a} = \dot{H} + H^2 = -\frac{1}{6}(\rho + 3p). \tag{9.3}$$

Here, $H = \frac{\dot{a}}{a}$ is the Hubble parameter, representing the expansion rate of the Universe. The Hubble time, $t \sim H^{-1}$, and the Hubble length, $d \sim H^{-1}$, set the scales for the age and size of the observable Universe, respectively. At the present time t_0, the scale factor is set to $a(t_0) = 1$, and the Hubble parameter has a current value of $H_0 = H(t_0) = 70\frac{\mathrm{km/s}}{\mathrm{Mpc}}$ [94].

One can define the equation of state parameter $w = p/\rho$, characterizing the relationship between energy density ρ and isotropic pressure p. Specific values of w correspond to different types of matter or energy: $w = 0$ for non-relativistic matter, $w = \frac{1}{3}$ for radiation or relativistic matter, and $w = -1$ for the cosmological constant (possibly associated with dark energy). Assuming a flat Universe, $k = 0$, the equations (9.2) and (9.3), give the solutions for the scale factor $a(t)$ as:

$$a(t) \sim \begin{cases} t^{\frac{2}{3}(1+w)} & w \neq -1, \\ \exp\{Ht\} & w = -1. \end{cases} \tag{9.4}$$

To describe the geometry and matter content of the Universe, one introduces the critical density ρ_c and the density parameter Ω:

$$\Omega - 1 = \frac{k}{(aH)^2}, \qquad \Omega = \frac{\rho}{\rho_c}, \qquad \rho_c = 3H^2 \qquad (8\pi G \equiv 1). \tag{9.5}$$

When $\rho = \rho_c$, the spatial geometry is flat, $k = 0$. The present knowledge, based on the observations of cosmic microwave background (CMB) and the large-scale structure, indicates that the Universe is flat, with $\Omega = 1$. Current estimates of the matter and energy composition of the Universe suggest the following distribution: 4.6% baryonic matter, 24.5% cold dark matter, and 70.9% dark energy (cosmological constant) [95]:

$$\Omega_b = 0.046, \qquad \Omega_{DM} = 0.245, \qquad \Omega_\Lambda = 0.709. \tag{9.6}$$

9.1. Big Bang Puzzles and Conditions for Inflation

According to the Big Bang Theory, the Universe began its evolution at $t = 0$ (one sets $a(t = 0) = 0$) from a state of extremely high energy density. Following this moment, the Universe went through a phase of decelerated expansion ($\dot{a} > 0$ and $\ddot{a} < 0$). However, to evolve to its current state, the Universe at the very beginning had to be in very precise, fine-tuned initial conditions, which raise several fundamental challenges. In this section, we briefly outline these issues, which are later addressed by the inflationary theory.

Flatness problem:
Decelerated expansion requires $\dot{a} > 0$ and $\ddot{a} < 0$, so that the $\dot{a}$ decreases over time. Substituting $aH = \dot{a} > 0$ to the equation (9.5) one can observe that $\frac{k}{(aH)^2} = \frac{k}{\dot{a}^2}$ grows with time. So even if we start from sufficiently large $\dot{a}$, so that $\Omega \approx 1$ at the beginning, it is an unstable fixed point. To obtain the flat Universe observed today, one needs Ω even closer to 1 in the past. For example, we require $|\Omega - 1| \leq \mathcal{O}(10^{-16})$ at the nucleosynthesis epoch and $|\Omega - 1| \leq \mathcal{O}(10^{-64})$ at the Planck epoch [94]. This is a very rigorous condition.

Horizon problem:
The photons that decoupled from the primordial plasma during recombination reveal almost perfect isotropy, with temperature variations in the cosmic microwave background (CMB) on the order of $\mathcal{O}(10^{-5})$ K. This suggests that the observed CMB regions should have been casually connected. However, the situation is different. Any two points separated by at least 1 degree in the sky have distinct past light cones that do not overlap [92]. The question arises: How can such distant regions of the Universe exhibit such extraordinary isotropy despite having no way to exchange information or energy to equilibrate?

9.1.1. Conditions for Inflation

Cosmic inflation solves the flatness and horizon problems by proposing a period of rapid exponential expansion in the very early Universe. This expansion drives Ω close to 1, regardless of its initial value, and ensures that tiny, casually connected regions expand to encompass the entire observable Universe, explaining its isotropy and homogeneity. The conditions for inflation are outlined below:

- **Accelerated expansion ($\ddot{a} > 0$):** Relating the scale factor to the Hubble parameter, one obtains the first slow-roll parameter, ϵ :

$$\frac{\ddot{a}}{a} = H^2 + \dot{H} = H^2\big(1-\epsilon\big), \qquad \epsilon = -\frac{\dot{H}}{H^2}, \tag{9.7}$$

  where acceleration $\ddot{a}$ corresponds to $\epsilon < 1$. Further, one defines the number of e-folds N as $\mathrm{d}N = H\mathrm{d}t = \mathrm{d}\ln a$, which gives $\epsilon = -\mathrm{d}\ln H/\mathrm{d}N < 1$.

- **Negative pressure:** Substituting the accelerated expansion condition $\ddot{a} > 0$ into equation (9.3) relates pressure p and energy density ρ as:

$$p < -\frac{1}{3}\rho \quad \Rightarrow \quad w < -\frac{1}{3}, \tag{9.8}$$

  which violates the strong energy condition for a perfect fluid.

- **Decreasing comoving horizon:** From $\dot{a} > 0$ and $\ddot{a} > 0$, the comoving Hubble radius $(aH)^{-1}$ decreases over time:

$$\frac{d}{dt}\Big(\frac{1}{aH}\Big) = -\frac{\ddot{a}}{(aH)^2} < 0. \tag{9.9}$$

  This ensures that Ω in equation (9.5) is driven to unity. After the inflation ends, $|\Omega - 1|$ increases with time, but a sufficiently long inflationary period keeps Ω close to 1. For inflation to resolve the horizon problem, $(aH)^{-1}$ must shrink by a factor of approximately 10^{28} times [92]. Assuming a constant Hubble parameter $H \approx const$ (which is a consequence of $\epsilon = -\mathrm{d}\ln H/\mathrm{d}N < 1$), this corresponds to an approximate number of e-folds:

$$N = \int \mathrm{d}\ln a = \int \frac{1}{aH}\mathrm{d}aH \approx \ln 10^{28} \approx 64. \tag{9.10}$$

- **Constant energy density:** From the continuity equation for a perfect fluid [92], $\dot{\rho} = -3H\big(\rho + p\big)$, combined with the second Friedman equation (9.3), one obtains:

$$\left|\frac{\mathrm{d}\ln\rho}{\mathrm{d}\ln a}\right| = 2\epsilon < 1. \tag{9.11}$$

  Therefore, inflation requires a nearly constant energy density, which cannot be achieved with conventional matter sources.

9.1.2. Scalar Field Inflationary Dynamics

The accelerated expansion of the Universe can be achieved using a model of a homogeneous scalar field, $\phi = \phi(t)$, to which we will refer as inflaton. Given its Lagrangian:

$$\frac{\mathcal{L}}{\sqrt{g}} = \frac{1}{2}\dot{\phi}^2 - V(\phi), \tag{9.12}$$

the stress-energy tensor is derived as:

$$T_{\mu\nu} = \partial_\mu\phi\partial_\nu\phi - g_{\mu\nu}\Big(\frac{1}{2}g^{\alpha\beta}\partial_\alpha\phi\partial_\beta\phi - V(\phi)\Big). \tag{9.13}$$

The energy density $\rho_\phi = T^0_0$ and pressure $p_\phi = -T^i_i$ of the scalar field are given by:

$$\rho_\phi = \frac{1}{2}\dot{\phi}^2 + V(\phi), \qquad p_\phi = \frac{1}{2}\dot{\phi}^2 - V(\phi). \tag{9.14}$$

The negative pressure condition from equation (9.8) leads to:

$$p_\phi < -\frac{1}{3}\rho_\phi \quad \Rightarrow \quad \dot{\phi}^2 < V(\phi), \tag{9.15}$$

indicating that the potential energy of the inflaton must dominate over its kinetic energy. This scenario requires a sufficiently flat potential.

The evolution of the inflaton field $\phi(t)$ and the scale factor $a(t)$ is governed by the Friedmann equation (9.2) and the equation of motion for the scalar field, respectively:

$$H^2 = \frac{1}{3}\left(\frac{1}{2}\dot{\phi}^2 + V(\phi)\right), \tag{9.16}$$

$$\ddot{\phi} + 3H\dot{\phi} + \frac{\partial V(\phi)}{\partial\phi} = 0. \tag{9.17}$$

The first slow-roll parameter ϵ, which quantifies the rate of change of the Hubble parameter, can be expressed as:

$$\epsilon = -\frac{\dot{H}}{H^2} = \frac{\frac{1}{2}\dot{\phi}^2}{H^2} = \frac{3\dot{\phi}^2}{2V(\phi) + \dot{\phi}^2}, \qquad \dot{H} = -\frac{1}{2}\dot{\phi}^2, \tag{9.18}$$

where (9.3) and (9.16) have been used. The condition for accelerated expansion, $\epsilon < 1$, leads again to the domination of potential energy $\dot{\phi}^2 < V(\phi)$.

For inflation to solve the cosmological problems, the accelerated expansion must last for at least $N \approx 60$ e-folds. This requires that ϵ remains small throughout inflation. To ensure this, a second slow-roll parameter, η, is introduced to describe the rate of change of ϵ:

$$\eta = \frac{\mathrm{d}\ln\epsilon}{\mathrm{d}N} = \frac{\dot{\epsilon}}{H\epsilon} = -2\frac{\dot{H}}{H^2} + 2\frac{\ddot{\phi}}{H\dot{\phi}} = 2\big(\epsilon - \delta\big), \tag{9.19}$$

where δ, the dimensionless acceleration of the scalar field, is defined as $\delta = -\ddot{\phi}/(H\dot{\phi})$. For inflation to persist, $|\eta| < 1$ and $|\delta| < 1$ must hold. These conditions ensure that the inflaton evolves slowly enough to sustain inflation while maintaining the required flatness of the potential.

9.1.3. Slow-roll Approximation

Inflation occurs and persists under the conditions $\epsilon \ll 1$, $|\eta| \ll 1$ and $|\delta| \ll 1$. We use these conditions to simplify the equations of motion (9.16) and (9.17), which is called the slow-roll approximation. When $\epsilon \ll 1$, the potential energy dominates over the kinetic energy and the Friedmann equation (9.16) simplifies to:

$$H^2 \approx \frac{1}{3}V, \tag{9.20}$$

and the Hubble expansion is determined almost entirely by the potential energy of the scalar field. The condition $|\delta| \ll 1$ leads to the neglect of the second derivative term in the scalar field equation (9.17), giving:

$$3H\dot{\phi} \approx -\frac{\partial V(\phi)}{\partial\phi}. \tag{9.21}$$

Using these approximations, the first slow-roll parameter ϵ can be expressed as:

$$\epsilon \approx \frac{M_{Pl}^2}{2}\left(\frac{V'(\phi)}{V(\phi)}\right)^2 \equiv \epsilon_V, \tag{9.22}$$

where the Planck mass has been reintroduced. Further, taking the derivative of (9.21), one defines:

$$\delta + \epsilon = -\frac{\ddot{\phi}}{H\dot{\phi}} - \frac{\dot{H}}{H^2} \approx M_{Pl}^2 \frac{V''(\phi)}{V(\phi)} \equiv \eta_V. \tag{9.23}$$

Here, ϵ_V and η_V are the potential slow-roll parameters. The successful inflation occurs when $\epsilon_V \ll 1$ and $|\eta_V| \ll 1$. During slow-roll, the following relations hold: $\epsilon_V \approx \epsilon$ and $\eta_V \approx 2\epsilon - \frac{1}{2}\eta$.

The number of e-folds during the slow-roll regime can be expressed as:

$$N = \int_{t^*}^{t_{end}} H(t)\mathrm{d}t = \int_{\phi^*}^{\phi_{end}} \frac{H}{\dot{\phi}}\mathrm{d}\phi = \frac{1}{M_{Pl}}\int_{\phi^*}^{\phi_{end}} \frac{|\mathrm{d}\phi}{\sqrt{2\epsilon}} \approx \frac{1}{M_{Pl}}\int_{\phi^*}^{\phi_{end}} \frac{|\mathrm{d}\phi|}{\sqrt{2\epsilon_V}}. \tag{9.24}$$

Here, $\phi^* = \phi(t^*)$ marks the beginning of inflation, whereas $\phi_{end} = \phi(t_{end})$ corresponds to the end of inflation. Usually ϕ_{end} is determined by the condition $\epsilon = 1$, though alternative conventions may also be used, as will be discussed in subsequent analysis.

9.1.4. Constraints on Inflation from ACT DR6

In this section, we shortly summarize the most important findings from the ACT DR6 results in combination with external datasets [96, 97], providing crucial constraints on the parameters characterizing cosmic inflation.

- **Tensor-to-scalar ratio ($r_{0.002}$):** This parameter measures the relative amplitude of primordial tensor perturbations (gravitational waves) to scalar perturbations (density fluctuations) generated during inflation. Observations of CMB polarization set up the upper limit on $r_{0.002}$ as:

$$r_{0.002} < 0.035 \qquad (95\%\ \mathrm{CL}). \tag{9.25}$$

- **Scalar spectral index (n_s):** The scalar spectral index characterizes the scale dependence of the power spectrum of scalar perturbations. A value of $n_s = 1$ corresponds to a scale-invariant spectrum, where fluctuations have the same amplitude across all scales. The value of n_s provides insight into the dynamics of inflation and the shape of the inflaton potential. Current constraints are:

$$n_s = 0.974 \pm 0.003 \qquad (68\%\ \mathrm{CL}). \tag{9.26}$$

  Both r and n_s parameters relate to the slow-roll parameters determined at the beginning of the inflation as:

$$r_{0.002} = 16\epsilon_*, \qquad n_s - 1 = -6\epsilon_* + 2\eta_*. \tag{9.27}$$

- **Scalar amplitude (A_s):** The scalar amplitude determines the initial conditions for the growth of cosmic structures, affecting the amplitude of temperature anisotropies and polarization in the CMB. Planck 2018 reports [95]:

$$\ln\left(10^{10}A_s\right) = 3.044 \pm 0.014. \tag{9.28}$$

  The scalar amplitude is related to the inflaton potential energy as:

$$A_s = \frac{2}{3\pi^2 r}\frac{V_*}{M_{Pl}^4}. \tag{9.29}$$

- **Energy scale of inflation:** From the constraints on A_s and r, the upper bound on the energy scale of inflation is determined as:

$$V_* = \frac{3\pi^2 A_s}{2} r M_{Pl}^4 < \left(1.6 \cdot 10^{16}\ \text{GeV}\right)^4 \qquad (95\%\ \text{CL}), \tag{9.30}$$

which corresponds to an upper limit on the Hubble parameter in slow-roll approximation:

$$\frac{H_*}{M_{Pl}} < 2.5 \cdot 10^{-5} \qquad (95\%\ \text{CL}). \tag{9.31}$$

These constraints provide essential information for constructing and testing models of inflation, linking theoretical predictions to observational data.

9.2. From Jordan to Einstein frame in Weyl geometry

In this and the forthcoming sections, we analyze the inflationary scenarios within the Higgs-dilaton model framework presented in this thesis. We start with a Lagrangian (5.13):

$$\frac{\mathcal{L}}{\sqrt{g}} = -\frac{1}{12}\left(\xi_0\phi_0^2 + \xi_1\phi_1^2\right)\tilde{R} - \frac{1}{4}\tilde{F}_{\mu\nu}\tilde{F}^{\mu\nu} + \frac{1}{2}\tilde{D}_\mu\phi_0\tilde{D}^\mu\phi_0 + \frac{1}{2}\tilde{D}_\mu\phi_1\tilde{D}^\mu\phi_1 - V(\phi_0,\phi_1), \tag{9.32}$$

invariant under Weyl conformal transformations (4.8). Expanding $\tilde{R}$ and $\tilde{D}_\mu\phi_i$, up to a total derivative, one gets:

$$\frac{\mathcal{L}}{\sqrt{g}} = -\frac{1}{12}\rho^2 R - \frac{q}{4}K_\mu\omega^\mu + \frac{q^2}{8}K\omega_\mu\omega^\mu + \frac{1}{2}\partial_\mu\phi_0\partial^\mu\phi_0 + \frac{1}{2}\partial_\mu\phi_1\partial^\mu\phi_1 - \frac{1}{4}\tilde{F}_{\mu\nu}\tilde{F}^{\mu\nu} - V(\phi_0,\phi_1), \tag{9.33}$$

where we defined:

$$\rho^2 = \xi_0\phi_0^2 + \xi_1\phi_1^2, \tag{9.34}$$

$$K = \rho^2 + \phi_0^2 + \phi_1^2 = (\xi_0+1)\phi_0^2 + (\xi_1+1)\phi_1^2, \qquad K_\mu = \partial_\mu K. \tag{9.35}$$

Next, we perform a transformation to the Einstein-frame, applying (4.8) on the metric and Riemannian Ricci scalar R[1], with:

$$\Omega^2 = \frac{\rho^2}{6M^2} = \frac{\xi_0\phi_0^2 + \xi_1\phi_1^2}{6M^2}. \tag{9.37}$$

The Lagrangian becomes:

$$\begin{aligned}\frac{\hat{\mathcal{L}}}{\sqrt{\hat{g}}} = &-\frac{1}{2}M^2\hat{R} + \frac{1}{\Omega^2}\left[\frac{1}{2}\partial_\mu\phi_0\partial^\mu\phi_0 + \frac{1}{2}\partial_\mu\phi_1\partial^\mu\phi_1 - \frac{q}{4}K_\mu\omega^\mu + \frac{q^2}{8}K\omega_\mu\omega^\mu\right] + \\ &+ \frac{3M^2}{4}\hat{g}^{\mu\nu}\left(\partial_\mu\ln\Omega^2\right)\left(\partial_\nu\ln\Omega^2\right) - \frac{1}{4}\tilde{F}_{\mu\nu}\tilde{F}^{\mu\nu} - \frac{V(\phi_0,\phi_1)}{\Omega^4}.\end{aligned} \tag{9.38}$$

To remove the $K_\mu\omega^\mu$ mixing term in (9.38), one introduces:

$$\hat{\omega}_\mu = \omega_\mu - \frac{1}{q}\partial_\mu\ln K, \tag{9.39}$$

[1] The Ricci scalar coupled to the scalar fields transforms under (4.8) as:

$$-\frac{1}{12}\rho^2 R \quad\to\quad -\frac{1}{2}M^2\hat{R} + \frac{3M^2}{4}\hat{g}^{\mu\nu}\left(\partial_\mu\ln\Omega^2\right)\left(\partial_\nu\ln\Omega^2\right). \tag{9.36}$$

which transforms the Lagrangian further to:

$$\begin{aligned}\frac{\hat{\mathcal{L}}}{\sqrt{\hat{g}}} =& -\frac{1}{2}M^2\hat{R}+\frac{1}{\Omega^2}\Big[\frac{1}{2}\partial_\mu\phi_0\partial^\mu\phi_0+\frac{1}{2}\partial_\mu\phi_1\partial^\mu\phi_1-\frac{1}{8}\frac{K_\mu K^\mu}{K}+\frac{q^2}{8}K\hat{\omega}_\mu\hat{\omega}^\mu\Big]+\\ &+\frac{3M^2}{4}\hat{g}^{\mu\nu}\big(\partial_\mu\ln\Omega^2\big)\big(\partial_\nu\ln\Omega^2\big)-\frac{1}{4}\hat{\tilde{F}}_{\mu\nu}\hat{\tilde{F}}^{\mu\nu}-\frac{V(\phi_0,\phi_1)}{\Omega^4}.\end{aligned} \tag{9.40}$$

The kinetic part of the above Lagrangian is non-canonical and reads:

$$\frac{\hat{\mathcal{L}}}{\sqrt{\hat{g}}}\Big|_{k.t.}=\frac{1}{\Omega^2}\Big[\frac{1}{2}\partial_\mu\phi_0\partial^\mu\phi_0+\frac{1}{2}\partial_\mu\phi_1\partial^\mu\phi_1-\frac{1}{8}\frac{K_\mu K^\mu}{K}\Big]+\frac{3M^2}{4}\hat{g}^{\mu\nu}\big(\partial_\mu\ln\Omega^2\big)\big(\partial_\nu\ln\Omega^2\big). \tag{9.41}$$

In terms of ϕ_i fields it simplifies to:

$$\frac{\hat{\mathcal{L}}}{\sqrt{\hat{g}}}\Big|_{k.t.}=\frac{3M^2\left(\xi_0\left(\xi_0+1\right)\phi_0^2+\xi_1\left(\xi_1+1\right)\phi_1^2\right)}{\left(\xi_0\phi_0^2+\xi_1\phi_1^2\right)^2\left(\left(\xi_0+1\right)\phi_0^2+\left(\xi_1+1\right)\phi_1^2\right)}\left(\phi_1\partial_\mu\phi_0-\phi_0\partial_\mu\phi_1\right)^2. \tag{9.42}$$

Since ω_μ field "ate" the K radial direction (9.39), one can choose the following polar coordinates:

$$\begin{aligned}\phi_0 =&\frac{1}{\sqrt{1+\xi_0}}\sqrt{K}\cos\theta,\\ \phi_1 =&\frac{1}{\sqrt{1+\xi_1}}\sqrt{K}\sin\theta,\end{aligned} \tag{9.43}$$

for which the kinetic part becomes the function of the θ angle only:

$$\frac{\hat{\mathcal{L}}}{\sqrt{\hat{g}}}\Big|_{k.t.}=3M^2(\xi_0+1)(\xi_1+1)\frac{\xi_0\cos^2\theta+\xi_1\sin^2\theta}{(\xi_0\cos^2\theta+\xi_1\sin^2\theta+\xi_0\xi_1)^2}\big(\partial_\mu\theta\big)\big(\partial^\mu\theta\big). \tag{9.44}$$

Changing the variable to $\tau=\tan\theta$, one gets:

$$\frac{\mathcal{L}}{\sqrt{g}}=-\frac{1}{2}M^2R-\frac{1}{4}\tilde{F}_{\mu\nu}\tilde{F}^{\mu\nu}+\frac{q^2}{8}\frac{K}{\Omega^2}\omega_\mu\omega^\mu+\frac{1}{2}F^2(\tau)\big(\partial_\mu\tau\big)\big(\partial^\mu\tau\big)-V(\tau), \tag{9.45}$$

where the hats have been omitted and:

$$F^2(\tau)=6M^2\big(\xi_0+1\big)\big(\xi_1+1\big)\frac{\xi_0+\xi_1\tau^2}{\big(\xi_0(\xi_1+1)+\xi_1\tau^2(\xi_0+1)\big)^2\big(\tau^2+1\big)}, \tag{9.46}$$

$$V(\tau)=36M^4\frac{\lambda_0\big(\xi_1+1\big)^2+\lambda_1\big(\xi_0+1\big)\big(\xi_1+1\big)\tau^2+\lambda_2\big(\xi_0+1\big)^2\tau^4}{\big(\xi_0(\xi_1+1)+\xi_1\tau^2(\xi_0+1)\big)^2}. \tag{9.47}$$

Note, that we identify the M scale with the Planck mass, M_{Pl}, as $-\frac{1}{2}M^2R$ is the Einstein-Hilbert term. The stationary solutions for the τ field from the Euler-Lagrange equations derived with the Lagrangian (9.45) are:

$$\tau=0,\qquad \tau^2=\frac{\left(\xi_1+1\right)\left(2\lambda_0\xi_1-\lambda_1\xi_0\right)}{\left(\xi_0+1\right)\left(2\lambda_2\xi_0-\lambda_1\xi_1\right)}\xrightarrow{\lambda_0=\lambda_1^2/4\lambda_2}-\frac{\lambda_1}{2\lambda_2}\cdot\frac{1+\xi_1}{1+\xi_0}. \tag{9.48}$$

With the parameter space condition from the Subsection 5.2.1, $\lambda_0=\frac{\lambda_1^2}{4\lambda_2}$, the potential values at the stationary solutions are:

$$V(\tau=0)=9M^4\frac{\lambda_1^2}{\lambda_2\xi_0^2}>0,\qquad V\Big(\tau=-\frac{\lambda_1}{2\lambda_2}\cdot\frac{1+\xi_1}{1+\xi_0}\Big)=0. \tag{9.49}$$

Figure 9.1 illustrates the potential (9.47) for example parameter space values so that the characteristic features for small and large values of τ are visible.

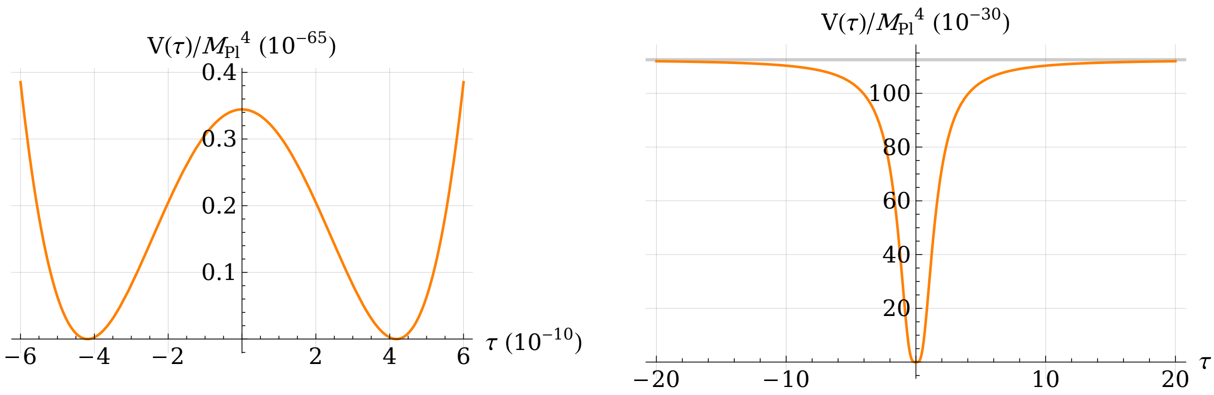

Figure 9.1: The plots of the potential $V(\tau)$ (9.47) for $\xi_0 = 10^{15}$ and $\xi_1 = 10^{10}$. For small τ, the two degenerate, non-zero minima are visible. The $\tau = 0$ is the maximum. For large τ values, the potential becomes constant, with value (9.59).

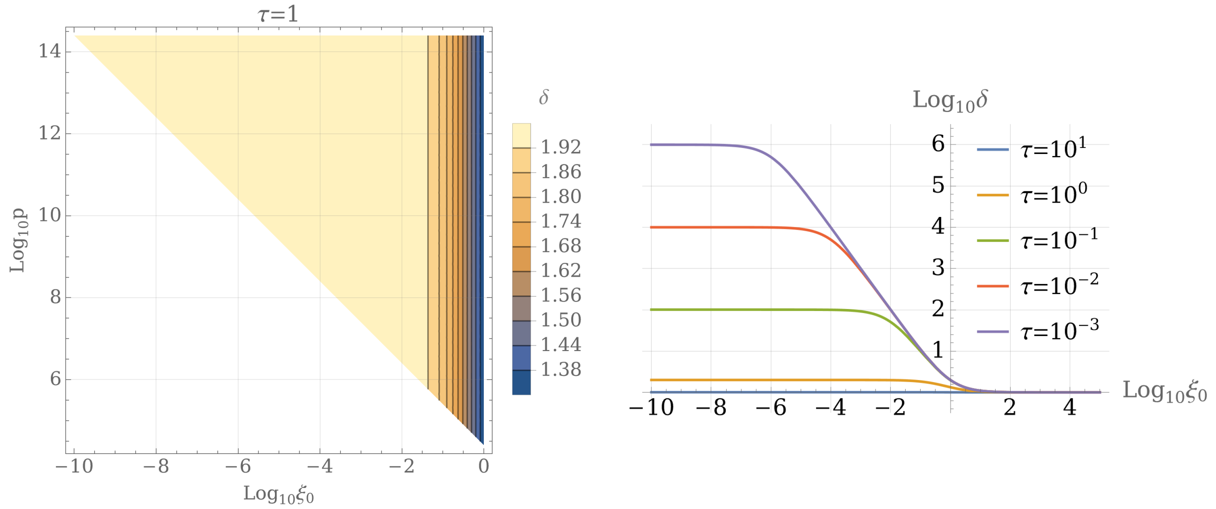

Figure 9.2: Plots of δ for different values of ξ_i and τ, where $\xi_1 = p \cdot \xi_0$. The exclusion of certain regions in the ξ_i parameter space follows from subsequent argumentation, as illustrated in Figure 9.3a. The right plot is evaluated for $p = 10^{14.4}$.

Analyzing the Lagrangian (9.45) further reveals that the Weyl vector field, ω_μ, effectively "eats" the radial component K and acquires a mass:

$$m_\omega^2(\tau) = \frac{q^2}{4}\frac{K}{\Omega^2} = \frac{3}{2}q^2 M^2 \frac{(\xi_0+1)(\xi_1+1)(\tau^2+1)}{\xi_0(\xi_1+1)+\xi_1\tau^2(\xi_0+1)} = \frac{3}{2}q^2 M^2 \cdot \delta. \tag{9.50}$$

For the values of ξ_i, studied later in this analysis, the δ parameter remains larger than 1 and $m_\omega^2 \gtrsim \frac{3q^2}{2}M^2$. The Weyl gauge coupling q can have values larger than 1 (as shown in Section 6.3), and ω_μ mass can be of the order of the Planck mass scale or larger. Figure 9.2 further supports this approximation. Consequently, for the energies below m_ω scale, the ω_μ field effectively decouples from the inflaton, for which the Lagrangian reads:

$$\frac{\mathcal{L}}{\sqrt{g}} = -\frac{1}{2}M^2 R + \frac{1}{2}F^2(\tau) g^{\mu\nu}\partial_\mu\tau\partial_\nu\tau - V(\tau). \tag{9.51}$$

We briefly outline the number of independent variables in the parameter space of our model. Using the parameter space conditions discussed in Subsection 5.2.1, namely:

$$\frac{1}{\lambda_1} = -16\left(\frac{6M_{Pl}^2}{\xi_0\langle\phi_1^2\rangle} - \frac{\xi_1}{\xi_0} + 1\right), \quad \lambda_2 = \frac{1}{32}(1+16\lambda_1), \quad \lambda_0 = \frac{\lambda_1^2}{4\lambda_2}, \tag{9.52}$$

and imposing the relation $\xi_1 = p \cdot \xi_0$, one can express all the quantities in terms of ξ_0 and p. This reduces the parameter space to just two independent variables.

9.3. Slow-Roll Inflation: Classical Level

With the Lagrangian of the form (9.51), the canonical field variable reads:

$$\sigma(\tau) = \int_{v_\tau}^{\tau} dx F(x). \tag{9.53}$$

The integral above can only be evaluated numerically, which complicates the calculation of inflationary slow-roll parameters. However, for the τ field with a non-canonical kinetic term, the slow-roll parameters can be modified to[2]:

$$\epsilon_V(\tau) = \frac{M_{Pl}^2}{2F^2(\tau)}\left(\frac{V'(\tau)}{V(\tau)}\right)^2, \tag{9.55}$$

$$\eta_V(\tau) = \frac{M_{Pl}^2}{F^2(\tau)}\left(\frac{V''(\tau)}{V(\tau)} - \frac{F'(\tau)}{F(\tau)}\frac{V'(\tau)}{V(\tau)}\right) \tag{9.56}$$

and the number of e-folds is:

$$N_e = \int_{\tau^*}^{\tau_{end}} \frac{d\tau}{\sqrt{2\epsilon_V(\tau)}}, \tag{9.57}$$

where τ_{end} is established as the end of inflation as $\eta_V(\tau_{end}) = -0.0095$[3], whereas τ^* is the beginning of inflation for which one has $\epsilon_V(\tau^*) \ll 1$ and $\eta_V(\tau^*) > -0.0095$.

In analyzing the parameter space of ξ_0 and p, we especially pay attention to the value of the inflationary potential (9.47) for large τ:

$$V_\infty = \lim_{\tau\to\infty} V(\tau) = \frac{36\lambda_2}{\xi_1^2} M_{Pl}^4, \tag{9.59}$$

which represents its maximum value potentially reached during inflation. This value is constrained from above by the Planck 2018 bound (9.30):

$$V_*^{1/4} < 1.6 \cdot 10^{16}\text{GeV}. \tag{9.60}$$

Figure 9.3a shows the region plot of the parameter space for ξ_0 and p that satisfies $V_\infty \leq V_*$, giving the constraint:

$$\log_{10} p \geq -\log_{10}\xi_0 + 4.4. \tag{9.61}$$

The second slow-roll parameter $\eta_V(\tau)$ has a non-zero limit when:

$$\lim_{\tau\to\infty} \eta_V(\tau) = \frac{1}{3}\Big(-2\xi_0 + \frac{\lambda_1\xi_1}{\lambda_2}\Big) = \eta_V(\infty) < 0. \tag{9.62}$$

[2]These modified formulas can be derived similarly to the standard expressions in Section 9.1, with the change of Lagrangian to (9.51). This leads to the energy density ρ_τ and pressure p_τ for the τ field:

$$\rho_\tau = \frac{1}{2}F(\tau)^2\dot{\tau}^2 + V(\tau), \qquad p_\tau = \frac{1}{2}F(\tau)^2\dot{\tau}^2 - V(\tau). \tag{9.54}$$

[3]The ACT DR6 in combination with external datasets [96,97] constraint the η_V value in the slow-roll regime:

$$\eta_V = -95^{+23}_{-30} \times 10^{-4} \qquad (68\%\ \text{CL}). \tag{9.58}$$

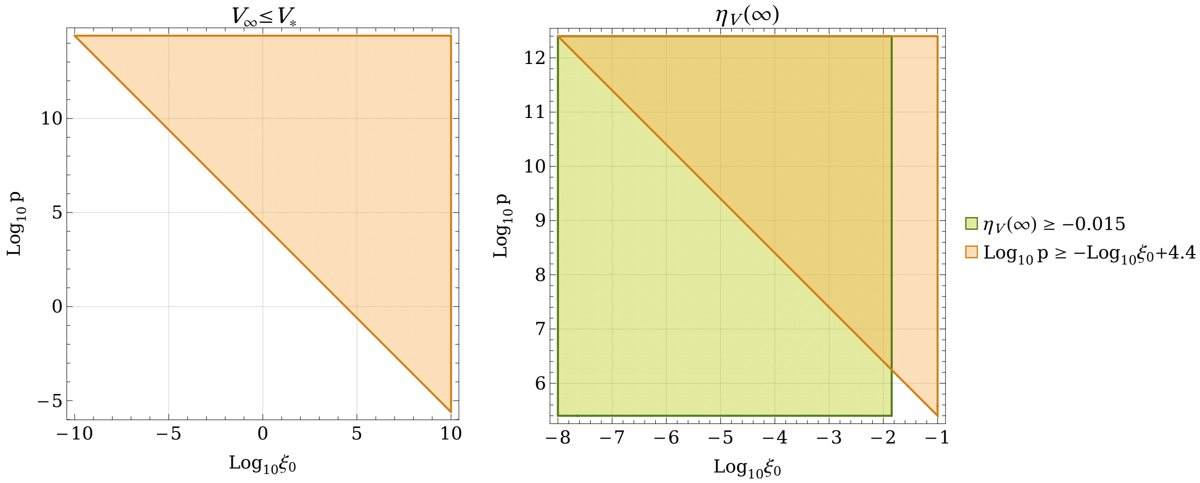

(a) (b)

Figure 9.3: (a): Region plot of the parameter space for which $V_\infty \leq V_*$. The constraint can be approximated by the inequality $\log_{10} p \geq -\log_{10} \xi_0 + 4.4$. (b): Plot illustrating the constraint $\eta_V(\infty) > -0.0095 - 0.0030$, resulting from (9.62), limiting ξ_0 to $\log_{10} \xi_0 \lesssim -1.727$.

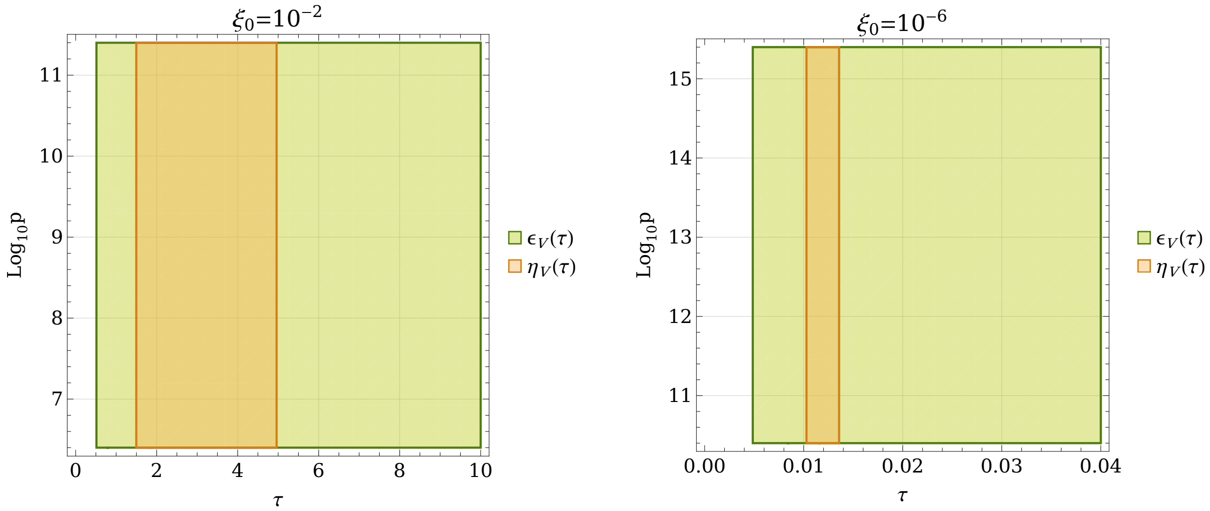

Figure 9.4: Plots of the parameter space satisfying the slow-roll conditions. The minimum p values correspond to the boundary values determined by inequality (9.61).

To fulfill slow-roll conditions during inflation, one obtains a constraint $\eta_V(\infty) > -0.0095-0.0030$, illustrated in Figure 9.3b. This results in inequality:

$$\log_{10} \xi_0 \lesssim -1.727. \tag{9.63}$$

The example regions of ξ_0, p and τ where the slow-roll parameters $\epsilon_V(\tau)$ and $\eta_V(\tau)$ fulfill the ACT DR6 conditions [96, 97]:

$$\epsilon_V < 0.0024, \qquad \eta_V = -95^{+23}_{-30} \cdot 10^{-4}, \tag{9.64}$$

ensuring successful inflation, are illustrated in Figure 9.4, where both regions do not depend on the choice of p value. The η_V condition imposes a more rigorous constraint on the parameter space.

Next, the number of e-folds is calculated using equation (9.57), and its value is evaluated for different starting points $\tau^* \geq \tau_{end}$. Choosing the τ^* values for which $N_e \in \langle 50, 60 \rangle$, one can determine the inflationary indexes as:

$$n_s = -6\epsilon_V(\tau^*) + 2\eta_V(\tau^*) + 1, \qquad r = 16\epsilon_V(\tau^*). \tag{9.65}$$

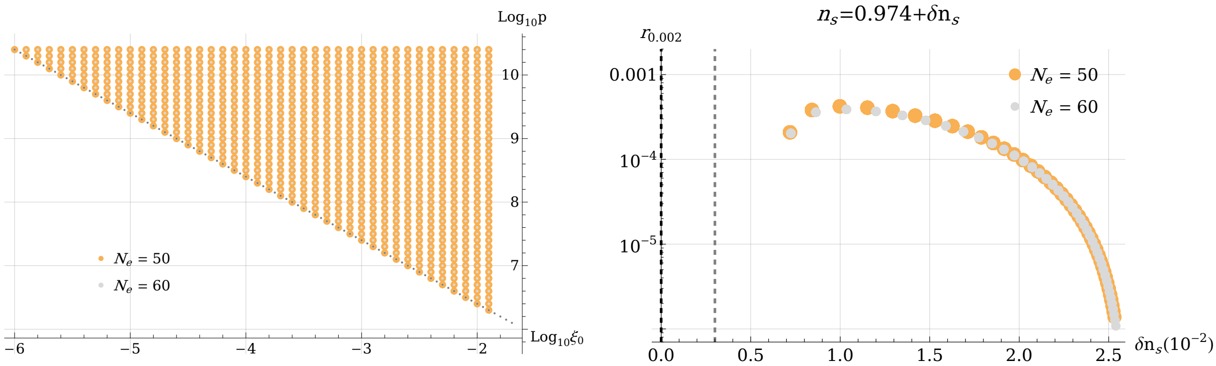

Figure 9.5: **Left:** Parameter space points used to generate the corresponding $r_{0.002}(n_s)$ plot on the right. The dark gray dotted line marks the constraint $\log_{10} p = -\log_{10} \xi_0 + 4.4$. **Right:** Tensor-to-scalar ratio $r_{0.002}$ as a function of the scalar spectral index n_s in the model with the inflaton field τ. The black dashed line corresponds to the experimental value, $n_s = 0.974$, and the gray dashed line to $n_s = 0.974 + 0.003$. Variations in ξ_0 and p lead to small differences in n_s, as illustrated in Figure 9.7.

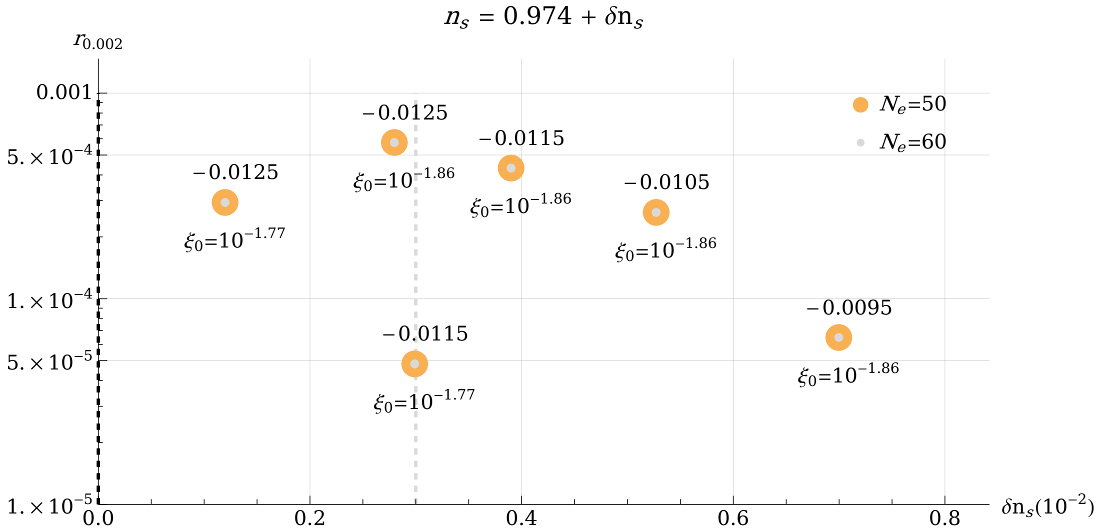

Figure 9.6: Tensor-to-scalar ratio $r_{0.002}(n_s)$ for $\xi_0 = 10^{-1.71}$ and $\xi_0 = -1.86$ with $p = 10^{6.5}$ at different inflationary endpoints, determined by $\eta_V(\tau_{end})$. The numerical labels above the points indicate the corresponding $\eta_V(\tau_{end})$ values. The black dashed line corresponds to the experimental value, $n_s = 0.974$, and the gray dashed line to $n_s = 0.974 + 0.003$.

Figure 9.5 shows the region of the parameter space used to calculate n_s and $r_{0.002}$, along with the function $r_{0.002}(n_s)$. When the end field point of inflation is defined as $\eta_V(\tau_{end}) = -0.0095$, the resulting n_s values are inconsistent with the ACT DR6 bound (9.26). Figure 9.7 illustrates the impact of ξ_0 and p on $r_{0.002}$ and n_s for $\eta_V(\tau_{end}) = -0.0095$. However, one can redefine the τ_{end}, consistently with (9.64), and affect the n_s values so that proper results are possible. These revised results, consistent with the bounds (9.25) and (9.26), are shown in Figure 9.6, where $\xi_0 = 10^{-1.86}$ and $\xi_0 = -1.77$ with $p = 10^{6.5}$. Figure 9.7 further illustrates how the values of ξ_0 and p impact $r_{0.002}$ and n_s.

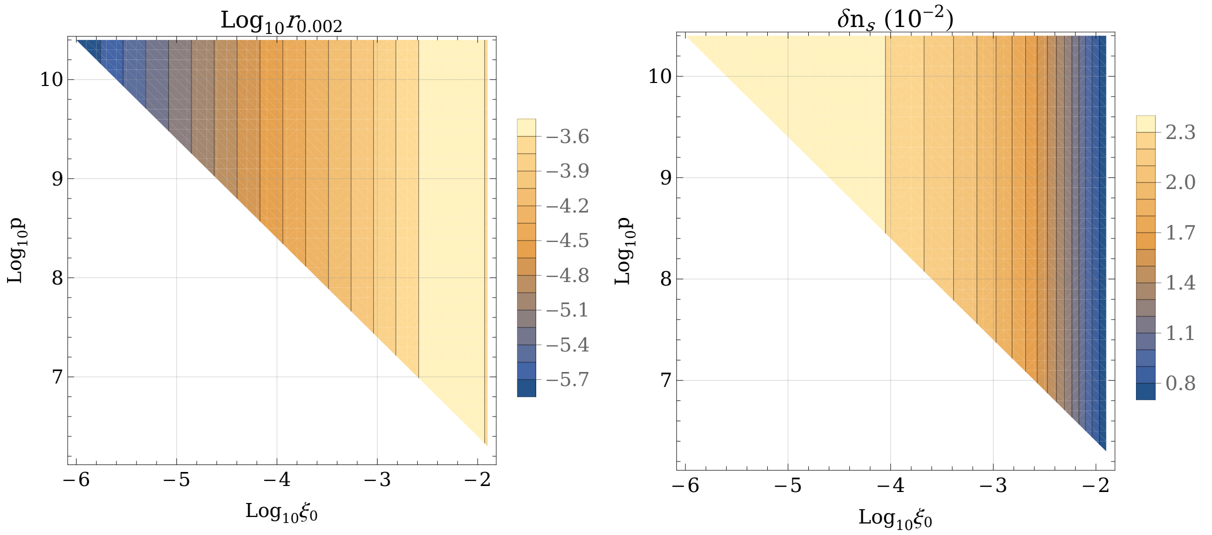

Figure 9.7: Plots illustrating the influence of ξ_0 and p on $r_{0.002}$ and n_s, with the endpoint of inflation set as $\eta_V(\tau_{end}) = -0.0095$, yielding $n_s = 0.974 + \delta n_s$.

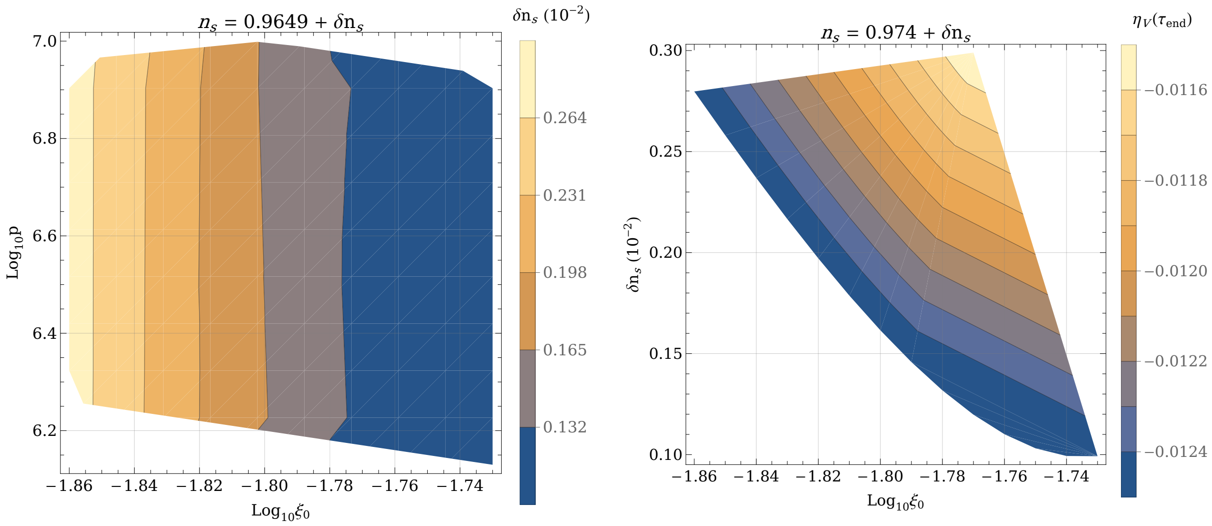

Figure 9.8: Plots illustrating the allowed parameter space to obtain n_s consistent with experiments. In the left plot, the p values were truncated; however, because n_s does not depend on p, the constraint applies only to ξ_0. For this reason, the right plot highlights exclusively the ξ_0 dependence.

9.4. Slow-Roll Inflation: Quantum Level

In the previous section, we demonstrated that inflation is possible within a classical framework for a certain parameter space. Here, we extend our analysis by implementing quantum corrections to the inflationary potential (9.47) by including one-loop effective potential and RG improving it by incorporating the renormalization group equations for the couplings.

When deriving the one-loop effective potential for the Higgs-dilaton sector in Chapter 5, we adopted the scale-symmetric quantum corrections approach, outlined in Chapter 3. This choice was motivated by the scale symmetry of the tree-level Jordan frame Lagrangian (5.28). However, this symmetry is broken in the Einstein frame, where the conformal transformation (4.8) introduces a mass scale M to canonize the gravitational sector. This raises an important question when deriving quantum corrections in inflationary theory: Should one use the Jordan frame one-loop potential and transform it to the Einstein frame via (4.8), or should one renormalize the theory directly in the Einstein frame? Moreover, are these two approaches equivalent?

In this chapter, we take a different approach compared to Chapter 5. Firstly, we no longer neglect the impact of the Weyl sector on the Higgs dilaton framework. Secondly, we want to account for quantum corrections associated with gravity, which are crucial in the context of inflation but were previously omitted. These considerations make the direct renormalization of the Einstein frame Lagrangian more suitable for our present analysis. However, obtaining the RG equations directly from the Einstein frame turns out to be a technically challenging task due to the complexity of the inflaton Lagrangian (9.51). Consequently, we follow the approach of [98], which shows that the one-loop effective potentials obtained in the Jordan and Einstein frames can be equivalent, provided that the renormalization is performed appropriately in each frame. In the Jordan frame, the renormalization is carried out with a field-dependent subtraction scale $\mu(\phi)$, consistent with the scale-symmetric prescription where μ depends on the dilaton field, as discussed in [21–25, 31, 55]. In contrast, the Einstein frame renormalization proceeds with a conventional constant scale, $\mu = const.$

Therefore, in this chapter, we compute the one-loop effective potential for the inflaton field τ directly in the Einstein frame, where the gravity sector is canonical. This allows us to apply standard methods, as in [99–101]. The beta functions, however, are derived following the Jordan frame prescription, which is more straightforward.

Following the approach of [41, 42, 89, 90], it is crucial to account for the propagator suppression factors, c_{ϕ_i}, which arise from modifications to the canonical commutation relations. In the presence of non-minimal couplings of the scalar field to gravity, such as the $\xi_i\phi_1^2R$ terms, the standard commutation relations, $\big[\phi(x), \dot{\phi}(y)\big]$, are altered. This originates from the fact that the scalar field's kinetic term is non-canonical in the Einstein frame. To derive the corresponding suppression factors, one utilizes the fact that the fields ϕ_i commute with their canonical momentum π_i when the gravity sector is canonical, i.e., in the Einstein frame. Let's denote the kinetic term of the Einstein frame Lagrangian (9.51) as:

$$\frac{\mathcal{L}_E}{\sqrt{g_E}}\bigg|_{k.t.} = \frac{1}{2}F^2(\tau)g_E^{0\nu}\partial_\nu\tau\partial_0\tau = \frac{1}{2}g_E^{0\nu}\partial_\nu\sigma\partial_0\sigma, \tag{9.66}$$

where the subscript E denotes the quantities in the Einstein frame, σ is the canonical field (9.53) and $F^2(\tau) = \big(\partial\sigma/\partial\tau\big)^2$. The canonical momentum for the scalar field ϕ_i reads:

$$\begin{aligned}\pi_i =& \frac{\partial\mathcal{L}_E\big|_{k.t.}}{\partial\dot{\phi}_i} = \sqrt{g_E}\frac{1}{2}g_E^{0\nu}\cdot\frac{\partial}{\partial\dot{\phi}_i}\Big(\partial_\nu\sigma\partial_0\sigma\Big) = \frac{1}{2}\Omega^2\sqrt{g}g^{0\nu}\cdot\frac{\partial}{\partial\dot{\phi}_i}\Big(\partial_\nu\sigma\partial_0\sigma\Big) = \\ =& \frac{1}{2}\Omega^2\sqrt{g}\cdot\frac{\partial}{\partial\dot{\phi}_i}\dot{\sigma}^2 = \frac{1}{2}\Omega^2\sqrt{g}\cdot 2\dot{\sigma}\frac{\partial\sigma}{\partial\phi_i} = \Omega^2\sqrt{g}\left(\frac{\partial\sigma}{\partial\phi_i}\right)^2\dot{\phi}_i = \Omega^2\sqrt{g}F^2(\tau)\left(\frac{\partial\tau}{\partial\phi_i}\right)^2\dot{\phi}_i,\end{aligned} \tag{9.67}$$

where Einstein frame metric functions transformed to the Jordan-frame ones have the forms $\sqrt{g_E} = \Omega^4\sqrt{g}$ and $g_E^{\mu\nu} = \Omega^{-2}g^{\mu\nu}$, with Ω^2 defined in (9.37). By imposing $\big[\phi_i(x), \pi_j(y)\big] = i\delta_{ij}\delta^{(3)}\big(\vec{x}-\vec{y}\big)$, one finds:

$$\big[\phi_i(x), \pi_i(y)\big] = \Omega^2\sqrt{g}F^2(\tau)\left(\frac{\partial\tau}{\partial\phi_i}\right)^2\big[\phi_i(x), \dot{\phi}_i(y)\big], \tag{9.68}$$

$$\big[\phi_i(x), \dot{\phi}_i(y)\big] = \frac{i}{a^3}\cdot c_{\phi_i}\cdot\delta^{(3)}\big(\vec{x}-\vec{y}\big), \tag{9.69}$$

where the suppression factors c_{ϕ_i} are defined as:

$$c_{\phi_i} = \frac{1}{\Omega^2\Big(\frac{\partial\sigma}{\partial\phi_i}\Big)^2} = \frac{1}{\Omega^2F^2(\tau)}\left(\frac{\partial\phi_i}{\partial\tau}\right)^2. \tag{9.70}$$

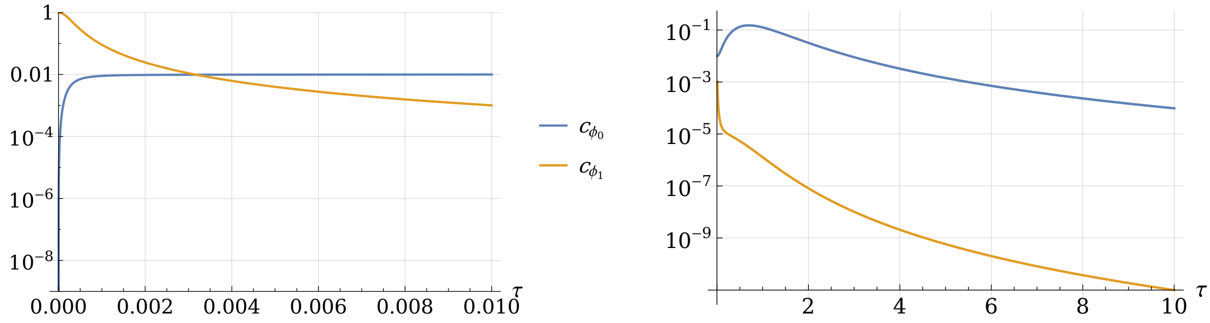

Figure 9.9: Plots of the suppression factors $c_{\phi_i}(\tau)$ (9.70), for $\xi_0 = 10^{-2}$ and $\xi_1 = 10^5$. Note the different τ scales on each plot. The low τ field value limits are $\lim_{\tau\to 0} c_{\phi_0} = 0$ and $\lim_{\tau\to 0} c_{\phi_1} = 1$.

The derivatives $\partial\phi_i\partial\tau$ can be determined from equation (9.43). Figure 9.9 illustrates the dependence of the suppression factors $c_{\phi_i}(\tau)$ on the inflaton field τ, for an example parameter space. These factors suppress the ϕ_i propagators, especially in the large-τ regime where inflation occurs. This suppression significantly affects the β-functions for Standard Model and dilaton couplings, as discussed in [41, 42, 89], from where all the β-functions for λ_i, ξ_i, and y_t, g_1 and g_2 can be read. Particularly, the β-functions for the non-minimal couplings ξ_i are:

$$\begin{aligned}\beta_{\xi_0} &= \frac{1}{94\pi)^2}\left(24c_0\lambda_0(\xi_0+1) + (3+c_1)\lambda_1(\xi_1+1)\right),\\ \beta_{\xi_1} &= \frac{1}{94\pi)^2}\left(4c_0\lambda_1(\xi_0+1) + \left(12(1+c_1)\lambda_2 - \frac{3}{2}(3g_1^2+g_2^2-4y_t^2)\right)(\xi_1+1)\right),\end{aligned} \tag{9.71}$$

where we set the notation $c_{\phi_i} = c_i$. For the SM couplings g_1, g_2, g_3 and y_t, we have:

$$\begin{gathered}\beta_{g_1} = \frac{1}{(4\pi)^2}\frac{40+c_1}{6}g_1^3, \quad \beta_{g_2} = \frac{1}{(4\pi)^2}\frac{-(20-c_1)}{6}g_2^3, \quad \beta_{g_3} = \frac{1}{(4\pi)^2}(-7g_3^3),\\ \beta_{y_t} = \frac{1}{(4\pi)^2}y_t\left(\frac{9}{2}c_1y_t^2 - \frac{17}{12}g_1^2 - \frac{9}{4}g_2^2 - 8g_3^2\right).\end{gathered} \tag{9.72}$$

We neglect the running of λ_0, λ_1, and ξ_0, as their beta functions are negligible. The significant changes occur in the RG equation of λ_2 coupling, which beta function is modified as follows [41, 42, 89]:

$$\beta_{\lambda_2} = \frac{1}{(4\pi)^2}\left(2c_0^2\lambda_1^2 + 24(1+3c_1^2)\lambda_2^2 - 6\lambda_2(3g_1^2+g_2^2-4y_t^2) + \frac{3}{32}((g_1^2+g_2^2)^2+2g_2^4) - \frac{3}{2}y_t^2\right). \tag{9.73}$$

In the limit $c_{\phi_0} \to 1$ and $c_{\phi_1} \to 1$, corresponding to unmodified commutation relations, (9.71), (9.72) and (9.73) reduce to the standard β-functions as provided in equation (A.1).

The running of the inflaton field is determined by the anomalous dimensions of the Higgs field $\gamma_H = \frac{d\ln\phi_1}{d\ln\mu}$ and the dilaton field $\gamma_G = \frac{d\ln\phi_0}{d\ln\mu}$, which are equal to [22, 63, 64]:

$$\gamma_H = \frac{2}{(4\pi)^2}\left(\frac{9}{4}g_1^2 + \frac{3}{4}g_2^2 - 3y_t^2\right), \qquad \gamma_G = 0. \tag{9.74}$$

Consequently, we obtain:

$$\frac{d\ln\tau}{d\ln\mu} = \frac{d}{d\ln\mu}\sqrt{\frac{1+\xi_1}{1+\xi_0}\frac{\phi_1}{\phi_0}} = \frac{d\ln\phi_1}{d\ln\mu} = \gamma_H. \tag{9.75}$$

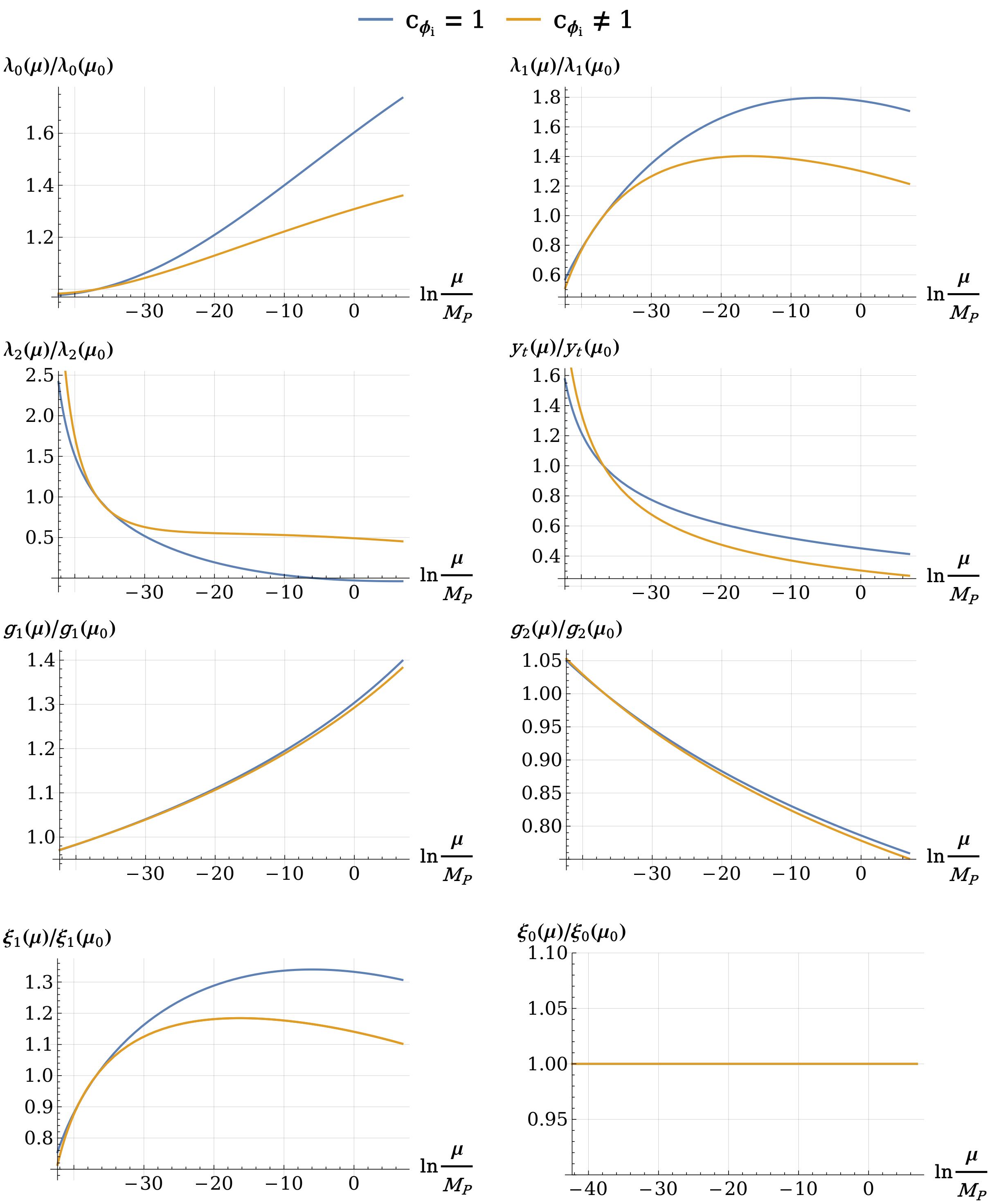

Figure 9.10: Running of the coupling constants $\lambda_0, \lambda_1, \lambda_2, \xi_0, \xi_1, g_1, g_2, g_3$ and y_t with the energy scale μ. The most significant effect is observed in the high-energy behavior of the λ_2, where suppression factors ensure that this coupling remains positive.

To RG improve the potential (9.86), we make the replacement $\tau \to \exp\big(\Gamma(\mu)\big)\tau$, where:

$$\Gamma(\mu) = \int_{\langle\phi_1\rangle}^{\mu} \gamma_H(\mu')d\ln\mu'. \tag{9.76}$$

Figures 9.10 and 9.11 illustrate the running of couplings and inflaton field with the energy scale μ in two cases: the regular scenario ($c_{\phi_i} = 1$) and the scenario including the suppression

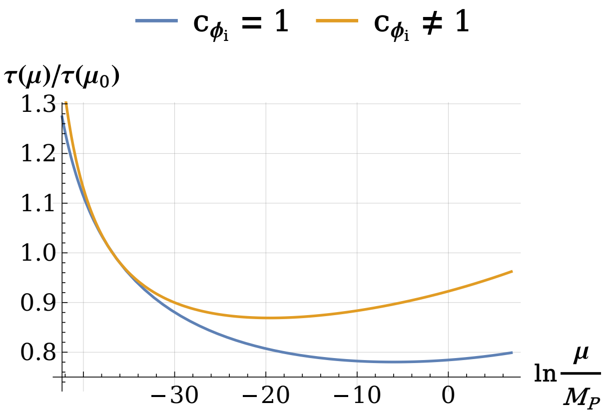

Figure 9.11: The running of the inflaton field τ with the energy scale μ, according to equation (9.75).

factors effects ($c_{\phi_i} \neq 1$). The initial values $\alpha_i(\mu_0)$, with $\mu_0 = \langle\phi_1\rangle = 250$ GeV, are given by:

$$I_{\lambda_0} = \frac{I_{\lambda_1}^2}{4I_{\lambda_2}}, \quad I_{\lambda_1} = -\frac{1}{16}\left(\frac{6M_P^2}{I_{\xi_0}\langle\phi_1^2\rangle} - p + 1\right)^{-1}, \quad I_{\lambda_2} = \frac{1}{32}\big(1 + 16I_{\lambda_1}\big), \quad I_{\xi_1} = p \cdot I_{\xi_0}, \tag{9.77}$$
$$I_{g_1} = 0.35940, \quad I_{g_2} = 0.64754, \quad I_{y_t} = 0.95113,$$

where the individual relations come from the parameter space analysis in Section 5.2.1.

The running of the couplings is independent of the initial conditions. The most significant difference appears in the Higgs-quartic coupling λ_2. Due to the suppression introduced by the c_{ϕ_i} factors, λ_2 remains positive across all energy scales, up to $10^3 M_P$, which is the maximum μ scale showed in the plots. This behavior arises because, in the presence of $c_{\phi_i} \neq 1$, the beta function of y_t is dominated by the negative contributions of the gauge couplings g_i. Consequently, at high energies, y_t takes smaller values compared to the case where $c_{\phi_i} = 1$. As a result, the negative contribution of y_t to the beta function of λ_2 is reduced, preventing λ_2 from turning negative at high energies.

One-loop effective potential for the inflation field τ is derived based on [99], where for the canonically normalized Lagrangian in the Einstein frame:

$$\frac{\mathcal{L}}{\sqrt{g}} = -\frac{1}{2}M_P^2 R + \frac{1}{2}g^{\mu\nu}\partial_\mu\sigma\partial_\nu\sigma - V(\sigma), \tag{9.78}$$

one-loop quantum corrections take the form[4]:

$$V_{1-\text{loop}}(\sigma) = V(\sigma) + \frac{1}{64\pi^2}\left[n_\sigma \mathcal{M}^4(\sigma)\log\frac{|\mathcal{M}^2(\sigma)|}{c_\sigma\mu^2} + n'_\sigma\frac{R^2}{144}\log\frac{|\mathcal{M}^2(\sigma)|}{\mu^2}\right], \tag{9.80}$$

where $c_\sigma = e^{3/2}$, $n_\sigma = 1$, $n'_\sigma = -\frac{2}{15}$, $\mathcal{M}^2(\sigma) = m^2(\sigma) - \frac{R}{6}$ and:

$$m^2(\sigma) = \frac{\partial^2 V(\sigma)}{\partial\sigma^2} = m^2(\tau) = \frac{1}{F^2(\tau)}\left(\frac{\partial^2 V(\tau)}{\partial\tau^2} - \frac{\partial V(\tau)}{\partial\tau}\frac{\partial F(\tau)/\partial\tau}{F(\tau)}\right), \tag{9.81}$$

where $V(\tau)$ and $F(\tau)$ are given in equations (9.47) and (9.46) respectively, $V(\sigma) = V(\tau)$ and consequently $V_{1-\text{loop}}(\sigma) = V_{1-\text{loop}}(\tau)$. During inflation, the space-time has the de Sitter form, and the curvature, $R = 12H_{inf}^2$, with large H_{inf}, gives a dominant contribution over $m^2(\tau)$.

[4]We apply the results from [99] during the inflation, where the space-time has the de Sitter form, with:

$$R = 12H^2, \qquad R_{\mu\nu}R^{\mu\nu} = 36H^4, \qquad R_{\mu\nu\rho\sigma}R^{\mu\nu\rho\sigma} = 24H^4. \tag{9.79}$$

The ϕ_1 field, being the Higgs boson neutral component, couples to the SM particles, which give important contributions to the potential at the one-loop level. The most dominant are $W^{\pm}$, Z^0 bosons, and the top quark, and G_i Goldstone bosons from (5.3), with the Jordan frame masses:

$$\begin{gathered} m_W^2(\phi_1) = \frac{g_2^2}{4}\phi_1^2, \qquad m_Z^2(\phi_1) = \frac{g_1^2+g_2^2}{4}\phi_1^2, \qquad m_t^2(\phi_1) = \frac{y_t^2}{2}\phi_1^2, \\ m_G^2(\phi_0,\phi_1) = 2\lambda_1\phi_0^2 + 4\lambda_2\phi_1^2. \end{gathered} \tag{9.82}$$

After transformation (4.8) to the Einstein frame, they depend on the inflaton field as follows:

$$\begin{gathered} \hat{m}_{W,Z}^2(\tau) = \frac{m_{W,Z}^2\big(\phi_1(\tau)\big)}{\Omega^2\big((\phi_0(\tau),\phi_1(\tau)\big)}, \qquad \hat{m}_t^2(\tau) = \frac{m_t^2\big(\phi_1(\tau)\big)}{\Omega^2\big((\phi_0(\tau),\phi_1(\tau)\big)}, \\ \hat{m}_G^2(\tau) = \frac{m_G^2\big(\phi_0(\tau),\phi_1(\tau)\big)}{\Omega^4\big((\phi_0(\tau),\phi_1(\tau)\big)}, \end{gathered} \tag{9.83}$$

where $\phi_i(\tau)$ can be read from (9.43). The SM particles' contribution to the one-loop effective potential then reads [99]:

$$V_{1-\text{loop}}(\tau)\Big|_{SM} = \frac{1}{64\pi^2}\sum_{i=W,Z,t}\left[n_i\mathcal{M}_i^4(\tau)\log\frac{|\mathcal{M}_i^2(\tau)|}{c_i\mu^2} + n_i'\frac{R^2}{144}\log\frac{|\mathcal{M}_i^2(\tau)|}{\mu^2}\right], \tag{9.84}$$

where:

$$\begin{array}{llll} \mathcal{M}_W^2(\tau) = \hat{m}_W^2(\tau) + \frac{R}{12}, & c_W = e^{5/6}, & n_W = 6, & n_W' = -\frac{34}{5}, \\ \mathcal{M}_Z^2(\tau) = \hat{m}_Z^2(\tau) + \frac{R}{12}, & c_Z = e^{5/6}, & n_Z = 3, & n_Z' = -\frac{17}{5}, \\ \mathcal{M}_t^2(\tau) = \hat{m}_t^2(\tau) + \frac{R}{12}, & c_t = e^{3/2}, & n_t = -12, & n_t' = \frac{38}{5}, \\ \mathcal{M}_G^2(\tau) = \hat{m}_G^2(\tau) + \frac{R}{6}\big(\xi_1 - 1\big), & c_G = e^{3/2}, & n_G = 3, & n_G' = -\frac{6}{15}. \end{array} \tag{9.85}$$

Finally, the full one-loop effective potential for the inflaton field τ reads:

$$V_{1-\text{loop}}(\tau) = V_{1-\text{loop}}(\tau)\Big|_{\sigma} + V_{1-\text{loop}}(\tau)\Big|_{SM}, \tag{9.86}$$

with the corresponding contributions given in equations (9.80) and (9.84).

To apply the RG improvement to the potential (9.86), an appropriate choice of the running energy scale μ is required to minimize quantum corrections, particularly the logarithmic terms in $V_{1-\text{loop}}(\tau)$. Based on the approximate constancy of energy scales during inflation, we adopt an approach with constant μ[5]. Given that the characteristic energy scale during inflation is the Hubble parameter H_{inf}, which remains nearly constant along with the potential energy during slow-roll, we set $\mu = H_{inf}$. The Hubble scale is determined numerically using the equation (9.20):

$$H_{inf}^2 = \frac{V_{1-\text{loop}}(\tau = 10^2, H_{inf}, \mu = H_{inf})}{3M_P^2}, \tag{9.87}$$

where $\tau = 10^2$ is chosen as the value at which the potential is sufficiently flat and lies within the inflationary regime.

The RG improvement of the potential (9.86) is implemented by solving the RG equations (9.71), (9.72) and (9.73) for ξ_i, λ_2, and the SM couplings, and then evaluating them at $\mu = H_{inf}$. As argued earlier in this chapter, we neglect the running of λ_0, λ_1, and ξ_0. Finally, the inflaton field is modified according to equations (9.75) and (9.76), leading to the replacement $\tau \to \exp\big(\Gamma(\mu = H_{inf})\big)\tau$.

[5] As discussed in [99], one can choose μ in a way that the logarithms vanish. However, this prescription introduces an ambiguity in the definition of μ, and the quantum potential behavior can still be compromised. A common alternative is to set $\mu = a \cdot f(\phi) + b \cdot R$, where $f(\phi)$ is a field-dependent function. In the framework considered here, this choice reduces to a constant μ in the inflationary regime of τ. For this reason, we adopt the constant-μ approach.

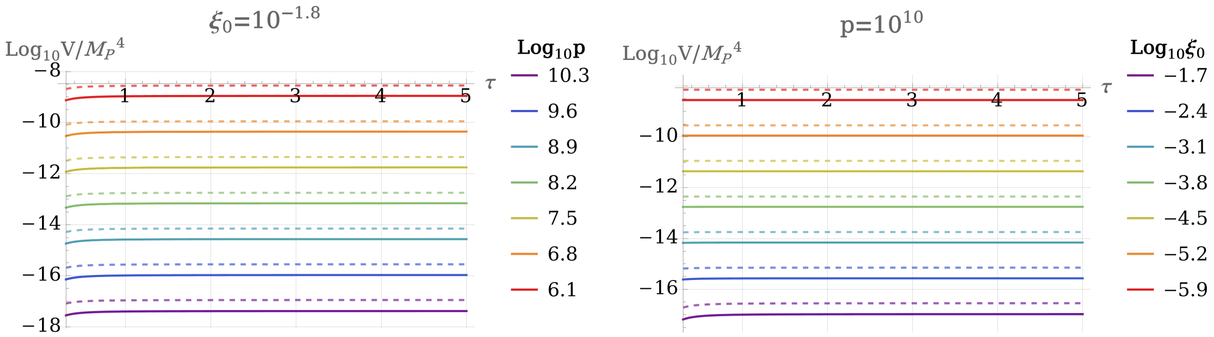

Figure 9.12: Plots of the RG-improved effective potential $V_{RGI}(\tau)$ (solid lines) and the tree-level potential $V(\tau)$ (dashed lines) for selected parameter space values. Quantum corrections reduce the potential values slightly, by less than an order of magnitude.

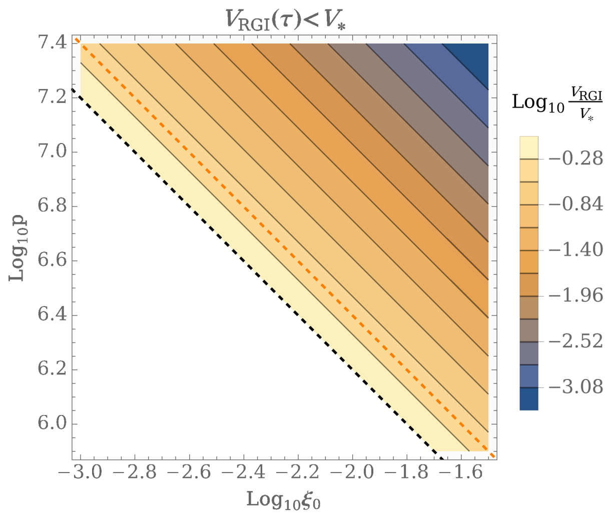

Figure 9.13: Region plot of the allowed values of ξ_0 and p for which $V_{RGI}(\tau)$ does not exceed the bound (9.60). The result can be approximated by the inequality $\log_{10} p \geq -\log_{10}\xi_0 + 4.2$, marked by the black dashed line. For comparison, the tree-level result $\log_{10} p \geq -\log_{10}\xi_0 + 4.4$ is indicated by the orange dashed line.

Figure 9.12 compares the RG-improved one-loop potential, $V_{1-\mathrm{loop}}(\tau, \mu = H_{inf}) = V_{RGI}(\tau)$, with the tree-level potential $V(\tau)$. The plots are shown for $\tau \geq 1$, where the choice of a constant μ is justified. Quantum corrections lower the potential energy. As a consequence, the parameter space satisfying the Planck 2018 bound (9.60) is enlarged compared to the tree-level case, as illustrated in Figure 9.13. The constraint can be approximated by the inequality $\log_{10} p \geq -\log_{10}\xi_0 + 4.2$.

The general expressions for the slow-roll parameters ϵ_V and η_V were derived for the one-loop effective potential $V_{1-\mathrm{loop}}(\tau)$ from equation (9.86). The couplings were then evaluated at the energy scale $\mu = H_{inf}$, and the inflaton field was rescaled as $\tau \to \exp\big(\Gamma(\mu_1)\big)\tau$. Following the same steps as in Section 9.3, we computed the scalar spectral index n_s and the tensor-to-scalar ratio $r_{0.002}$, focusing on $N_e = 50$. Since the results for $N_e = 60$ are nearly identical, they are omitted for clarity. The function $r_{0.002}(n_s)$ is illustrated in Figure 9.14, along with a comparison to the tree-level case. The endpoint of inflation in this plot is defined by the condition $\eta_V(\tau_{end}) = -0.0095$. As in the classical scenario, the obtained n_s values are inconsistent with (9.26). Therefore, we further analyze the impact of the $\eta_V(\tau_{end})$ choice on $r_{0.002}(n_s)$, consistently with (9.64). This dependence is illustrated in Figure 9.15 for $\xi_0 = 10^{-1.86}$ and $\xi_0 = 10^{-1.77}$ with $p = 10^{6.5}$, along with a comparison to the tree-level case. The results demonstrate that physically

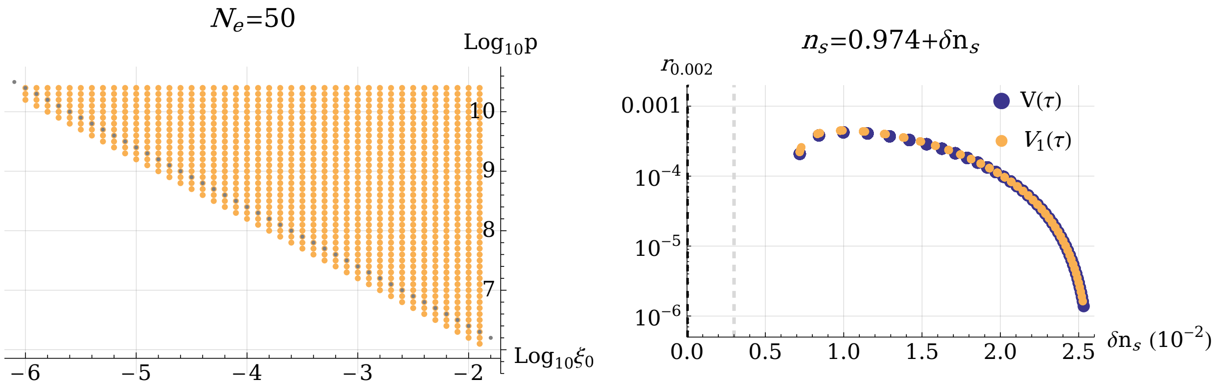

Figure 9.14: **Left:** Parameter space points used to derive the $r_{0.002}(n_s)$ function shown in the right panel. The dotted gray line marks the boundary of the tree-level constraint, given by $\log_{10} p \geq -\log_{10} \xi_0 + 4.4$. **Right:** The function $r_{0.002}(n_s)$, computed using the RG improved potential $V_{RGI}(\tau)$, for the endpoint of inflation defined as $\eta_V(\tau_{end}) = -0.0095$ and $N_e = 50$. The results are compared with the tree-level $r_{0.002}(n_s)$ function for the same parameters, as illustrated in Figure 9.5.

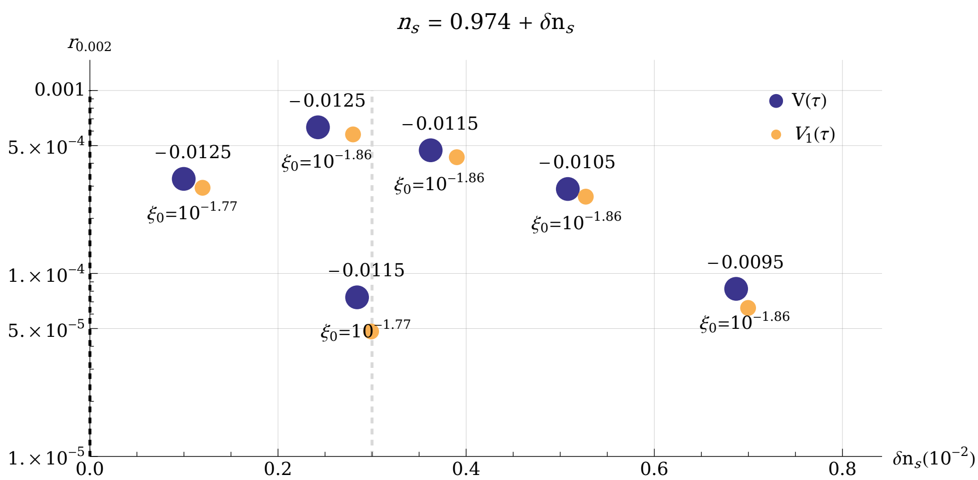

Figure 9.15: Tensor-to-scalar ratio $r_{0.002}(n_s)$ for $\xi_0 = 10^{-1.71}$ and $\xi_0 = -1.86$ with $p = 10^{6.5}$ at different inflationary endpoints, determined by $\eta_V(\tau_{end})$ and $N_e = 50$. The numerical labels above the points indicate the corresponding $\eta_V(\tau_{end})$ values. The black dashed line corresponds to the experimental value, $n_s = 0.974$, and the gray dashed line to $n_s = 0.974 + 0.003$. The results are compared with the tree-level $r_{0.002}(n_s)$ function for the same parameters, as illustrated in Figure 9.6.

viable results of n_s can be achieved within the Higgs-dilaton model. Finally, since the quantum corrections introduce only minor deviation from the tree-level results, the impact of ξ_0 and p on n_s and $r_{0.002}$ for $\eta_V(\tau_{end}) = -0.0095$ follows the same pattern as in the tree-level analysis, as shown in Figure 9.7.

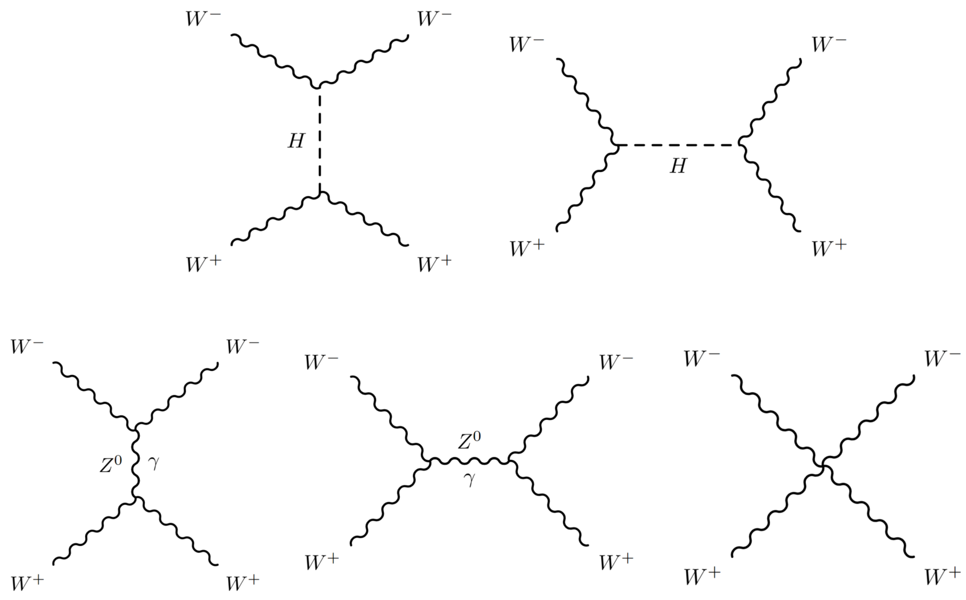

Figure 9.16: Diagrams contributing to $W_L^+W_L^- \to W_L^+W_L^-$ scattering amplitude.

9.5. Unitarity Bounds

In the Einstein frame, the gravity is in its canonical form. Therefore, the unitarity cutoff resulting from the interactions involving gravitons is of the order of the Planck mass. However, the SM gauge sector changes due to the conformal transformation (4.8) and changing to the polar coordinates (9.43). This can induce unitarity violation above some energy scale, which we aim to find below.

We analyze the behavior of scattering amplitudes for specific processes, particularly the longitudinal W boson scattering $W_L^+W_L^- \to W_L^+W_L^-$. Figure 9.16 illustrates the relevant Feynman diagrams contributing to this process. In the high-energy limit $(s, t \gg m_W^2)$, the leading contributions from the $s-$ and $t-$channel exchange of the photon and Z^0, along with the 4-point gauge interaction give [102–104]:

$$\mathcal{A}(W_L^+W_L^- \to W_L^+W_L^-)\Big|_{\text{gauge}} = -\frac{1}{4}g_2^2\frac{1}{m_W^2}u + \mathcal{O}(1), \tag{9.88}$$

where u is the Mandelstam variable, $u = 4m_W^2 - s - t$. This amplitude grows with energy, signaling a potential violation of unitarity at high energies. However, the Higgs boson exchange in the s and t channels introduces a contribution of [102–104]:

$$\mathcal{A}(W_L^+W_L^- \to W_L^+W_L^-)\Big|_{\text{Higgs}} = +\frac{1}{4}g_2^2\frac{1}{m_W^2}u + \mathcal{O}(1), \tag{9.89}$$

which precisely cancels the problematic energy-growing term in the SM, ensuring a well-behaved amplitude in the high-energy limit. However, in the theories where the Higgs-W interaction is modified, such as our model, this cancellation may not occur.

We now examine the unitarity constraints in the Einstein frame Lagrangian of inflationary theory presented in this work. The charged $W^\pm$ bosons couple to the neutral Higgs component ϕ_1 through the interaction term:

$$\frac{\mathcal{L}_{Higgs-W}}{\sqrt{g}} \sim \frac{g_2^2}{4}g^{\mu\nu}W_\mu^+W_\nu^- \cdot \phi_1^2. \tag{9.90}$$

After applying a conformal transformation and changing to polar coordinates, this becomes:

$$\frac{\hat{\mathcal{L}}_{Higgs-W}}{\sqrt{\hat{g}}} \sim \frac{1}{\Omega^2}\frac{g_2^2}{4}\hat{g}^{\mu\nu}W_\mu^+W_\nu^- \cdot \frac{1}{1+\xi_1}K \cdot \frac{\tau^2}{1+\tau^2}, \tag{9.91}$$

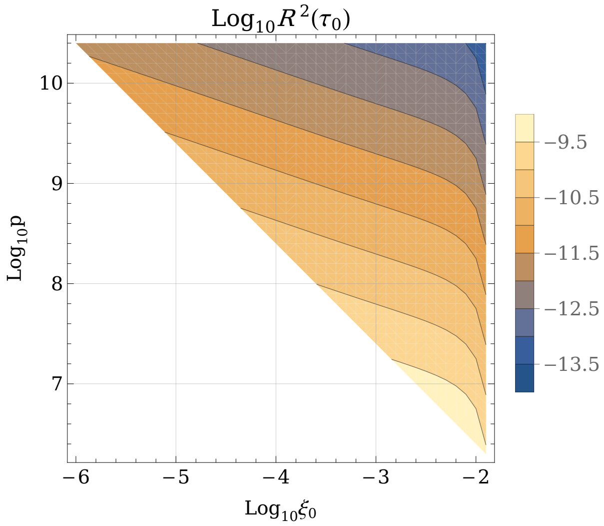

Figure 9.17: Plot of the $R^2(\tau_0)$ parameter, defined in (9.98). The τ_0 values for each plot point were determined as a τ^* for a corresponding parameter space point.

where Ω^2 is defined in equation (9.37). K is an arbitrary scale, chosen to obtain proper vacuum expectation values for ϕ_i fields in equation (9.43):

$$K = \left(-\frac{2\lambda_2}{\lambda_1}\big(1+\xi_0\big) + \big(1+\xi_1\big)\right)\langle\phi_1^2\rangle, \qquad \langle\phi_1\rangle = 250 \text{ GeV}. \tag{9.92}$$

Consequently, the Higgs$-W$ interaction is modified to:

$$\frac{\hat{\mathcal{L}}_{Higgs-W}}{\sqrt{\hat{g}}} \sim \frac{g_2^2}{4}\hat{g}^{\mu\nu}W_\mu^+W_\nu^- \cdot f(\tau), \tag{9.93}$$

where:

$$f(\tau) = \frac{1}{\Omega^2}\frac{K}{1+\xi_1}\frac{\tau^2}{1+\tau^2} = 6M^2\frac{(1+\xi_0)\tau^2}{\xi_0(1+\xi_1)+\xi_1(1+\xi_0)\tau^2}. \tag{9.94}$$

With the non-canonical kinetic term for the inflaton field:

$$\frac{1}{2}F^2(\tau)\hat{g}^{\mu\nu}\partial_\mu\tau\partial_\nu\tau = \frac{1}{2}\hat{g}^{\mu\nu}\partial_\mu\sigma\partial_\nu\sigma, \qquad F(\tau) = \frac{\partial\sigma}{\partial\tau}, \tag{9.95}$$

we expand (9.93) around the τ_0 background, with $\tau = \tau_0 + \delta\tau$ and $\delta\tau \cdot F(\tau_0) = \delta\sigma$:

$$\frac{\hat{\mathcal{L}}_{Higgs-W}}{\sqrt{\hat{g}}} \sim \frac{g_2^2}{4}\hat{g}^{\mu\nu}W_\mu^+W_\nu^- \cdot \left(f(\tau_0) + \frac{f'(\tau_0)}{F(\tau_0)}\delta\sigma + \frac{f''(\tau_0)}{2F^2(\tau_0)}\delta\sigma^2 + \dots \right). \tag{9.96}$$

Consequently, the $WW\sigma$ vertex with canonical σ field reads:

$$g_{WW\sigma} = \frac{g_2^2}{4}\frac{f'(\tau_0)}{F(\tau_0)}. \tag{9.97}$$

Defining the relative change of the interaction as:

$$R(\tau_0) = \frac{g_{WW\sigma}}{g_2 m_W(\tau_0)} = \frac{1}{2}\frac{f'(\tau_0)}{F(\tau_0)\sqrt{f(\tau_0)}}, \tag{9.98}$$

the amplitude for the Higgs exchange now reads:

$$\mathcal{A}\big(W_L^+W_L^- \to W_L^+W_L^-\big)\Big|_{\text{Higgs}} \simeq +\frac{1}{4}g_2^2\frac{R^2(\tau_0)}{m_W^2}u + \mathcal{O}(1). \tag{9.99}$$

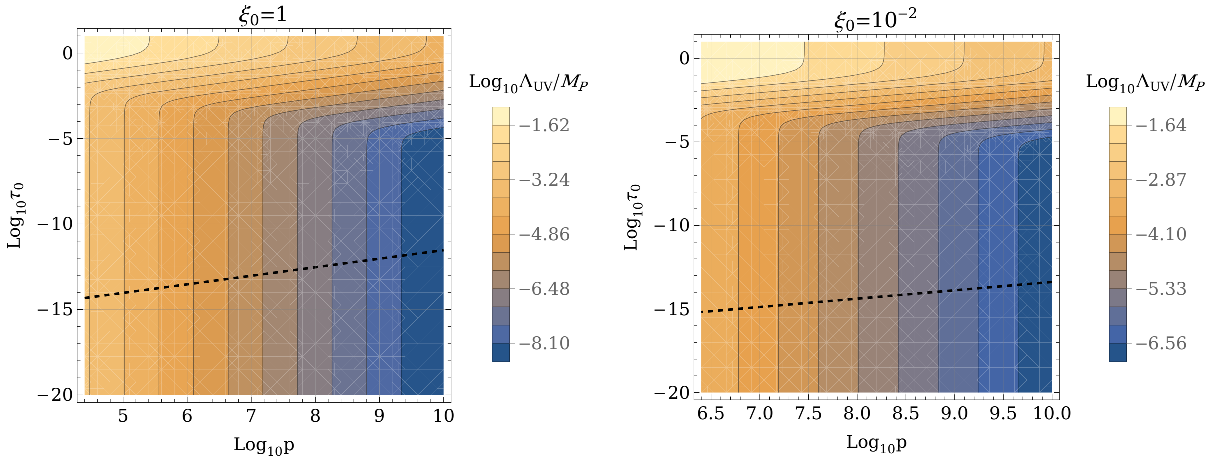

Figure 9.18: Cutoff scale Λ_{UV} as a function of τ_0 for different parameter-space points. The black dashed line indicates the vacuum expectation value $\langle \tau_0 \rangle$.

In the SM, $R = 1$ and the Higgs exchange process cancels the amplitude in (9.88)[6]. In the case of the theory presented in this paper, we examine the cancellation of amplitudes and the resulting unitary cutoff by the sum of both amplitudes:

$$\mathcal{A}(W_L^+ W_L^- \to W_L^+ W_L^-) \simeq \frac{g_2^2}{4} \frac{u}{m_W^2(\tau_0)} \Big(-1 + R^2(\tau_0) \Big). \tag{9.100}$$

Figure 9.17 presents the $R^2(\tau_0)$ values for different ξ_0, p and $\tau_0 = \tau^*$ for a given parameter space with $\eta_V(\tau_{end}) = -0.0095$ and $N_e = 50$. Values are significantly smaller than 1. Therefore, the unitarity cutoff in the inflationary background is dominated by the gauge bosons' contribution:

$$\Lambda_{UV}\Big|_{R\ll 1} \sim \sqrt{8\pi}\frac{m_W(\tau_0)}{g_2/2} = 8\sqrt{3\pi} M_P \tau_0 \sqrt{\frac{1+\xi_0}{\xi_0(1+\xi_1)+\xi_1(1+\xi_0)\tau_0^2}} \xrightarrow[\xi_0 \ll 1, \tau_0 \lesssim 1]{\xi_1 \gg 1} \frac{M_P}{\sqrt{\xi_1}}. \tag{9.101}$$

The cutoff always exceeds the values of inflationary potential $V(\tau)^{1/4}$. For a background value $\tau_0 = \tau^*$, the cutoff exceeds the inflationary energy scale $V(\tau^*)^{1/4}$ by a factor of 11.9236, ensuring the validity of our results. The asymptotic behavior $M_P/\sqrt{\xi_1}$ matches the cutoff in the inflationary regime found in Higgs inflation models with a non-minimal coupling in the inflationary large field background [105, 106].

The full τ_0-dependent cutoff reads:

$$\Lambda_{UV} = \sqrt{8\pi}\frac{m_W(\tau_0)}{g_2/2}\frac{1}{\sqrt{-1+R^2(\tau_0)}}, \tag{9.102}$$

and is illustrated in Figure 9.18. In the vacuum limit ($\tau_0 \ll 1$), the cutoff is significantly lower than in the inflationary background, in particular:

$$\Lambda_{UV} \xrightarrow[\xi_0 \ll 1, \tau_0 \ll 1]{\xi_1 \gg 1} \frac{M_P}{\xi_1}. \tag{9.103}$$

The asymptotic behavior (9.103) agrees with the Higgs inflation models from the literature [105, 106].

[6] The pure Yang-Mills sector is invariant under transformation to the Einstein frame.

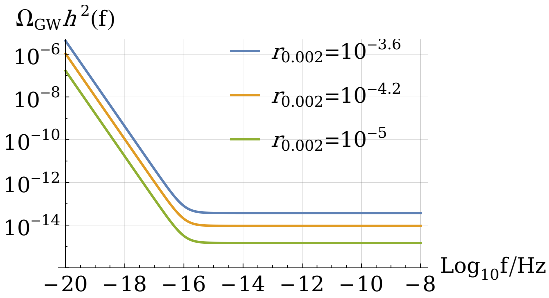

(a) Gravitational wave spectrum (9.105) for three values of $r_{0.002}$ obtained from the analysis in Section 9.4.

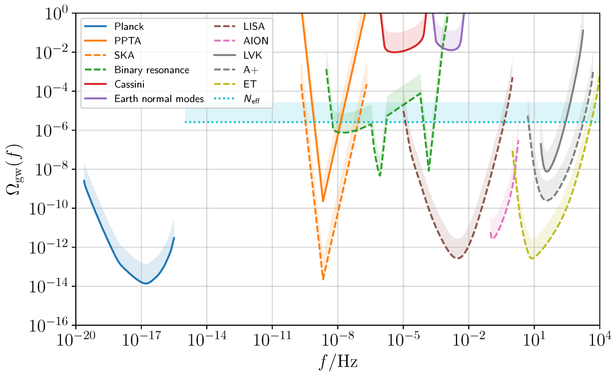

(b) Detection sensitivity ranges of current gravitational wave experiments. Figure taken from [110].

Figure 9.19

9.6. Gravitational Waves Spectrum

During inflation, tensor metric perturbations, which are small deviations h_{ij} from the background FLRW metric:

$$ds^2 = a^2(\eta)\Big[-\mathrm{d}\eta^2 + \big(\delta_{ij} + h_{ij}\big)\mathrm{d}x^i\mathrm{d}x^j\Big], \tag{9.104}$$

originate from quantum fluctuations of the gravitational field. As inflation progresses, they are amplified and stretched to super-Hubble scales, resulting in a nearly scale-invariant spectrum [107, 108]. Upon re-entering the Hubble horizon in the post-inflationary era, they evolve as classical gravitational waves (GWs), forming a stochastic background that could, in principle, be detected by experiments such as LISA, ET, CMB B-mode polarization searches, and future gravitational wave observatories.

The GW energy density spectrum $\Omega_{GW}(f)$ represents the spectrum observed today after the GW frequencies have been redshifted due to the Universe's expansion. Assuming a standard cosmic history, including nonrelativistic matter and radiation evolution, it is given by [107,108]:

$$\Omega_{GW}(f) = \frac{3}{128} r_{0.002} A_s \Omega_r \left(\frac{f}{f_*}\right)^{n_t} \left[\frac{1}{2}\left(\frac{f_{eq}}{f}\right)^2 + \frac{16}{9}\right], \tag{9.105}$$

where A_s is the scalar amplitude (9.28), $\Omega_r = 3.72 \cdot 10^{-5}$ is the current value of radiation energy density, f_* is the pivot frequency, given by $f_* = \frac{0.05\ \mathrm{Mpc}^{-1}}{2\pi} \approx 7.75 \cdot 10^{-16}$ Hz, f_{eq} is the frequency corresponding to matter-radiation equality, with $f_{eq} \approx 2.02 \cdot 10^{-16}$, and n_t is the tensor spectral index, which at first order is related to the slow-roll parameter ϵ_V as $n_t = -2\epsilon_V$. The cosmological parameter values used here are consistent with Planck 2018 results [109] and references [107, 108]. The slow-roll parameter ϵ_V is evaluated at τ_*, hence, n_t can be expressed in terms of $r_{0.002}$ as $n_t = -\frac{r_{0.002}}{8}$.

Figure 9.19b provides the sensitivity ranges of current GW detection experiments across different frequencies. The frequency range accessible to each experiment determines the epoch and scale of the early Universe that can be probed. The lowest frequencies, detectable by CMB B-mode polarization searches done by the Planck satellite, correspond to the physics at the largest cosmological scales, tracking the earliest times and the highest energy scales of inflation.

Figure 9.19a presents the predicted GW spectrum for values of $r_{0.002}$ derived within the scale symmetric Higgs-dilaton model, as shown in Figure 9.15. Comparing these results with the sensitivity ranges in Figure 9.19b, we conclude that the predicted GW signal lies within the detectable range, providing a potential test of the framework developed in this work.

Chapter 10

Conclusions

This thesis has studied a scale symmetric extension of the Standard Model Higgs scalar sector by coupling the Higgs field to Weyl conformal gravity, from which the new sector, the dilaton, naturally emerges. This approach offers a natural resolution to the hierarchy problem and answers the question about mass scales generation without the need for explicit dimensionful parameters.

One of the key contributions of this work is the analysis of spontaneous scale symmetry breaking (SSSB) at high temperatures. The results have profound implications for early Universe cosmology. We incorporated temperature corrections into the one-loop effective potential of the Higgs-dilaton model and demonstrated that scale symmetry is dynamically broken during the system's evolution in an expanding hot Universe. This, confirmed by numerical simulations of the Higgs and dilaton fields, serves as a viable mechanism for mass generation, in which, with appropriate initial conditions, a physically stable vacuum state is reached, consistent with our present knowledge about physical observables.

Moreover, we provided an independent analysis of the decoupling limit of the dilaton, showing that it is strongly connected to the gravity sector decoupling. We derived that in their decoupling limits, the standard Higgs scalar sector in flat spacetime is recovered. Furthermore, we examined the implications of the Weak Gravity Conjecture (WGC) in the Higgs-dilaton model. We presented the constraints imposed by the WGC on the Weyl gauge coupling, ensuring theoretical consistency.

Our work also addressed inflation within the scale-invariant Higgs-dilaton model. We demonstrated that embedding the theory in Weyl geometry introduces significant modifications to the inflationary dynamics, particularly when a kinetic term for the dilaton is included. We analyzed the slow-roll conditions in the classical potential and then incorporated quantum correction through the running of couplings in an appropriate renormalization prescription for the inflationary scenario analyzed in this work. The results showed that a viable parameter space exists where inflationary predictions align with the experimental data. Finally, we discussed potential unitarity violation, highlighting the energy scale constraints needed for a consistent, effective theory of inflation. We finished with a brief analysis of the Gravitational Waves spectrum resulting within the Higgs-dilaton model.

This work contributes to the broader effort of finding a fundamental framework in theoretical physics, where mass scales emerge naturally from symmetry principles rather than being introduced as arbitrary parameters. However, several open questions remain that should be addressed to understand the theory further. Future work should focus on the application of presented ideas to a quantum gravity framework, possibly within string theory or asymptotically safe gravity models. Moreover, the parameter space sufficient to obtain proper mass scales, such as the Higgs mass, Higgs vev, and especially the Planck scale, is beyond the reach of current or even future experiments. Therefore, one should seek experimental validation of the theory, potentially through Dark Matter abundance analysis or more in-depth thermal corrections incorporation. More precise results may impact the nature of electroweak symmetry breaking in the Higgs-dilaton model, especially driving it more to a first-order phase transition, which is possibly required for a proper baryogenesis mechanism.

In conclusion, this dissertation has demonstrated that scale-invariant extensions of the Standard Model offer a promising direction for addressing unresolved problems in particle physics and cosmology. While challenges remain, the insights gained from this work lay the foundation for further investigations into the role of scale symmetry in fundamental physics.

Appendix A

One-loop Beta Functions

We define $B_i = (4\pi)^2 \cdot \beta_i = (4\pi)^2 \cdot \frac{d}{d\ln z}\alpha_i$ with $\alpha_i = \{\lambda_0, \lambda_1, \ldots, g_1, g_2, g_3, y_t\}$. The one-loop β functions for g_1, g_2, g_3 and y_t, along with their boundary values, can be found, for example, in [64,111] (it is important to note that the notation used in our work may differ from that in the referenced sources). Here, we list the β functions for λ_i obtained in Chapter 5 and SM couplings setting notation proper for this work.

$$
\begin{aligned}
B_0 &= 8\big(9\lambda_0^2 + \lambda_1^2\big),\\
B_1 &= 8\lambda_1\big(3\lambda_0 + 2\lambda_1 + 6\lambda_2\big) + 3\lambda_1\big(-3g_1^2 - g_2^2 + 4y_t^2\big),\\
B_2 &= 2\big(\lambda_1^2 + 48\lambda_2^2 + 30\lambda_1\lambda_3\big) + \frac{3}{32}\left(g_1^4 + 2g_1^2g_2^2 + 3g_2^4 - 16y_t^4 + 64\lambda_2\big(-3g_1^2 - g_2^2 + 4y_t^2\big)\right),\\
B_3 &= 24\lambda_3\big(3\lambda_0 - 4\lambda_1 + 15\lambda_2\big) + 9\lambda_3\big(-3g_1^2 - g_2^2 + 4y_t^2\big),\\
B_4 &= 6\lambda_3\big(2\lambda_1 + 75\lambda_3\big) + 12\lambda_4\big(-3g_1^2 - g_2^2 + 4y_t^2\big),\\
B_5 &= 144\lambda_3^2 + 15\lambda_5\big(-3g_1^2 - g_2^2 + 4y_t^2\big),\\
B_6 &= 18\lambda_3^2 + 18\lambda_6\big(-3g_1^2 - g_2^2 + 4y_t^2\big).
\end{aligned}
$$

$$
\begin{aligned}
B_{g_1} &= \frac{41}{6}g_1^3,\\
B_{g_2} &= -\frac{19}{6}g_2^3,\\
B_{g_3} &= -7g_3^3,\\
B_{y_t} &= y_t\left(\frac{9}{2}y_t^2 - \frac{17}{12}g_1^2 - \frac{9}{4}g_2^2 - 8g_3^2\right).
\end{aligned}
\tag{A.1}
$$

The RG factor z tracks the dependence on the subtraction scale $\mu(\langle\phi_0\rangle) = z \cdot \langle\phi_0\rangle$. For the coupling constants to be evaluated at the scale $\langle\phi_1\rangle = 250$ GeV, we define $z_0 = \frac{\langle\phi_1\rangle}{\langle\phi_0\rangle}$. To apply the RG improvement to the quantum potential, we let the parameters run with the dilaton field ϕ_0, namely:

$$
z_0 = \frac{\mu(\langle\phi_0\rangle)}{\langle\phi_0\rangle} \xrightarrow{\text{RG improvement}} z = \frac{\mu(\phi_0)}{\langle\phi_0\rangle} = \frac{z_0 \cdot \phi_0}{\langle\phi_0\rangle}. \tag{A.2}
$$

Consequently, coupling constants are now functions of the dilaton:

$$
\beta_i = z\frac{d\alpha_i}{dz} \quad \Rightarrow \quad \alpha_i\,(z) = \alpha_i(\phi_0). \tag{A.3}
$$

Initial values used to obtain plots in Figure A.2 are evaluated at the scale $\mu(\langle\phi_0\rangle) = z_0\langle\phi_0\rangle =$

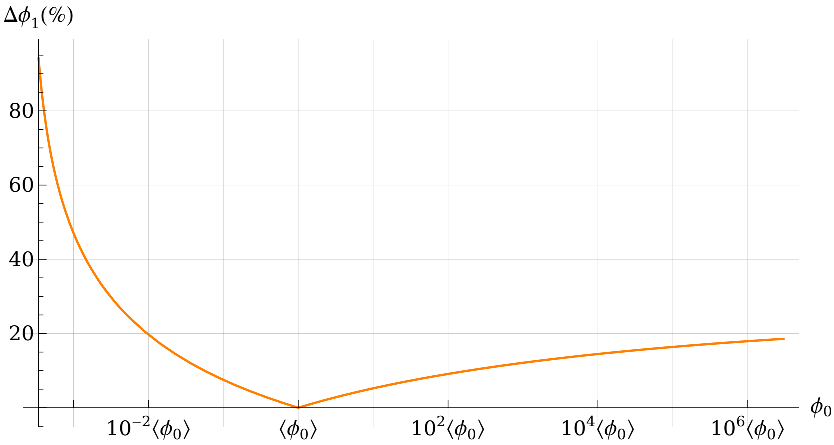

Figure A.1: $\Delta\phi_1$ defined in (A.8), illustrating the running of the ϕ_1 field according to (A.7).

$\langle\phi_1\rangle$, and read (notation: $L_i = \lambda_i(\langle\phi_0\rangle)$):

$$L_0 = \frac{L_1^2}{4L_2}, \quad L_1 = -10^{-6}, \quad L_2 = 0.03125, \quad L_3 = 10^{-5}L_0, \quad L_4 = L_5 = L_6 = 0, \tag{A.4}$$

$$L_{g_1} = 0.35940, \quad L_{g_2} = 0.64754, \quad L_{g_3} = 1.1666, \quad L_{y_t} = 0.95113. \tag{A.5}$$

In Figure A.2, we provide the results of running for λ_0, λ_1, λ_2 and SM couplings g_1, g_2 and y_t. Couplings λ_n for $n > 2$ were not plotted due to their negligible running, as their corresponding beta functions indicate.

A.1. Anomalous Dimension and the Field Running

Having the β functions for all the couplings in δ_H, where [22, 63, 64]:

$$Z_H = 1 + \frac{1}{\epsilon}\frac{\delta_H}{(4\pi)^2}, \qquad \delta_H = \frac{9}{4}g_1^2 + \frac{3}{4}g_2^2 - 3y_t^2, \qquad \gamma_H = -\frac{1}{2}\frac{\partial \ln Z_H}{\partial \ln z} = \frac{\partial \ln \phi_1}{\partial \ln z} = \frac{2}{(4\pi)^2}\delta_H, \tag{A.6}$$

one can solve the differential equation for ϕ_1 field:

$$\frac{\partial \ln \phi_1}{\partial \ln z} = \frac{2}{(4\pi)^2}\left[\frac{9}{4}g_1^2 + \frac{3}{4}g_2^2 - 3y_t^2\right], \tag{A.7}$$

with initial value, $\phi_1(z_0)$ evaluated at z_0. Deviation from this initial value will illustrate the significance of the quantum corrections in the field running. In Figure A.1, we plot this difference, defined as:

$$\Delta\phi_1 = \frac{|\phi_1(z) - \phi_1(z_0)|}{|\phi_1(z_0)|} \cdot 100\% = \frac{|\phi_1(\phi_0) - \phi_1(\langle\phi_0\rangle)|}{|\phi_1(\langle\phi_0\rangle)|} \cdot 100\%. \tag{A.8}$$

A.2. Plots of Running Couplings

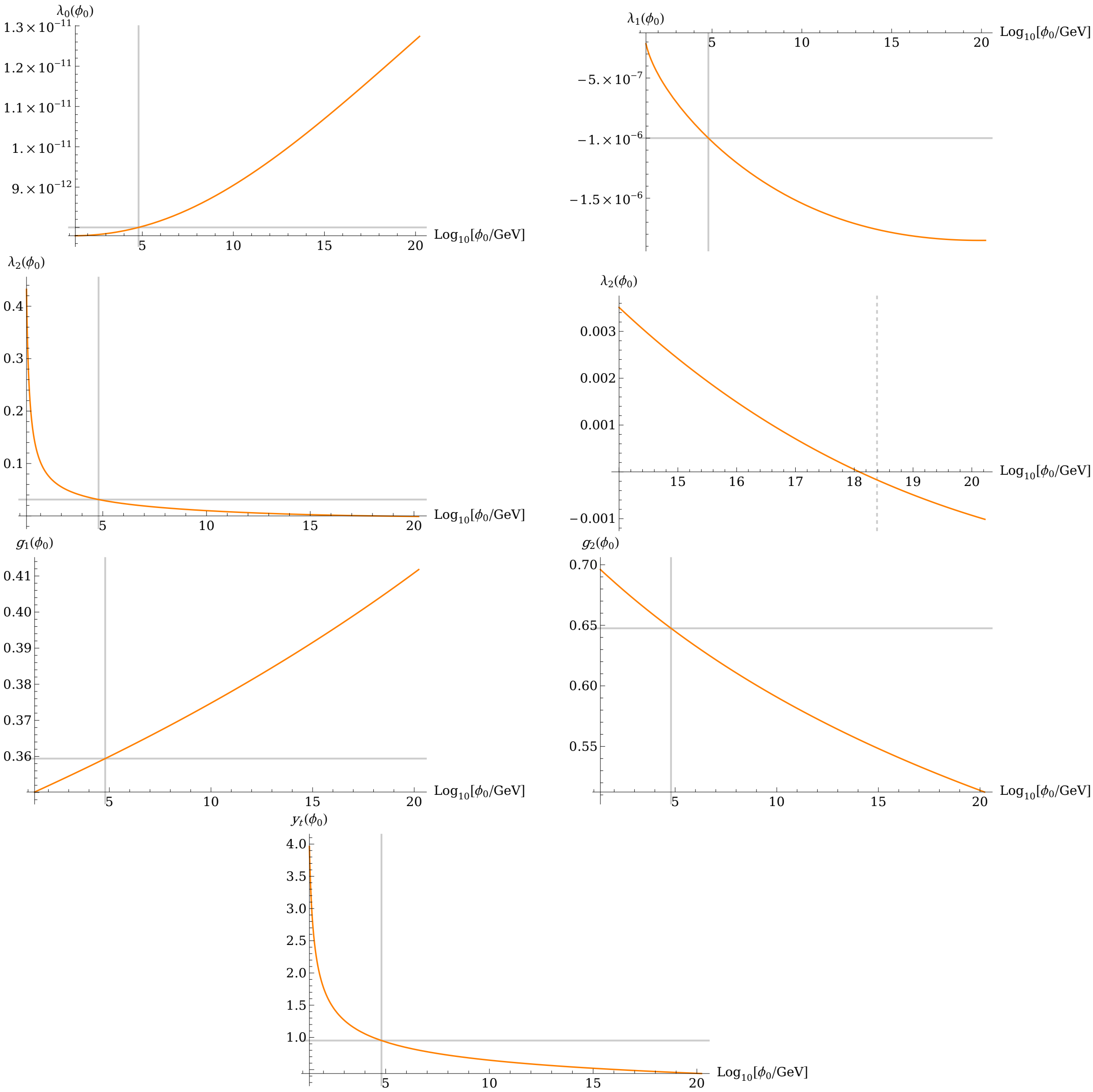

Figure A.2: Plots of running for λ_0, λ_1, λ_2 and SM couplings g_1, g_2 and y_t with the dilaton field value ϕ_0. Initial values were chosen as in equations (A.4) and (A.5). Solid grid lines correspond to the $\langle\phi_0\rangle$ value on the x axis and L_i on the y axis. The dashed grid line on the second plot for λ_2 running marks the Planck scale $M_P = 2.44\cdot10^{18}$ GeV.

Appendix B

Ensemble Average of the Annihilation and Creation Operators Products

B.1. Scalars:

To obtain formulas for thermal averages of $\langle a^\dagger a\rangle$ and $\langle aa^\dagger\rangle$, let's consider the discrete dimensionless operators a_i and $a_i^\dagger$:

$$a_i \equiv \sqrt{\delta V_k^3}\cdot a(\vec{k}_i), \qquad a_i^\dagger \equiv \sqrt{\delta V_k^3}\cdot a^\dagger(\vec{k}_i), \tag{B.1}$$

where continuous momentum $\vec{k}$ is replaced by a set of discrete values $\{\vec{k}_1, \vec{k}_2, \ldots\}$ and δV_k^3 is the volume of a momentum-space cell. The integral over d^3k and Dirac delta change to sum and Kronecker delta, respectively:

$$\int \frac{d^3k}{(2\pi)^3} \quad\rightarrow\quad \delta V_k^3 \sum_{i=0}^{\infty}, \qquad\qquad (2\pi)^3\delta^{(3)}(\vec{k}-\vec{k}') \quad\rightarrow\quad \frac{1}{\delta V_k^3}\delta_{ij}. \tag{B.2}$$

The plane-wave decomposition of the scalar field $\phi(x)$ for discrete momenta is:

$$\phi(x) = \sqrt{\delta V_k^3}\sum_i \frac{1}{\sqrt{2\omega_i}}\Big[a_i e^{-ik_ix} + a_i^\dagger e^{ik_ix}\Big], \tag{B.3}$$

where $\omega_i^2 = \vec{k}_i^{\,2} + m^2$ and the normally ordered Hamiltonian reads:

$$H = \sum_i \omega_i a_i^\dagger a_i = \sum_i \omega_i N_i, \tag{B.4}$$

with $N_i = a_i^\dagger a_i$ being the particle number operator. Discrete creation and annihilation operators satisfy commutation relations:

$$[a_i, a_j^\dagger] = \delta_{ij}, \qquad [a_i, a_j] = [a_i^\dagger, a_j^\dagger] = 0. \tag{B.5}$$

The Fock space is spanned by the orthonormal basis of states $|n_1, n_2, n_3, \ldots\rangle$, which are the energy H and particle number $N = \sum_i N_i$ eigenstates:

$$\begin{aligned} H|n_1,n_2,n_3,\ldots\rangle &= \Big(\sum_i \omega_i n_i\Big)|n_1,n_2,n_3,\ldots\rangle, \\ N|n_1,n_2,n_3,\ldots\rangle &= \Big(\sum_i n_i\Big)|n_1,n_2,n_3,\ldots\rangle. \end{aligned} \tag{B.6}$$

The annihilation and creator operators act on the $|n_1, n_2, n_3, \ldots\rangle$ in the following way:

$$\begin{aligned} a_i|n_1, n_2, n_3, \ldots\rangle &= \sqrt{n_i}|n_1, n_2, \ldots, n_i - 1, \ldots\rangle, \\ a_i^\dagger|n_1, n_2, n_3, \ldots\rangle &= \sqrt{n_i + 1}|n_1, n_2, \ldots, n_i + 1, \ldots\rangle. \end{aligned} \tag{B.7}$$

The set of $|n_1, n_2, n_3, \ldots\rangle$ states is complete; therefore, the thermal average of an operator A takes form:

$$\langle A\rangle = \frac{1}{\mathrm{Tr}e^{-\beta H}} \sum_{n_1} \sum_{n_2} \ldots \langle n_1, n_2, \ldots |e^{-\beta H} A|n_1, n_2, \ldots\rangle, \tag{B.8}$$

where:

$$\mathrm{Tr}e^{-\beta H} = \sum_{n_1} \sum_{n_2} \ldots \langle n_1, n_2, \ldots |e^{-\beta H}|n_1, n_2, \ldots\rangle = \sum_{n_1} \sum_{n_2} \ldots e^{-\beta\omega_1 n_1} e^{-\beta\omega_2 n_2} \ldots \tag{B.9}$$

For a chosen n_i we get:

$$\sum_{n_i=0}^{\infty} e^{-\beta\omega_i n_i} = 1 + e^{-\beta\omega_i} + e^{-2\beta\omega_i} + e^{-3\beta\omega_i} + \ldots = \frac{1}{1 - e^{-\beta\omega_i}}, \tag{B.10}$$

and the partition function is:

$$Z = \mathrm{Tr}e^{-\beta H} = \prod_i \frac{1}{1 - e^{-\beta\omega_i}}. \tag{B.11}$$

In the two point correlation functions $\Delta^\pm$, combinations of products of a_i and $a_j^\dagger$ appear. Since we have (B.7), the only non-zero possibilities are:

$$\begin{aligned} \langle n_1, n_2, \ldots, n_i, \ldots |a_i a_j^\dagger|n_1, n_2, \ldots, n_j, \ldots\rangle &= \sqrt{(n_i + 1)(n_j + 1)}\delta_{ij}, \\ \langle n_1, n_2, \ldots, n_i, \ldots |a_i^\dagger a_j|n_1, n_2, \ldots, n_j, \ldots\rangle &= \sqrt{n_i n_j}\delta_{ij}. \end{aligned} \tag{B.12}$$

Hence $\langle a_i a_j\rangle = \langle a_i^\dagger a_j^\dagger\rangle = 0$ for any i, j and:

$$\begin{aligned} \langle a_i a_i^\dagger\rangle &= \frac{1}{Z} \sum_{n_1} \sum_{n_2} \ldots \langle n_1, n_2, \ldots |e^{-\beta H} a_i a_i^\dagger|n_1, n_2, \ldots\rangle = \frac{1}{Z} \sum_{n_1} \sum_{n_2} \ldots \Big(e^{-\beta\omega_1 n_1} e^{-\beta\omega_2 n_2} \ldots\Big)(n_i + 1) = \\ &= \frac{1}{Z} \left(\prod_k^{k\neq i} \sum_{n_k} e^{-\beta\omega_k n_k}\right) \sum_{n_i} e^{-\beta\omega_i n_i}(n_i + 1) = \frac{1}{Z} \left(\prod_k^{k\neq i} \frac{1}{1 - e^{-\beta\omega_k}}\right) \cdot \left(\frac{1}{(1 - e^{-\beta\omega_i})^2}\right) = \\ &= \frac{1}{Z} \left(\prod_k \frac{1}{1 - e^{-\beta\omega_k}}\right) \cdot \frac{1}{1 - e^{-\beta\omega_i}} = \frac{1}{Z} \cdot Z \cdot \frac{1}{1 - e^{-\beta\omega_i}} = \Big(1 + \frac{1}{e^{\beta\omega_i} - 1}\Big). \end{aligned} \tag{B.13}$$

Similarly for $a_i^\dagger a_i$ we get:

$$\begin{aligned} \langle a_i^\dagger a_i\rangle &= \frac{1}{Z} \sum_{n_1} \sum_{n_2} \ldots \langle n_1, n_2, \ldots |e^{-\beta H} a_i^\dagger a_i|n_1, n_2, \ldots\rangle = \frac{1}{Z} \sum_{n_1} \sum_{n_2} \ldots \Big(e^{-\beta\omega_1 n_1} e^{-\beta\omega_2 n_2} \ldots\Big)(n_i) = \\ &= \frac{1}{Z} \left(\prod_k^{k\neq i} \sum_{n_k} e^{-\beta\omega_k n_k}\right) \sum_{n_i} e^{-\beta\omega_i n_i}(n_i) = \frac{1}{Z} \left(\prod_k^{k\neq i} \frac{1}{1 - e^{-\beta\omega_k}}\right) \cdot \left(\frac{e^{-\beta\omega_i}}{(1 - e^{-\beta\omega_i})^2}\right) = \\ &= \frac{1}{Z} \left(\prod_k \frac{1}{1 - e^{-\beta\omega_k}}\right) \cdot \frac{e^{-\beta\omega_i}}{1 - e^{-\beta\omega_i}} = \frac{1}{Z} \cdot Z \cdot \frac{e^{-\beta\omega_i}}{1 - e^{-\beta\omega_i}} = \frac{1}{e^{\beta\omega_i} - 1}. \end{aligned} \tag{B.14}$$

Thus, we obtained:

$$\begin{aligned}\langle a_i a_j^\dagger\rangle &= [1+n_B(\omega_i)]\delta_{ij},\\ \langle a_i^\dagger a_j\rangle &= n_B(\omega_i)\delta_{ij},\end{aligned} \tag{B.15}$$

where $n_B(\omega_i) = \frac{1}{\exp(\beta\omega_i)-1}$ is the Bose-Einstein distribution function. Taking a continuous limit, we finally have:

$$\begin{aligned}&\langle a(\vec{p})a^\dagger(\vec{k})\rangle = [1+n_B(\omega_k)](2\pi)^3\delta^{(3)}(\vec{p}-\vec{k}),\\ &\langle a^\dagger(\vec{p})a(\vec{k})\rangle = n_B(\omega_k)(2\pi)^3\delta^{(3)}(\vec{p}-\vec{k}).\end{aligned} \tag{B.16}$$

B.2. Fermions

Similarly, we define the discrete dimensionless operators $a_{s,i}, a_{s,i}^\dagger, b_{s,i}$ and $b_{s,i}^\dagger$ for fermions:

$$a_{s,i} \equiv \sqrt{\delta V_k^3}\cdot a_s(\vec{k}_i), \qquad a_{s,i}^\dagger \equiv \sqrt{\delta V_k^3}\cdot a_s^\dagger(\vec{k}_i), \qquad b_{s,i} \equiv \sqrt{\delta V_k^3}\cdot b_s(\vec{k}_i), \qquad b_{s,i}^\dagger \equiv \sqrt{\delta V_k^3}\cdot b_s^\dagger(\vec{k}_i), \tag{B.17}$$

and discrete dimensionless vectors $u_{s,i}$, $\bar{u}_{s,i}$, $v_{s,i}$ and $\bar{v}_{s,i}$:

$$u_{s,i} = \frac{1}{\sqrt{\delta V_k}}u_s(\vec{k}_i), \qquad \bar{u}_{s,i} = \frac{1}{\sqrt{\delta V_k}}\bar{u}_s(\vec{k}_i), \qquad v_{s,i} = \frac{1}{\sqrt{\delta V_k}}v_s(\vec{k}_i), \qquad \bar{v}_{s,i} = \frac{1}{\sqrt{\delta V_k}}\bar{v}_s(\vec{k}_i). \tag{B.18}$$

The plane-wave decomposition of the fermionic field $\psi(x)$ for the discrete momenta is:

$$\psi(x) = \delta V_k^2 \sum_s \sum_i \frac{1}{\sqrt{2\omega_k}}\Big[a_{s,i}u_{s,i}e^{-ik_i x} + b_{s,i}^\dagger v_{s,i}e^{ik_i x}\Big], \tag{B.19}$$

$$\bar{\psi}(x) = \delta V_k^2 \sum_s \sum_i \frac{1}{\sqrt{2\omega_k}}\Big[a_{s,i}^\dagger \bar{u}_{s,i}e^{ik_i x} + b_{s,i}\bar{v}_{s,i}e^{-ik_i x}\Big], \tag{B.20}$$

where $\omega_i^2 = \vec{k}_i^2 + m^2$ and the normally ordered Hamiltonian:

$$H = \sum_i \omega_i\big(a_{s,i}^\dagger a_{s,i} + b_{s,i}^\dagger b_{s,i}\big) = \sum_i \omega_i N_i, \tag{B.21}$$

with $N_i = a_{s,i}^\dagger a_{s,i} + b_{s,i}^\dagger b_{s,i}$ being the particle number operator. Discrete creation and annihilation operators satisfy anti-commutation relations:

$$\{a_{s,i}, a_{r,j}^\dagger\} = \{b_{s,i}, b_{r,j}^\dagger\} = \delta_{sr}\delta_{ij}, \qquad \{a_{s,i}, a_{r,j}\} = \{a_{s,i}^\dagger, a_{r,j}^\dagger\} = \{b_{s,i}, b_{r,j}\} = \{b_{s,i}^\dagger, b_{r,j}^\dagger\} = 0. \tag{B.22}$$

The Fock space is spanned by the orthonormal basis of states $|n_1, n_2, n_3, \ldots\rangle$, where n_i refers to the number of particles with given momenta $\vec{k}_i$ and spin s_i. This time, the Pauli exclusion principle forbids more than one fermion occupying a single state. Therefore, n_i numbers can take on values 0 or 1 only, and the momenta assigned to each n_i must be different. In the following part, we will use only the $a_{s,i}$ and $a_{s,i}^\dagger$ operators, since the calculations and results for $b_{s,i}$ and $b_{s,i}^\dagger$ operators are the same. The annihilation and creation operators act on the $|n_1, n_2, n_3, \ldots\rangle$ in the following way:

$$\begin{aligned}a_{s_i,i}|n_1,n_2,n_3,\ldots\rangle &= \sqrt{n_i}|n_1,n_2,\ldots,n_i-1,\ldots\rangle, && \text{for } n_i = 1,\\ a_{s_i,i}|n_1,n_2,n_3,\ldots\rangle &= 0, && \text{for } n_i = 0,\\ a_{s_i,i}^\dagger|n_1,n_2,n_3,\ldots\rangle &= \sqrt{n_i+1}|n_1,n_2,\ldots,n_i+1,\ldots\rangle, && \text{for } n_i = 0,\\ a_{s_i,i}^\dagger|n_1,n_2,n_3,\ldots\rangle &= 0, && \text{for } n_i = 1.\end{aligned} \tag{B.23}$$

The set of $|n_1, n_2, n_3, \ldots\rangle$ states is complete, therefore, the thermal average of an operator A takes the form:

$$\langle A\rangle = \frac{1}{\mathrm{Tr}e^{-\beta H}} \sum_{n_1}\sum_{n_2} \ldots \langle n_1, n_2, \ldots | e^{-\beta H} A | n_1, n_2, \ldots\rangle, \tag{B.24}$$

where any $n_i = 0, 1$ and:

$$\mathrm{Tr}e^{-\beta H} = \sum_{n_1}\sum_{n_2} \ldots \langle n_1, n_2, \ldots | e^{-\beta H} | n_1, n_2, \ldots\rangle = \sum_{n_1}\sum_{n_2} \ldots e^{-\beta\omega_1 n_1} e^{-\beta\omega_2 n_2} \ldots \tag{B.25}$$

For a chosen n_i we get:

$$\sum_{n_i=0}^{1} e^{-\beta\omega_i n_i} = 1 + e^{-\beta\omega_i}, \tag{B.26}$$

and the partition function is:

$$Z = \mathrm{Tr}e^{-\beta H} = \prod_i (1 + e^{-\beta\omega_i}). \tag{B.27}$$

In the two point correlation functions $\Delta_F^{\pm}$, combinations of products of $a_{s_i,i}$, $a^\dagger_{s_j,j}$, $b_{s_i,i}$, $b^\dagger_{s_j,j}$ appear. Since we have (B.23), the only non-zero possibilities are:

$$\begin{aligned}
&\langle n_1, n_2, \ldots, n_i, \ldots | a_{s_i,i} a^\dagger_{s_j,j} | n_1, n_2, \ldots, n_j, \ldots\rangle = \sqrt{(n_i+1)(n_j+1)}\,\delta_{ij}\delta_{s_i s_j}, &&\text{for } n_i = n_j = 0,\\
&\langle n_1, n_2, \ldots, n_i, \ldots | a^\dagger_{s_i,i} a_{s_j,j} | n_1, n_2, \ldots, n_j, \ldots\rangle = \sqrt{n_i n_j}\,\delta_{ij}\delta_{s_i s_j}, &&\text{for } n_i = n_j = 1.
\end{aligned} \tag{B.28}$$

Hence $\langle a_{s_i,i} a_{s_j,j}\rangle = \langle a^\dagger_{s_i,i} a^\dagger_{s_j,j}\rangle = 0$ for any i, j and for $\langle a_{s_i,i} a^\dagger_{s_j,j}\rangle$ we get:

$$\begin{aligned}
\langle a_{s_i,i} a^\dagger_{s_i,i}\rangle &= \frac{1}{Z}\sum_{n_1}\sum_{n_2} \ldots \langle n_1, n_2, \ldots | e^{-\beta H} a_{s_i,i} a^\dagger_{s_i,i} | n_1, n_2, \ldots\rangle = \\
&= \frac{1}{Z}\sum_{n_1}\sum_{n_2} \ldots \Big(e^{-\beta\omega_1 n_1} e^{-\beta\omega_2 n_2} \ldots\Big)(n_i+1)\Big|_{n_i=0} = \\
&= \frac{1}{Z}\left(\prod_k^{k\neq i} \sum_{n_k=0}^{1} e^{-\beta\omega_k n_k}\right) \cdot e^{-\beta\omega_i n_i}(n_i+1)\Big|_{n_i=0} = \frac{1}{Z}\left(\prod_k^{k\neq i}\left(1 + e^{-\beta\omega_k}\right)\right) \cdot \left(\frac{1+e^{-\beta\omega_i}}{1+e^{-\beta\omega_i}}\right) = \\
&= \frac{1}{Z}\left(\prod_k \left(1 + e^{-\beta\omega_k}\right)\right) \cdot \frac{1}{1+e^{-\beta\omega_i}} = \frac{1}{Z} \cdot Z \cdot \frac{1}{1+e^{-\beta\omega_i}} = \Big(1 - \frac{1}{e^{\beta\omega_i}+1}\Big).
\end{aligned} \tag{B.29}$$

Similarly for $\langle a^\dagger_{s_i,i} a_{s_j,j}\rangle$ we get:

$$\begin{aligned}
\langle a^\dagger_{s_i,i} a_{s_i,i}\rangle &= \frac{1}{Z}\sum_{n_1}\sum_{n_2} \ldots \langle n_1, n_2, \ldots | e^{-\beta H} a^\dagger_{s_i,i} a_{s_i,i} | n_1, n_2, \ldots\rangle = \frac{1}{Z}\sum_{n_1}\sum_{n_2} \ldots \Big(e^{-\beta\omega_1 n_1} e^{-\beta\omega_2 n_2} \ldots\Big)(n_i)\Big|_{n_i=1} = \\
&= \frac{1}{Z}\left(\prod_k^{k\neq i} \sum_{n_k} e^{-\beta\omega_k n_k}\right) \cdot e^{-\beta\omega_i n_i}(n_i)\Big|_{n_i=1} = \frac{1}{Z}\left(\prod_k^{k\neq i}\left(1 + e^{-\beta\omega_k}\right)\right) \cdot e^{-\beta\omega_i} \cdot \left(\frac{1+e^{-\beta\omega_i}}{1+e^{-\beta\omega_i}}\right) = \\
&= \frac{1}{Z}\left(\prod_k \left(1 + e^{-\beta\omega_k}\right)\right) \cdot \frac{e^{-\beta\omega_i}}{1+e^{-\beta\omega_i}} = \frac{1}{Z} \cdot Z \cdot \frac{e^{-\beta\omega_i}}{1+e^{-\beta\omega_i}} = \frac{1}{e^{\beta\omega_i}+1}.
\end{aligned} \tag{B.30}$$

Thus, we obtained:

$$\begin{aligned} \langle a_{s_i,i} a^{\dagger}_{s_j,j} \rangle &= [1 - n_F(\omega_i)]\delta_{ij}\delta_{s_i s_j}, \\ \langle a^{\dagger}_{s_i,i} a^{s_j,j} \rangle &= n_F(\omega_i)\delta_{ij}\delta_{s_i s_j}, \end{aligned} \tag{B.31}$$

where $n_F(\omega_i) = \frac{1}{\exp(\beta\omega_i)+1}$ is the Fermi distribution function. Taking a continuous limit, we finally have:

$$\begin{aligned} &\langle a_s(\vec{p}) a^{\dagger}_r(\vec{k}) \rangle = [1 - n_F(\omega_k)](2\pi)^3 \delta^{(3)}(\vec{p} - \vec{k})\delta_{sr}, \\ &\langle a^{\dagger}_s(\vec{p}) a_r(\vec{k}) \rangle = n_F(\omega_k)(2\pi)^3 \delta^{(3)}(\vec{p} - \vec{k})\delta_{sr}. \end{aligned} \tag{B.32}$$

Appendix C

Resummation of Higher-Order Daisy Diagrams

C.1. Scalars and First-Order Contribution

Let's revisit the effective potential at finite temperature for scalars. From equations (7.72), (7.78) and (7.79), we have:

$$V_1(\phi_c) = \int \frac{d^3p}{(2\pi)^3}\left[\frac{\omega}{2} + \frac{1}{\beta}\log\left(1 - e^{-\beta\omega}\right)\right] = \delta V_1^{\text{vac}} + \delta V_1^{\text{med}}, \tag{C.1}$$

where we denote the zero-temperature contribution, referred to as the vacuum contribution, by δV_1^{vac}:

$$\delta V_1^{\text{vac}} = \frac{1}{2}\int \frac{d^4p}{(2\pi)^4}\log\left(p^2 + m^2(\phi_c)\right), \tag{C.2}$$

and δV_1^{med} represents the finite-temperature part, which we refer to as the medium contribution:

$$\delta V_1^{\text{med}} = \frac{T}{2\pi^2}\int_0^\infty dp\, p^2 \log\left(1 - e^{-\beta\sqrt{\vec{p}^2 + m^2(\phi_c)}}\right) = \frac{T^4}{2\pi^2} J_B\left[m^2(\phi_c)/T^2\right]. \tag{C.3}$$

The zero-temperature part δV_1^{vac} is divergent in the ultraviolet limit of large momenta $p \to \infty$ and infrared-safe when $p \to 0$. This issue for a particular model considered in this work was already discussed and resolved in Chapter 5. What is more, since this is the ultraviolet divergence of the vacuum QFT, its effects don't affect the finite-temperature part and thermodynamics of the system. This is why we refer to this part as the vacuum contribution.

The behavior of the temperature (medium) contribution to $V_1(\phi_c)$ is determined by the function under the integral in (C.3). In the ultraviolet limit, we have:

$$\lim_{p\to\infty} p^2 \log\left(1 - e^{-\beta\sqrt{\vec{p}^2 + m^2(\phi_c)}}\right) = 0, \qquad \text{if } m^2 \in \mathbb{R} \text{ and } \beta > 0, \tag{C.4}$$

where the conditions for m and β are analytically satisfied. The infrared limit is simply zero:

$$\lim_{p\to 0} p^2 \log\left(1 - e^{-\beta\sqrt{\vec{p}^2 + m^2(\phi_c)}}\right) = 0. \tag{C.5}$$

Therefore, the temperature-dependent part of the one-loop effective potential is both ultraviolet and infrared-safe.

In statistical quantum field theory, it is commonly observed that ultraviolet divergences, as opposed to infrared divergences, arise only from the vacuum sector of the theory. To see this, let's consider a relativistic gas of particles with high momenta, where T is much bigger than the masses of gas particles. The particle density ρ scales as T^3, hence the inter-particle spacing is of order $\rho^{-1/3} \sim T^{-1}$. The ultraviolet limit $p \to \infty$ corresponds to distances $x \to 0$. Since the temperature is finite, ultraviolet divergences occur at distances $x \ll T^{-1}$, much smaller than the inter-particle spacing. As a consequence, the medium, which is the relativistic gas, has no impact in this context, and the renormalization procedure needs to address only the vacuum part of QFT.

C.2. Scalars and Second-Order Contribution

In the previous section, we saw that we can disregard the vacuum part of the effective potential at finite temperature as it has no thermodynamic consequences for our theory. However, there is an important issue within the boson thermal contribution that needs to be addressed: the imaginary part of the potential, coming from the $m^3(\phi_c)T$ term, which can be refined by resuming the most dominant infrared contributions. This process leads to the so-called daisy-resummed potential. The reader can find similar analysis in [34, 73, 76, 77, 86, 112].

In standard quantum field theory, we typically employ a perturbative approach, expanding the theory order by order in the dimensionless coupling constant. However, in thermal field theories, some diagrams that seem to be of higher order might be as significant as lower-order ones. This occurs due to contributions from corrections known as hard thermal loops, which can lead to problems with infrared divergences, particularly in massless theories. For a clearer understanding, let us revisit the massless scalar ϕ^4 model and compute higher-order corrections to the effective potential. One of the possible two-loop diagrams is:

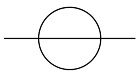

$$= (-i\lambda)^2 \left(\frac{i}{\beta}\right)^2 \sum_{n,\ell=-\infty}^{+\infty} \int \frac{d^3p}{(2\pi)^3} \frac{d^3k}{(2\pi)^3} \frac{i}{\omega_n^2 - \vec{p}^2} \frac{i}{\omega_\ell^2 - \vec{k}^2} \frac{i}{(\omega_n + \omega_\ell)^2 - (\vec{p} + \vec{k})^2}, \tag{C.6}$$

where ω_n and ω_ℓ are bosonic Matsubara frequencies. This contribution is infrared divergent for the zero Matsubara modes. Indeed, for $n = \ell = 0$ we have $\omega_n = \omega_\ell = 0$ and:

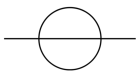

$$\Bigg|_{n=\ell=0} \sim \int \frac{d^3p}{(2\pi)^3} \frac{d^3k}{(2\pi)^3} \frac{1}{\vec{p}^2} \frac{1}{\vec{k}^2} \frac{1}{(\vec{p} + \vec{k})^2} \sim \int dp\, dk\, \frac{1}{(\vec{p} + \vec{k})^2} \tag{C.7}$$

is divergent for $p \to 0$ and $k \to 0$. We encounter the same problem for the following two-loop diagram:

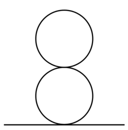

$$\Bigg|_{n=\ell=0} \sim \int \frac{d^3p}{(2\pi)^3} \frac{d^3k}{(2\pi)^3} \left(\frac{1}{\vec{p}^2}\right)^2 \frac{1}{\vec{k}^2} \sim \int dp\, dk\, \frac{1}{\vec{p}^2}, \tag{C.8}$$

which diverges for $p \to 0$. To address the problem of infrared sensitivity in the loop expansion, we need to sum all the divergent terms order by order. This process effectively cancels these divergences. As we will demonstrate, the result is a contribution of order $\lambda^{3/2}$, rather than the λ^2 or higher, as one would expect from a naive perturbation approach. It is important to note that the infrared divergences originate only from the bosonic loops and their zero Matsubara modes. Fermions do not experience the infrared problem and therefore do not require resummation, as they don't have zero-valued Matsubara mode.

Let us look at the high-temperature limit of a couple of diagrams and see which are the most important in this regime. At one-loop, we have:

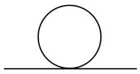

$$\sim \frac{\lambda}{\beta} \sum_{n=-\infty}^{\infty} \int \frac{d^3p}{(2\pi)^3} \frac{1}{\omega_n^2 + \vec{p}^2 + m^2} = \frac{\lambda}{2} \int \frac{d^3p}{(2\pi)^3} \frac{1}{\sqrt{\vec{p} + m^2}} \left[1 + \frac{2}{e^{\beta\sqrt{\vec{p}^2 + m^2}} - 1}\right], \tag{C.9}$$

where in the last equality, we separated contributions for zero and finite temperature, as can be done for any diagram. The zero-temperature part undergoes the usual one-loop renormalization. The temperature part can be expressed as the derivative of the thermal bosonic function J_B:

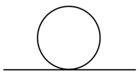

$$\Bigg|_{T>0} \sim \frac{\lambda}{2\pi^2}\int_0^\infty dp\; p^2 \frac{1}{\sqrt{\vec{p}^2+m^2}}\frac{1}{e^{\beta\sqrt{\vec{p}^2+m^2}}-1} = \frac{\lambda}{\pi^2\beta^2}\cdot\frac{\partial J_B[a^2]}{\partial a^2}\Bigg|_{a^2=\frac{m^2}{T^2}}. \tag{C.10}$$

Using the high temperature expansion of J_B (7.81), we obtain:

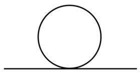

$$\Bigg|_{T>0} \sim \lambda\left[\frac{T^2}{12} - \frac{Tm}{4\pi} + \dots\right]. \tag{C.11}$$

Consequently, at high temperatures, this one-vertex bubble diagram behaves like λT^2.

Next, we consider two-loop diagrams. The following one has 1 one-vertex bubble and 1 two-vertex bubble:

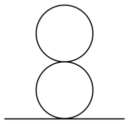

$$\begin{aligned}&\sim\Big(\lambda T^2\Big)\cdot\frac{\lambda}{\beta}\sum_{n=-\infty}^{\infty}\int\frac{d^3p}{(2\pi)^3}\left(\frac{1}{\omega_n^2+\vec{p}^2+m^2}\right)^2 = \\ &=\Big(\lambda T^2\Big)\cdot\lambda\int\frac{d^3p}{(2\pi)^3}\frac{1}{4P^3}\left[1+2\frac{e^{\beta P}(1+\beta P)-1}{(e^{\beta P}-1)^2}\right],\end{aligned} \tag{C.12}$$

where we denoted $\vec{p}^2+m^2 = P^2$. For the temperature-dependent part, the most dominant terms at high temperature are:

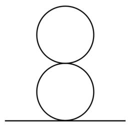

$$\begin{aligned}\Bigg|_{T>0} &\sim\lambda T^2\cdot\lambda\int_0^\infty dp\; p^2\cdot\frac{1}{4P^3}\cdot 2\frac{e^{\beta P}(1+\beta P)-1}{(e^{\beta P}-1)^2} = \\ &=\lambda T^2\cdot\big(-\lambda\big)\frac{\partial^2 J_B[a^2]}{(\partial a^2)^2}\Bigg|_{a^2=\frac{m^2}{T^2}} \sim \lambda T^2\cdot\frac{\lambda T}{m}.\end{aligned} \tag{C.13}$$

The two-loop sunset diagram is more complicated, and at the high temperature, it contributes as [113]:

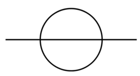

$$\Bigg|_{T>0} \sim \lambda^2 T^2 \log\frac{m}{T}. \tag{C.14}$$

By comparing the temperature dependence of all the possible two-loop diagrams in equations (C.13) and (C.14), it is clear that at high temperatures, the contribution from the diagram (C.13) significantly dominates.

At the three-loop level, a possible diagram consists of 2 one-vertex bubbles and 1 three-vertex bubble, which, performing the same calculations as for previous diagrams, contributes as:

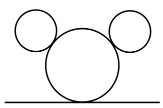

$$\Bigg|_{T>0} \sim (\lambda T^2)^2\cdot\lambda\cdot\beta^2\frac{\partial^3 J_B[a^2]}{(\partial a^2)^3}\Bigg|_{a^2=\frac{m^2}{T^2}} \sim (\lambda T^2)^2\cdot\frac{\lambda T}{m^3}. \tag{C.15}$$

Whereas a diagram with 1 one-vertex bubble and two two-vertex bubbles gives:

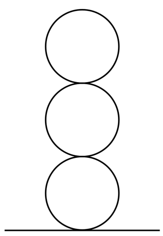

$$\Bigg|_{T>0} \sim (\lambda T^2)\cdot\left(\frac{\lambda T}{m}\right)^2, \tag{C.16}$$

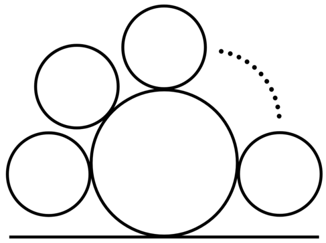

Figure C.1: Daisy $(N+1)$-loop diagram, with N one-vertex loops attached to $(N+1)$-vertex loop.

and a diagram with a one-vertex loop attached to the sunset diagram at high temperature behaves as [78]:

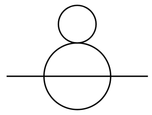

$$\Big|_{T>0} \sim \lambda^3 \frac{T^4}{m^2}. \tag{C.17}$$

Comparing the results of diagrams (C.15), (C.16), and (C.17), we find that at high temperatures, the most significant contribution comes from the diagram (C.15).

It turns out that at every loop level, the most dominant high-temperature contribution comes from the so-called daisy diagram, shown in Figure C.1, with N loops attached to the one-loop self-energy diagram. The contribution from such a diagram is given by:

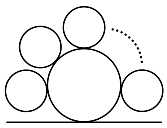

$$\Big|_{T>0} \sim \left(\lambda T^2\right)^N \cdot \frac{\lambda}{\beta} \sum_{n=-\infty}^{n=+\infty} \int \frac{d^3p}{(2\pi)^3} \frac{1}{\left(\omega_n^2 + \vec{p}^2 + m^2\right)^{N+1}}. \tag{C.18}$$

We aim to sum daisy diagrams from $N=0$ (corresponding to the one-loop order diagram (C.10)) to $N=\infty$. To accurately compute the contribution from this sum, we need to proceed carefully and include all the numerical factors:

- each vertex gives $\left(-i\frac{\lambda}{2}\right)$ factor and we have $N+1$ vertices;
- each one-vertex loop contributes as $\frac{i}{\beta}\sum_{n=-\infty}^{n=+\infty}\int \frac{d^3p}{(2\pi)^3}\frac{-i}{\omega_n^2+\vec{p}^2+m^2}$, where $\omega_n = \frac{2\pi n}{\beta}$ and we have N such loops;
- we have $N+1$ lines between vertices, each with propagator $\frac{-i}{\omega_\ell^2+\vec{k}^2+m^2}$, integrated over the loop momenta k, so it gives $\frac{i}{\beta}\sum_{\ell=-\infty}^{\ell=+\infty}\int\frac{d^3k}{(2\pi)^3}\left(\frac{-i}{\omega_\ell^2+\vec{k}^2+m^2}\right)^{N+1}$;
- for 2 external lines, we get the ϕ_c^2 factor;
- the symmetry factor is $\frac{1}{2}\frac{(N+1)!}{(N+1)!} = \frac{1}{2}$, from the following argumentation: we have $(N+1)!$ combinations for choosing vertices, mirror symmetry of the graph gives the factor $\frac{1}{2}$ and the $\frac{1}{(N+1)!}$ factor comes from the loop expansion (2.26);
- there's an extra global factor of i coming from the definition of the generating functional W;

Therefore, the daisy $(N+1)$-loop diagram gives:

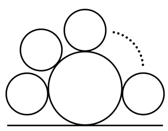

$$\begin{aligned} &= i\phi_c^2 \cdot \sum_{N=0}^{N=+\infty} \left(-i\frac{\lambda}{2}\right)^{N+1} \frac{1}{2} \cdot \left[\frac{i}{\beta}\sum_{n=-\infty}^{n=+\infty}\int \frac{d^3p}{(2\pi)^3}\frac{-i}{\omega_n^2+\vec{p}^2+m^2}\right]^N \times \\ &\times \frac{i}{\beta}\sum_{\ell=-\infty}^{\ell=+\infty}\int\frac{d^3k}{(2\pi)^3}\left[\frac{-i}{\omega_\ell^2+\vec{k}^2+m^2}\right]^{N+1}. \end{aligned} \tag{C.19}$$

The p integral gives:

$$\frac{1}{\beta}\sum_{n=-\infty}^{n=+\infty}\int\frac{d^3p}{(2\pi)^3}\frac{1}{\omega_n^2+\vec{p}^2+m^2}=\int\frac{d^3p}{(2\pi)^3}\frac{1}{2\sqrt{\vec{p}^2+m^2}}\left[1+\frac{2}{e^{\beta\sqrt{\vec{p}^2+m^2}}-1}\right], \tag{C.20}$$

where we have separated the zero and finite temperature parts. As we have shown before in equation (C.10), the $T>0$ term is:

$$\begin{aligned}&\frac{1}{2\pi^2}\int_0^\infty dp\ p^2\frac{1}{\sqrt{\vec{p}+m^2}}\frac{1}{e^{\beta\sqrt{\vec{p}^2+m^2}}-1}=\frac{1}{\pi^2\beta^2}\cdot\frac{\partial J_B[a^2]}{\partial a^2}\bigg|_{a^2=\frac{m^2}{T^2}}=\\&\frac{T^2}{12}-\frac{T}{4\pi}|m|-\frac{m^2}{16\pi^2}\log\frac{m^2}{a_bT^2}+\ldots\approx\frac{T^2}{12},\end{aligned} \tag{C.21}$$

where we used the high-temperature expansion of J_B (7.81). So far, we have:

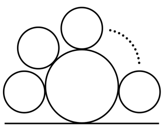 $$=-6\beta\phi_c^2\sum_{N=0}^{N=+\infty}\sum_{\ell=-\infty}^{\ell=+\infty}\int\frac{d^3k}{(2\pi)^3}\left[\frac{-\frac{\lambda T^2}{24}}{\omega_\ell^2+\vec{k}^2+m^2}\right]^{N+1}. \tag{C.22}$$

Let us observe that:

$$\begin{aligned}\sum_{\ell=-\infty}^{\ell=+\infty}\int\frac{d^3k}{(2\pi)^3}\frac{1}{\left(\omega_l^2+\vec{k}^2+m^2\right)^{N+1}}&=\frac{\beta}{N!}\Big(-\frac{\partial}{\partial m^2}\Big)^N\left(\frac{1}{\beta}\sum_{\ell=-\infty}^{\ell=+\infty}\int\frac{d^3k}{(2\pi)^3}\frac{1}{\omega_l^2+\vec{k}^2+m^2}\right)\\&=\frac{\beta}{N!}\Big(-\frac{\partial}{\partial m^2}\Big)^N\left(\frac{T^2}{12}-\frac{T}{4\pi}|m|-\frac{m^2}{16\pi^2}\log\frac{m^2}{a_bT^2}+\ldots\right),\end{aligned} \tag{C.23}$$

where we used (C.20) and (C.21). Consequently:

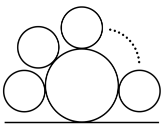 $$\begin{aligned}&=6\beta^2\phi_c^2\cdot\frac{\lambda T^2}{24}\sum_{N=0}^{N=+\infty}\Big(-\frac{\lambda T^2}{24}\Big)^N\frac{1}{N!}\Big(-\frac{\partial}{\partial m^2}\Big)^N\left(\frac{T^2}{12}-\frac{T}{4\pi}|m|+\ldots\right)=\\&=\beta^2\phi_c^2\cdot\frac{\lambda T^2}{4}\exp\left(\frac{\lambda T^2}{24}\frac{\partial}{\partial m^2}\right)\left(\frac{T^2}{12}-\frac{T}{4\pi}|m|+\ldots\right).\end{aligned} \tag{C.24}$$

Next, we use the property:

$$f(x+a)=f(x)+a\cdot f'(x)+\frac{a^2}{2!}f''(x)+\frac{a^3}{3!}f^{(3)}(x)+\ldots=\sum_{n=0}^{\infty}\frac{a^n}{n!}f^{(n)}(x)=\exp\Big(a\cdot\frac{\partial}{\partial x}\Big)f(x), \tag{C.25}$$

which gives:

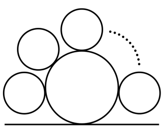 $$=\phi_c^2\cdot\frac{\lambda}{4}\left(\frac{T^2}{12}-\frac{T}{4\pi}\Big(m^2+\frac{\lambda T^2}{24}\Big)^{1/2}+\ldots\right). \tag{C.26}$$

The infinite sum of daisy diagrams results in the correction of order $\lambda^{3/2}$. Next, let us revisit the one-loop mass correction diagram and calculate it precisely:

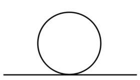 $$=i\Big(-i\frac{\lambda}{2}\Big)\frac{\phi_c^2}{2}\frac{i}{\beta}\sum_{n=-\infty}^{\infty}\int\frac{d^3p}{(2\pi)^3}\frac{-i}{\omega_n^2+\vec{p}^2+m^2}\xrightarrow{T>0}\phi_c^2\cdot\frac{\lambda}{4}\left(\frac{T^2}{12}-\frac{T}{4\pi}|m|+\ldots\right), \tag{C.27}$$

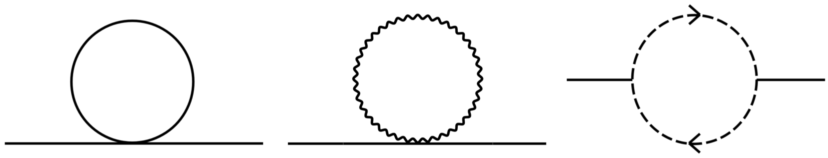

Figure C.2: Example contributions to the scalar self-energy correction from a scalar (solid line), gauge boson (wavy line), and fermion (dashed line) loop.

where (C.20) and (C.21) were used. Comparing (C.26) and (C.27), it becomes clear that the resummation corresponds to modifying the tree-level mass to the thermal effective mass at leading order:

$$m^2 \quad \rightarrow \quad m^2_{eff}(T) = m^2 + \frac{\lambda T^2}{24} = m^2 + \Pi(T). \tag{C.28}$$

The diagram (C.27) is known as the first-order self-energy or polarization tensor, often denoted by $\Pi(T)$. When a scalar field interacts with other particles, such as gauge bosons or fermions, determining $\Pi(T)$ involves calculating the sum of all one-loop contributions from these particles, as illustrated in Figure C.2. However, there is a more efficient way to obtain $\Pi(T)$. Consider a theory with a scalar field ϕ having a tree-level field-dependent mass $m^2(\phi) = m^2 + \frac{\lambda}{2}\phi^2$, which also gives mass to other particles: the gauge boson with $m^2_{GB}(\phi) \sim \phi^2$ and the fermion with $m^2_F(\phi) \sim \phi^2$. For this scalar field, the one-loop temperature-dependent effective potential (7.106) at high temperature without resummation is given by:

$$\begin{aligned} V_1(\phi, T) =& \frac{T^4}{2\pi^2}\left[J_B\Big(\frac{m^2(\phi)}{T^2}\Big) + 3J_B\Big(\frac{m^2_{GB}(\phi)}{T^2}\Big) - 12J_F\Big(\frac{m^2_F(\phi)}{T^2}\Big)\right] \approx \\ \approx& \left(\frac{m^2(\phi)}{24} + \frac{m^2_{GB}(\phi)}{8} + \frac{m^2_F(\phi)}{4}\right)T^2 - \frac{29\pi^2}{180}T^4 + \ldots \end{aligned} \tag{C.29}$$

Since the polarization tensor $\Pi(T)$ contributes as the temperature part to the effective mass, it can be obtained by taking the second derivative of this high-temperature expression with respect to the field ϕ:

$$\Pi(T) = \frac{\partial^2 V_1(\phi, T)}{\partial \phi^2} \approx \frac{\lambda T^2}{24} + \frac{3m^2_{GB}(\phi)T^2}{2\phi^2} + \frac{3m^2_F(\phi)T^2}{\phi^2}. \tag{C.30}$$

One would obtain the same result by summing the Figure C.2 diagrams.

From the analysis in this section, it follows that to account for all critical thermal correction effects, one must work with the resumed thermal potential given by:

$$\delta V_{T+daisy} = \frac{T^4}{2\pi^2}\left[\sum_{i=\text{bosons}} n_i \cdot J_B\left(\frac{(m_i^2)_{eff}(\phi_c, T)}{T^2}\right) + \sum_{j=\text{fermions}} n_j \cdot J_F\left(\frac{m_j^2(\phi_c)}{T^2}\right)\right], \tag{C.31}$$

where thermal mass corrections apply only to the bosons because fermions don't experience infrared divergences due to the absence of zero Matsubara mode.

Appendix D

Thermal Equilibrium

We investigate the temperature ranges within which the dilaton field ϕ_0 is in thermal equilibrium. This analysis is purely approximate since it is quite clear that for small $|\lambda_1|$, the dilaton can't reach the equilibrium state. To achieve the results, we calculate the cross-section, as detailed in [114]:

$$\frac{d\sigma}{dt} = \frac{1}{64\pi \cdot s} \frac{1}{|\vec{p}_{1CM}|^2} |\mathcal{M}|^2, \tag{D.1}$$

where s and t are Mandelstam variables, and $\vec{p}_{1CM}$ denotes the momentum of an incoming particle in the center-of-mass frame. The essential steps and formulas can be found in [114]. We adopt the following approximations:

$$m_{\phi_0} \approx m_G = 0, \qquad m_{\phi_1} \approx m_H = 125 \text{ GeV}. \tag{D.2}$$

Considering the $\lambda_1 \phi_0^2 \phi_1^2$ interaction term as the sole $\phi_0\phi_1$ interaction present in the potential $V(\phi_0, \phi_1)$, we arrive at $|\mathcal{M}|^2 = 16\lambda_1^2$. Consequently, two processes are possible:

- ELASTIC $\phi_0\phi_1 \to \phi_0\phi_1$:

$$\sigma(s) = \frac{\lambda_1^2}{\pi \cdot s},$$

- INELASTIC $\phi_1\phi_1 \to \phi_0\phi_0$:

$$\sigma(s) = \frac{\lambda_1^2}{\pi\sqrt{s\left(s - 4m_H^2\right)}}.$$

While elastic interactions help maintain the kinetic equilibrium of the dilaton ϕ_0 by redistributing its momentum, they do not change its particle number density. Therefore, if the primary concern is whether ϕ_0 can reach thermal equilibrium, the inelastic processes are more critical. This is because inelastic interactions directly impact the number density of dilaton, making them essential for establishing thermal equilibrium. The thermally averaged cross-section for an inelastic process reads [115]:

$$\langle \sigma \cdot v \rangle_{INEL} = \frac{1}{8K_2(m_H/T)^2 \cdot m_H^4 T} \int_{4m_H^2}^{\infty} ds \cdot \lambda(s, m_H, m_H) \frac{\sigma(s)}{\sqrt{s}} K_1(\sqrt{s}/T), \tag{D.3}$$

where $K_i(x)$ is a modified Bessel function of $i - th$ kind and:

$$\lambda(x, y, z) = \left[x - (y+z)^2\right] \cdot \left[x - (y-z)^2\right]. \tag{D.4}$$

A system of particles can be considered to be in thermal equilibrium with good accuracy if their interaction rate, denoted by Γ, satisfies the following inequality:

$$\Gamma \gtrsim H, \tag{D.5}$$

where H represents the Hubble parameter. During the radiation-dominated era, the Hubble parameter can be expressed as:

$$H(T) = \frac{1}{\sqrt{3}M_{Pl}}\sqrt{\frac{\pi^2}{30}g_* T^4}. \tag{D.6}$$

Here, g_* is the effective number of degrees of freedom for relativistic particles in the hot Universe, and $M_P = 2.44 \cdot 10^{18}$ GeV is the Planck mass. For the considered case of thermal equilibrium of dilaton, the interaction rate is equal to [116]:

$$\Gamma = n^{EQ}_{\phi_0} \cdot \langle \sigma \cdot v \rangle_{INEL}, \tag{D.7}$$

where $n^{EQ}_{\phi_0}$ is the number density of relativistic ϕ_0 particles, as if they would be in equilibrium:

$$n^{EQ}_{\phi_0} = \frac{\zeta(3)}{\pi^2}T^3, \tag{D.8}$$

with $\zeta(3) \approx 1.20206$. Consequently, we can analyze the ratio:

$$\frac{\Gamma(T)}{H(T)} = f(T), \tag{D.9}$$

as a function of temperature. For temperatures exceeding 0.1 GeV, used in the analysis of the time evolution of the fields, the effective number of degrees of freedom is approximately $g_* \approx 100$ [88]. Figure D.1 illustrates the results for various values of λ_1. The inelastic interactions can ensure that the dilaton field, ϕ_0, reaches thermal equilibrium for $\lambda_1 \gtrsim -10^{-5}$.

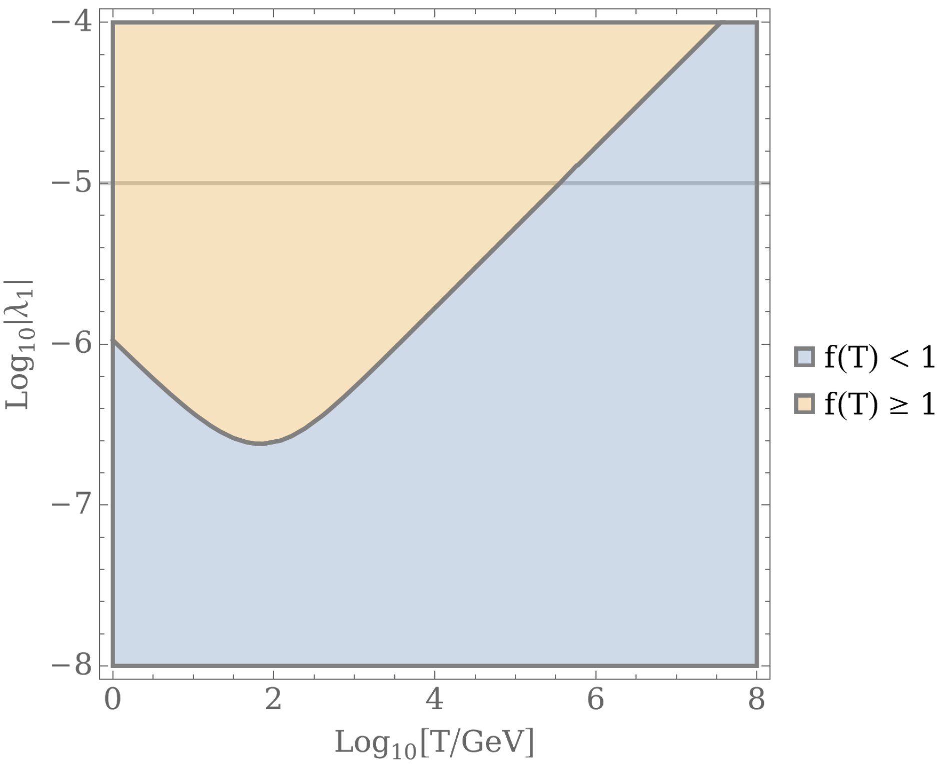

Figure D.1: Plot of the function $f(T) = \frac{\Gamma(T)}{H(T)}$ for different λ_1 coupling values and temperature range used in the time evolution of the fields.

Appendix E

Temperature Fluctuations of the Scalar Field

The normal distribution is described by the formula:

$$f(x) = \frac{1}{\sigma\sqrt{2\pi}} \exp\left\{ -\frac{1}{2}\left(\frac{x-\mu}{\sigma}\right)^2 \right\}, \tag{E.1}$$

where $\mu = \langle x \rangle$ is the mean value of the x variable, defined in equation (7.2), and σ is the standard deviation:

$$\sigma = \sqrt{\langle x^2 \rangle - \langle x \rangle^2}. \tag{E.2}$$

In the following, we use the same method and results as in Appendix B. For the free scalar field, equation (7.19), the temperature averages of single field values and its time derivative are zero:

$$\langle \phi \rangle = 0, \qquad \langle \dot{\phi} \rangle = 0. \tag{E.3}$$

This statement changes in light of the analysis from Chapter 8, as the fields have non-zero potential and can be in thermal equilibrium. In that case, the mean value for the single field value is its vacuum expectation value, $\langle \phi \rangle_T$, determined by its interactions, and can be non-zero. The field derivative thermal average stays zero $\langle \dot{\phi} \rangle_T = 0$. Consequently, the standard deviations read:

$$\sigma_\phi = \sqrt{\langle \phi^2 \rangle_T - \langle \phi \rangle_T^2}, \qquad \sigma_{\dot{\phi}} = \sqrt{\langle \dot{\phi}^2 \rangle_T}. \tag{E.4}$$

For the two field values, we get:

$$\begin{aligned} \langle \phi^2 \rangle &= \int \frac{d^3k}{(2\pi)^3} \frac{1}{\omega_k}\left[n_B(\omega_k) + \frac{1}{2} \right] = \frac{1}{2\pi^2} \int_0^\infty dk\ \frac{k^2}{\omega_k}\left[n_B(\omega_k) + \frac{1}{2} \right], \\ \langle \dot{\phi}^2 \rangle &= \int \frac{d^3k}{(2\pi)^3} \omega_k \left[n_B(\omega_k) + \frac{1}{2} \right] = \frac{1}{2\pi^2} \int_0^\infty dk\ k^2 \omega_k \left[n_B(\omega_k) + \frac{1}{2} \right], \end{aligned} \tag{E.5}$$

where:

$$\omega_k^2 = \vec{k}^2 + m^2, \qquad n_B(\omega_k) = \frac{1}{\exp\{\beta\omega_k\} - 1}, \tag{E.6}$$

and the $\frac{1}{2}$ being the vacuum contribution and $n_B(\omega_k)$ the thermal contribution. Therefore:

$$\langle \phi^2 \rangle_T = \frac{1}{2\pi^2} \int_0^\infty dk\ k^2 \omega_k n_B(\omega_k), \qquad \langle \dot{\phi}^2 \rangle_T = \frac{1}{2\pi^2} \int_0^\infty dk\ k^2 \omega_k n_B(\omega_k). \tag{E.7}$$

Changing the integration variable to $x = \beta\omega_k$, one gets:

$$\langle \phi^2 \rangle_T = \frac{1}{2\pi^2} \frac{1}{\beta^2} \int_{\beta m}^\infty dx\ \frac{\sqrt{x^2 - \beta^2 m^2}}{e^x - 1}, \qquad \langle \dot{\phi}^2 \rangle_T = \frac{1}{2\pi^2} \frac{1}{\beta^4} \int_{\beta m}^\infty dx\ \frac{x^2\sqrt{x^2 - \beta^2 m^2}}{e^x - 1}. \tag{E.8}$$

One can define, [117]:

$$J^{(\nu)}\big[A,B\big] = \int_A^\infty \frac{\left(x^2 - A^2\right)^{\nu/2}}{e^{x-B} - 1} + \int_A^\infty \frac{\left(x^2 - A^2\right)^{\nu/2}}{e^{x+B} - 1}, \tag{E.9}$$

$$K^{(\nu)}\big[A,B\big] = \int_A^\infty \frac{x^2\left(x^2 - A^2\right)^{\nu/2}}{e^{x-B} - 1} + \int_A^\infty \frac{x^2\left(x^2 - A^2\right)^{\nu/2}}{e^{x+B} - 1}, \tag{E.10}$$

so that:

$$\langle\phi^2\rangle_T = \frac{1}{4\pi^2}\frac{1}{\beta^2}J^{(1)}\big[\beta m, 0\big], \qquad \langle\dot{\phi}^2\rangle_T = \frac{1}{4\pi^2}\frac{1}{\beta^4}K^{(1)}\big[\beta m, 0\big]. \tag{E.11}$$

Expanding the above quantities for high temperature, $T \gg m \Rightarrow \beta m \ll 1$, one obtains [117]:

$$\langle\phi^2\rangle_T \approx \frac{T^2}{12}, \qquad \langle\dot{\phi}^2\rangle_T \approx \frac{\pi^2}{30}T^4. \tag{E.12}$$

Consequently, the high-temperature standard deviations are:

$$\sigma_\phi = \sqrt{\frac{T^2}{12} - \langle\phi\rangle_T^2}, \qquad \sigma_{\dot{\phi}} = \frac{\pi}{\sqrt{30}}T^2. \tag{E.13}$$

Bibliography

[1] M. Shaposhnikov and D. Zenhausern, *Scale invariance, unimodular gravity and dark energy*, *Phys. Lett. B* **671** (2009) 187–192, [arXiv:0809.3395].

[2] J. Garcia-Bellido, J. Rubio, M. Shaposhnikov, and D. Zenhausern, *Higgs-dilaton cosmology: From the early to the late universe*, *Phys. Rev. D* **84** (2011) 123504, [arXiv:1107.2163].

[3] F. Bezrukov, G. K. Karananas, J. Rubio, and M. Shaposhnikov, *Higgs-dilaton cosmology: an effective field theory approach*, *Phys. Rev. D* **87** (2013), no. 9 096001, [arXiv:1212.4148].

[4] P. G. Ferreira, C. T. Hill, and G. G. Ross, *Scale-independent inflation and hierarchy generation*, *Phys. Lett. B* **763** (2016) 174–178, [arXiv:1603.05983].

[5] P. G. Ferreira, C. T. Hill, and G. G. Ross, *Inertial spontaneous symmetry breaking and quantum scale invariance*, *Phys. Rev. D* **98** (2018), no. 11 116012, [arXiv:1801.07676].

[6] P. G. Ferreira, C. T. Hill, and G. G. Ross, *Weyl current, scale-invariant inflation and planck scale generation*, *Phys. Rev. D* **95** (2017), no. 4 043507, [arXiv:1610.09243].

[7] A. Salvio and A. Strumia, *Agravity*, *JHEP* **06** (2014) 080, [arXiv:1403.4226].

[8] G. K. Karananas, M. Shaposhnikov, A. Shkerin, and S. Zell, *Scale and Weyl invariance in Einstein-Cartan gravity*, *Phys. Rev. D* **104** (2021), no. 12 124014, [arXiv:2108.05897].

[9] D. Ghilencea, *Stueckelberg breaking of weyl conformal geometry and applications to gravity*, *Phys. Rev. D* **101** (2020), no. 4 045010, [arXiv:1904.06596].

[10] D. Ghilencea, *Spontaneous breaking of weyl quadratic gravity to einstein action and higgs potential*, *JHEP* **03** (2019) 049, [arXiv:1812.08613].

[11] D. Ghilencea and H. M. Lee, *Weyl gauge symmetry and its spontaneous breaking in the standard model and inflation*, *Phys. Rev. D* **99** (2019), no. 11 115007, [arXiv:1809.09174].

[12] D. M. Ghilencea, *Weyl R^2 inflation with an emergent Planck scale*, *JHEP* **10** (2019) 209, [arXiv:1906.11572].

[13] I. Oda, *Planck scale from broken local conformal invariance in Weyl geometry*, *PoS* **CORFU2019** (2020) 070, [arXiv:2003.12256].

[14] I. Oda, *Emergence of Einstein Gravity from Weyl Gravity*, arXiv:2003.01437.

[15] I. Oda, *Planck scale from broken local conformal invariance in weyl geometry*, *Adv. Stud. Theor. Phys.* **14** (2020), no. 1-4 9–28, [arXiv:1909.09889].

[16] I. Oda, *Planck and electroweak scales emerging from conformal gravity*, *PoS CORFU2018* (2019) 057, [arXiv:1903.09309].

[17] D. M. Ghilencea, *Gauging scale symmetry and inflation: Weyl versus Palatini gravity*, *Eur. Phys. J. C* **81** (2021), no. 6 510, [arXiv:2007.14733].

[18] D. M. Ghilencea, *Standard Model in Weyl conformal geometry*, *Eur. Phys. J. C* **82** (2022), no. 1 23, [arXiv:2104.15118].

[19] D. M. Ghilencea and T. Harko, *Cosmological evolution in Weyl conformal geometry*, arXiv:2110.07056.

[20] D. M. Ghilencea, *Non-metric geometry as the origin of mass in gauge theories of scale invariance*, *Eur. Phys. J. C* **83** (2023), no. 2 176, [arXiv:2203.05381].

[21] M. Shaposhnikov and D. Zenhausern, *Quantum scale invariance, cosmological constant and hierarchy problem*, *Phys. Lett. B* **671** (2009) 162–166, [arXiv:0809.3406].

[22] D. Ghilencea, Z. Lalak, and P. Olszewski, *Standard model with spontaneously broken quantum scale invariance*, *Phys. Rev. D* **96** (2017), no. 5 055034, [arXiv:1612.09120].

[23] D. Ghilencea, *Manifestly scale-invariant regularization and quantum effective operators*, *Phys. Rev. D* **93** (2016), no. 10 105006, [arXiv:1508.00595].

[24] D. M. Ghilencea, *Quantum implications of a scale invariant regularization*, *Phys. Rev. D* **97** (2018), no. 7 075015, [arXiv:1712.06024].

[25] Z. Lalak and P. Olszewski, *Vanishing trace anomaly in flat spacetime*, *Phys. Rev. D* **98** (2018), no. 8 085001, [arXiv:1807.09296].

[26] M. Weißwange, D. M. Ghilencea, and D. Stöckinger, *Quantum scale invariance in gauge theories and applications to muon production*, *Phys. Rev. D* **107** (2023), no. 8 085008, [arXiv:2208.01293].

[27] M. Weißwange, *Master thesis*, 2021. Available at: https://iktp.tu-dresden.de/IKTP/pub/21/Masterarbeit_Matthias_Weisswange.pdf.

[28] D. M. Ghilencea, Z. Lalak, and P. Olszewski, *Two-loop scale-invariant scalar potential and quantum effective operators*, *Eur. Phys. J. C* **76** (2016), no. 12 656, [arXiv:1608.05336].

[29] S. Coleman, *Aspects of Symmetry.* Cambridge University Press, 1985.

[30] S. R. Coleman and E. J. Weinberg, *Radiative Corrections as the Origin of Spontaneous Symmetry Breaking*, *Phys. Rev. D* **7** (1973) 1888–1910.

[31] P. Olszewski, *Electroweak vacuum in standard model and in its extension motivated by scale symmetry*, .

[32] M. Sher, *Electroweak Higgs Potentials and Vacuum Stability*, *Phys. Rept.* **179** (1989) 273–418.

[33] F. Karsch, T. Neuhaus, A. Patkos, and J. Rank, *Critical Higgs mass and temperature dependence of gauge boson masses in the SU(2) gauge Higgs model*, *Nucl. Phys. B Proc. Suppl.* **53** (1997) 623–625, [hep-lat/9608087].

[34] M. Laine and A. Vuorinen, *Basics of Thermal Field Theory*, vol. 925. Springer, 2016.

[35] Z. Lalak and P. Michalak, *Spontaneous scale symmetry breaking at high temperature*, *JHEP* **05** (2023) 206, [arXiv:2211.09045].

[36] Z. Lalak and P. Michalak, *Inflation in the Scale Symmetric Standard Model and Weyl geometry*, arXiv:2506.14617.

[37] O. Lebedev and H. M. Lee, *Higgs Portal Inflation*, *Eur. Phys. J. C* **71** (2011) 1821, [arXiv:1105.2284].

[38] H. M. Lee, *Light inflaton completing Higgs inflation*, *Phys. Rev. D* **98** (2018), no. 1 015020, [arXiv:1802.06174].

[39] P. G. Ferreira, C. T. Hill, J. Noller, and G. G. Ross, *Scale-independent R^2 inflation*, *Phys. Rev. D* **100** (2019), no. 12 123516, [arXiv:1906.03415].

[40] O. Lebedev, *The Higgs portal to cosmology*, *Prog. Part. Nucl. Phys.* **120** (2021) 103881, [arXiv:2104.03342].

[41] H. M. Lee, *Running inflation with unitary Higgs*, *Phys. Lett. B* **722** (2013) 198–206, [arXiv:1301.1787].

[42] R. N. Lerner and J. McDonald, *Distinguishing Higgs inflation and its variants*, *Phys. Rev. D* **83** (2011) 123522, [arXiv:1104.2468].

[43] K. Enqvist, S. Nurmi, T. Tenkanen, and K. Tuominen, *Standard Model with a real singlet scalar and inflation*, *JCAP* **08** (2014) 035, [arXiv:1407.0659].

[44] M. Piani and J. Rubio, *Higgs-Dilaton inflation in Einstein-Cartan gravity*, *JCAP* **05** (2022), no. 05 009, [arXiv:2202.04665].

[45] G. K. Karananas, M. Shaposhnikov, and S. Zell, *Scale invariant Einstein-Cartan gravity and flat space conformal symmetry*, *JHEP* **11** (2023) 171, [arXiv:2307.11151].

[46] A. Zee, *Quantum field theory in a nutshell.* Princeton University Press, 2003.

[47] L. Ryder, *Quantum Field Theory.* Cambridge University Press, 1996.

[48] M. D. Schwartz, *Quantum Field Theory and the Standard Model.* Cambridge University Press, 2014.

[49] M. E. Peskin and D. V. Schroeder, *An Introduction to Quantum Field Theory.* Westview Press, 1995.

[50] R. Ticciati, *Quantum Field Theory for Mathematicians.* Cambridge University Press, 1999.

[51] C. Delaunay, C. Grojean, and J. D. Wells, *Dynamics of non-renormalizable electroweak symmetry breaking*, *JHEP* **04** (2008) 029, [arXiv:0711.2511].

[52] H. Kleinert and V. Schulte-Frohlinde, *Critical Properties of ϕ^4-Theories.* World Scientific, 2001.

[53] F. Englert, C. Truffin, and R. Gastmans, *Conformal invariance in quantum gravity*, *Nucl. Phys. B* **117** (1976) 407–432.

[54] S. Deser, *Scale invariance and gravitational coupling*, *Annals Phys.* **59** (1970) 248–253.

[55] C. Tamarit, *Running couplings with a vanishing scale anomaly*, *JHEP* **12** (2013) 098, [arXiv:1309.0913].

[56] H. Weyl, *Gravitation and electricity*, *Sitzungsber. Preuss. Akad. Wiss. Berlin (Math. Phys.)* **1918** (1918) 465.

[57] T. Fulton, F. Rohrlich, and L. Witten, *Conformal invariance in physics*, *Rev. Mod. Phys.* **34** (1962) 442–457.

[58] P. A. M. Dirac, *Long range forces and broken symmetries*, *Proc. Roy. Soc. Lond. A* **333** (1973) 403–418.

[59] W. Drechsler and H. Tann, *Broken weyl invariance and the origin of mass*, *Found. Phys.* **29** (1999) 1023–1064, [gr-qc/9802044].

[60] E. Scholz, *Higgs and gravitational scalar fields together induce weyl gauge*, *Gen. Rel. Grav.* **47** (2015), no. 2 7, [arXiv:1407.6811].

[61] Particle Data Group, *Review of Particle Physics: Astrophysical Constants*, *Progress of Theoretical and Experimental Physics* **2020** (2021), no. 8 083C01. https://pdg.lbl.gov/2021/reviews/rpp2020-rev-astrophysical-constants.pdf.

[62] Particle Data Group, *Review of Particle Physics: Higgs Boson*, *Progress of Theoretical and Experimental Physics* **2023** (2023), no. 8 083C01. https://pdg.lbl.gov/2023/reviews/rpp2023-rev-higgs-boson.pdf.

[63] M. B. Einhorn and D. R. T. Jones, *The effective potential, the renormalisation group and vacuum stability*, *JHEP* **04** (2007) 051, [hep-ph/0702295].

[64] D. Buttazzo, G. Degrassi, P. P. Giardino, G. F. Giudice, F. Sala, A. Salvio, and A. Strumia, *Investigating the near-criticality of the higgs boson*, *JHEP* **12** (2013) 089, [arXiv:1307.3536].

[65] S. P. Martin, *Taming the goldstone contributions to the effective potential*, *Phys. Rev. D* **90** (2014), no. 1 016013, [arXiv:1406.2355].

[66] J. Elias-Miro, J. R. Espinosa, and T. Konstandin, *Taming infrared divergences in the effective potential*, *JHEP* **08** (2014) 034, [arXiv:1406.2652].

[67] H. C. Ohanian, *Weyl gauge-vector and complex dilaton scalar for conformal symmetry and its breaking*, *Gen. Rel. Grav.* **48** (2016), no. 3 25, [arXiv:1502.00020].

[68] J. F. Donoghue, M. M. Ivanov, and A. Shkerin, *EPFL Lectures on General Relativity as a Quantum Field Theory*, arXiv:1702.00319.

[69] C. M. Hirata, "Lecture x: Linearized gravity." http://www.tapir.caltech.edu/~chirata/ph236/2011-12/. Caltech, 2011 Nov 09.

[70] M. van Beest, J. Calderón-Infante, D. Mirfendereski, and I. Valenzuela, *Lectures on the Swampland Program in String Compactifications*, *Phys. Rept.* **989** (2022) 1–50, [arXiv:2102.01111].

[71] E. Palti, *The Swampland: Introduction and Review*, *Fortsch. Phys.* **67** (2019), no. 6 1900037, [arXiv:1903.06239].

[72] E. Palti, *A Brief Introduction to the Weak Gravity Conjecture*, *LHEP* **2020** (2020) 176.

[73] S. Mrówczyński, "Introduction to statistical quantum field theory - lecture notes." https://www.ujk.edu.pl/strony/Stanislaw.Mrowczynski/Statistical-QFT.html.

[74] J. I. Kapusta and C. Gale, *Finite-temperature field theory: Principles and applications.* Cambridge Monographs on Mathematical Physics. Cambridge University Press, 2011.

[75] J. I. Kapusta and P. V. Landshoff, *FINITE TEMPERATURE FIELD THEORY*, *J. Phys. G* **15** (1989) 267–285.

[76] L. Dolan and R. Jackiw, *Symmetry Behavior at Finite Temperature*, *Phys. Rev. D* **9** (1974) 3320–3341.

[77] P. B. Arnold and O. Espinosa, *The Effective potential and first order phase transitions: Beyond leading-order*, *Phys. Rev. D* **47** (1993) 3546, [hep-ph/9212235]. [Erratum: Phys.Rev.D 50, 6662 (1994)].

[78] M. Quiros, *Finite temperature field theory and phase transitions*, in *ICTP Summer School in High-Energy Physics and Cosmology*, pp. 187–259, 1, 1999. hep-ph/9901312.

[79] T. Matsubara, *A New approach to quantum statistical mechanics*, *Prog. Theor. Phys.* **14** (1955) 351–378.

[80] M. Kierkla, A. Karam, and B. Swiezewska, *Conformal model for gravitational waves and dark matter: a status update*, *JHEP* **03** (2023) 007, [arXiv:2210.07075].

[81] T. Prokopec, J. Rezacek, and B. Świeżewska, *Gravitational waves from conformal symmetry breaking*, *JCAP* **02** (2019) 009, [arXiv:1809.11129].

[82] S. Arunasalam, A. Kobakhidze, C. Lagger, S. Liang, and A. Zhou, *Low temperature electroweak phase transition in the Standard Model with hidden scale invariance*, *Phys. Lett. B* **776** (2018) 48–53, [arXiv:1709.10322].

[83] L. Marzola, A. Racioppi, and V. Vaskonen, *Phase transition and gravitational wave phenomenology of scalar conformal extensions of the Standard Model*, *Eur. Phys. J. C* **77** (2017), no. 7 484, [arXiv:1704.01034].

[84] V. Vaskonen, *Electroweak baryogenesis and gravitational waves from a real scalar singlet*, *Phys. Rev. D* **95** (2017), no. 12 123515, [arXiv:1611.02073].

[85] F. Sannino and J. Virkajarvi, *First order electroweak phase transition from (non)conformal extensions of the standard model*, *Phys. Rev. D* **92** (2015), no. 4 045015, [arXiv:1505.05872].

[86] M. E. Carrington, *The effective potential at finite temperature in the standard model*, *Phys. Rev. D* **45** (1992) 2933–2944.

[87] L. D. Rose, C. Marzo, and A. Urbano, *On the fate of the standard model at finite temperature*, *JHEP* **05** (2016) 050, [arXiv:1507.06912].

[88] L. Husdal, *On effective degrees of freedom in the early universe*, *Galaxies* **4** (2016), no. 4 78, [arXiv:1609.04979].

[89] R. N. Lerner and J. McDonald, *Gauge singlet scalar as inflaton and thermal relic dark matter*, *Phys. Rev. D* **80** (2009) 123507, [arXiv:0909.0520].

[90] D. S. Salopek, J. R. Bond, and J. M. Bardeen, *Designing Density Fluctuation Spectra in Inflation*, *Phys. Rev. D* **40** (1989) 1753.

[91] B. A. Bassett, S. Tsujikawa, and D. Wands, *Inflation dynamics and reheating*, *Rev. Mod. Phys.* **78** (2006) 537–589, [astro-ph/0507632].

[92] D. Baumann, *Inflation*, in *Theoretical Advanced Study Institute in Elementary Particle Physics: Physics of the Large and the Small*, pp. 523–686, 2011. arXiv:0907.5424.

[93] D. Baumann, *Cosmology.* Cambridge University Press, 7, 2022.

[94] A. R. Liddle and D. H. Lyth, *Cosmological inflation and large scale structure.* 2000.

[95] **Planck** Collaboration, Y. Akrami et al., *Planck 2018 results. X. Constraints on inflation*, *Astron. Astrophys.* **641** (2020) A10, [arXiv:1807.06211].

[96] **ACT** Collaboration, T. Louis et al., *The Atacama Cosmology Telescope: DR6 Power Spectra, Likelihoods and ΛCDM Parameters*, arXiv:2503.14452.

[97] **ACT** Collaboration, E. Calabrese et al., *The Atacama Cosmology Telescope: DR6 Constraints on Extended Cosmological Models*, arXiv:2503.14454.

[98] K. Falls and M. Herrero-Valea, *Frame (In)equivalence in Quantum Field Theory and Cosmology*, *Eur. Phys. J. C* **79** (2019), no. 7 595, [arXiv:1812.08187].

[99] T. Markkanen, S. Nurmi, A. Rajantie, and S. Stopyra, *The 1-loop effective potential for the Standard Model in curved spacetime*, *JHEP* **06** (2018) 040, [arXiv:1804.02020].

[100] T. Markkanen, T. Tenkanen, V. Vaskonen, and H. Veermäe, *Quantum corrections to quartic inflation with a non-minimal coupling: metric vs. Palatini*, *JCAP* **03** (2018) 029, [arXiv:1712.04874].

[101] O. Czerwińska, Z. Lalak, and L. Nakonieczny, *Stability of the effective potential of the gauge-less top-Higgs model in curved spacetime*, *JHEP* **11** (2015) 207, [arXiv:1508.03297].

[102] K. Cheung, C.-W. Chiang, and T.-C. Yuan, *Partially Strong WW Scattering*, *Phys. Rev. D* **78** (2008) 051701, [arXiv:0803.2661].

[103] M. Szleper, *The Higgs boson and the physics of WW scattering before and after Higgs discovery*, arXiv:1412.8367.

[104] G. Valencia and S. Willenbrock, *The Goldstone Boson Equivalence Theorem and the Higgs Resonance*, *Phys. Rev. D* **42** (1990) 853–859.

[105] A. Ito, W. Khater, and S. Rasanen, *Tree-level unitarity in Higgs inflation in the metric and the Palatini formulation*, *JHEP* **06** (2022) 164, [arXiv:2111.05621].

[106] G. K. Karananas, M. Shaposhnikov, and S. Zell, *Field redefinitions, perturbative unitarity and Higgs inflation*, *JHEP* **06** (2022) 132, [arXiv:2203.09534].

[107] C. Caprini and D. G. Figueroa, *Cosmological Backgrounds of Gravitational Waves*, *Class. Quant. Grav.* **35** (2018), no. 16 163001, [arXiv:1801.04268].

[108] P. D. Lasky et al., *Gravitational-wave cosmology across 29 decades in frequency*, *Phys. Rev. X* **6** (2016), no. 1 011035, [arXiv:1511.05994].

[109] **Planck** Collaboration, N. Aghanim et al., *Planck 2018 results. VI. Cosmological parameters*, *Astron. Astrophys.* **641** (2020) A6, [arXiv:1807.06209]. [Erratum: Astron.Astrophys. 652, C4 (2021)].

[110] A. I. Renzini, B. Goncharov, A. C. Jenkins, and P. M. Meyers, *Stochastic Gravitational-Wave Backgrounds: Current Detection Efforts and Future Prospects*, *Galaxies* **10** (2022), no. 1 34, [arXiv:2202.00178].

[111] C. Ford, D. R. T. Jones, P. W. Stephenson, and M. B. Einhorn, *The effective potential and the renormalization group*, *Nucl. Phys. B* **395** (1993) 17–34, [hep-lat/9210033].

[112] E. Senaha, *Symmetry Restoration and Breaking at Finite Temperature: An Introductory Review*, *Symmetry* **12** (2020), no. 5 733.

[113] R. R. Parwani, *Resummation in a hot scalar field theory*, *Phys. Rev. D* **45** (1992) 4695, [hep-ph/9204216]. [Erratum: Phys.Rev.D 48, 5965 (1993)].

[114] "Review of kinematics." URL: https://pdg.lbl.gov/2018/reviews/rpp2018-rev-kinematics.pdf.

[115] F. D'Eramo, N. Fernandez, and S. Profumo, *Dark matter freeze-in production in fast-expanding universes*, *JCAP* **02** (2018) 046, [arXiv:1712.07453].

[116] E. W. Kolb and M. S. Turner, *The Early Universe*, vol. 69 of *Front. Phys.* 1990.

[117] V. Mukhanov, *Physical Foundations of Cosmology*. Cambridge University Press, 2005.